STUDIES ON THE INTERACTION OF SMALL FLUORESCENT MOLECULES/NUCLEOSIDE WITH DUPLEX, G-QUADRUPLEX AND CALF THYMUS DNA

A

thesis submitted to the
Indian Institute of Technology Guwahati
for the degree of Doctor of Philosophy in Chemistry

Submitted by

Manoj Kumar Pradhan
Roll.No.11612211

Department of Chemistry
Indian Institute of Technology Guwahati
Guwahati – 781039

DECLARATION

I declare that the thesis entitled "**STUDIES ON THE INTERACTION OF SMALL FLUORESCENT MOLECULES/NUCLEOSIDE WITH DUPLEX, G-QUADRUPLEX AND CALF THYMUS DNA**" submitted by me for the degree of Doctor of Philosophy is the record of research work carried out by me during the period from July 2011 to December 2016 under the guidance and supervision of Dr. Subhendu Sekhar Bag, associate professor, Indian Institute of Technology Guwahati and has not formed the basis for the award of any degree, diploma, associateship, fellowship, titles in this University or in any other University or other similar institutions of higher learning.

Manoj Kumar Pradhan
Roll No.: 11612211

Department of Chemistry,
Indian Institute of Technology Guwahati,
Guwahati – 781 039, India
March, 2017

Dr. Subhendu Sekhar Bag, Ph.D.
Associate Professor
Department of Chemistry
Indian Institute of Technology
Guwahati -781039
Assam, INDIA

Ph: +91-361-258-2324 (O)
Ph: +91-361-258-4324 (R)
Fax: +91-361-258-2349

E-mail: ssbag75@yahoo.co.in
ssbag75@iitg.ernet.in

CERTIFICATE

This is to certify that the research work presented in this thesis entitled **"STUDIES ON THE INTERACTION OF SMALL FLUORESCENT MOLECULES/NUCLEOSIDE WITH DUPLEX, G-QUADRUPLEX AND CALF THYMUS DNA"** is an authentic record of the results obtained from the research work carried out by **Mr. Manoj Kumar Pradhan** under my supervision in the Department of Chemistry, Indian Institute of technology Guwahati, India. This work is original and has not been submitted elsewhere for any degree or award.

IIT Guwahati
March, 2017

Dr. Subhendu Sekhar Bag
(Thesis Supervisor)

This dissertation is dedicated to my beloved parents for their endless love, support and encouragement…

Science is organized knowledge. Wisdom is organised LIFE

Immanuel Kant

ACKNOWLEDGEMENTS

Throughout the last five and half years, many people have dedicated their own time and effort towards helping me, who have made this dissertation possible. First and foremost, I would like to express my sincere gratitude to my advisor **Dr. Subhendu Sekhar Bag**, associate professor, IIT Guwahati, Assam, for giving me the opportunity to work on my PhD studies in his group. I have been amazingly fortunate to have an advisor who gave me the freedom to explore on my own, and at the same time the guidance to recover when my steps faltered. His keen interest and encouragement serves as a constant support during all the time of research and writing of this thesis.

Besides my advisor, I would like to thank the rest of my thesis committee members: **Prof. Bhisma Kumar Patel** (CHY), **Dr. Kalyanasis Sahu** (CHY) and **Dr. Chandan Das** (CE), for their insightful comments and encouragement.

I am thankful to the **CIF IIT Guwahati** for providing instrument facilities. I am grateful to university grants commission (**UGC**) for providing me Fellowship for my PhD programme.

I wish to thank my former and present labmates, **Rajen da**, **Sangita di**, **Subhashis**, **Afsana**, **Suman**, **Suranjan** and **Hiranya**, for their cooperation, support and pleasant company throughout my research work. I would like to thank all my PhD batchmates for making a friendly environment. My best thank goes to **Harikrishna** and **Santosh** for being always with me during my good and bad times. Besides, I would like to thank all my juniors, friends and seniors of chemistry and other departments of IIT Guwahati, who are attached with me and have made my stay in the campus colourful.

And last but not least, my heart-felt gratitude goes to my whole family for their unconditional love and support throughout my study my parents (**Mr. Pitabasa Pradhan** and **Mrs. Sita Pradhan**) who have been a constant source of inspiration throughout my life. Today I am here because of their sacrifices, blessings, love and affection. I am so grateful to my grandmother Late. **Ajodhya Pradhan**. Without them, this thesis would never have been written.

Sincerely,

Manoj Kumar Pradhan

ABSTRACT

The dissertation entitled **"STUDIES ON THE INTERACTION OF SMALL FLUORESCENT MOLECULES/NUCLEOSIDE WITH DUPLEX, G-QUADRUPLEX AND CALF THYMUS DNA"** contains a total of 5 Chapters. **Chapter 1** is a review chapter in which briefly described on the structural features of B-DNA and G-quadruplex DNAs and there possible different binding mode (covalent and non-covalent) with small molecules/nucleoside was highlighted. **Chapter 2** focused on detection of SNPs with a wavelength shifting oligonucleotide probe, **Chapter 3** focused on the label free detection of mismatched, abasic and bulge DNA utilising a fluorescent unnatural tetrazolyl pyrene nucleoside probe ($^{TzPy}B^{Do}$), **Chapter 4** focused on the discrimination of higher order G-quadruplex over monomeric G-quadruplexes, single stranded and double stranded DNAs using $^{TzPy}B^{Do}$ as fluorescent switch on probe. **Chapter 5** deals with fluorescence switch-on sensing of ct-DNA utilising solvatochromic fluorescent naphthalimide probes.

Chapter 1: Interaction of Small Fluorescent Molecules/Nucleosides with DNA: A Review

This is a review chapter, which briefly described structural features of DNA (duplex), G-quadruplexes and possible different binding of modes with small molecules (**Figure A1**).

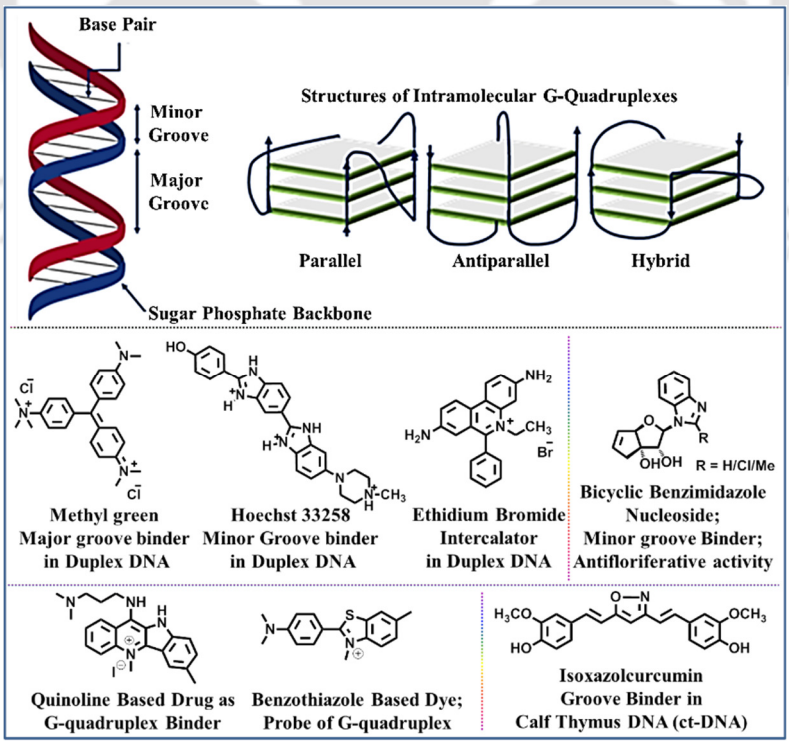

Figure A1. The structure of DNA duplex and G-quadruplex DNA and some fluorescent molecules/nucleosides with their role in DNA detection.

Chapter 2: Synthesis of Fluorescent Oligonucleotide Probe Containing 5'-(2-napthyl)-2'-deoxy Uridine and Its Application in SNPs Genotyping

This chapter describes the synthesis of an environment sensitive fluorescent nucleoside (^{Naph}U), which exhibited excellent solvatocromic photophysical properties. It was incorporated into short oligonucleotide sequence for homogeneous DNA detection. Study of photophysical property revealed that the novel naphthalene labeled uridine nucleoside displayed solvatochromism (Dioxane, λ_{em} = 380 to Water, λ_{em} = 453 nm). Upon incorporation into oligonucleotides, the absorption spectrum of ^{Naph}U was characterized by a minimal hypsochromic shift and a hyperchromicity, in particular, when hybridized to form the fully matched duplex, (^{Naph}U/A base pair). The emission spectra of the perfect matched DNA showed an increased intensity with 26 nm blue-shift suggesting that the naphthyl group positioned in a compact hydrophobic microenvironment pointing toward the duplex groove region. In contrary, with mismatched duplexes the absorption spectra were characterized by bathochromic shift in wavelength and hypochromic effect. The fluorescence was partially quenched. So, the naphthalene labeled modified oligonucleotide was able to magnificently discriminate between the Watson-Crick base pairing against non-Watson-Crick base pairing via wavelength shifting and enhancement of fluorescence emission intensity (**Figure A2**).

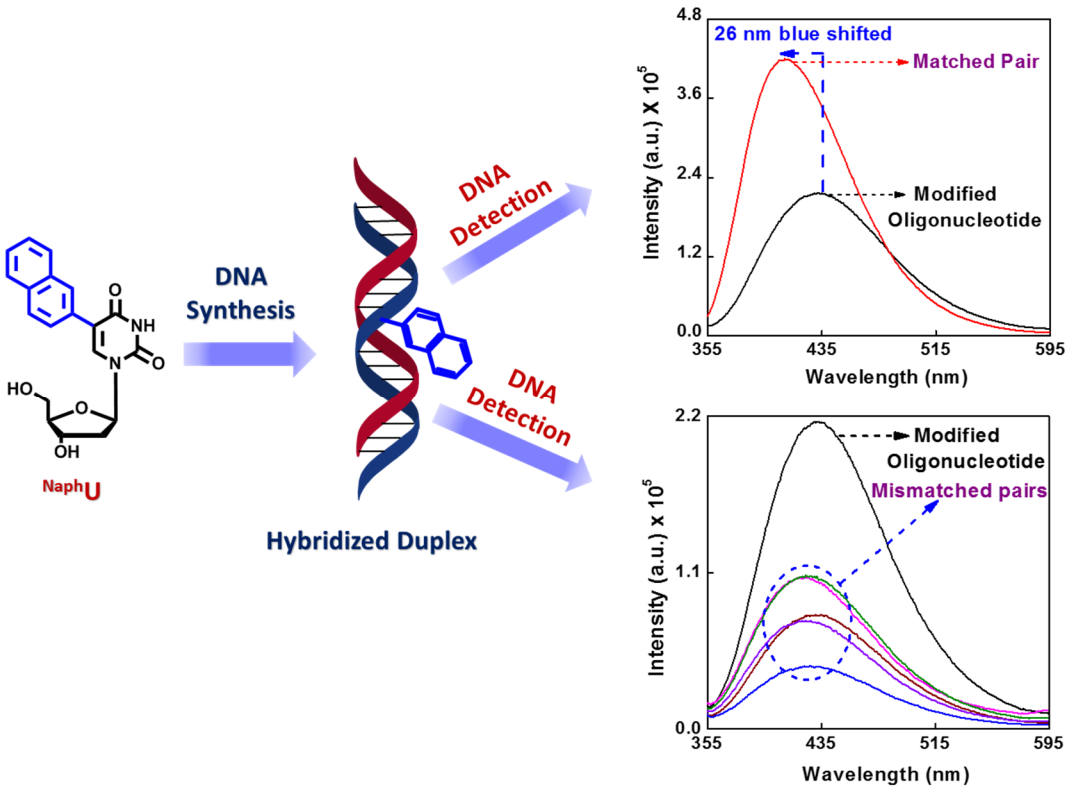

Figure A2. Overall representation of ^{Naph}U incorporated into ODN for DNA detection.

Chapter 3: Studies on the Label Free Detection of Mismatched, Abasic and Bulge DNA Utilizing Fluorescent Tetrazolyl Pyrene Unnatural Nucleoside

Chapter 3 describes label free detection of DNA lesions. In the label-free approach, fluorescent ligands are not covalently attached to the nucleic acid backbone but it interacts noncovalently with DNA through a number of binding modes such as intercalation, groove-binding, end-stacking or electrostatic interactions. Mismatched (non-Watson–Crick) base pairs represent the most common type of DNA damage, as they are formed permanently in living cells due to erroneous insertion, deletion and misincorporation of bases. Thus, using an unnatural tetrazolylpyrene nucleoside ($^{TzPy}B^{Do}$) as a fluorescent probe the detection of homo pyrimidine mismatches, abasic site positioned opposite to pyrimidines and pyrimidine-bulge DNA over fully matched double stranded DNA was accomplished. Comparing to the fluorescence spectra of fully matched (FM) duplex homo pyrimidine mismatched (T/T or C/C) duplexes showed fluorescence enhancement upto 24 fold for T/T mismatch and 32 fold for C/C mis-matched duplex whereas FM duplex had only by 10 fold with respect to the bare nucleoside probe **TzPy**. Also, the fold increase of fluorescence intensity compared to the bare probe observed in the presence of an abasic site opposite to pyrimidines was 19 fold for Φ–C and 14 fold for Φ-T and only 5 fold for FM duplex. The analysis of the emission spectra for bulge DNA revealed that the fold increase of fluorescence intensity compared to the only probe observed when excited at 370 nm was 37 and 43, respectively for T- and C-bulge DNAs and 5 for FM duplex (**figure A3**). The binding of the probe to all the three mutated DNA duplexes was supported by an increase in the thermal melting of the mutated DNA in presence of unnatural nucleoside, **TzPy**. The proposed binding of TzPy to mutated DNAs presented in **Scheme A1**.

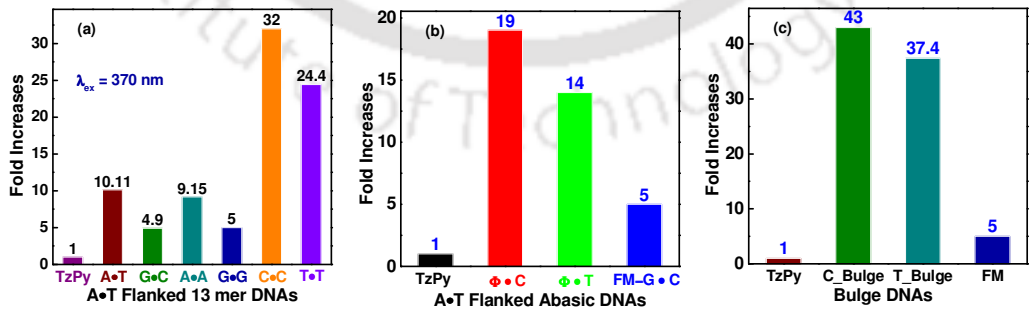

Figure A3. (a) Fluorescence fold increases for A/T flanked mismatched and matched DNAs, (b) Fluorescence fold increases for A/T flanked abasic DNAs and (c) Fluorescence fold increases for A/T flanked pyrimidine bulge DNAs.

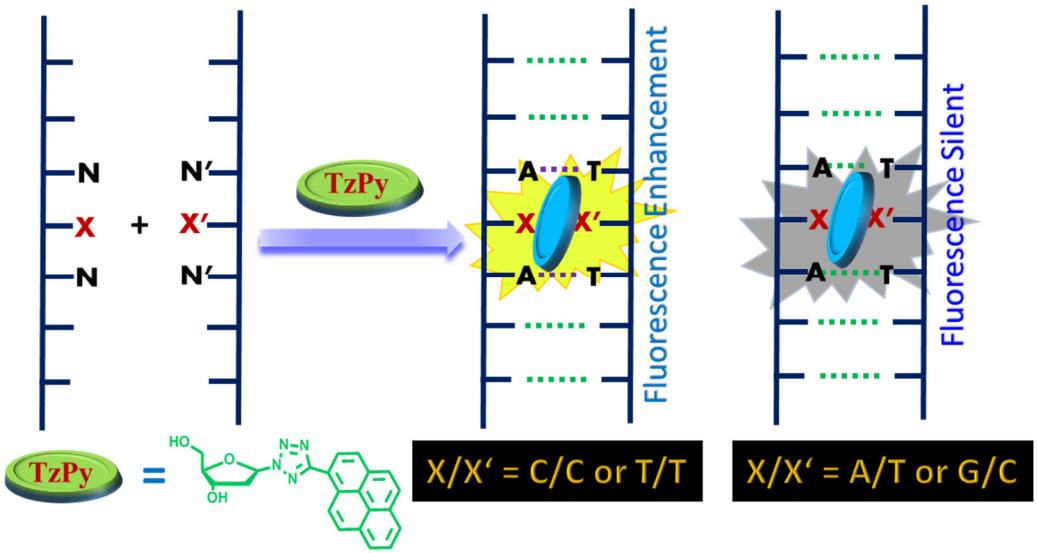

Scheme A1. Proposed bind of **TzPy** to A/T flanked homo pyrimidine mismatched duplexes and matched duplex (X, X' = C/C or T/T, X = C/T, X' = Abasic or bulge site).

Chapter 4: Studies on the Label Free Detection of G-Quadruplex DNA Utilizing Fluorescent Tetrazolyl Pyrene Unnatural Nucleoside

Chapter 4 describes the detection of higher order human telomeric G-quadruplex DNA over monomeric G-quadruplexes and other canonical topology of DNA. In humans, telomeric DNA consists of a duplex region composed of hundreds of TTAGGG repeats, ending in a shorter G-rich single-stranded protrusion, which can fold into unique, highly stable four-stranded helices known as G-quadruplexes. Higher-order G-quadruplex structure is more biologically relevant, and the multimeric quadruplex units can be a predominant factor in recognizing long telomeric DNA *in vivo*. Thus, ligands bind to higher-order long telomeric DNA is essential.

So, the probe tetrzolyl pyrene unnatural nucleoside ($^{TzPy}\mathbf{B}^{Do}$) successfully and specifically bound to dimeric G-qudrupex with generation of about 9-fold increase in fluorescent emission intensity compared to monomeric G-quadruplex (**Figure A4**). We proposed that the tetrzolyl pyrene unnatural nucleoside bound at the cleft between two consecutive G-quadruplexes and hold via intercalative stacking interaction. The UV-visible spectra shown a bathochromic shift of about 11 nm and hyperchromicity suggesting that the probe bind to the compact hydrophobic region of dimeric G-quadruplex (**Figure A4**). From thermal denaturation study it was also revealed that there was no effect on monomer G-quadruplex whereas 2 °C temperature was

increased for dimeric G-qudruplex in presence of the probe. The proposed binding mode of the probe to dimeric G-quadruplex presented in **Scheme A2** below.

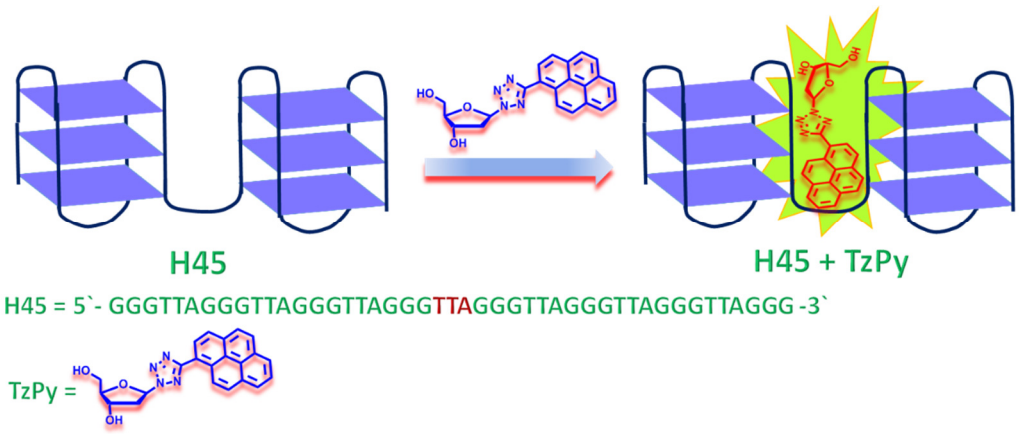

Scheme A2. TzPy proposed to bind at the cleft between two consecutive G-quadruplexes (H45).

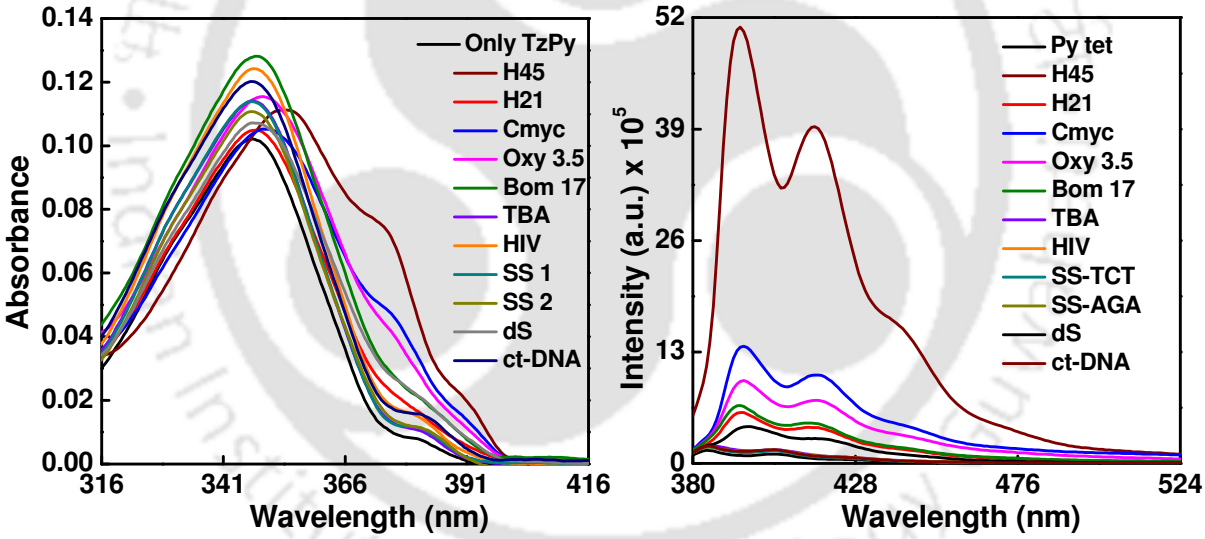

Figure A4. UV-visible and fluorescence emission spectra of un-natural nucleoside (10 μM) in presence of different G-quadruplex forming sequences, ct-DNA, duplex and single stranded DNAs (each DNA concentration = 4 μM).

Chapter 5: Studies on the Synthesis, Photophysical Properties of Naphthalimide and Fluorescence Switch-on Sensing of ct-DNA

Chapter 5 briefly describes the synthesis of highly solvatochromic molecules (**5.10** and **5.11**) and exploited in bio sensing application. Thus, we successfully synthesized highly solvatochromic donor/acceptor substituted naphthalimide based fluorophores and investigated

their photophysical properties. The synthesized naphthalimides containing propargyl ends showed highly solvatochromic intramolecular charge transfer (ICT) features as was revealed from the UV–visible, fluorescence and DFT/TDDFT calculation. Fluorescence life times for the imide fluorophores also supported our observation of ICT. Furthermore, both the donor/acceptor substituted naphthalimide fluorophores were exploited in sensing calf-thymus DNA via switch-on fluorescence response. The absorption maxima of fluorophore showed a negligible effect on the change in wavelength position and enhanced absorbance intensity as ct-DNA was added gradually. Similarly, upon gradual addition of ct-DNA, the emission intensity (λ_{em} = 525 nm) of the fluorophore **5.11** was found to be significantly enhanced with slightly red shifted pattern. The emission became saturated at 75 μM concentration of ct-DNA against 30 μM probe concentration (**Figure A5**). On the other hand, fluorophore **5.10** showed a sudden enhancement of fluorescence intensity with very little blue shifted pattern at probe : ct-DNA concentration ratio of 1:1. The association constant of probe **5.11** with ct-DNA was also determined by a Benesi-Hildebrand plot which was found to be 3.98 × 104 M^{-1} with an experimental free energy of binding, G = – 6.3 kcal/mol.

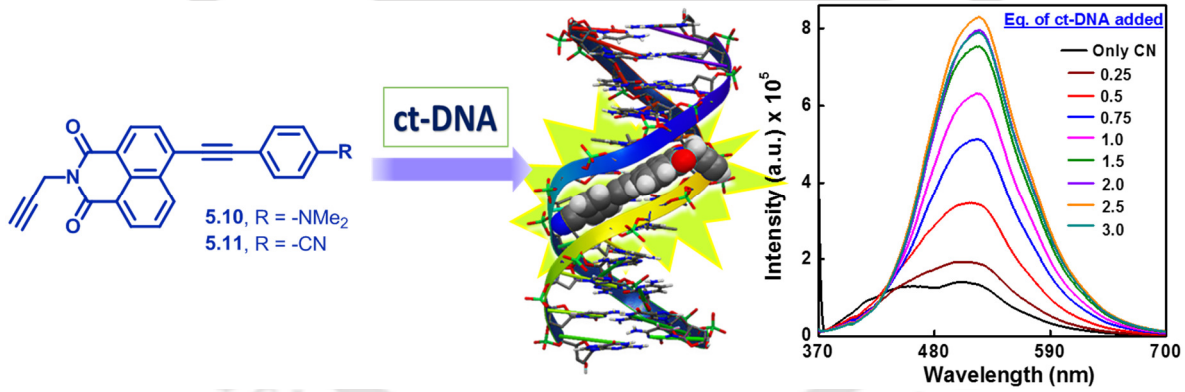

Figure A5. Binding interaction of probe **5.11** to ct-DNA and its fluorescence response.

List of Articles Published/ Communicated

1. Subhendu Sekhar Bag, **Manoj Kumar Pradhan**, Rajen Kundu and Subhashis Jana, Highly solvatochromic fluorescent naphthalimides: Design, synthesis, photophysical properties and fluorescence switch-on sensing of ct-DNA, *Bioorg. Med. Chem. Lett*. **2013**, *23*, 96.
2. Subhendu Sekhar Bag, **Manoj Kumar Pradhan**, Suman Kalyan Das, Subhashis Jana, and Raghunath Bag, Wavelength Shifting Oligonucleotide Probe for the Detection of Adenosine of a Target DNA with Enhanced Fluorescence Signal, *Bioorg. Med. Chem. Lett*. **2014**, *24*, 4678.
3. Subhendu Sekhar Bag, Subhashis Jana, **Manoj Kumar Pradhan** and Sunit Pal, Trichromophoric Pentapeptide: Impact of β-Sheet Conformation on Dual Path to Excimer Emission and Sensing of BSA Protein, *RSC Advances* **2016**, *6*, 72654.
4. Subhendu Sekhar Bag, Sangita Talukdar, Suman Kalyan Das, **Manoj Kumar Pradhan**, and Sumen Mukherjee, Donor/Acceptor Chromophores Decorated Triazolyl Unnatural Nucleosides: Synthesis, Photophysical Properties and Study of Interaction with BSA, *Org. Biomol. Chem*. **2016**, *14*, 5088.
5. Subhendu Sekhar Bag, Subhashis Jana and **Manoj Kumar Pradhan**, Synthesis and Photophysical Properties of Triazolyl-Donor/Acceptor Chomophores Decorated Unnatural Amino Acids and Application of Triazolylperylene Amino Acid in Sensing BSA, *Bioorg. Med. Chem*. **2016**, *24*(16), 3579.
6. Subhendu Sekhar Bag, Suman Kalyan Das, **Manoj Kumar Pradhan** and Subhashis Jana, Hybridization Accompanying FRET Event in Labeled Natural Nucleoside-Unnatural Nucleoside Containing Chimeric DNA Duplexes, *J. Photochem. Photobio., B* **2016**, *162*, 669.
7. Subhendu Sekhar Bag, **Manoj Kumar Pradhan** and Sangita Talukdar, Trifunctional Fluorescent Unnatural Nucleoside: Label Free Detection of T-T/C-C Base Mismatches, Abasic Site and Bulge DNA, *J. Photochem. Photobio., B* **2017**, *173*, 165.

Article 3, 4, 5 and 6 are not part of the present thesis

Communicated

1. Subhendu Sekhar Bag, **Manoj Kumar Pradhan** and Sangita Talukdar, Trifunctional Fluorescent Unnatural Nucleoside: Label Free Discrimination of higher order G-

quadruplex over monomer G-quadruplex, duplexes and single strand DNAs (Communicated).

List of Conferences/Symposiums

1. **Pradhan, M. K**.; Bag, S. S., Wavelength Shifting Oligonucleotide Probe for DNA Detection with Enhanced Fluorescence Signal, *10th International Symposium on Bio-Organic Chemistry, IISER Pune, January 11-15, 2015.*
2. **Pradhan, M. K**.; Bag, S. S., Wavelength Shifting oligonucleotide probe for the discrimination between matched and mismatched duplex of a target DNA with enhanced fluorescence signal, *Frontiers in Chemical Sciences 2014, IIT Guwahati, December 04-06, 2014*.

CONTENTS

Title	Page No.
ABBREVIATIONS and NOTATIONS	**xiii-xvi**
LIST OF FIGURES	**xvii-xxiv**
LIST OF SCHEME	**xxiv**
LIST OF TABLES	**xxiv-xxv**

CHAPTER 1. Interaction of Small Fluorescent Molecules/Nucleosides with DNA: A Review

1.1	Introduction	1-2
1.2	Structural Features of DNA	2-5
1.3	Non-covalent Interactions of Small Molecules with Duplex-DNA	5-6
1.3.1	Duplex-DNA Intercalators	6-7
1.3.2	Duplex-DNA Groove-Binding Molecules	7-9
1.3.3	Intercalator–Minor-Groove Binding Hybrid Molecules	9-10
1.4	Fluorescent Nucleoside Analogs For SNP Detection in DNA	10-18
1.5	Label Free DNA Detection	18-22
1.6	Structural Features of G-Quadruplex DNA	22-25
1.6.1	G-Quadruplex Binding Probes	25-31
1.7	References	32-36

CHAPTER 2. Synthesis of Fluorescent Oligonucleotide Probe Containing 5'-(2-napthyl)-2'-deoxy Uridine and Its Application in SNPs Genotyping

2.1	Introduction	37-40
2.2	Background	40
2.3	Objective	41-43
2.4	Result and Discussion	43-59
2.4.1	Synthesis of Naphthalene Labeled Fluorescent Nucleoside	43-44
2.4.2	Study of Photophysical Properties of Naphthalene Labeled Fluorescent Nucleoside	44-46
2.4.3	Theoretical Calculation	47-50

2.4.4		Synthesis and Characterization of the Oligonucleotide Probe	50-52
2.4.5		DNA Detection by Measuring Photophysical Properties	52-59
	2.4.5.1	Spectral Study of ODN **1** and ODN **9** with Its Various Duplexes	52-56
	2.4.5.2	Evaluation of Thermal Stability of the Duplexes Derived From ODN **1**	56-57
	2.4.5.3	Circular Dichroism Measurement	57-58
	2.4.5.4	Molecular Modeling Study	58-59
2.5		Conclusion	59
2.6		Experimental Section	60-63
2.7		NMR Spectra of ^{Naph}**U** Nucleoside	64-67
2.8		References	68-72

CHAPTER 3. Studies on the Label Free Detection of Mismatched, Abasic and Bulge DNA Utilizing Fluorescent Tetrazolyl Pyrene Unnatural Nucleoside

3.1		Introduction	73
3.2		DNA Mismatch Detection	74-75
3.3		Abasic Site Detection	75-78
3.4		Bulge DNA Detection	78-80
3.5		Background	80-81
3.6		Objective	81-82
3.7		Result and Discussion	82-100
3.7.1		Study of Photophysical Properties of **TzPy** in Dioxane-Water Mixture	82-84
3.7.2		DNA Mismatch Detection	84-93
	3.7.2.1	Spectral Study of **TzPy** with Various Form of Match and Mismatch Duplexes Having Both AT/AT and GC/GC Flanking	84-89
	3.7.2.2	Effect of **TzPy** On the Thermal Stability of Various Match and Mismatch Duplexes Having Both AT/AT and GC/GC Flanking Base Pairs	89-91
	3.7.2.3	Effect of **TzPy** On the Circular Dichroism Spectra of Various Match and Mismatch Duplexes Having Both AT/AT and GC/GC Flanking Base Pairs	91-93

3.7.3		Detection of Abasic Site (AP site) Positioned Opposite to Pyrimidines in Duplex DNA	93-96
	3.7.3.1	Spectral Study of **TzPy** with Abasic Site Positioned Opposite to Pyrimidine in AT/AT Flanking Duplex DNA	94-95
	3.7.3.2	Effect of **TzPy** On the Thermal Stability of Abasic Site Positioned Opposite to Pyrimidine in AT/AT Flanking Duplex DNA	95-96
	3.7.3.3	Effect of **TzPy** On the Circular Dichroism of Abasic Site Positioned Opposite to Pyrimidine in AT/AT Flanking Duplex DNA	96
3.7.4		Detection of Pyrimidine Bulge DNAs	97-100
	3.7.4.1	Spectral Study of **TzPy** with AT/AT Flanking Pyrimidine-Bulge	98-99
	3.7.4.2	Effect of **TzPy** On the Thermal Stability of Pyrimidine-Bulge	99-100
	3.7.4.3	Effect of **TzPy** On the Circular Dichroism of Pyrimidine-Bulge	100
3.8		Conclusion	101
3.9		Experimental Section	101-102
3.10		References	103-104

CHAPTER 4 Studies on the Label Free Detection of G-Quadruplex DNA Utilizing Fluorescent Tetrazolyl Pyrene Unnatural Nucleoside

4.1		Introduction	105
4.2		Detection of Higher-Order G-Quadruplexes	105-110
4.3		Background	110-111
4.4		Objective	111-112
4.5		Result and Discussion	112-122
4.5.1		Spectral Study of **TzPy** with Various Kind of G-quadruplex DNA Detection	112-116
4.5.2		Effects of **TzPy** On Circular Dichroism Spectra of G-quadruplexes	116-117
4.5.3		Comparative Binding Study of **TzPy** with Human Monomeric G4 (Hum21) and Human Dimeric G4 (Hum45)	117-120
4.5.4		Binding Affinity of **TzPy** to Dimeric G4 (Hum45) DNA	120-121
4.5.5		Effect of **TzPy** On the Thermal Stability of Hum21 and Hum45	121-122

4.6 Conclusion 122
4.7 Experimental Section 123-124
4.8 References 124-126

CHAPTER 5 Studies on the Synthesis, Photophysical Properties of Naphthalimide and Fluorescence Switch-on Sensing of ct-DNA

5.1 Introduction 127-132
5.2 Background 132
5.3 Objective 132-133
5.4 Results and Discussions 133-149
5.4.1 Synthesis of Donor/Acceptor Labeled Naphthalimide Solvatocromic Fluoroprobe 133-134
5.4.2 Crystallographic Description of **5.10** 134-135
5.4.3 Spectral Study of **5.10** and **5.11** in Different Solvent 135-141
5.4.4 Lippert and Mataga Plots 141-144
5.4.5 Studies On the Interaction of Fluorophores **5.10** and **5.11** with ct-DNA 144-149
5.4.5.1 UV-visible Study of **5.10** and **5.11** with ct-DNA 144-145
5.4.5.2 Fluorescence Study of **5.10** and **5.11** with ct-DNA 145-146
5.4.5.3 Evaluation of Binding Constant "Benesi-Hildebrand Plot" 146-147
5.4.5.4 DNA Melting Experiments 147
5.4.5.5 Evaluation of Binding Mode of the Fluorophore **5.10** and **5.11** with ct-DNA by a Dye (Ethidium Bromide) Displacement Study 148
5.4.5.6 Molecular Modeling Study 148-149
5.5 Conclusion 149-150
5.6 Experimental Section 150-157
5.7 ^{1}H and ^{13}C NMR Spectra 158-161
5.8 References 162-164

Summary and Outlook 165-166

ABBREVIATIONS

A	Adenine
ACN	Acetonitrile
ATMND	2-amino-5,6,7-trimethyl- 1,8-naphthyridine
AF	Ammonium formate
AP site	Apurinic/apyrimidinic site
BDF	Base-discriminating fluorescent
BER	Berberine
BEU	Berberrubine
B3LYP	Becke, three-parameter, Lee-Yang-Parr
C	Cytosine
CD	Circular dichroism
CHE	Chelerythrine
ct-DNA	Calf thymus DNA
CT	Charge transfer
CH_3CN	Acetonitrile
$CHCl_3$	Chloroform
COP	Coptisine
COR	Coralyne
$^{4\text{-CPE}}$**NI**	4-(4-cyanophenylethynyl)-*N*-(2-propynyl)-1,8-naphthalimide
Cy-hex	Cyclohexane
DANP	2,7-diamino-1,8-naphthyridine
DATPE	1,2-Bis{4-[(trimethylammonium)- butoxy]phenyl}-1,2-tetraphenylethene dibromide
DCPC	3,5-diamino-6-chloro-2-pyrazine carbonitrile
7-DeG	7-Deazaguanine
DFT	Density functional theory
Diox	1,4-Dioxane
DIPEA	*N,N*-Diisopropyl ethyl amine
$^{4\text{-DMAPE}}$**NI**	4-(4-*N,N*-dimethylaminophenylethynyl)-*N*-(2-propynyl)-1,8-naphthalimide
DMA	Dimethoxyamphetamine
DMAP	*N, N*-Dimethylamino pyridine
DMF	Dimethyl formamide

DMSO	Dimethyl sulfoxide
DMTrCl	4,4′-dimethoxytrityl chloride
DNA	Deoxyribonucleic acid
ds DNA	Double-stranded DNA
dU	2`-deoxyuridine
EB	Ethidium Bromide
ENX	Enoxacin
EtOAc	Ethylacetate
EtOH	Ethanol
ESF	Environmentally sensitive fluorescent
EPI	Epiberberine
Et_3N	Triethylamine
Eq.	Equivalent
FM	Fully matched
FRET	Fluorescence Resonance Energy Transfer
FQs	Fluoroquinolones
G	Guanine
Hex	Hexane
HIV	Human immunodeficiency virus
HOMO	Highest Occupied Molecular Orbital
HPLC	High Performance Liquid Chromatography
ICT	Internal charge transfer
ICT	Intramolecular Charge Transfer
ITC	Isothermal titration calorimetry
JAT	Jatrorrhizine
KOH	Potassium hydroxide
K_2CO_3	Potassium carbonate
LE	Locally-Excited
LOM	lomefloxacin
LUMO	Lowest Unoccupied Molecular Orbital
MALDI-ToF	Matrix Assisted Laser Desorption Ionization-Time of Flight
MeOH	Methanol
mM	Mili molar

MO	Molecular orbital
6 MP	6 mercaptopurine
μM	Micro molar
Nd–NAP	Neodymium–naproxen complex
NIT	Nitidine
NMR	Nuclear Magnetic Resonance
nm	Nano meter
^{Naph}**U**	Naphthalene labelled uridine nucleoside
ODN	Oligodeoxyribonucleotide
ONs	Oligo nucleotides
ORTEP	Oak Ridge Thermal Ellipsoid Plot
PAL	Palmatine
PCR	Polymerase chain reaction
Py	Pyrene
RNA	Ribonucleic acid
SAN	Sanguinarine
SNPs	Single nucleotide polymorphisms
SSA	Sodium saccharin
ss-DNA	Single-stranded DNA
T	Thymine
TBA	Thrombin binding aptamer
TBZ	Tetrabenazine
TD-DFT	Time dependent density functional theory
TFA	Trifluoroacetic Acid
TFE	Trifluoroethanol
THF	Tetrahydrofuran
ThT	Thioflavin T
TLC	Thin layer chromatography
TMS	Trimethylsilyl
TO	Thiazole Orange
^{TzPy}**B**^{Do}	Tetrazollylpyrene unnatural nucleoside
TzPy	Tetrazollylpyrene unnatural nucleoside
T_m	Thermal melting

UV	Ultra violate
UV-Vis	Ultraviolet-Visible
WOR	Worenine

NOTATIONS

Φ	Quantum Yield
ε	Molar extinction co-efficient
τ	Decay time
Å	Angstrom (10^{-8}cm)
λ	Wave Length
T_m	Thermal melting (DNA)
δ	Chemical shift in NMR
s	singlet
d	Doublet
t	triplet
q	quartet
m	multiplet
bs	broad singlet
dd	double doublet
dt	doublet of triplet
ddd	doublet of doublet of doublet
J	coupling constant in Hz
I	Fluorescence intensity
I_0	Fluorescence intensity (only probe)
υ	Frequency
η	Viscosity
G	Instrumental correction factor

LIST OF FIGURES

Figure	Title	Page No.
1.1	Structure of Nucleotide and Nitrogen Containing Purine and Pyrimidine Bases	3
1.2	Structure of the Watson and Crick H-bonding between A-T and G-C	4
1.3	Structure of DNA minor and major grove	4
1.4	Graphical presentation to show the difference between Watson-Crick and Hoogsteen pairing	5
1.5	Representation of base stacking and H-bonding between bases	5
1.6	Chemical structure of some DNA intercalators	7
1.7	Examples of polypyrroles	8
1.8	Examples of bis(benzimidazoles)	9
1.9	Example of a combilexin	10
1.10	Chemical structure of X-pyrene nucleoside	11
1.11	(a) Pyrene-modified phosphoramidite monomers	12
1.12	Chemical structure of thiophene-modified ribonucleoside triphosphate 1.18	12
1.13	(a) Oligonucleotides used by Aso et.al., and (b) pyrene-labeled 3-deaza-2'-deoxyadenosines $py^{3z}A$ (1.19)	13
1.14	(a) Chemical stucture of purine nucleoside,1.20, ^{cna}A (X) and (b) Oligonucleotides used in SNP detection by Suzuki et.al	14
1.15	Structure of PRODAN-labeled nucleosides ^{PDN}X	15
1.16	Structure of pyrene-labeled nucleosides ^{py}U and ^{py}C	16
1.17	Structure of the 5-labelled thiopheneuridines and oligonucleotides used by Capobianco *et.al*	17
1.18.	Structure of (dU^{phen}) and the oligonucleotide used by Hurley *et.al*	18
1.19	Macrocyclic bisintercalators BisA and 9,10-BisAN	19
1.20	Chemical structures of CF_3-AMND and AMND. Proposed binding modes of these ligands with (A) cytosine and (B) thymine (two possible patterns) are also shown	20
1.21	Chemical structure of ATMND–TO and DMP–BO	21
1.22	Chemical structures of isoquinoline alkaloids (IAs) used by Wang et al	22

1.23	Graphical presentation of G–G Hoogsteen mode of hydrogen bonds, G-quartet stacked to G-quadruplex structure ($M^+ = Na^+, K^+ NH_4^+$).	23
1.24	Classification of G-quadruplex structures	24
1.25	Examples of binding mode of small molecule with G-quadruplex	25
1.26	Molecular structures of 1,3-phenylene-bis(piperazinyl benzimidazole) skeleton unit	26
1.27	Structure of Thioflavin T (ThT)	27
1.28	Structures of thiazole orange and isaindigotone fusion dyes,1.51a-c	27
1.29	Structures of the indolo[3,2-c]quinoline derivatives	28
1.30	Compound lead 1.55a and structural modifications	30
1.31	structure of BPBC composed of benzimidazole and carbazole moieties	31
2.1	Chemical Structure of nucleoside 2.1 and 2.2a-d	38
2.2	Structure of nucleoside triphosphates dA^RTP and dU^RTP and their R groups	39
2.3	Structure of BodU, 2.5 and Bo, 2.6	39
2.4	Structure of AQ-dU nucleoside 2.7	40
2.5	Proposed C/C and T/T flanking ^{Naph}**U** incorporated ODN **1** and ODN **9**	42
2.6	(a) UV-visible, (b) fluorescence emission (λ_{ex} = 310 nm) and (c) fluorescence normalised emission of naphthalene linked 2`-deoxyuridine, (^{Naph}**U, 2.11**) in different solvent	45
2.7	(a) UV-visible, (b) fluorescence emission (λ_{ex} = 310 nm) and (c) fluorescence normalised emission of naphthalene linked 2`-deoxyuridine, (^{Naph}**U, 2.11**) in dioxane-water mixture of solvent	45
2.8	MO diagram with electronic transition of compound ^{Naph}**U** (**2.11**)	48
2.9	Calculated UV-Visible spectrum of nucleoside ^{Naph}**U** (**2.11**)	48
2.10	HPLC traces of synthesized crude and purified oligonucleotide probe containing fluorescent nucleoside, ^{Naph}**U**	52
2.11	(a) UV-visible, (b) expanded UV-visible, (c) emission and (d) excitation spectra of probe oligonucleotide (ODN **1**) containing nucleoside, ^{Naph}**U**, and its various duplexes with natural bases A, G, C, T and ^{Me}C and Abasic DNA (Φ)	53

2.12	(a) UV-visible, (b) emission spectra of probe oligonucleotide (ODN **9**) containing nucleoside, ^{Naph}**U**, and its various duplexes with natural bases A, G, C, T and ^{Me}C and Abasic DNA (Φ)	55
2.13	*Tm* curve of (ODN **1** = 5'-CGCAAC **X** CAACGC-3') containing nucleoside, ^{Naph}**U** (= X), and its various duplexes with natural bases A, G, C, T and ^{Me}C and Abasic DNA (Φ)	56
2.14	(a) Circular Dichroism (CD) and (b) Induced CD spectra of probe oligonucleotide (ODN **1**) containing nucleoside, ^{Naph}U, and its various duplexes with natural bases A, G, C, T and ^{Me}C and Abasic DNA	58
2.15	AMBER* energy minimized conformations in water of the duplex ODN **1•2**	59
2.16	^{1}H NMR spectra of Naphthyl boronic ester (**2.9**)	64
2.17	^{1}H NMR 5-(2-naphthyl)-2'-deoxyuridine (**2.11**)	65
2.18	^{13}C NMR 5-(2-naphthyl)-2'-deoxyuridine (**2.11**)	66
2.19	^{1}H NMR spectra of DMTr protected ^{Naph}**U** nucleoside (**2.12**)	67
3.1	Structure of 2-amino-5,6,7-trimethyl- 1,8-naphthyridine (ATMND)	74
3.2	Structure of bisanthracene macrocycle 3.2	75
3.3	Possible binding mode of amiloride with T in the AP site-containing DNA duplexes	76
3.4	Chemical structures of DCPC and amiloride	76
3.5	Structure of berberine, 3.5 and the sequences used by Wu[7] *et al*. X = AP site (dSpacer, tetrahydrofuran residual) for AP site-containing DNAs. Fully matched DNAs (FM-DNA) with X/Y = G/C and A/T are used as controls	78
3.6	Structures of PyDANP	79
3.7	Chemical structure of DANP, 3.7	7.9
3.8	7-Deazaguanine, 3.8 (7-DeG), deazaguanine-based hydrogen-bonding ligand	80
3.9	Chemical structure of **TzPy**, (**3.9**) and Proposed bind of **TzPy** DNAs	82
3.10	(a) UV-visible (b) inset normalised UV-visible of **TzPy** (c) normalised UV-visible absorbance in dioxane and buffer and (d) fluorescence emission spectra (λ_{ex} = 350 nm) in dioxane with increasing percent of water	83

3.11	(a) UV-visible, (b) emission (c) in set fold increase in fluorescence of the probe (10 μM) in absence and presence of various mismatched/matched DNA duplexes (4 μM, pH 7), (d) UV-visible of **TzPy** with increase concentration of AT/AT flanking C•C mismatch duplex and (e) color change under UV- transilluminator	86
3.12	(a) UV-visible and (b) fluorescence emission spectra of the probe (10 μM) in absence and presence of GC/GC flanking various mismatch/match DNA duplexes (4 μM, pH 7)	88
3.13	(a) UV-visible, (b) fluorescence emission spectra of the probe (10 μM) in absence and presence of increasing concentration of AT/AT flanking C•C mismatch duplex, ODN **1•2**, X•Y = C•C, (4 μM, pH 7)	89
3.14	Melting temperature curve (T_m) of A:T flanking various match and mismatch duplexes, ODN **1•2**, X•Y = (a) A•T, (b) A•A, (c) G•G, (d) C•C and (e) T•T in absence and presence of **TzPy**	90
3.15	Melting temperature curve (T_m) for G:C flanking various match and mismatch duplexes, ODN **1•2**, X•Y = (a) A•T, (b) A•A, (c) G•G, (d) C•C, (e) T•T in absence and presence of **TzPy**	91
3.16	Circular Dichroism (CD) spectra of of AT/AT flanking various match and mismatch duplexes, ODN **1•2**, X•Y = (a) A•T, (b) A•A, (c) G•G, (d) C•C, (e) T•T in absence and presence of **TzPy**	92
3.17	Circular Dichroism (CD) spectra of of GC/GC flanking various match and mismatch duplexes, ODN **1•2** (X•Y = (a) A•T, (b) A•A, (c) G•G, (d) C•C, and (e) T•T) in absence and presence of **TzPy**	93
3.18	Pictorial presentation of the proposed binding of **TzPy** to abasic site opposite to pyrimidines (X = C/T)	94
3.19	(a) UV-visible, (b) emission and (c) in set fold increase in fluorescence of the probe **TzPy** (10 μM) in presence and absence of AP site in opposite to pyrimidine base ODN **2•1** (X = C and T) and full match DNA duplexes (4 μM, pH 7)	95
3.20	Melting temperature curve (T_m) for AT/AT flanking abasic site opposite to pyrimidine duplexes, ODN **2•1**, Y•X = (a) Φ•C, (b) Φ•T and (c) full match duplex in absence and presence of **TzPy**	96

3.21	Circular Dichroism (CD) spectra for AT/AT flanking abasic site opposite to pyrimidine duplexes, ODN **2•1**, Y•X = (a) Φ•C, (b) Φ•T and (c) full match duplex in absence and presence of **TzPy**	96
3.22	Pictorial presentation of the proposed binding of **TzPy** to pyrimidines (X = C/T) bulge	97
3.23	(a) UV-visible, (b) emission and (c) in set fold increase in fluorescence of the probe **TzPy** (10 μM) in presence and absence of pyrimidine bulge ODN **2•5** (T_T/ACA and T_T/ATA) and full match DNA duplexes (4 μM, pH 7)	99
3.24	Thermal melting curve of AT/AT flanking pyrimidine bulge and fully matched duplex, ODN **2•5**, (a) C-bulge, (b) T-bulge and (c) fully match pair in absence and presence of **TzPy**	100
3.25	Circular Dichroism (CD) spectra of AT/AT flanking pyrimidine-bulge and fully matched duplex, ODN **2•5**, (a) C-bulge, (b) T-bulge and (c) fully match pair in absence and presence of **TzPy**	100
4.1	Pictorial presentation of the preferred binding of a chiral metallosupramolecular complex to dimeric G-quadruplex over a monomeric G- quadruplex	106
4.2	Structure of dimeric berberine 4.2	107
4.3	Chemical structures of the two tetraphenylethene (TPE) derivatives used by Zhang[23] *et.al*	108
4.4	The chemical structures of TMPyP4 and TMPipEOPP	109
4.5	The chemical structures of IZNP-1	110
4.6	Proposed bind of **TzPy** to the cleft between the G-qudruplex of Hum45	112
4.7	(a) UV-visible, (b) emission (c) fluorescence fold increase (d) steady state anisotropy of the probe (10 μM) in absence and presence of ss-DNA, ds-DNA, ct-DNA, Cmyc, Oxy3.5, TBA, HIV, Hum21 and Hum45	114
4.8	Color change under UV-transilluminator in presence of **TzPy**	115
4.9	Circular dichroism spectra of Hum45, Hum21, Bom 17, Oxy 3.5, Cmyc, TBA and HIV in presence and absence of **TzPy**	117

4.10	(a) UV-visible and (b) fluorescence emission spectra and (c) steady state anisotropy of **TzPy** (10 μM) in absence and presence of Hum21 (4 μM, pH 7)	118
4.11	(a) UV-visible and (b) fluorescence emission spectra and (c) steady state anisotropy of **TzPy** (10 μM) in absence and presence of Hum45 (4 μM, pH 7)	119
4.12	Benesi-Hildebrand plot for **TzPy** with increasing concentration of Hum45	121
4.13	T_m profile for Hum21 and Hum45 in absence and presence of **TzPy**	122
5.1	Structure of Highly photocarcinogenic and phototoxic fluoroquinolones (FQs), lomefloxacin (LOM) and enoxacin (ENX)	128
5.2	Structure of sodium saccharin SSA	129
5.3	Structure of neodymium–naproxen complex (Nd–NAP)	129
5.4	Structure of daphnetin	130
5.5	Structure of 6 mercaptopurine (6 MP)	130
5.6	Structure of farrerol	131
5.7	Structure of gefitinib	131
5.8	Structure of anthraquinone derivative (AOMan)	132
5.9	Structure of **5.10** and **5.11**	133
5.10	ORTEP molecular diagram with ellipsoid at 50% probability of **5.10**	135
5.11	Crystal structure (a-b) showing inter planar distance and the two planes formed by two pendent acetylenic arms. (c) Crystal network of the molecule **5.10**	135
5.12	(a) UV-visible spectra for 5.10 and (b) UV-visible spectra for **5.11** in different solvents	136
5.13	(a) emission and (b) normalized emission spectra of **5.10** (**$^{4\text{-DMAPE}}$NI**) in different solvents (λ_{ex} = 445 – 465 nm). (c) Colours in different solvents after irradiation of 5.10 in UV light (λ = 254 nm)	137
5.14	(a) normalized absorbance and emission spectra of **5.10** (**$^{4\text{-DMAPE}}$NI**) in solid state (λ_{ex} = 560 nm). (b) Time resolved fluorescence spectra of **5.10** in both solvent and solid state	138
5.15	(a) emission and (b) normalized emission spectra of **5.11** (**$^{4\text{-CPE}}$NI**) in different solvents (λ_{ex} = 370 nm)	139

5.16	Time resolved fluorescence spectra of (a) **5.10** and (b) **5.11** in different solvent of varying polarity	140
5.17	Excited-state energy levels of probe **5.10** based on TD-DFT calculations. The surface plots represent densities of the MOs with the largest contribution to the *CI*-eigenvectors	141
5.18	Excited-state energy levels of probe **5.11** based on TD-DFT calculations. The surface plots represent densities of the MOs with the largest contribution to the *CI*-eigenvectors	141
5.19	Plots of $\tilde{\nu}_{abs}$ & $\tilde{\nu}_{fl}$ values against solvent polarity parameter Δf for fluorophore (a) **5.10** and (b) **5.11** (c) Plots of $\Delta\tilde{\nu}$ values against Δf in different solvents for **5.10** and **5.11** and the corresponding dipole moment and excitation energy values	143
5.20	(a) UV-visible of fluorophore **5.10** and (b) UV-visible spectra of fluorophore **5.11** in presence of increasing concentration of ct-DNA. [Probe] = 30 µM and [ct-DNA] = 7.5, 15, 22.5, 30, 37.5, 45, 60 and 75 µM	145
5.21	(a) Emission spectra of fluorophore **5.11** (λ_{ex} = 370 nm) and (b) Emission spectra of fluorophore **5.10** (λ_{ex} = 460 nm) in presence of increasing concentration of ct-DNA. [Probe] = 30 µM and [ct-DNA] = 0, 7.5, 15, 22.5, 30, 45, 60 and 75µM	146
5.22	Benesi- Hildebrand plot of fluorophore **5.11** in presence of increasing ct-DNA concentration. [fluorophore **5.11**] = 30 µM and [ct-DNA] = 15, 22.5, 30, 45, 60 and 75 µM	147
5.23	T_m study of ct-DNA in presence of fluorophore **5.11**	147
5.24	(a) Emission spectra (λ_{ex} = 520 nm) of EB, EB-ct-DNA complex and EB-ct-DNA complex mixed with **5.10**. (b) Emission spectra (λ_{ex} = 520 nm) of EB, EB-ct-DNA complex and EB-ct-DNA complex mixed with fluorophore **5.11**. [EB] = 6 µM, [ct-DNA] = 25 µM and [Probe **5.10** or **5.11**] = 7.5, 15, 22.5, 30, 37.5, 45, 60 and 75 µM	148
5.25	Amber* energy minimized geometry of **5.11** with DNA, showing the minor groove binding of the probe **5.11**. The DNA sequence was 5'-d(*CP*GP*CP*GP*AP*AP*TP*TP*CP*GP*CP*G)-3', (PDB Id: 1DNH)	149

5.26 ^{1}H NMR of synthesized compound **5.10** 158
5.27 ^{13}C NMR of synthesized compound **5.10** 159
5.28 ^{1}H NMR of synthesized compound **5.11** 160
5.29 ^{13}C NMR of synthesized compound **5.11** 161

LIST OF SCHEMES

Schemes	Title	Page No.
2.1	Synthesis of naphthalene labeled fluorescent nucleoside **2.11**	44
2.2	Synthesis of fluorescently labeled ODNs	51
5.1	Synthesis of donor/ accepter labeled naphthalimide fluorophore **5.10** and **5.11**	134

LIST OF TABLES

Table	Title	Page No.
2.1	Photophysical summary of the ^{Naph}**U** (**2.11**) in different solvents	46
2.2	Photophysical summary of the ^{Naph}**U** (**2.1**) in dioxane-water mixture of solvents	46
2.3	Summary of TD-DFT calculation	49
2.4	Synthesized fluorescently labeled ODNs and their MALDI-TOF MS	51
2.5	Oligonucleotide sequences used for DNA detection study	53
2.6	Summary of photophysical propertiies of probe oligonucleotide (ODN **1**) containing nucleoside, ^{Naph}**U**, and its various duplexes with A, G, C, T and ^{Me}C and AP site (Φ)	54
2.7	Thermal melting temperatures of duplex ODNs	57
3.1	Photophysical summary of Dioxane-water mixture of solvent	84
3.2	DNA sequences used in this study	84
3.3	Photophysical Summary and Thermal melting (T_m) of **TzPy** non-natural nucleoside with AT/AT flanking various mismatch/match DNA duplexes	87

3.4	Photophysical Summary and Thermal melting (T_m) of **TzPy** non-natural nucleoside with GC/GC flanking various mismatch/match DNA duplexes	89
3.5	Photophysical summary of **TzPy** with AT/AT flanking Abasic site DNAs	95
3.6	Photophysical summary of **TzPy** with AT/AT flanking Bulge DNAs	99
4.1	DNA sequences used in this study	113
4.2	Photophysical Summary of **TzPy** non-natural nucleoside with various G-quadruplexes, single and duplexes DNAs	115
4.3	Photophysical summary of **TzPy** with Hum21	118
4.4	Photophysical Summary of **TzPy** with Hum45	119
4.5	T_m values and Binding constant (K_a) values of H21 and H45 with **TzPy**	121
5.1	Photophysical Summary of **5.10** ($^{4\text{-DMAPE}}$**NI**)	138
5.2	Photophysical Summary of Fluorophore **5.11** ($^{4\text{-CPE}}$**NI**)	139
5.3	Summary table of and of the fluorophores and fluorescent nucleoside and solvent polarity parameter (Δf)	143
5.4	Summary table of $\Delta\tilde{\nu}$ of the fluorophores and solvent polarity parameter (Δf)	143
5.5	Summary of Physical parameters of **5.10** and **5.11**	144
5.6	UV-visible, Fluorescence and T_m values of ct-DNA in presence of Fluorophore **5.11** ($^{4\text{-CPE}}$**NI**)	146
5.7	Summary of TD-DFT Calculations	155

Chapter 1

Interaction of Small Fluorescent Molecules/Nucleosides with DNA: A Review

1.1. Introduction

Fluorescence spectroscopy one of the most informative and sensitive analytical techniques, widely used in diverse areas like biochemistry, biophysics, material sciences, pharmacology, biotechnology, genetic analysis, photochemical, nanotechnology and biochemical processes.[1] The parameters obtained from the fluorescence techniques provides information of the surrounding microenvironments of the medium and give very important information about the local structure, physical properties and dynamics of such systems. Fluorescence technique are very simple, sensitive, highly specific and cost effective. Fluorescence also harmless to the sample under investigation. Living cells can be studied with no adverse effects.

The investigation on the binding interaction of DNA-small molecules is helpful to understand the mechanism of interaction and to improve newer drug design. Currently, the study of the interaction between small molecules and DNA has become a hot topic in the area of chemistry, biochemistry and medicine.[2] Small molecules bind to DNA mainly through covalent or non-covalent interaction. Both the covalent and non-covalent interaction of small molecule to DNA provide the basic idea about nucleic acid structure, dynamics and recognition events.[3] Fluorescent small molecule/nucleoside analogs that are sensitive to their local environment, demonstrating changes in the fluorescent properties when induced by changes in polarity, pH, or even structure, have become powerful tools for the investigation of nucleic acid structure, dynamics, and recognition.[3-6] When a fluorescent probe makes complexes with bio-macromolecules such as DNA and protein or comes into interaction, the fluorophore's emission property may be modulated such as fluorescence can be enhanced/quenched and/or emission wavelength can be shifted to red/blue region thereby enabling visual observations of the bio-macromolecular species. Considerable attention has been focused on new DNA-binding and modifying agents from natural products to wholly synthetic design as probes of DNA structure and as potential chemotherapeutic agents. Several fluorescent bio-probes have been reported based on the fluorophore's properties like intercalation, stacking, and/or groove binding for DNA detection with a generation of a distinct fluorescence signal.[4-6] The natural products like Hoechst 33258,[4a] netropsin,[4b] distamycin,[4c] etc., have received special attention for their specific binding in minor groove due to their modular nature, reduced size, and diminished conformational freedom.[4] Groove binding/intercalative interaction, the most commonly studied, is the noncovalent stacking interaction resulting from the insertion of a planar heterocyclic aromatic ring between the base pairs of the DNA double helix. However,

many of the explored fluorophores are found to suffer from self- quenching, short emission wavelength, or not suitable for use in buffers solutions; thus makes them inefficient biosensors. Therefore, there is a need to design probes which is low or zero emitting in buffer but upon interaction with the biomolecules, it fluoresces significantly. Thus, the development of new fluorescent probes for sensing bio-macromolecules is a highly demanding and desirable goal to the chemists, biochemists and biologists.

On the other hand, because of their significant biological and clinical importance, recently, there has been a growing interest in single nucleotide polymorphisms (SNPs) typing.[5] A great deal of efforts has been paid by various research groups all over the world for the development of SNP genotyping technologies, chemistry, fluorescently labeled oligonucleotide probes.

1.2. Structural Features of DNA

Nearly half a century ago (1953) James Watson and Francis Crick first proposed the structure of the classical deoxyribonucleic acid (DNA) double helix.[7] DNAs are the most important class of bio-macromolecule which storage the genetic information get transferred from parents to offspring.[7-9] DNA consists of two biopolymer strands coiled around each other to form a double helix. The two DNA strands are known as polynucleotides because they are composed of simpler units called nucleotides. DNA has polynucleotide chains with each nucleotide being composed of 2-deoxyribose sugar, a phosphate group and a nitrogenous base [7,9,10]. The nitrogenous bases shown in **Figure 1.1** are purines (adenine, **A** and guanine, **G**) and pyrimidines (thymine, **T** and cytosine, **C**). The deoxyribose sugar and the phosphate group provide a backbone for the nitrogenous bases that are directly attached to the deoxyribose unit [7,9]. Each nitrogen base has a different structure and is capable of forming specific hydrogen bonds due to the presence of electron-accepting and donating sites. DNA consists of two chains twisted around each other (double helix), they look like a spiral staircase or twisted ladder type of form and the sides of the ladder are made up of deoxyribose/ribose (a sugar) and phosphates. The twisted ladder type form is due to the Watson and Crick base pairing that can bind to a complementary strand through hydrogen bonding. According to Watson and Crick base pairing (**Figure 1.2**), A binds to T and G binds to C, and therefore the amount of A is always equal to T and G equal to C in a specific sample of DNA.[11] It is worth noting that the G–C base pair is stronger than the A–T base pair due to the number of hydrogen bonds. The binding effect is cooperative, and leads to a stable double-stranded structure that is right-handed helical under

normal base-pairing conditions (sometimes known as Watson and Crick base pairing), the helix is known as the B-form, and contains major and minor grooves (**Figure 1.3**). The spatial arrangement of base pairs leads to the formation of major and minor grooves [12,13]. The region where the two strands are close to each other (deep–narrow) is called minor grove while the region where they are away from each other (shallow–wide) is called major groove (**Figure 1.3**). At a molecular level, the environment of each type of groove is different [14]. The major groove has multiple sites of interaction, thus offering comparatively strong binding to drugs/ligands [13,15]. It has a width of 11.6 Å and depth of 8.5 Å.[16] The major groove provides easy access for bulky molecules. [17] On the other hand, the minor groove has less binding sites and is smaller in size, with a depth of 8.2 Å and width 6.0 Å. However, minor groove has the benefit that it is usually untenanted and thus available for attack to small drug molecules. As most of the antibiotic and anticancer drugs have been reported to have small molecules so minor groove is their main binding site. [16,18]

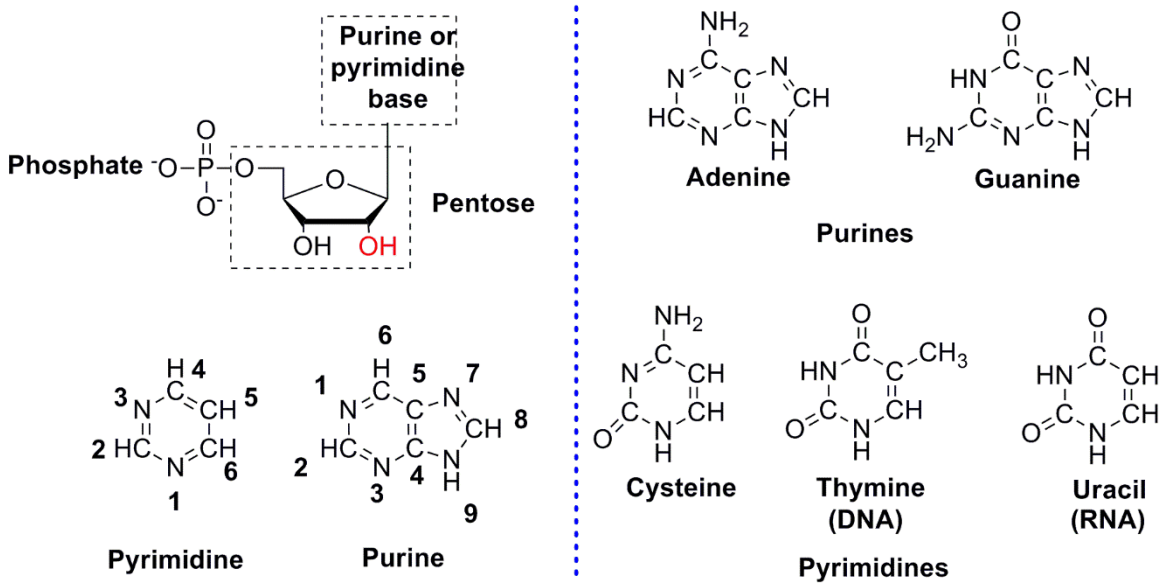

Figure 1.1. Structure of nucleotide and nitrogen containing purine and pyrimidine bases.

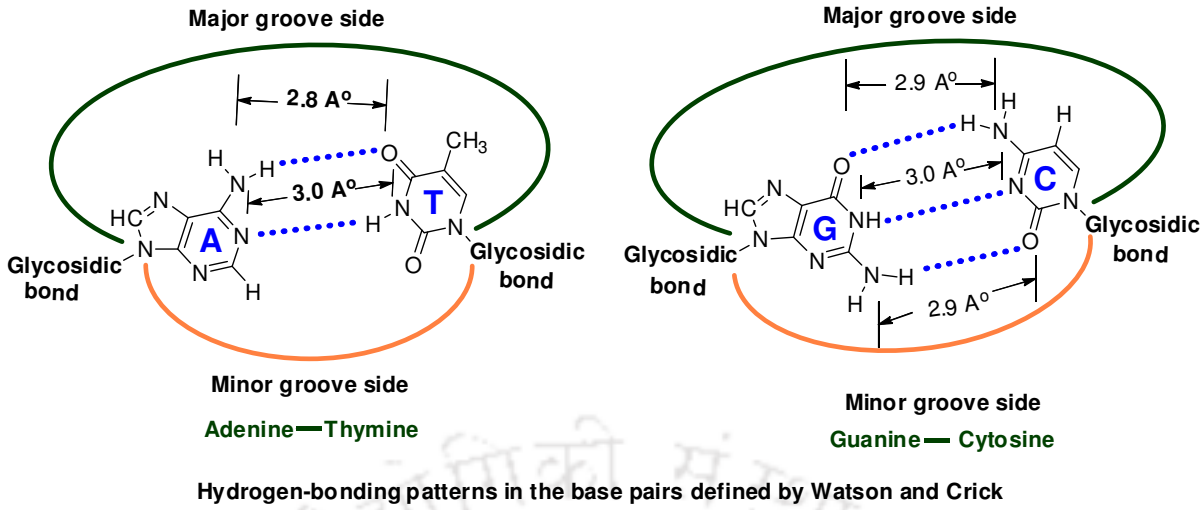

Figure 1.2. Structure of the Watson and Crick H-bonding between A—T and G—C.

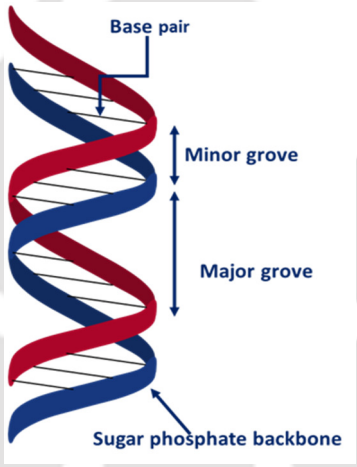

Figure 1.3. Structure of DNA minor and major grove.

On the other hand, beyond Watson and Crick base pairing in duplex DNA, there exist another type of base pairing/H-bonding known as Hoogsteen base pairing. Watson-Crick base pairing occurred only when both the bases are in anti-conformation. On the contrary, in Hoogsteen base pairing the bases are in opposite conformation, one is *syn* and another is *anti* (**Figure 1.4**).[7b] The nucleotide base adenine (A) is "flipped" in Hoogsteen pairing as compared to Watson-Crick pairing (**Figure 1.4**). It has been thought for quite some time that Hoogsteen pairing only occurs in DNA when it is either damaged or bound to some other molecule (like a protein or a drug). A recent study, however, shows that this is not the case. In fact, Hoogsteen pairing seems to be a part of DNA's design. In guanine rich oligo nucleotide sequence, Hoogsteen base pairing observed between guanine and guanine and they formed the stable G-quatret or quadruplex, known as G-quadruplex, which is stabilized by Hoogsteen hydrogen

bonding.[19] Thus, far from being an indication of damage or external binding, it seems to be a means by which DNA increases it complexity so as to store more information.

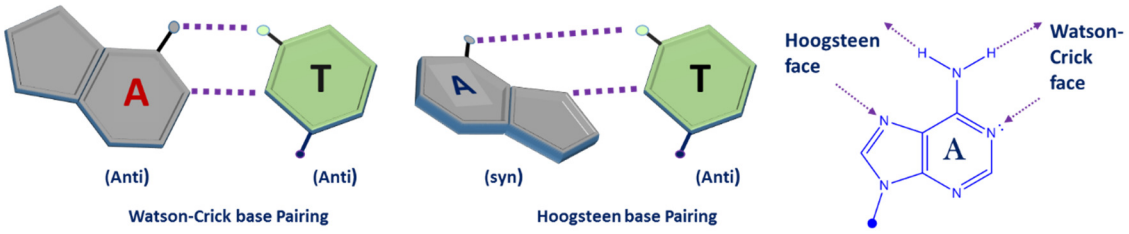

Figure 1.4. Graphical presentation to show the difference between Watson-Crick and Hoogsteen pairing.

Inter-strand hydrogen bonding is obviously important driving force to the formation of DNA duplexes, but it is by no means the only contributing factor. The individual bases in duplexes form strong stacking interactions which are major contributors to duplex stability as base stacking is much more prevalent in duplexes than in single strands (**Figure 1.5**). Base-stacking interactions are hydrophobic and electrostatic in nature and depend on the aromaticity of the bases and their dipole moments.[20] So, base-stacking interaction markedly plays a role in stabilising DNA duplexes.

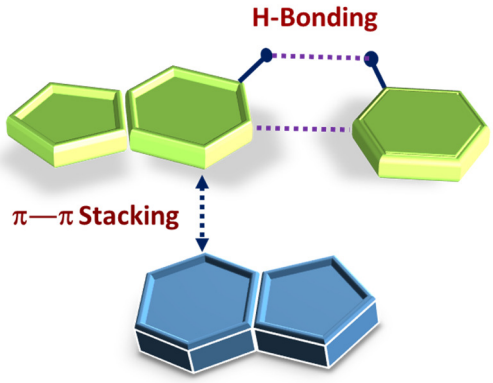

Figure 1.5. Representation of base stacking and H-bonding between bases.

1.3. Non-covalent Interactions of Small Molecules with Duplex-DNA

Currently, the study of the interaction between small molecules and DNA has attracted research in both academic and pharmaceutical industries.[21] In some cases the ligand/DNA interaction results in DNA structural distortion or damage that impedes replication or transcription, for example, by blocking the movement of helicases, topoisomerases and polymerases. However, small molecules bound upon DNA may alter or inhibit DNA

function[22,23]. Therefore, the investigation on the binding interaction of DNA with small molecules is helpful to understand the mechanism of interaction and to improve new drug design. The non-covalent interaction mode of small molecules with DNA can be broadly categorized into three modes: (i) nonspecific electrostatic binding, (ii) intercalation and (iii) groove binding. Ligands may bind to nucleic acids utilizing more than one mode.

Nonspecific electrostatic binding refers to the indiscriminate interactions between positively charged ions (e.g. Na^+, K^+ or Mg^{2+}) or polyamines (e.g. spermine, spermidine) that cluster around the negatively charged sugar–phosphate backbone. Although this binding mode governs the behavior of electrolytes and water in the nucleic acid's vicinity, it has little effect on ligands that occupy much larger surface area.

1.3.1. Duplex-DNA Intercalators

Intercalation describes the insertion of polyaromatic, planar molecules between consecutive base pairs. [24,25] Some planar heterocyclic molecules act as intercalators which stack between adjacent DNA base pairs resulting in significant π-electron overlap without forming covalent bonds and breaking up the hydrogen bonding interactions between the DNA base pairs. Therefore, DNA-intercalator complex is stabilized by π–π stacking interaction. Molecules that bind to double-stranded DNA (ds-DNA) by intercalative mode have been significantly used as drugs (**Figure 1.6**). Intercalation is generally independent of base-pair sequence. Intercalators generally cause more significant distortion of the native conformations of DNA, a factor that contributes to the disruption of protein binding.

Ethidium bromide and the antimalarial quinacrine (**Figure 1.6**) are well known intercalators.[26] An important contributor to the binding affinity of ethidium bromide and quinacrine to DNA is the stacking interaction of the respective heteroaromatic rings with the DNA base pairs. In case of quinacrine, the cationic sidechain contributes to complex stability by electrostatic interactions with the negative phosphate units of the groove.

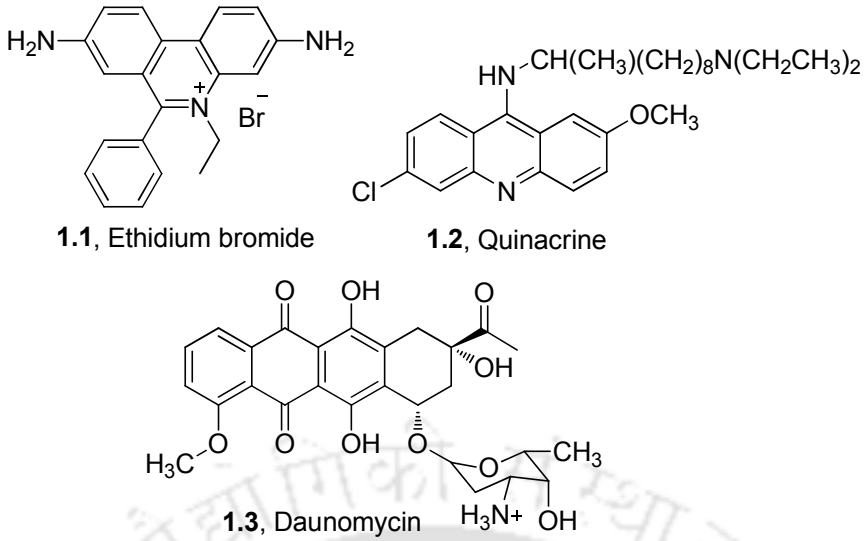

1.1, Ethidium bromide **1.2**, Quinacrine

1.3, Daunomycin

Figure 1.6. Chemical structure of some DNA intercalators.

1.3.2. Duplex-DNA Groove-Binding Molecules

Groove binding is typically governed by electrostatics and van der Waals forces. Some molecules with several aromatic rings can bind to the minor groove of DNA via van der Waals interaction and hydrogen bonding interaction.[5,6] Groove binders are typically positively charged crescent shaped linked aromatic rings. Minor groove binding molecules are generally isohelical to the curve of the minor groove of DNA and facilitate binding through van der Waals interactions and these molecules can form hydrogen bonding interaction with base pairs.[5,6]

Polypyrrole antibiotics distamycin A and netropsin are well known minor groove binder (**Figure 1.7**).[27] These compounds are characterized by repeating pyrrole units connected by amide bonds and ending with one or more positively charged nitrogen atoms. They are capable of interacting with the minor groove of B form DNA based on their curved shape, which matches well with the topology of double-stranded DNA. Distamycin has also been shown by NMR to bind to G-quadruplex DNA but this is by intercalating between the terminal G-planes and the bases that flank the G-quartet structure.[28] More recent analogues of distamycin A have had greater success as potential anti-cancer drugs because of an improved cytoxicity/myelotoxicity ratio such as brostacillin (PNU-166196) (**Figure 1.7**).[29]

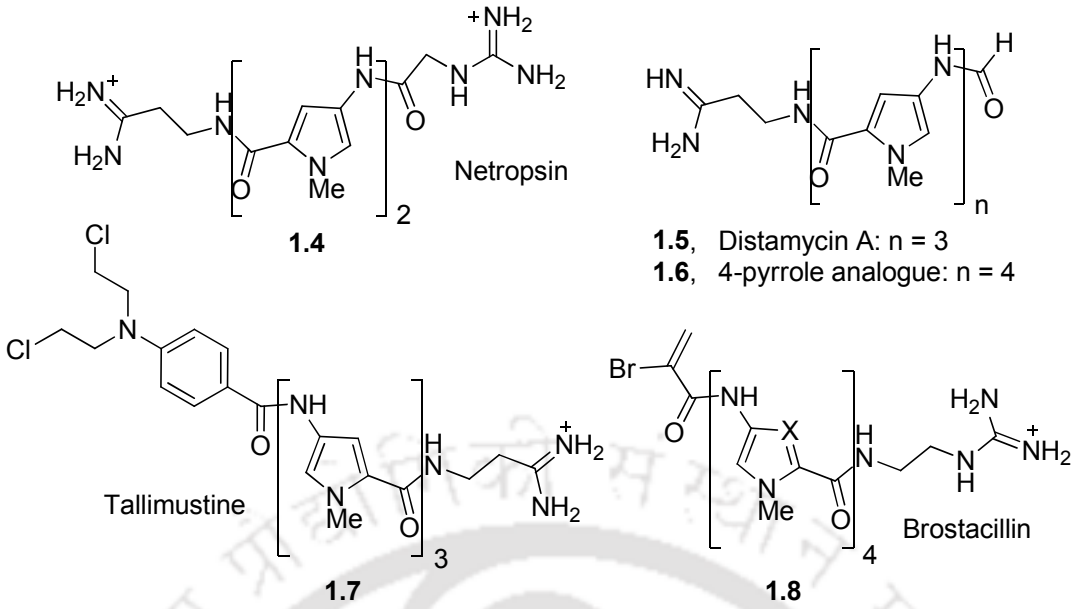

Figure 1.7. Examples of polypyrroles.

The bis(benzimidazole) compounds, Hoechst 33342 and 33258 (**Figure 1.8**) also bind in the minor groove of DNA and show AT sequence selectivity[30]. These compounds are additionally useful because they are fluorescent dyes and have been widely used as such. Hoechst 33258 (pibenzimol) has undergone Phase I clinical evaluation as an anti-cancer agent[31]; the mechanism of cytotoxicity has been suggested as inhibition of topoisomerase[32] and DNA helicase.[33] Recent studies have been undertaken to determine the exact nature of the interaction between Hoechst 33258 and DNA using a variety of methods in the hope of better understanding the number of factors that contribute to the affinity and sequence specific binding of small molecules with DNA.[34] Two other Hoechst derivatives DMA, a bisbenzimidazole, and TBZ, a tribenzimidazole (**Figure 1.8**) have been synthesised and their increased sequence and structure selective binding via enhanced fluorescence emission has been demonstrated.[35] Hoechst 33258 has been shown to bind to G-quadruplex DNA in the promoter region of the c-MYC gene in vitro, but it is not clear how the ligand interacts with the DNA structure.[36]

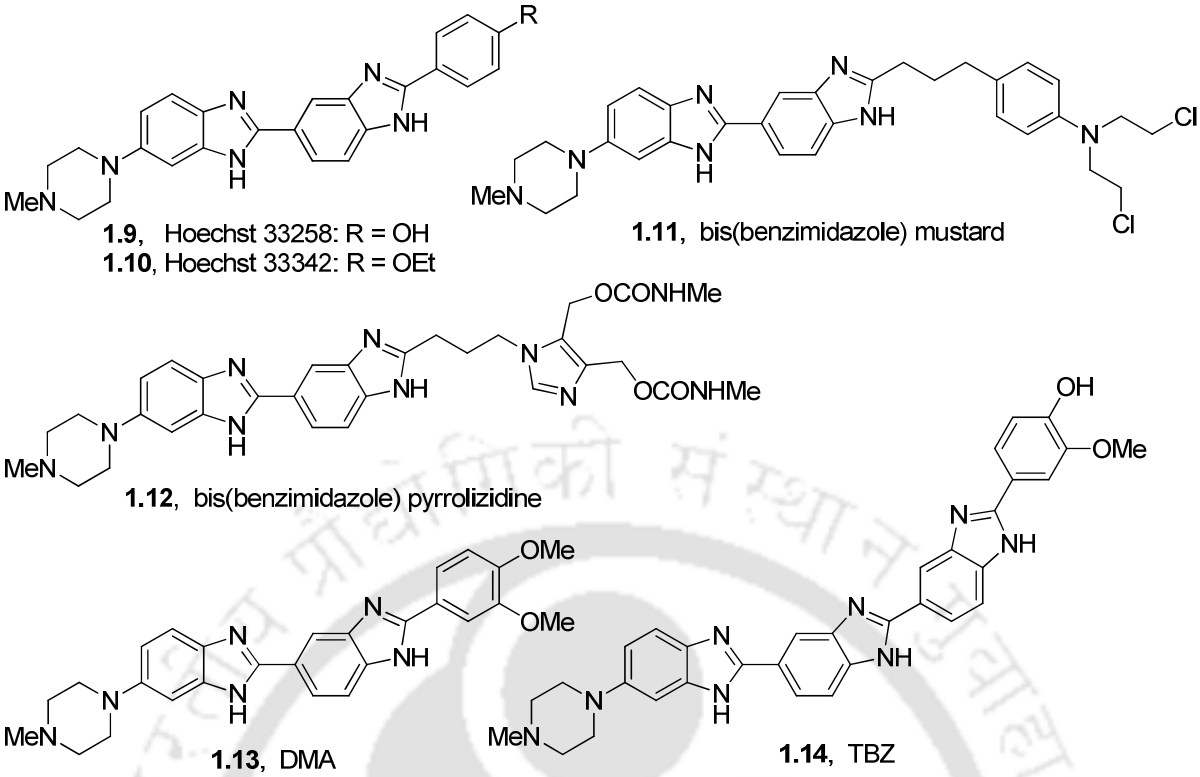

Figure 1.8. Examples of bis(benzimidazoles).

1.3.3. Intercalator–minor-groove Binding Hybrid Molecules

The hybrid molecules containing both intercalating and minor-groove binding functionalities can interact more strongly with DNA than those having either of the individual functionality.[37,38] These hybrid molecules, because of their dual binding mode of action, are called combilexins.

The well-known and potent antitumour drug, NetAmsa (**Figure 1.9**), is a good example of the combilexins. This is derived from a covalent combination of a minor-groove binder, netropsin and an intercalator, amsacrine. This molecule shows three modes of binding with duplex DNA: (i) sequence-specific recognition of the minor groove of the DNA double-helix via the netropsin moiety; (ii) intercalation of the acridine chromophore inside the duplex DNA, and (iii) threading of the methane sulfonanilino group into the major groove.[37]

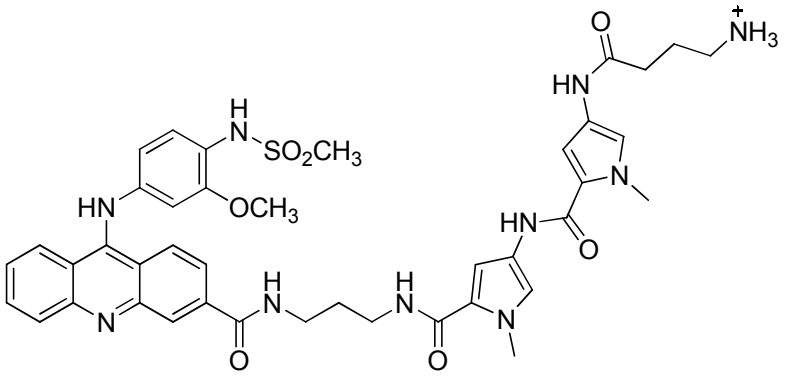

1.15, NetAmsa

Figure 1.9. Example of a combilexin.

1.4. Fluorescent Nucleoside Analogs for SNP Detection in DNA

The detection of single nucleotide polymorphism or single base mutation either *in vivo* or *in vitro* within a gene has attracted attention due to their relevance to certain diseases including cancer, HIV *etc*., and ultimately for the development of personalized drug/medicine.[39,40-44] Emissive oligonucleotides play very important role to identify SNPs by hybridized to their target DNA. The fluorescent nucleoside probes are typically placed across from the base of interest yielding markedly different signals depending upon their pairing partner. Saito and co-workers have named such fluorescent nucleosides as base discriminating fluorescent (BDF) nucleosides.[45] A large number of research works in this regard have been reported in literature. Few of them are discussed below.

Lou[46] *et. al*., synthesised a new cytosine analogue X-pyrene (**Figure 1.10**), incorporation of which into short oligo nucleotide sequences stabilize duplexes via enhanced π-stacking, H-bonding and electrostatic interactions to greatly increase the stability of bulged DNA duplexes and DNA/RNA hybrids. X-pyrene is highly selective for guanine as a partner and duplex stability was reduced dramatically when X-pyrene or a neighboring base was mismatched. From fluorescence point of view, a decreased emission of light from a fluorescent oligonucleotide upon binding to its complementary DNA strand was an indication of strong stacking, for example through intercalation into the double helix,[47-49] which leads to quenching by surrounding base pairs.[47,50] A large decrease in fluorescence (~ 95%) was observed for bulged A, C and T, but not for bulged G, where the reduction was only about 25%. The different behavior of bulged guanine is probably caused by the presence of a G-rich core that leads to stable G-quadruplex formation.[51,52] To confirm the quadruplex hypothesis, complementary oligonucleotides with deoxyinosine replacing one of the four consecutive deoxyguanosines of

the G-rich core were used to prevent G-quadruplex formation. This led to normal duplex formation and strong fluorescence quenching using less than 1.5 equivalents of the complementary strand. Almost 90% quenching was observed with the deoxyinosine in the middle of the G4 repeat.

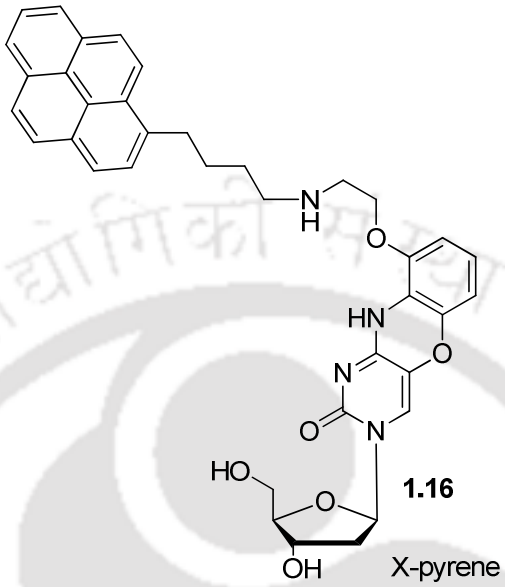

Figure 1.10. Chemical structure of X-pyrene nucleoside.

Li[53] *et. al*., synthesized a series of novel nucleotide phosphoramidites (**Figure 1.11**) and incorporated site-specifically in DNA oligonucleotide probes with pyrene-modified phosphate. These oligodeoxynucleotide (ODN) probes almost had no inherent fluorescence emission with pyrene modification at 3′ phosphate of corresponding nucleotides as a result of the photoinduced electron-transfer quenching effect of nucleobases (thymidine ~ cytidine > guanosine ≫ adenosine). Almost no fluorescence emission was observed for the single-stranded S0 with a quantum yield less than 0.015. However, when S0 was hybridized to its complementary strand S2, a dramatic increase in fluorescence emission was observed with two clearly sharp peaks at 378 and 398 nm and the quantum yield was measured to be 0.313. However, strong fluorescence emission was observed only with the perfectly matched duplex for the probes with pyrene modified at 3′ phosphate of thymidine and cytidine. These rationally designed ODN probes successfully worked as “turn on” fluorescence oligonucleotide sensors for single-nucleotide polymorphism (SNP) and were also successfully used for sensing SNP in PCR applications and the BRAF single-mutation site of human melanoma.

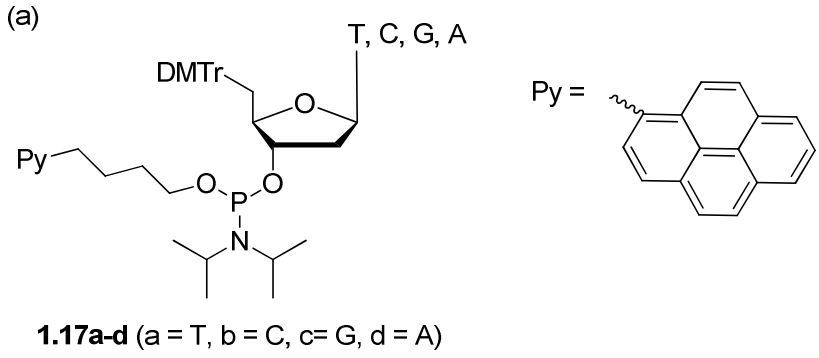

(b)

S0	5`- TCAACATCAG**T$_{py}$**CTGATAAGCT - 3`
S1	5`- TCAACATCAGTCTGATAAGCT - 3`
S2	3` - AGTTGTAGTCAGACTATTCGA - 5`
Mm1	3` - AGTTGTAGTCA**N$_1$**ACTATTCGA - 5`
Mm2	3` - AGTTGTAGTCA**N$_2$**ACTATTCGA - 5`

N1 = A, T, C **N2 = C, G, T**

Figure 1.11. (a) Pyrene-modified phosphoramidite monomers and (b) oligonucleotide sequences used in their work, with bold type representing pyrene modification at 3′ phosphate of thymidine and N1 and N2 being mismatched nucleobases.

Srivatsan[54] *et.al.*, synthesized a highly emissive base discriminating fluorescent nucleobase thieno[3,4-d] pyrimidine analogue (**Figure 1.12**) and incorporated into RNA enzymatically. The ribonucleoside triphosphate **1.18** can be enzymatically incorporated into RNA oligonucleotides using T7 RNA polymerase and the resulting fluorescent constructs can be employed as hybridization probes, positively porting the presence of a C mismatch by enhanced emission photophysically distinguish between perfect and mismatched base pairing upon hybridization to DNA oligonucleotides.

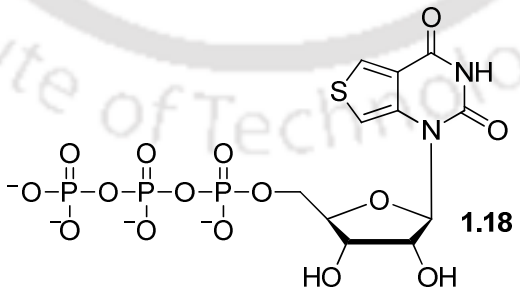

Figure 1.12. Chemical structure of thiophene-modified ribonucleoside triphosphate **1.18**.

Aso[55] *et.al.*, explored the synthesis of a Pyrene-labeled 3-deaza-2'-deoxyadenosine comprising a non-π-conjugated linker py^{3z}A (**1.19, Figure 1.13**) and incorporated into oligideoxynucleotide. Oligodeoxynucleotide (ODN) probes containing py^{3z}A (**1.19**) exhibited

remarkable fluorescence quenching only when the opposite base of the complementary strand was the perfectly matched thymine. This was observed because of their close proximity at the sterically restricted DNA minor groove, whereas py^{3z}A (**1.19**) was highly emissive in mismatched duplexes because of spatial separation of pyrene and 3-deazaadenine (**Figure 1.13**). Further evidence was suggested by thermal denaturation and circular dichroism study. The melting temperatures of perfectly matched duplexes **ODN1(py^{3z}A)/cODN1(T)** and **ODN2(py^{3z}A)/cODN2(T)** were considerably higher than those observed for mismatched duplexes **ODN1(py^{3z}A)/cODN1(N)** and **ODN2(py^{3z}A)/cODN2(N)** (N = C, G, or A), respectively, suggesting that py^{3z}A (**1.19**) formed stable Watson–Crick base pairs, identified thymine upon incorporation into ODN probes, and hybridized with target ODNs.

(a) Oligonucleotides synthesised and used by Aso *et.al.*

ODNs	Sequences	
ODN1(X)	5` d(CGCAACXCAACGC)-3`	X = py^{3z}A or A
ODN2(X)	5` d(CGCAATXTAACGC)-3`	X = py^{3z}A or A
cODN1(N)	5` d(GCGTTGNGTTGCG)-3`	N = A, G, C, or T
cODN2(N)	5` d(GCGTTANATTGCG)-3`	N = A, G, C, or T
Probe(AGT)	5` d(GGCTCCCpy$^{3z}$ATCAGGGA)-3`	
AGT(N)	5` d(TCCCTGANGGGAGCC)-3`	N = C or T

(b)

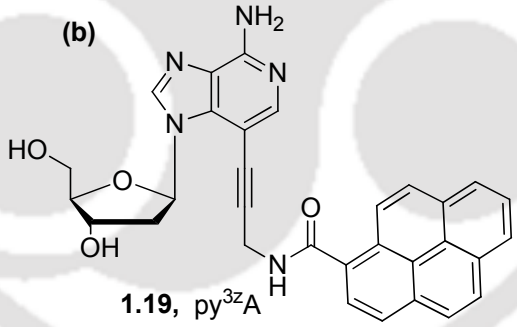

1.19, py^{3z}A

(3-deazaadenine base)

Figure 1.13. (a) Oligonucleotides used by Aso *et.al*., and (b) pyrene-labeled 3-deaza-2'-deoxyadenosines py^{3z}A **(1.19)**.

Suzuki[56] *et.al*., investigated a novel environmentally sensitive fluorescent (ESF) purine nucleoside, ^{cna}A **(1.20, Figure 1.14)**. The base-modified fluorescent nucleoside ^{cna}A exhibited remarkable solvatochromicity and environmentally sensitive dual fluorescence. ^{cna}A labeled DNA probes was found to sense the corresponding thymine (T) in a target DNA/RNA sequence (**Figure 1.14**) by a distinct change in emission wavelength. Also melting temperature of DNA **1 (^{cna}A)/DNA 2 (T)** was considerably higher than that observed in other mismatched duplexes in a sodium phosphate buffer (pH 7.0), suggesting that ^{cna}A (**1.20**) could form a stable base pair

only with thymine (T). In contrast, when the 6-ethynyl-2-naphthonitrile moiety is inside the groove because of the lack of base pairing (with abasic sites or mismatched cases), the configuration of the modified base of ^{cna}A becomes coplanar at the hydrophobic site between flanking base pairs. Thus, a significant electronic interaction between 8-aza-7-deazaadenine and 6-ethynyl-2-naphthonitrile moieties occurred which resulted in a broad unstructured ICT emission at a longer wavelength. The absorption spectrum of ^{cna}A in perfectly matched duplex is considerably blue-shifted and different from that in mismatched duplexes, suggesting that the ground state structure of ^{cna}A in matched duplexes is also quite different from that in mismatched duplexes. The ^{cna}A (**1.20**) exhibited remarkable solvatochromicity and environmentally sensitive dual fluorescence, which originate from the coplanar and non-coplanar conformers of the nucleobase and naphthalene moieties.

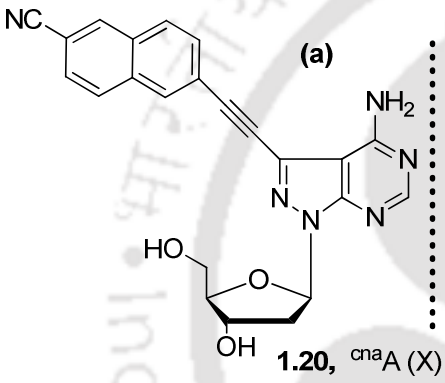

1.20, ^{cna}A (X)

(a) **(b)**

Oligonucleotides synthesised and used by Suzuki *et.al.*

	Sequences	
DNA I(**X**)	5` d(CGCAAT **X** TAACGC)-3`	**X = ^{cna}A or A**
DNA 2(**N**)	5` d(GCGTTA **N** ATTGCG)-3`	**N = T, G, C, A, Ab**
RNA 1(**N**)	5` r(GCGUUA **N** AUUGCG)-3`	**N = U, G, C, A**

*Ab = abasic site.

Figure 1.14. (a) Chemical stucture of purine nucleoside,**1.20**, ^{cna}A (X) and (b) Oligonucleotides used in SNP detection by Suzuki *et.al*.

Tainaka[57] *et.al*., reported the new type of solvatochromic fluorophore 6-propionyl-2-dimethylaminonaphthalene (PRODAN) labeled nucleoside (^{PDN}X, X = U, C, A, and G) and the photochemical properties of oligodeoxyribonucleotides (ODNs) containing them (**Figure 1.15**). The ^{PDN}X containing DNA exhibited unique photochemical behavior in sensitive response to the nature of the complementary base of ^{PDN}X. Based on the chemistry of PRODAN, four novel fluorescent nucleosides, ^{PDN}X (X = U, C, A, and G), to which a PRODAN fluorophore was attached at pyrimidine C5 or purine C8 were synthesised. The ^{PDN}X labeled DNA changed the Stokes shift values depending on the DNA structure. From the photochemistry point of view, fully matched duplex containing ^{PDN}X exhibited an excitation spectrum at a longer wavelength and a smaller Stokes shift value, compared with those of ^{PDN}X in a single-stranded state and mismatched duplexes. The bathochromic shift of the excitation spectrum of ^{PDN}X and lower energy excitation resulted in fluorescence emissions selective to

the Watson-Crick pairing base. The base-selective emission of ^{PDN}U facilitated multicolored SNP typing through the combination with BDF probes with a shorter emission wavelength.

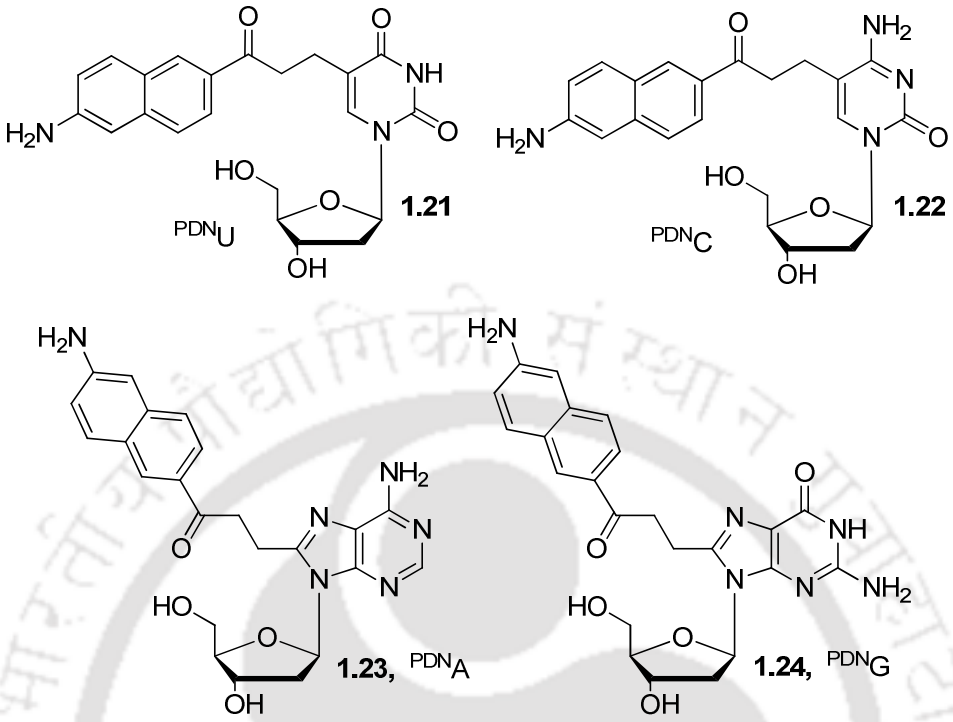

Figure 1.15. Structure of PRODAN-labeled nucleosides ^{PDN}X.

Okamoto[58] *et.al*., explored two novel pyrene labeled base-discriminating fluorescent (BDF) nucleosides ^{Py}U and ^{Py}C (**Figure 1.16**) toward single nucleotide polymorphism (SNP) typing. The fluorescence spectrum of the duplex containing a $^{Py}U/A$ base pair showed a strong emission at 397 nm upon excitation at 327 nm. In contrast, the fluorescence of duplexes containing $^{Py}U/N$ base pairs (N = C, G, or T) was considerably weaker. The proposed structure of the duplex containing a matched $^{Py}U/A$ base pair suggested that the high polarity near the pyrenecarboxamide group was responsible for the strong A-selective fluorescence emission. Moreover, the fluorescence of the duplex containing a $^{Py}U/A$ base pair was not quenched by a flanking C/G base pair. The duplex containing the C derivative, ^{Py}C, selectively emitted fluorescence when the base opposite ^{Py}C was G. In contrast, when the pyrene fluorophore was intercalated into a DNA duplex due to the lack of base-pairing (mismatched), the BDF base would exhibited no emission due to the location of the fluorophore at a highly hydrophobic site in the groove. The melting temperature of ODN1(^{Py}U)/ODN1` (A) was 7 to 9 °C higher than that observed for other mismatched duplexes. The high stability of duplex ODN1($^{Py}U$)/ODN1`(A) suggested that ^{Py}U forms a stable base pair only with A. Sequence of

ODN1 (^{Py}**U**) = 5′-d(CGCAAT^{Py}**U**TAACGC)-3′ and ODN1` (A) = 5′-d(GCGTTA**N**ATTGCG)-3′ (N = A, C, G or T).

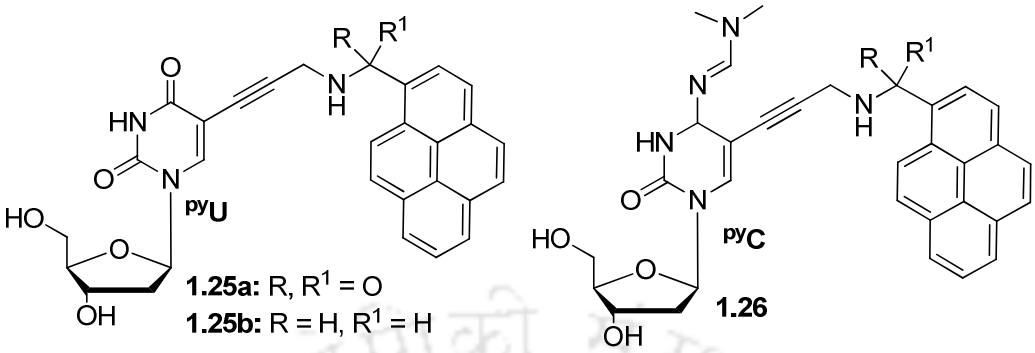

Figure 1.16. Structure of pyrene-labeled nucleosides ^{py}U and ^{py}C.

Capobianco[59] *et.al*., explored four deoxyuridine derivatives (**Figure 1.17**) in which bi- or terthiophene moieties have been conjugated to the 5-position of a 2′-deoxyuridine with or without an ethynyl spacer. By using phosporamidite chemistry they inserted each of these labeled compounds at the center of an oligonucleotide. The oligonucleotide probes were designed to hybridize with model oligonucleotides corresponding to a region known to contain an SNP (A to G transition), that occurs in some patients that present a mutated form of haemoglobin. The labeled oligonucleotides were used as probes to discriminate perfectly complementary strand and that with a single nucleotide mismatch facing the modified uridines via change in fluorescence emission. Upon hybridization, remarkable differences (up to 47%) of the emitted light were observed depending on the uridine facing base,

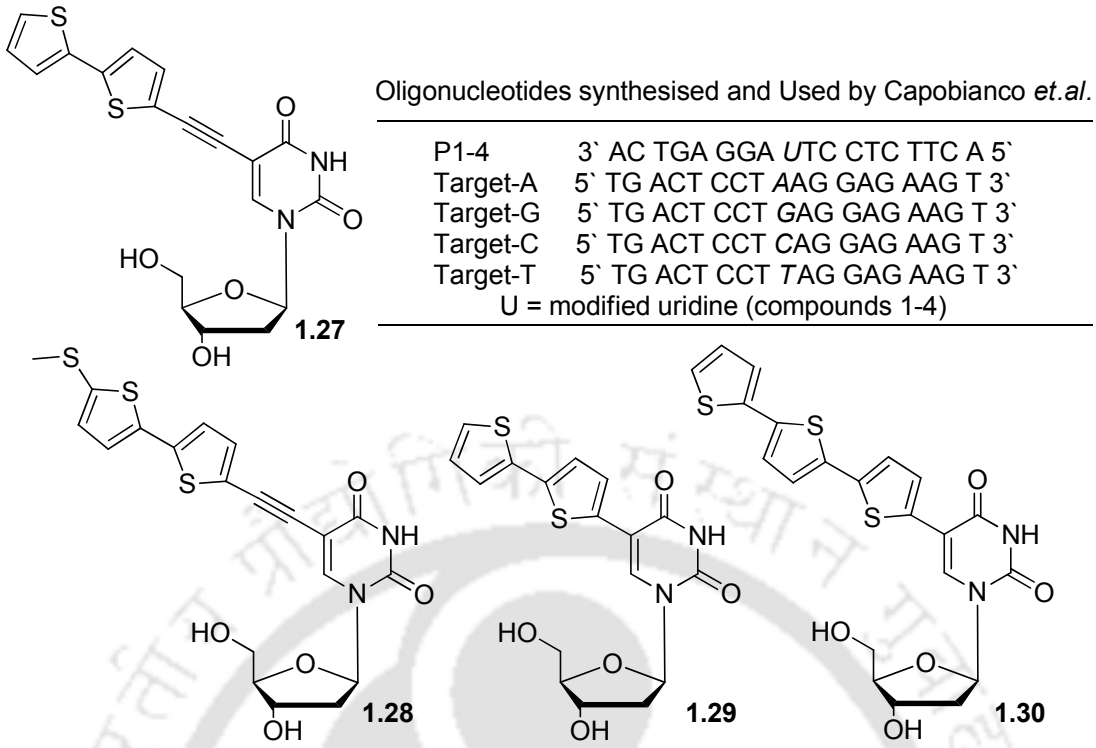

Figure 1.17. Structure of the 5-labelled thiopheneuridines and oligonucleotides used by Capobianco *et.al*.

Hurley[60] *et.al*., explored 1,10-Phenanthroline labeled uridine nucleoside incorporated to oligonucleotides to distinguish between perfectly matched and mismatched base pairing in target complementary oligonucleotides. The building block for synthesized fluorescent oligonucleotides was a modified 2`-deoxyuridine **1.31** (dU^{phen}) (**Figure 1.18**), where the 5-position on the heterocyclic base was conjugated to a 1,10-phenanthroline at the 3 position via an ethynyl linker. Extending the conjugation of 1,10-phenanthroline via ethynyl linkages provided a unique family of intense microenvironment sensitive nucleoside probe. Its fluorescence emission as a free nucleoside and within a single-stranded oligonucleotide was different from that observed when incorporated into a DNA duplex. Additionally, the emission-monitored denaturation curves of internally modified dU^{phen} duplexes were characteristic of the nucleotide opposite the fluorescent base and allowed one to distinguished between the perfectly matched and various mismatched complementary oligonucleotides. The emission of the fluorescent oligonucleotides changed upon hybridization, and was sensitive to the formation of a Watson-Crick vs mismatched base pairing.

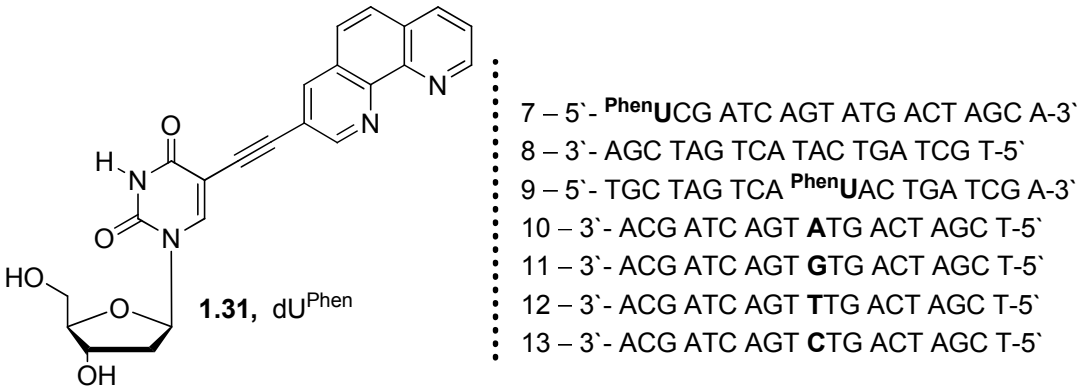

Figure 1.18. Structure of (dU^{phen}) and the oligonucleotide used by Hurley *et.al*.

1.5. Label Free DNA Detection

Detection of single nucleotide polymorphism (SNP) or single base mutation by covalently modified oligonucleotides are costly, tedious and time consuming. However, in this method the covalently modified oligonucleotides have to be synthesized for each particular SNP site, which is not convenient for large-scale SNP screening. On the other hand, there is an alternative approach, which does not require the covalent modification of the probe oligonucleotides. So, SNP or single base mutation (mutated DNAs) could also be easily detected by this method, known as, "label-free" method. In this method the small-molecule ligands (mismatch binders) which selectively bind to the mismatched base pairs in heteroduplexes. Upon selective binding to mismatched site in the DNA, the fluorescence response of these ligands would be modulated. Also this method is simple, less time consuming and moderate cost. To date, a large number of research works in this regard have been reported in literature. Few of them are discussed below.

As for example, Teulade-Fichou[61-65] *et.al*., synthesised bisacridine macrocycle BisA (**Figure 20**), as a receptor for nucleotides and nucleosides in aqueous solutions.[61] Further studied showed that BisA macrocycle binds to the loop region of DNA hairpins,[62] and could promote formation of hairpins from the thermodynamically more stable duplexes.[63] BisA was also a very efficient ligand for selective binding and photocleavage of abasic sites with an orphan thymine base in double-stranded DNA. [64,65]

In 2003, Weinhold and Teulade-Fichou[66] exploited BisA (**Figure 1.19**) as probe for this defected of TX-type mismatch sites in DNA. BisA probe was highly efficient to recognise TX-type mismatch sites (X = T, C, or G), with a strong preference for homopyrimidine mismatches (TT and TC), as evidenced by the large increase of melting temperatures of mismatch-containing 17-mer duplexes (e.g. ΔT_m = 5.8 °C) for the TT-mismatched duplex in

the presence of just one equivalent of BisA. In contrast, almost no change of the melting profile of the fully matched TA duplex was observed. It was proposed that binding of the macrocycle at the mismatch site was accompanied by flipping of one of the mismatched thymine residues out of the base stack, as evidenced by its higher susceptibility to oxidation by permanganate in the presence of BisA.[66]

The higher mismatch-binding affinity of 2,6-BisNP (**Figure 1.19**) compared with BisA (**Figure 1.19**) was somewhat unexpected in the view of better π-stacking properties of electron-poor acridine with nitrogenous bases. It appears, however, that naphthalene has more favourable size for binding the mismatch, while the larger acridine leads to steric clashes with the sugar residues upon intercalation.

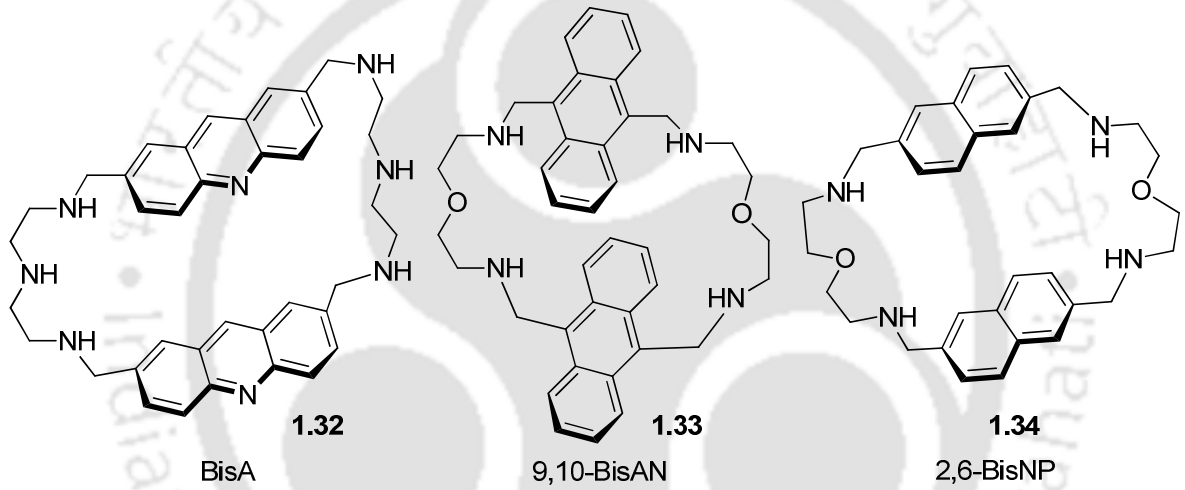

Figure 1.19. Macrocyclic bisintercalators BisA and 9,10-BisAN.

Sato *et al*., explored the binding study of a naphthyridine derivative, CF_3-AMND (**Figure 1.20**) with a trifluoromethyl group to cytosine opposite an abasic site in DNA duplexes.[67] The binding characteristics of CF_3-AMND to AP site-containing DNA duplexes were examined by UV-visible absorption and fluorescence measurements. The binding of CF_3-AMND was compared with the parent AMND in order to investigate the influence of the CF_3 group. The addition of a fully matched DNA duplex having no AP sites did not cause any fluorescence response of CF_3-AMND, indicating negligible intercalative binding of CF_3-AMND. Also, almost no response is observed for AP site-containing DNA duplexes carrying the A target and only slight responses for G and T targets. In contrast, significant fluorescence quenching is observed for C, where the fluorescence intensity at 403 nm decreased by as much as 75%. The absorption intensity of CF_3-AMND remarkably decreased upon addition of the

AP site-containing DNA duplexes carrying C whereas the absorption changes were slight for fully-matched DNA duplexes and AP site-containing DNA duplexes carrying the G, A, or T target. The CF_3-AMND shows highly selective binding to C in AP site-containing DNA duplexes. This might be due to the introduction of a CF_3 substituent into the parent AMND significantly improved the binding selectivity for C.

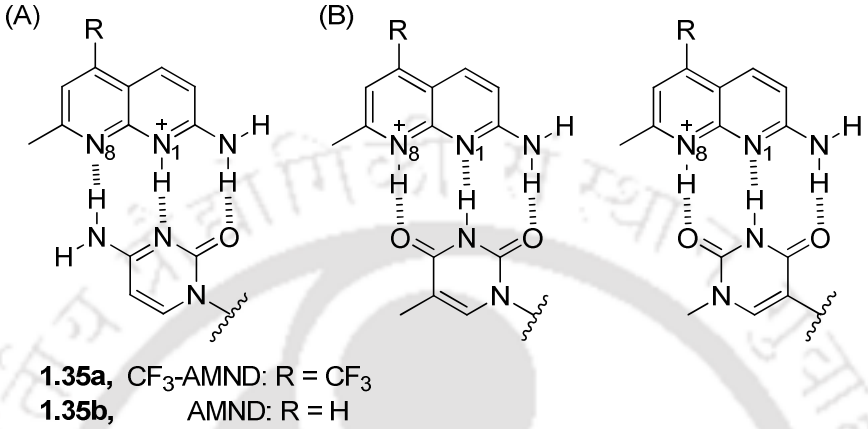

Figure 1.20. Chemical structures of CF_3-AMND and AMND. Proposed binding modes of these ligands with (A) cytosine and (B) thymine (two possible patterns) are also shown.

Sato *et al.*,[68] explored the binding study of ATMND–TO and DMP–BO (**Figure 1.21**) to AP site containing DNA and fully matched DNA. The fluorescence of the TO moiety was found to be negligible in the absence of DNA duplexes, resulting from the nonradiative energy loss by free rotation of the benzothiazole and quinoline rings of the TO moiety. In contrast, the addition of DNA duplexes caused a significant increase in the fluorescence intensity of the TO moiety. The responses were much pronounced for AP site-containing DNA duplexes compared to the fully-matched DNA duplex containing no AP sites, which suggested a favorable binding of ATMND–TO to the AP site-containing DNA duplexes. ATMND–TO exhibited the largest response for the target C in which the fluorescence intensity increased more than 1000-fold. The ATMND–TO also showed a large response for the target T, whereas the responses were small for purine nucleobases. While DMP–BO (**Figure 1.21**) showed G-selectivity with a light-up response at 483 nm (blue), ATMND–TO showed C- and T-selective light-up responses at 530 nm (green).

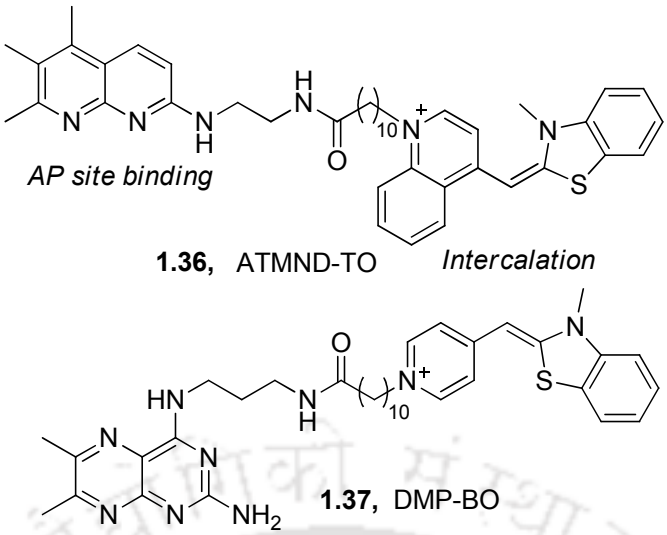

Figure 1.21. Chemical structure of ATMND–TO and DMP–BO.

Wang *et al*.,[69] investigated the fluorescence behavior of isoquinoline alkaloids including palmatine (PAL), berberine (BER), epiberberine (EPI), jatrorrhizine (JAT), coptisine (COP), coralyne (COR), worenine (WOR), berberrubine (BEU), sanguinarine (SAN), chelerythrine (CHE), and nitidine (NIT) (**Figure 1.22**) upon binding with the AP nanocavity. Among the isoquinoline alkaloids used, PAL was an efficient emitter to recognize the AP nanocavity over the fully matched DNA. The PAL was non-fluorescent alone in solution and its fluorescence enhancement occurred for all of the AP nanocavity sequence environments, which has not been achieved by other used probes.

The interactions of these alkaloids with the fully matched DNA containing no AP nanocavity caused small changes in fluorescence. In contrast fluorophore for the AP nanocavity-containing DNA against fully matched DNA, PAL showed brightest emission intensity response to the AP nanocavity binding. These results suggested that the substituent pattern of methoxyl groups in PAL favoured its binding affinity to the AP nanocavity in comparison with the other alkaloids (**Figure 1.22**). The increased melting temperature also supported the strong binding of PAL with the AP nanocavity containing DNAs. This type of strong interaction was also confirmed by the significant red-shifts in the absorption spectra of PAL upon the AP nanocavity binding especially within the 300– 400 and 400–500 nm ranges.

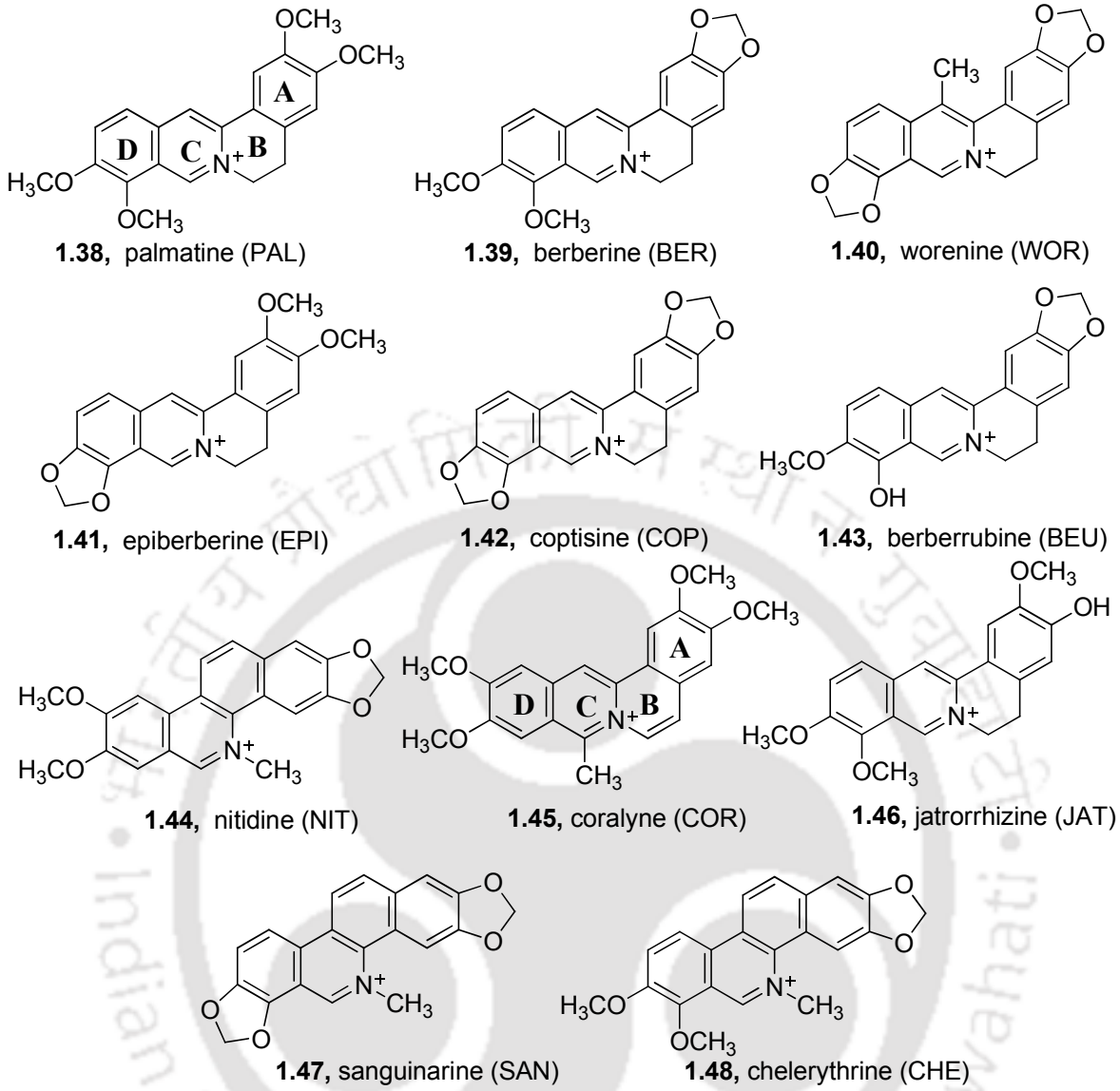

Figure 1.22. Chemical structures of isoquinoline alkaloids (IAs) used by Wang et al.

1.6. Structural Features of G-Quadruplex DNA

Label free DNA detection strategy that has been also popular with the use in non-canonical DNA secondary structures such as the G-quadruplex in conjunction with a G-quadruplex-specific fluorescent molecule. The unique structural features exhibited by the diverse array of G-quadruplex topologies offer the potential for highly specific interactions between the fluorophore and the functional oligonucleotide.

In 1910, gelatinous aggregates from the guanine-rich DNA solution was first observed. However, their exact nature was discovered by Davis [70] *et al.*, in 1962, who proposed that these gels form planar guanine tetramers which stack into a secondary structure termed G-quadruplex (**Figure 1.23**). DNA containing guanine-rich sequences can fold into a four-stranded DNA

helical secondary structure through guanine-guanine Hoogsteen H-bonding termed a G- tetrads or G-quartet. These G-quartets have large π-surfaces, and hence they tend to stack on each other due to π–π stacking as well as enabled cations to intercalate between the G-quartets (**Figure 1.23**). Because of the combined electrostatic effects of the phosphodiester backbone and converging arrangement of guanine O6 carbonyl groups, an exceptionally large negative potential exists in the central channel of the G-quadruplex.[71] To satisfy this repulsion, G-quadruplexes prepared under physiological conditions contain desolvated mono cations such as, sodium/potassium ions stacked between, or among, each planar G-tetrad.[72] As a result, G-quadruplex structures can exhibit thermodynamic stabilities comparable to, or even greater than the corresponding duplex structures.[73] This planar scaffold may adopt different structures in the presence of different cations, in particular K^+ and to a lesser extent NH_4^+ and Na^+. These cations interact with the lone pairs on the O6 atoms surrounding the central core.[74] The K^+ form is considered to be biologically more relevant due to its higher intracellular concentration (~ 140 mM) than that of Na^+ (5–15 mM). The precise location of cations between tetrads depends on the nature of the ions: Na^+ ions are observed in a range of geometries, whereas K^+ ions are always equidistant from each tetrad plane. The K^+ in general is preferred over Na^+ by G-quadruplexes as K^+ has a better coordination with eight guanine O6s and lower dehydration energy.[74] Unlike double-stranded DNA, the topology of these G-quadruplex structures exhibit extensive structural diversity and polymorphism, which depends on various factors:[75] 1) oligonucleotide strand/DNA sequence; 2) strand orientations (e.g. parallel, antiparallel, hybrid); 3) type and size of loops (e.g. diagonal, lateral, double chain reversal); 4) the number of telomeric repeats; 5) the oligonucleotide concentration; and 6) the stabilizing cation or solution environment (e.g. Na^+, K^+ and dehydration conditions).

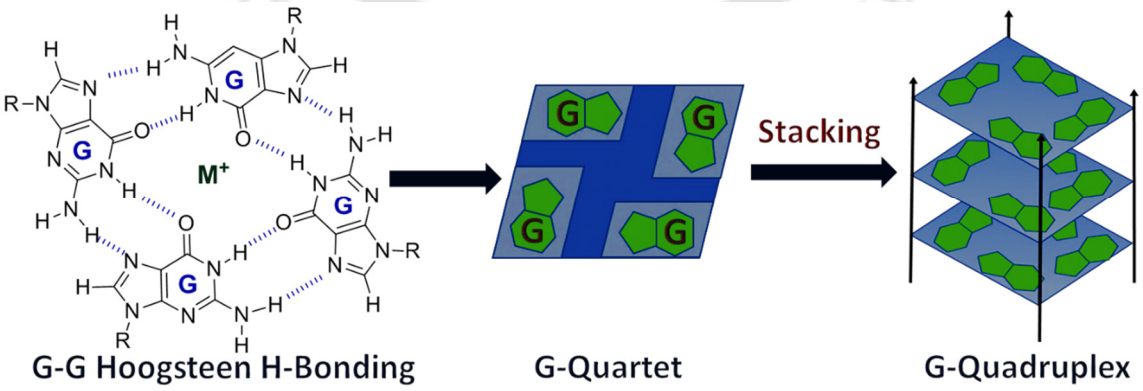

Figure 1.23. Graphical presentation of G–G Hoogsteen mode of hydrogen bonds, G-quartet stacked to G-quadruplex structure ($M^+ = Na^+$, K^+ NH_4^+).

The G4 formation most likely occurs during the processes of transcription, replication, and recombination, when the DNA duplex is actively denatured.[76] G-quadruplex structures can be intermolecular and intramolecular (**Figure 1.24**); the intramolecular quadruplexes are biologically more relevant since their structure may be altered upon interaction with appropriate ligands and proteins. The G4s can be classified into three main conformations (**Figure 1.24**) (i.e., parallel, antiparallel, and mixed parallel/antiparallel structures).[77] When the guanine tracts are oriented in opposite directions with loops above and below the terminal G-quartets, the G-quadruplex is called "antiparallel" (**Figure 1.24**). When all guanines tracts are oriented in the same direction with loops located on the sides of the G-quartets, the G-quadruplex is called "parallel" (**Figure 1.24**). Hybrid structures combining both kinds of loops and strand orientations also exist. However, complete prediction of a G-quadruplex conformation appears to be difficult. Thus, structural characterization of G-quadruplexes seems to be necessary to understand each G-quadruplex structure and its ligand interactions. [78]

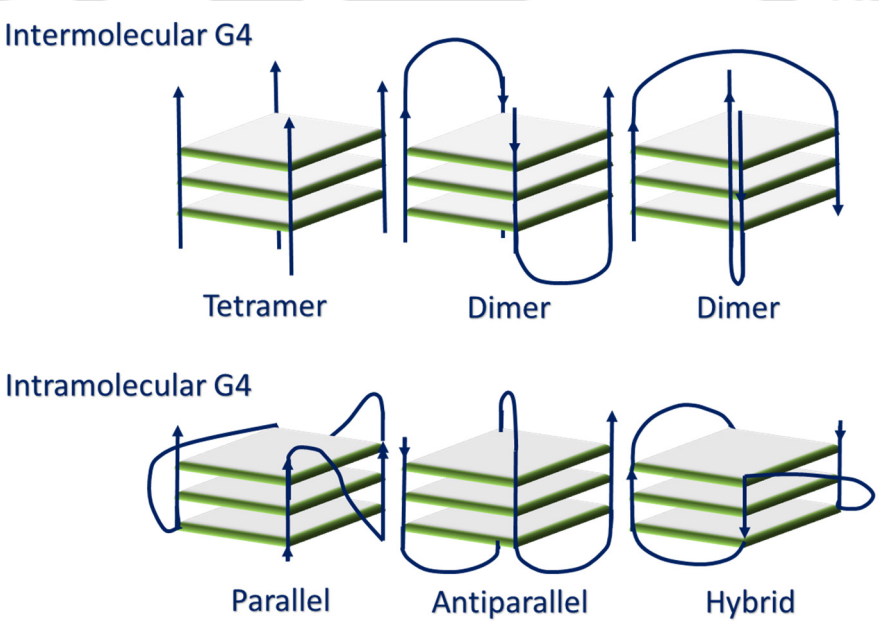

Figure 1.24. Classification of G-quadruplex structures.

The topology of G-quadruplexes provide a distinctive structure for a small molecule to specifically target G-quadruplexes over duplex, triplex or other nucleic acid secondary structure and even target specific G-quadruplex structures. The interaction modes of small molecules with a G-quadruplex usually follow these several principles[79]: (1) They can stack with the G-quartet through π–π interactions. Ligands with an extended planar aromatic system, which are similar to a G-quartet in size and shape, facilitate stacking on the G-quartet. This

aromatic system can be a rigid flat or twisted surface (**Figure 1.25**). (2) They can interact with the loops and grooves. Small molecules would interact with the loops and grooves of the G-quadruplex. Cationic substituents usually have stronger binding affinities with the anionic phosphate backbone (**Figure 1.25**). (3) They can interact with the negative electrostatic center of the G-quadruplex by electrostatic interaction with the cationic center of the aromatic core (**Figure 1.25**).

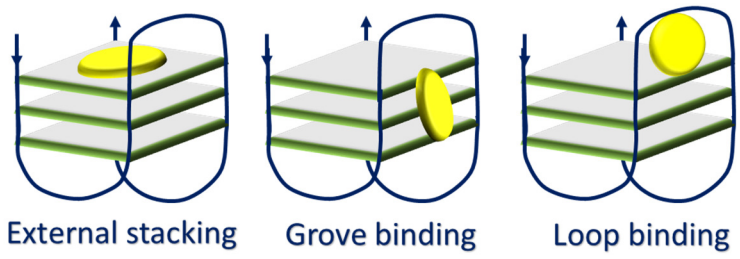

Figure 1.25. Examples of binding mode of small molecule with G-quadruplex.

1.6.1. G-Quadruplex Binding Probes

Apart, the design of highly efficient G4 ligands remains challenging, in part due to our limited knowledge of the binding modes with many G4s, some of which can be dynamic and polymorphic in structure. G-quadruplex elements in telomeres and in the genome are emerging targets for drug discovery, potentially leading to the development of new drugs with eventually improved selectivity and efficiency over conventional chemotherapeutics. Therefore, the development of new organic molecules that specifically bind to G4s, especially certain types of G4s, is important for the basic research, clinical diagnosis, and therapy. A large number of research works in this regard have been reported in literature. Few of them are discussed below.

In DNA-drug interaction some organic compounds (drug) achieving stabilization of telomeric DNA in G-quadruplex conformation has been an important insight to develop high specific new anticancer drug agents. There are relatively few organic molecules known to induce their formation and/or alter the topology of the preformed quadruplex DNA. Jain[80] *et.al*., explored four compounds having the 1,3-phenylene-bis(piperazinyl benzimidazole) unit (**Figure 1.26**) interactions with the 24-mer telomeric DNA sequences from *Tetrahymena thermophilia* $d(T_2G_4)_4$ using high-resolution techniques such as circular dichroism (CD) spectropolarimetry, CD melting, emission spectroscopy, and polyacrylamide gel electrophoresis. In the presence of one of three ions (Li^+, Na^+, or K^+), the new compounds had a high affinity for G-quadruplex DNA, and the strength of the binding with G-quadruplex

depends on (i) phenyl ring substitution, (ii) the piperazinyl side chain, and (iii) the type of monovalent cation present in the buffer. These compounds were able to abet the conversion of the intramolecular quadruplex into parallel stranded intermolecular G-quadruplex DNA. Notably, these compounds were also capable of inducing and stabilizing the parallel stranded quadruplex from randomly structured DNA in the absence of any stabilizing cation. The kinetics of the structural changes induced by these compounds could be followed by recording the changes in the CD signal as a function of time. These compounds would have significantly lower affinity for the duplex DNA via either mode of binding (minor groove binding and intercalation). Intrestingly, these compounds not only stabilized and altered the structure of the preformed *Tetrahymena* G-quadruplex but also induce formation of the quadruplex in the absence of added cations.

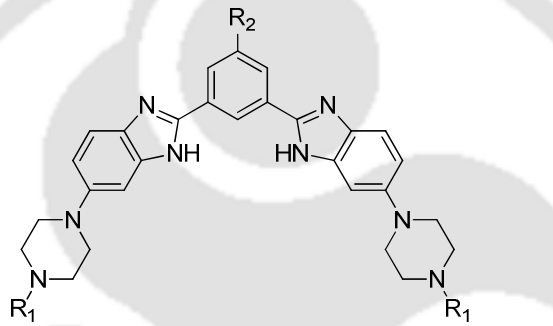

1.49a, EtBzMe $R_1 = CH_3$, $R_2 = OCH_2CH_3$
1.49b, EtBzEt $R_1 = CH_2CH_2OH$, $R_2 = OCH_2CH_3$
1.49c, HyBzMe $R_1 = CH_3$, $R_2 = OH$
1.49d, HyBzEt $R_1 = CH_2CH_2OH$, $R_2 = OH$

Figure 1.26. Molecular structures of 1,3-phenylene-bis(piperazinyl benzimidazole) skeleton unit.

Mohanty[81] *et.al*., demonstrated that the water soluble fluorogenic dye, Thioflavin T (ThT, **Figure 1.27**) in a dual role of exclusively inducing quadruplex folding in the 22AG (22AG: 5′- AGGGTTAGGGTTAGGGTTAGGG-3′) human telomeric DNA, both in the presence and absence of Tris buffer/salt, and sensing the same through its fluorescence light-up behaviour having emission enhancement of the order of 2100- fold in the visible region. In 50 mM Tris (pH 7.2) solution, 22AG–ThT showed parallel quadruplex structure, which switched to antiparallel form just by the addition of K^+ ions in the range 10–50 mM. Moreover, addition of ThT cooperatively stabilizes the K^+ induced antiparallel quadruplexes by a ΔT_m ~11 °C. The distinction of ThT as a quadruplex inducer has been contrasted with the well-known quadruplex binder dye TO. It has been illustrated that TO did not induce any quadruplex folding in the 22AG strand in the absence of salt. The striking fluorescence light-up signal by

ThT dye on binding to the human telomeric G-quadruplex, in the absence and presence of K^+, was shown to be highly specific compared to the less than 250-fold enhancement observed with other single/double-strand DNA forms.

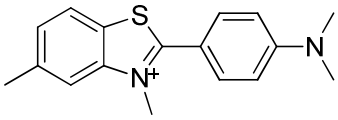

1.50, Thioflavin T (ThT)

Figure 1.27. Structure of Thioflavin T (ThT).

Yan[82] *et.al*., exploited three novel dyes (**1.51a-c, Figure 1.28**) for visual detection and differentiation of G-quadruplexes from single and duplex DNA structures. Compound **1.51c** exhibited a predominant H-aggregation band around 535 nm in buffer; upon titration with G-quadruplex-forming oligonucleotide (pu27), dramatic changed of the absorption peaks were observed. The peak around 535 nm gradually decreased with addition of G-quadruplex and eventually led to the appearance of a new peak around 600 nm assigned to its monomeric state, which was consistent with the disassembly of the H-aggregates of **1.51c**. The red shift for the disassembly of the H-aggregates of **1.51c** to its monomers gave rise to a clear and visible color change from purplish red to blue. Thus, **1.51c** could be used as a rapid and facile indicator for a variety of G-quadruplexes. Including G-quadruplexes pu27, c-kit1, HTG21, and tetramer could remarkably increase the absorbance at 600 nm. In contrast, non-quadruplexes, including single strands (dA21 and dT21), linear duplex CT-DNA (calf thymus DNA), and self-complementary duplex strand (ds15) could hardly affect the aggregation state of **1.51c** under the same condition, with only slight decrease of the absorbance. So, compound **1.51c** could be used for label-free visual detection of a variety of G-quadruplexes with high specificity.

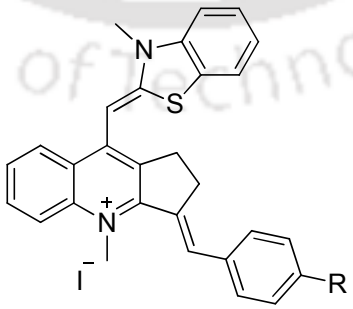

1.51a, R = H
1.51b, R = $N(CH_3)_2$
1.51c, R = NO_2

Figure 1.28. Structures of thiazole orange and isaindigotone fusion dyes, **1.51a-c**.

Lavrado[83] *et.al*., synthesised a small library of mono- and disubstituted alkyldiamine 5-methylindolo[3,2-c]quinolones (IQc) derivatives (**Figure 1.29**), and explored their capacity to induce G4 stabilization and characterize, at a molecular level, using the human telomeric G4 structure (HT21) (HT21 = 5`-GGGTTAGGGTTAGGGTTAGGG-3`) as a model. IQc derivatives **1.53d** and **1.54d** (**Figure 1.29**) stabilized the antiparallel G4 topology of HT21 and formed a complex with two ligands per G4 unit. Molecular modeling simulations revealed that the disubstituted IQc derivative **1.54d** bound to the antiparallel human telomeric G4 in two equivalent and non-independent binding sites, in which the second binding event appeared to be conditioned by an induced fit to the G4 structure.

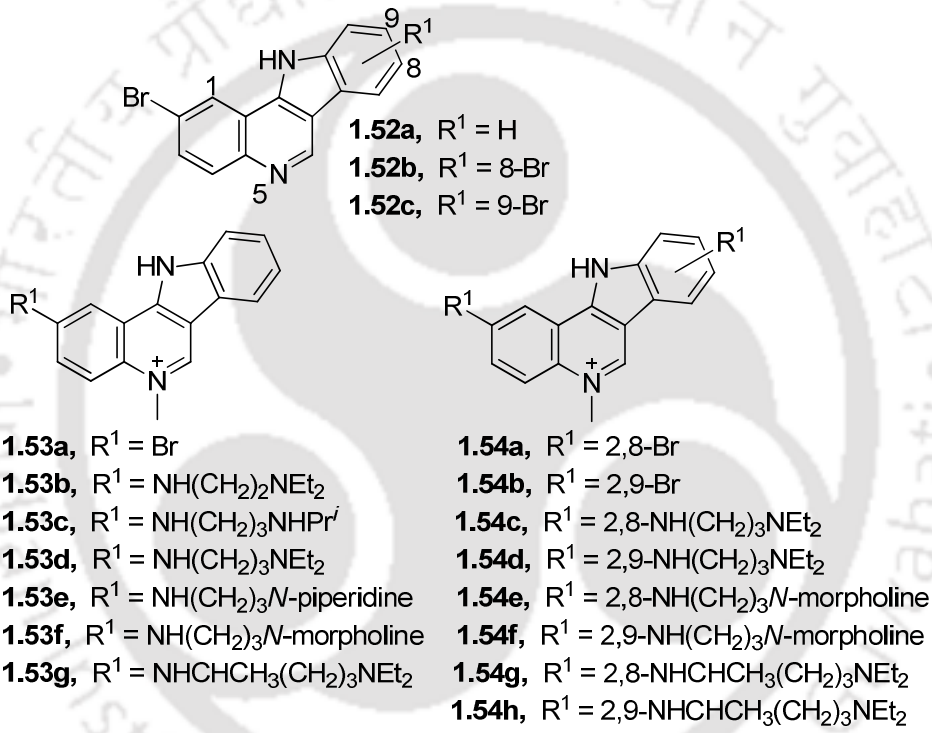

Figure 1.29. Structures of the indolo[3,2-c]quinoline derivatives.

Amato[84] *et.al*., explored starting from the lead compound **1.55a**, a series of analogues with structural modifications of the substituents and the core have been designed, synthesized, and evaluated as effective and selective G4 binding ligands (**Figure 1.30**) and evaluated as G-quadruplex binders. The *in vitro* G-quadruplex-binding properties of the compounds were investigated employing both human telomeric and oncogene promoter G-quadruplexes with different folding topologies as targeted using circular dichroism spectroscopy, nuclear magnetic resonance studies and molecular docking. The hydrazine-based compounds (**Figure 1.30**) identified of potent G-quadruplex stabilizers with high selectivity over duplex DNA. However, the compounds having a different core from that of compound **1.55a** (**1.55f**, **g**, and

h) were also shown to increase the stability of duplex DNA and therefore they are not selective for G4s. On the other hand, compounds **1.55b-d** displayed a marked preference for binding to parallel G4s over duplex and antiparallel G4s. In line with the *in vitro* assays, biological experiments demonstrated that hydrazine derivatives could effectively trap G4 structures in the nuclei of cells. Remarkably, derivative **1.55c** was more effective than the lead compound **1.55a** in inhibiting human U2OS and HCT116 cancer cell growth as well as in stabilizing G4s in osteosarcoma cells.

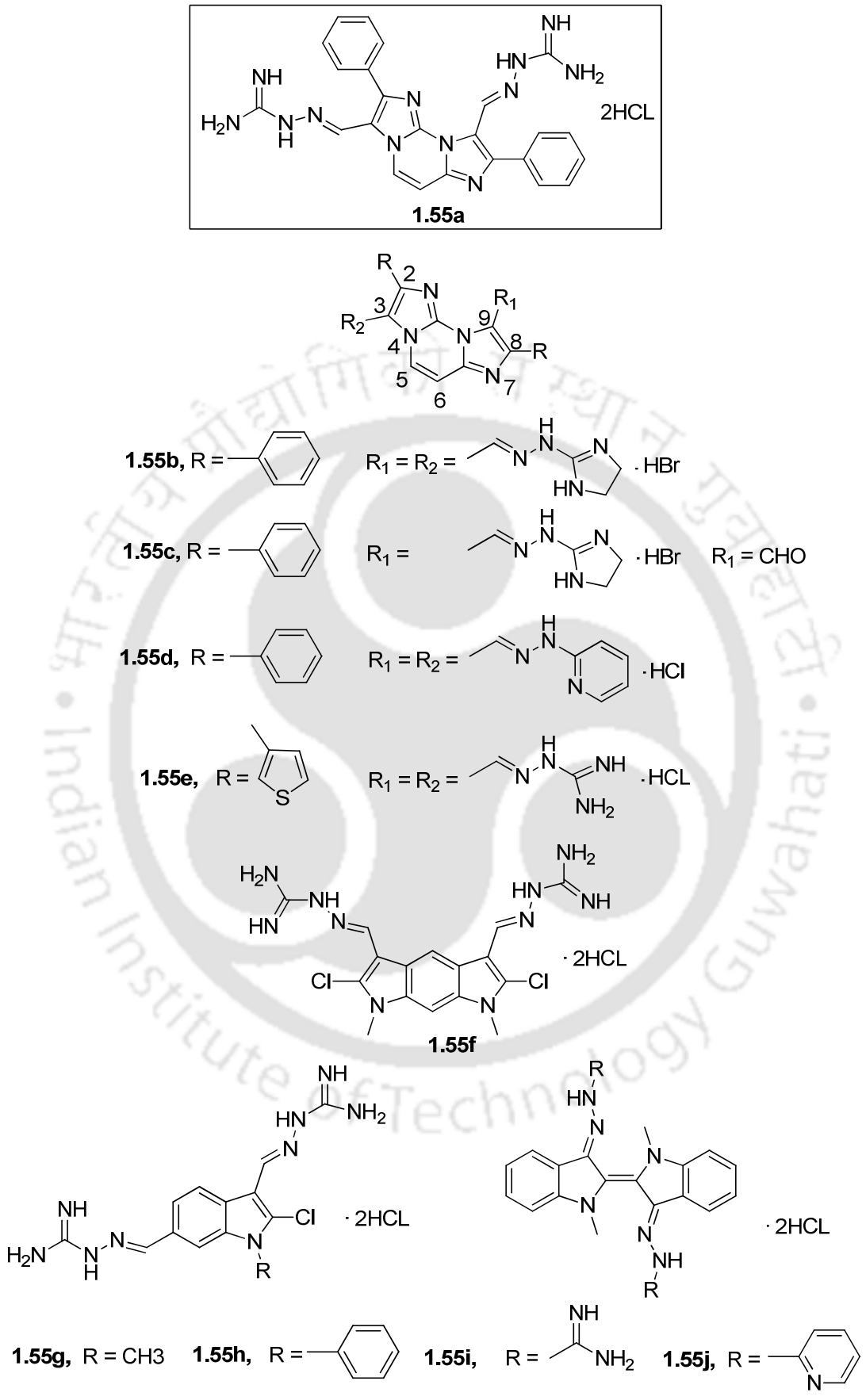

Figure 1.30. Compound lead 1.55a and structural modifications.

Jin[85] *et.al*., explored the design and synthesis of a new light up fluorescent probe, BPBC (**Figure 1.31**) composed of benzimidazole and carbazole moieties and evaluated as effective and selective parallel G4 binding fluorescence light-up Probe. A crescent-shaped dye BPBC exhibited good selectivity to parallel G4s over other G4s, which may be due to the larger size of the planar core. The UV−visible absorption spectra of BPBC showed that G4-binding, especially parallel G4 binding, caused a new absorption band to appear at around 400 nm. BPBC exhibited almost no fluorescence in the aqueous buffer condition. The fluorescence of BPBC was switched on upon binding to parallel G4s (about 335−1800-fold). But for the antiparallel G4s, the fluorescence enhancement was much smaller. The single stranded/duplex DNA could not enhance the fluorescence of BPBC. This optical selectivity allowed BPBC to serve to discriminate parallel G4s from other DNA forms. BPBC was bound to G4s through end-stacking on the G-quartet surface. The apparent binding constants (K_a's) of parallel G4s were calculated to be $0.8–5 \times 10^6$, based on results of fluorimetric titration.

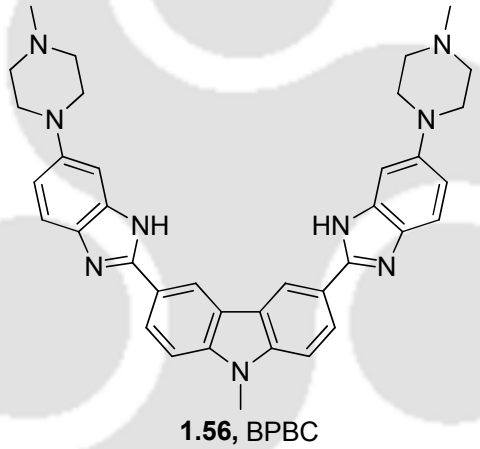

1.56, BPBC

Figure 1.31. Structure of BPBC composed of benzimidazole and carbazole moieties.

1.7. References

1. Lakowicz, J. R. *Principles of Fluorescence Spectroscopy*, 3rd ed.; Springer: New York, **2006**.
2. Sinkeldam, R. W.; Greco, N. J.; Tor, Y. *Chem. Rev*. **2010**, *110*, 2579.
3. (a) Sun, J.; Garestier, G; Hélène, C. *Curr Opin Struct Biol* **1996**, *6*, 327. (b) Kuryavyi, W.; Jovin, T. *Nat. Genet*. **1995**, *9*, 339. (c)Wojcewski, C.; Stolze, K.; Engles, J. W. *Synlett* **1999**, 1667.
4. (a) Teng, M. K.; Usman, N.; Frederick, C. A.; Wang, A. H. *Nucleic Acids Res*. **1988**, *16*, 2671. (b) Tabernero, L.; Verdaguer, N.; Coll, M.; Fita, I.; van der Marel, G. A.; van Boom, J. H.; Rich, A.; Aymami, J. *Biochemistry* **1993**, *32*, 8403. (c) Coll, M.; Frederick, C. A.; Wang, A. H.; Rich, A. *Proc. Natl. Acad. Sci. USA* **1987**, *84*, 8385. (d) Larsen, T. A.; Goodsell, D. S.; Cascio, D.; Grzeskowiak, K.; Dickerson, R. E. *J. Biomol. Struct. Dyn*. **1989**, *7*, 477. (e) Kielkopf, C. L.; Erkkila, K. E.; Hudson, B. P.; Barton, J. K.; Rees, D. C. *Nat. Struct. Biol*. **2000**, *7*, 117. (f) Lovejoy, K. S.; Todd, R. C.; Zhang, S.; McCormick, M. S.; D'Aquino, J. A.; Reardon, J. T.; Sancar, A.; Giacomini, K. M.; Lippard, S. J. *Proc. Natl. Acad. Sci. USA* **2008**, *105*, 8902.
5. (a) Watson, J. D. *Molecular biology of the gene*, 6th ed.; Pearson/ Benjamin Cummings; Cold Spring Harbor Laboratory Press: Cold Spring Harbor, NY, **2008**. (b) Bartel, D. P. *Cell* **2009**, *136*, 215. (c) Eddy, S. R. *Nat. Rev. Genet*. **2001**, *2*, 919. (d) Mattick, J. S.; Makunin, I. V. *Hum. Mol. Genet*. **2006**, *15*, R17. (e) Montange, R. K.; Batey, R. T. *Annu. Rev. Biophys*. **2008**, *37*, 117. (f) Munninger, K. O.; Chang, S. H *Biochem. Biophys. Res. Commun*. **1972**, *46*, 1837. (g) Maelicke, A.; Vonderha, F; Cramer, F. *Biopolymers* **1973**, *12*, 27. (h) Paszyc, S.; Rafalska, M. *Nucleic Acids Res*. **1979**, *6*, 385. (i) McCloskey, J. A.; Crain, P. F.; Edmonds, C. G.; Gupta, R.; Hashizume, T.; Phillipson, D. W.; Stetter, K. O. *Nucleic Acids Res*. **1987**, *15*, 683. (j) Stimson, S. M. M.; Reuter, S. M. A. *J. Am. Chem. Soc*. **1941**, *63*, 697. (k) Peon, J.; Zewail, A. H. *Chem. Phys. Lett*. **2001**, *348*, 255. (l) Serrano-Andres, L.; Merchan, M. *J. Photochem. Photobiol., C* **2009**, *10*, 21. (m) Leonard, N. J.; Tolman, G. L. *Ann. N. Y. Acad. Sci*. **1975**, *255*, 43.
6. (a) Sun, J.; Garestier, G; Hélène, C. *Curr Opin Struct Biol* **1996**, *6*, 327. (b) Kuryavyi, W.; Jovin, T. *Nat. Genet*. **1995**, *9*, 339. (c) Wojcewski, C.; Stolze, K.; Engles, J. W. *Synlett* **1999**, 1667.

7. (a) Watson, J.D.; Crick, F.H.C. J. *Am. Med. Assoc.* **1993**, *269*, 1966. (b) Nikolova, E. N.; Kim, E.; Wise, A. A.; O'Brien, P. J.; Andricioaei, I.; Al-Hashimi, H. M. *Nature* **2011**, *470*, 498.
8. Weiling, F. *Am. J. med. Genet*. **1991**, *40*, 1.
9. Watson, J.D.; Crick, F.H.C. *Nature* **1953**, *171*, 737.
10. Alberts, B.; Johnson, A.; Lewis, J.; Raff, M.; Roberts, K.; Wlater, P. *Molecular Biology of the Cell, fourth ed., Garland Science, New York, Amsterdam*, **2002**, 120.
11. Fonseca, G.C.; Bickelhaupt, F.M.; Snijders, J.G.; Baerends, E.J. *Chem. Eur. J*. **1999**, *5*, 3581.
12. Wing, R.; Drew, H.; Takano, T.; Broka, C.; Tanaka, S.; Itakura, K.; Dickerson, R. *Nature* **1980**, *287*, 755.
13. Kielkopf, C.L.; White, S.; Szewczyk, J.W.; Turner, J.M.; Baird, E.E.; Dervan, P.B. Rees, D.C. *Science* **1998**, *282*, 111.
14. Lown, J.W. *J. Mol. Recognit*. **1994**, *7*, 79.
15. Pabo, C.O.; Sauer, R.T. *Annu. Rev. Biochem*. 1984, 53, 293.
16. Neidle, S. *Natl. Prod. Rep*. **2001**, *18*, 291.
17. Takeda, Y.; Ohlendorf, D.H.; Anderson, W.F.; Matthews, B.W. *Science* **1983**, *221*, 1020.
18. Gao, X.; Mirau, P.; Patel, D.J. *J. Mol. Biol*. 1992, 223, 259.
19. Paul, A.; Bhattacharya, S. *Curr. Sci.* **2012**, *102*, 212.
20. Demeunynck, M.; Bailly, C.; Wilson, W. D. *DNA and RNA Binders: From Small Molecules to Drugs*, Wiley-VCH Verlag GmbH, Weinheim, **2003**.
21. Demeunynck, M.; Bailly, C.; Wilson, W. D. *Wiley-VCH Verlag GmbH, Weinheim,* **2003**.
22. Blackburn, G. M.; Gait, M. J.; Loakes, D.; Williams, D. M. Nucleic Acids in Chemistry and Biology, *Oxford University Press, Oxford*, **2006**.
23. Watson, J. D.; Crick, F. H. C. *Nature*, **1953**, *171*, 737.
24. Lerman, L. S. *J. Mol. Biol*., **1961**, *3*, 18.
25. Persil, O.; Hud, N. V. *Biotechnol*., **2007**, *25*, 433.
26. Clement, B.; Jung, F., *Drug Metab. Dispos*., **1994**, *22*, 486.
27. P. Cozzi, *Farmaco*, **2000**, *55*, 168.
28. Cocco, M.J.; Hanakahi, L.A.; Huber, M.D.; Maizels, N. *Nucleic Acids Res*. **2003**, *31*, 2944.

29. Sabatino, M.A.; Colombo, T.; Geroni, C.; Marchini, S.; Broggini, M. *Clin. Cancer Res*. **2003**, *9*, 5402.
30. Baraldi, P.G.; Bovero, A.; Fruttarolo, F.; Preti, D.; Tabrizi, M.A.; Pavani, M.G.; Romagnoli, R. *Med. Res. Rev*. **2004**, *24*, 475.
31. Patel, S.R.; Kvols, L.K.; Rubin, J.; O'Connell, M.J.; Edmonson, J.H.; Ames, M.M.; Kovach, J.S. *Invest. New Drugs.* **1991**, *9*, 53.
32. Singh, M.P.; Joseph, T.; Kumar, S.; Bathini, Y.; Lown, J.W. *Chem. Res. Toxicol*. **1992**, *5*, 597.
33. Soderlind, K.J.; Gorodetsky, B.; Singh, A.K.; Bachur, N.R.; Miller, G.G.; Lown, J.W. *Anticancer Drug Des*. **1999**, *14*, 19.
34. Kiser, J.R.; Monk, R.W.; Smalls, R.L.; Petty, J.T. *Biochemistry* **2005**, *44*, 16988.
35. Tawar, U.; Jain, A.K.; Chandra, R.; Singh, Y.; Dwarakanath, B.S.; Chaudhury, N.K.; Good, L.; Tandon, V. *Biochemistry* **2003**, *42*, 13339.
36. Maiti, S.; Chaudhury, N.K.; Chowdhury, S. *Biochem. Biophys. Res. Commun*. **2003**, *310*, 505.
37. Bourdouxhe, C.; Colson, P.; Houssier, C.; Henichart, J. P.; Waring, M. J.; Denny, W. A.; Bailly, C. *Anticancer Drug Des*. **1995**, *10*, 131.
38. David-Cordonnier, M. H. et al. *Eur. J. Med. Chem*. **2007**, *42*, 752.
39. Whitcombe, D.; Theaker, J.; Guy, S. P.; Brown, T.; Little, S. *Nat. Biotechnol.* **1999**, *17*, 804.
40. Cheung, V. G.; Gregg, J. P.; Gogolin-Ewens, K. J.; Bandong, J.; Stanley, C. A.; Baker, L.; Higgins, M. J.; Nowak, N. J.; Shows, T. B.; Ewens, W. J.; Spielman, R. S. *Nat. Genet*. **1998**, *18*, 225.
41. Howell, W. M.; Jobs, M.; Gyllensten, U.; Brookes, A. J. *Nat. Biotechnol*. **1999**, *17*, 87.
42. Lyamichev, V.; Mast, A. L.; Hall, J. G.; Prudent, J. R.; Kaiser, M. W.; Takova, T.; Kwiatkowski, R. W.; Sander, T. J.; de Arruda, M.; Arco, D. A.; Neri, B. P.; Brow, M. A. D. *Nat. Biotechnol*. **1999**, *17*, 292.
43. Pastinen, T.; Raitio, M.; Lindroos, K.; Tainola, P.; Peltonen, L.; Syvanen, A. C. *Genome Res*. **2000**, *10*, 1031.
44. Tyagi, S.; Bratu, D. P.; Kramer, F. R. *Nat. Biotechnol*. **1998**, *16*, 49.
45. (a) Okamoto, A.; Tanaka, K.; Fukuta, T.; Saito, I. *J. Am. Chem. Soc*. **2003**, *125*, 9296. (b) Okamoto, A.; Tainaka, K.; Saito, I. *Chem. Lett*. **2003**, *32*, 684.
46. Lou, C.; Dallmann, A.; Marafini, P.; Gao, R.; Brown, T. *Chem. Sci.,* **2014**, *5*, 3836.
47. Rist, M. J.; Marino, J. P. *Curr. Org. Chem*., **2002**, *6*, 775.

48. Sandin, P.; Wilhelmsson, L. M.; Lincoln, P.; Powers, V. E. C.; Brown, T.; Albinsson, B. *Nucleic Acids Res*., **2005**, *33*, 5019.
49. Telser, J.; Cruickshank, K. A.; Morrison, L. E.; Netzel, T. L. *J. Am. Chem. Soc*., **1989**, *111*, 6966.
50. Wilson, J. N.; Cho, Y. J.; Tan, S.; Cuppoletti, A.; Kool, E. T. *Chem Bio Chem*, **2008**, *9*, 279.
51. Huppert, J. L. *FEBS J*., **2010**, *277*, 3452.
52. Bochman, M. L.; Paeschke, K.; Zakian, V. A. *Nat. Rev. Genet*., **2012**, *13*, 770.
53. Li, P.; He, H.; Wang, Z.; Feng, M.; Jin, H.; Wu, Y.; Zhang, L.; Zhang, L.; Tang, X. *Anal. Chem*. **2016**, *88*, 883.
54. Srivatsan, S. G.; Weizman, H.; Tor. Y. *Org. Biomol. Chem*., **2008**, *6*, 1334.
55. Aso, T.; Saito, K.; Suzuki, A.; Saito. Y. *Org. Biomol. Chem*., **2015,** *13*, 10540.
56. Suzuki, A.; Nemoto, N.; Saito, I.; Saito. Y. *Org. Biomol. Chem.*, **2014**, *12*, 660.
57. Tainaka, K.; Tanaka, K.; Ikeda, S.; Nishiza, K.-I.; Unzai, T.; Fujiwara, Y.; Saito, I.; Okamoto. A. *J. Am. Chem. Soc.,* **2007**, *129*, 4776.
58. Okamoto, A.; Kanatani, K.; Saito. I. *J. Am. Chem. Soc.,* **2004**, *126*, 4820.
59. Capobianco, M. L.; Cazzato, A.; Alesi, S.; Barbarella. G. *Bioconjugate Chem***. 2008**, *19,* 171.
60. Hurley, D. J.; Seaman, S. E.; Mazura, J. C.; Tor. Y. *Org. Lett*., **2002**, *4* (4), 2305.
61. Teulade-Fichou, M.-P.; Vigneron, J.-P.; Lehn, J.-M. *Supramol. Chem*. **1995**, *5*, 139.
62. Slama-Schwok, A.; Teulade-Fichou, M.-P.; Vigneron, J.-P.; Taillandier, E.; Lehn, J.-M. *J. Am. Chem. Soc.* **1995**, *117*, 6822.
63. Slama-Schwok, A.; Peronnet, F.; Hantz-Brachet, E.; Taillandier, E.; Teulade-Fichou, M.-P.; Vigneron, J.-P.; Best-Belpomme M.; Lehn, J.-M. *Nucleic Acids Res*. **1997**, *25*, 2574.
64. Berthet, N.; Michon, J.; Lhomme, J.; Teulade-Fichou, M.-P.; Vigneron, J. P.; Lehn, J.-M. *Chem.–Eur. J*. **1999**, *5*, 3625.
65. Jourdan, M.; Garcia, J.; Lhomme, J.; Teulade-Fichou, M.-P.; Vigneron, J.-P.; Lehn, J.-M. *Biochemistry*, **1999**, *38*, 14205.
66. David, A.; Bleimling, N.; Beuck, C.; Lehn, J.-M.; Weinhold, E.; Teulade-Fichou, M.-P. *ChemBioChem*, **2003**, *4*, 1326.
67. Sato, Y.; Zhang, Y.; Seino, T.; Sugimoto, T.; Nishizawa, S.; Teramae, N. *Org. Biomol. Chem*. **2012**, *10*, 4003.

68. Sato, Y.; Kudo, M.; Toriyabe, Y.; Kuchitsu, S.; Wang, C. -x.; Nishizawa, S.; Teramae, N. *Chem. Commun*. **2014**, *50*, 515.
69. Wang, Y.; Hu, Y.; Wu, T.; Zhang, L.; Liu, H.; Zhou, X.; Shao, Y. *Spectrochimica Acta Part A: Molecular and Biomolecular Spectroscopy* **2016**, *153*, 645.
70. Gellert, M.; Lipsett, M. N.; Davies, D. R., *Proc. Natl. Acad. Sci. USA*, **1962**, *48*, 2013.
71. Mondragn-Snchez, J. A.; Santamaria, R.; Ço-Jurez, R. G. *Biopolymers* **2011**, *95*, 641.
72. Davis, J. T. *Angew. Chem. Int. Ed*. **2004**, *43*, 668.
73. Risitano, A.; Fox, K. R. *Biochemistry* **2003**, *42*, 6507.
74. Hud, N. V.; Plavec, J., *Royal Society of Chemistry Publishing, Cambridge*, **2006**, 100.
75. Bidzinska, J.; Cimino-Reale, G.; Zaffaroni, N.; Folini, M. *Molecules* **2013**, *18*, 12368.
76. Maizels, N. *Nat. Struct. Mol. Biol*. **2006**, *13*, 1055.
77. Burge, S.; Parkinson, G. N.; Hazel, P.; Todd, A. K.; Neidle, S. *Nucleic Acids Res*. **2006**, *34*, 5402.
78. Brooks, T. A.; Kendrick, S.; Hurley, L. *FEBS J*. **2010**, *277*, 3459.
79. Yan, Y.; Tan, J.; Ou, T.; Huang, Z.; Gu, L. *Expert Opin. Ther. Pat.* **2013**, *23*, 1495.
80. Jain, A. K.; Reddy, V. V.; Paul, A.; Muniyappa, K.; Bhattacharya, S. *Biochemistry* **2009**, *48*, 10693.
81. Mohanty, J.; Barooah, N.; Dhamodharan, V.; Harikrishna, S.; Pradeepkumar, P. I.; Bhasikuttan, A.C. *J. Am. Chem. Soc*. **2013**, *135*, 367.
82. Yan, J-W.; Ye, W-J.; Chen, S-B.; Wu, W-B.; Hou, J-Q.; Ou, T-M.; Tan, J-H.; Li, D.; Gu, L-Q.; Huang, Z-S. *Anal. Chem*. **2012**, *84*, 6288.
83. Lavrado, J.; Ohnmacht, S. A.; Correia, I.; Leitao, C.; Pisco, S.; Gunaratnam, M.; Moreira, R.; Neidle, S.; Santos, D. J. V. A.; Paulo, A. *ChemMedChem* **2015**, *10*, 836.
84. Amato, J.; Morigi, R.; Pagano, B.; Pagano, A.; Ohnmacht, S.; Magis, A. D.; Tiang, Y-P.; Capranico, G.; Locatelli, A.; Graziadio, A.; Leoni, A.; Rambaldi, M.; Novellino, E.; Neidle, S.; Randazzo, A. *J. Med. Chem*. **2016**, *59*, 5706.
85. Jin, B.; Zhang, X.; Zheng, W.; Liu, X.; Qi, C.; Wang, F.; Shangguan, D. *Anal. Chem*. **2014**, *86*, 943.

Chapter 2

Synthesis of Fluorescent Oligonucleotide Probe Containing 5'-(2-napthyl)-2'-deoxy Uridine and Its Application in SNPs Genotyping

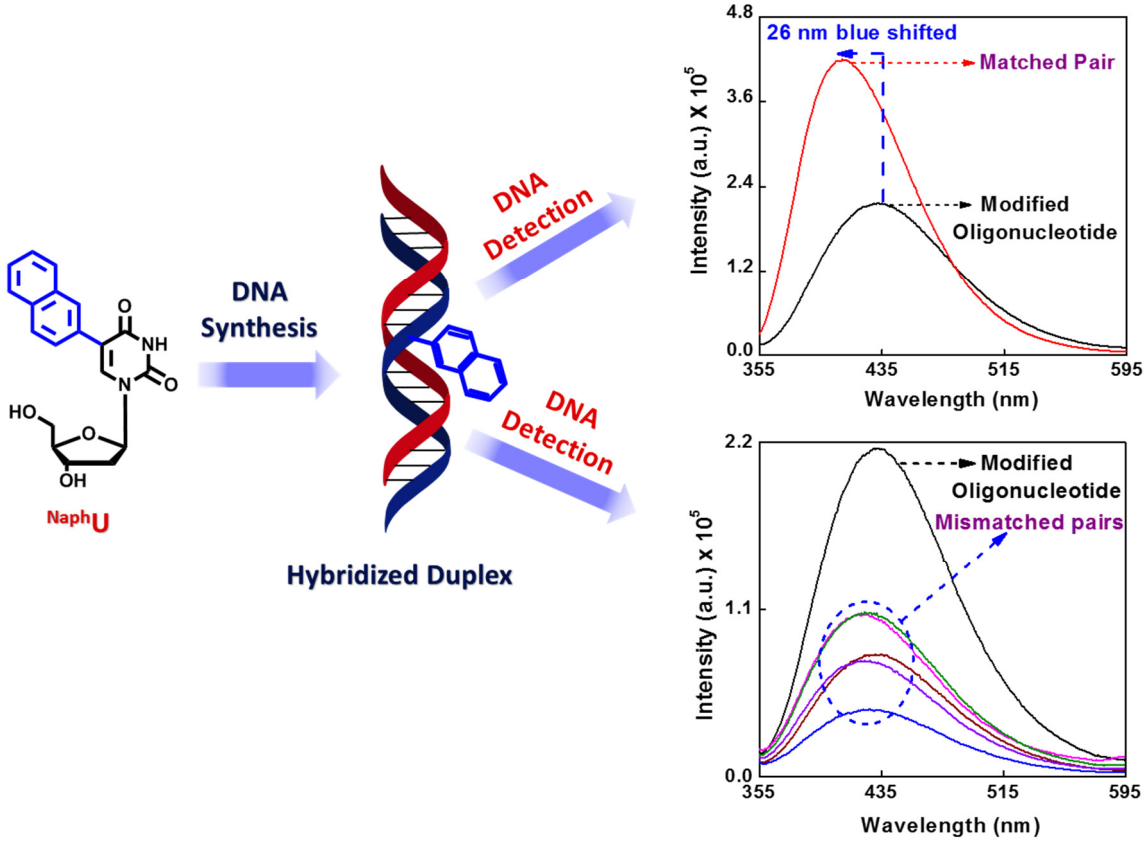

2.1. Introduction

Base-modified environmentally sensitive fluorescence (ESF) nucleosides which permit Watson–Crick base pair formation, are useful tools for structural studies of nucleic acids as well as for the detection of target genes and single nucleotide polymorphism (SNP) typing when incorporated into DNA.[1] Therefore, several classes of base-modified ESF nucleosides, mostly C5-substituted pyrimidine nucleosides, exhibiting interesting solvatochromic properties, have been reported.[1–3] The fluorophores can be attached to nucleic acids in several ways: to phosphate or sugar moiety or to nucleobase via a conjugate or nonconjugate linker, or a fluorophore can even replace a nucleobase. The fluorophores attached via longer nonconjugate aliphatic linkers are generally used for the detection in sequencing[4] or FRET techniques[5] and are favourable for decreasing the steric hindrance in enzymatic reactions and during DNA hybridization. The fluorescent nucleoside analogues, where a fluorophore is linked directly[6] or via conjugate tether[7] or replacing a nucleobase either by a fused analogue[8] or even by a structurally unrelated molecule,[9] typically respond well to hybridization (base-discriminating fluorophores, BDF) and formation of secondary structures. Even the use of a nonconjugate but short propargylamide linker for attachment of fluorophores resulted in the specific response of the fluorescence to single nucleotide polymorphism (SNP).[10] However, there are few reports on ESF nucleosides that discriminate local structural changes in DNA by a drastic change in emission wavelength.[1f,11] Detection of single nucleotide polymorphism (SNP)[12] in nucleic acid diagnostic steel a fundamentally challenging task for scientist. Such biological mutated base pairs directly linked to certain diseases or reflect susceptibility to specific therapeutics.[13] So, a lot approach towards the detection of SNPs have been developed.[14,15] Saito[16] *et. al*. first introduced a concept of base-discriminating fluorescent (BDF) nucleosides with "mix and read" strategy for SNP typing. According to their concept, base-discriminating fluorescent (BDF) modified nucleobases upon hybridisation to a given target distinguish the fully matched and mismatched bases in duplex DNA by producing a sharp change in their photophysical characteristics.[17] Several other research works in this regard have been reported in literature. Few of them are discussed below.

Srivatsan[20a] *et al*., synthesised a microenvironment-sensitive fluorescent 2'-deoxyuridine analogue that is based on a 5-(benzofuran-2-yl)pyrimidine core, nucleoside **2.1** (**Figure 2.1**) incorporated into DNA oligo nucleotides (ONs) and its photophysical properties within these ONs was explored. Photophysical characterisation showed that the fluorescence properties of the nucleoside **2.1** within ONs are significantly influenced by flanking bases,

especially by guanosine. Nucleoside **2.1** successfully detected the presence of an abasic site in RNA highlights the potential of **2.1** as a fluorescent probe.

Greco[20b] *et al*., explored the synthesis and photophysical characteristics of a series of simple and responsive thymidine analogues, where a 2′-deoxy-U core is conjugated to aromatic five-membered heterocycles, including furan, thiophene, oxazole, and thiazole (**Figure 2.1**). Nucleosides **2.2a-d** incorporated into oligonucleotides, among them the furan analogue **2.2a** was exposed to positively signal in the presence of DNA abasic sites.

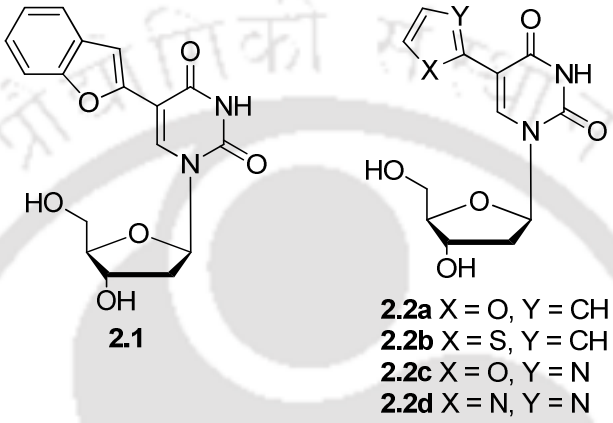

Figure 2.1. Chemical Structure of nucleoside **2.1** and **2.2a-d**.

Eight novel nucleosides dA^R, dU^R and nucleoside triphosphates dA^RTP, dU^RTP bearing multimode fluorescent and ^{19}F NMR detectable BIF, BFU, BOX, and ABOX (**Figure 2.2**) labeling groups were designed and prepared by single-step aqueous cross-coupling reactions of halogenated nucleosides or dNTPs with biarylboronates by Riedl[20c] *et.al*., The fluorophores incorporated to DNA are able to sense the changes in the structure of the DNA strand by the increased intensity in fluorescence during the transformation from hairpin to double strand, which has been confirmed simultaneously by ^{19}F NMR measurement. The fluorophores are also able to detect the site-specific single nucleotide mismatches in the G-rich sequence by decreased fluorescence intensity. However, the effects are sequence dependent. The best fluorophore for study of structural changes is dU^{BFU}, which is only slightly fluorescent when exposed to water (hairpin or deletions) but gives good emission in ss- or ds-DNA. The most electron-donating flanking guanosine nucleotides cause decreasing dU^{BFU} fluorescence and quenching of the dU^{BOX} and dU^{ABOX} violet emissions. Several modifications dA^{BIF}, dA^{BOX}, and dU^{BFU} showed base-discrimination in the sequence containing adjacent guanosine and thus could be used for mismatch detection in electron-donating flanking sequences.

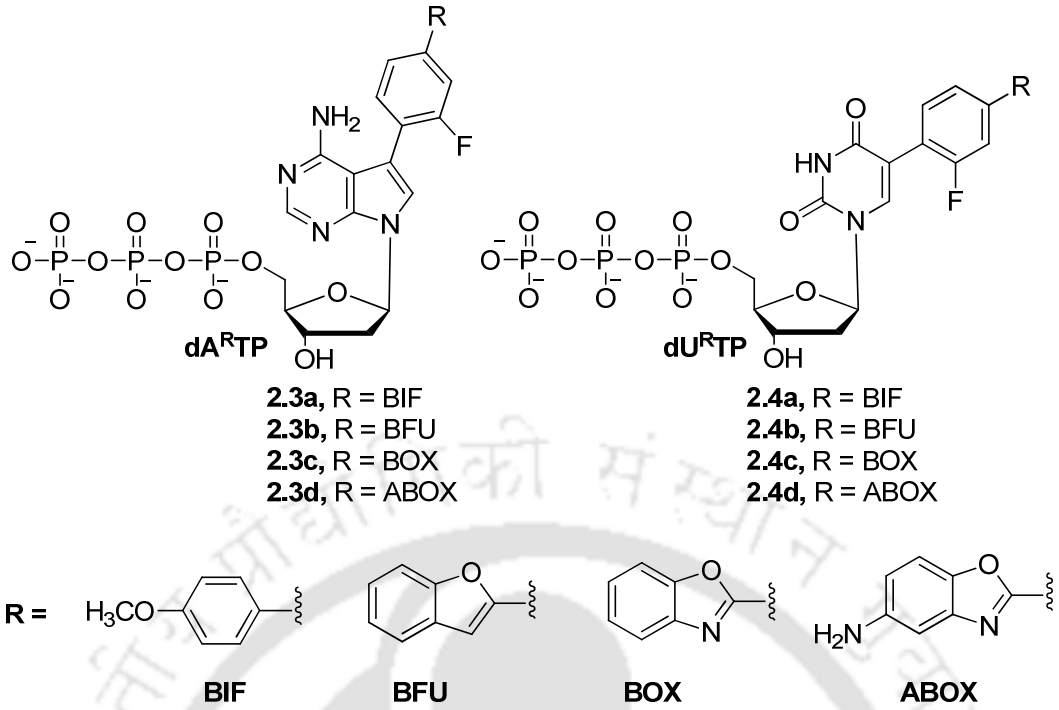

Figure 2.2. Structure of nucleoside triphosphates dA^{R}TP and dU^{R}TP and their R groups.

Ehrenschwender[20d] *et. al*., exploited 4,4-Difluoro-4-bora-3a,4a-diaza-s-indacene (BODIPY) as a fluorescent label could be incorporated into DNA by two conceptually different ways: the non-nucleosidic DNA base surrogate Bo, **2.6** (**Figure 2.3**) exhibited high brightness but no preferential base pairing properties, whereas the BODIPY-modified uridine BodU, **2.5** (**Figure 2.3**) has reduced quantum yields but showed preferred Watson-Crick base pairing with adenine.

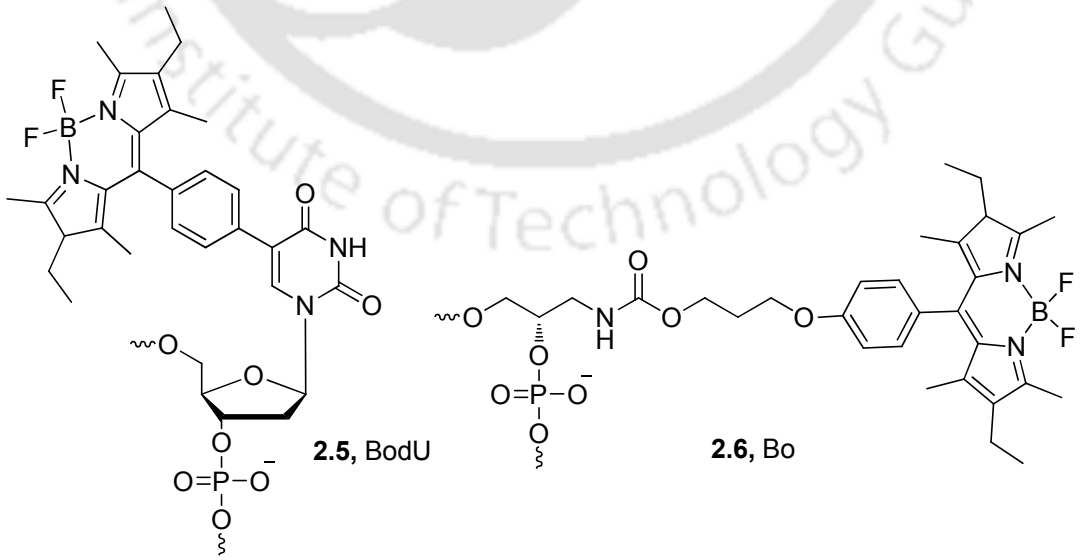

Figure 2.3. Structure of **BodU, 2.5** and **Bo, 2.6.**

Jacobsen[20e] *et al*., explored the synthesis of an AQ-dU nucleoside **2.7** (**Figure 2.4**) with conjugation between the anthraquinone and the uridine moiety. Nucleoside **2.7** exploited in studies of charge transfer processes in DNA and incorporated into oligonucleotides, and electrochemical studied of their used for detection of complementary oligonucleotides. The covalently attached anthraquinone to the uridine moiety induced a strong electronic interaction evident from the bathochromic shift of absorbance between **2.7** and pure anthraquinone (e.g. λ_{max} (anthraquinone) = 324 nm → λ_{max} (**2.7**) = 365 nm).

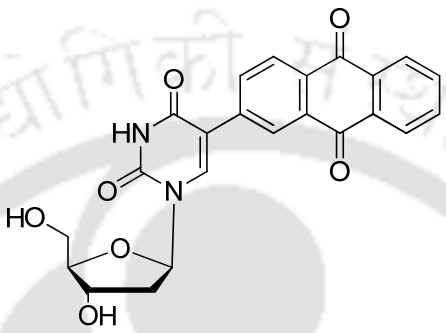

2.7, AQ-dU nucleoside

Figure 2.4. Structure of AQ-dU nucleoside **2.7.**

2.2. Background

Hybridization sensitive fluorescent DNA labels have attracted immense research interest in investigating interbiomolecular interactions in DNA and nucleic acid analysis, such as the detection of single nucleotide polymorphisms (SNPs). Creation of such kind of hybridization sensitive probe nucleoside can be achieved either by attaching an organic chromophore via a rigid acetylenic linker or a more compact single C–C covalent bond to DNA bases. Several such probes with fluorophore attached via an acetylenic linker have been reported successfully for the detection of SNPs. However, to attain higher sensitivity, there is still a great demand for the further development of newly designed base modified ESF nucleosides possessing a stronger fluorescence emission with a larger Stokes shift. The directly linked aromatic organic chromophores are expected to possess strong electronic coupling with the π-electron cloud of the nucleobases which would install modulated optical property into the nucleoside. Since long, organic chromophores via multiple C–C covalent bonds have been used to link with DNA bases as label and utilized for genetic analysis. However, less attention was paid for the synthesis of oligonucleotide probe with more compact fluorescence nucleoside useable for the detection of SNPs.

2.3. Objective

From the literature study and above background it is revealed that there exist only two few examples of organic chromophores, such as anthraquinone and pyrene which are directly linked with 2′-deoxyuridine via a single C–C bond and have been utilized for DNA detection or studying DNA mediated charge transport processes. To the best of our knowledge, directly linked naphthalene or its derivatives are not reported as a probe of DNA analysis. Moreover, there is no report in the design of single C–C linked fluorophore labeled solvatochromic nucleoside that discriminates between the bases of a target DNA opposite of the labeled nucleoside of the probe DNA via a shift in emission wavelength along with distinctly enhanced emission intensity. We expected that strong electronic coupling between aromatic chromophore linked directly via a single C-C bond and the uridine nucleus would yield modulated optical properties and if incorporated into a DNA could sense the opposite base of a target DNA via a change in absorption and emission light.

With this above background, idea and as a part of our ongoing research effort for the design of microenvironment sensitive fluorescent nucleoside and to get a better discrimination between Watson-Crick base pairing (matched pair) and non-Watson-Crick base pairing (mis-match pair) we decided to explore a new naphthalene-based SNP sensor for use in small DNA oligonucleotides for SNPs genotyping and therefore, we framed our objective as follows:

(a) Synthesis of naphthyl uridine (^{Naph}**U**) and study of solvatochromic property

(b) Incorporation into a short DNA

(c) Study of SNP detection with the fluorescently labeled oligonucleotide probe. Thus, we wanted to study of photophysical properties of naphthalene appended 2`-deoxyurdine incorporated ODN **1**/ODN **9** and their various duplexes formed upon hybridization with complementary fully matched and single base mismatched oligonucleotide sequences.

(d) The DNA sequences wanted to synthesise are: (i) ODN **1**: 5'-d(CGCAAC^{Naph}**U**CAACGC)-3'-containing C/C flanking base pair; (ii) ODN **9**: 5'-d(CGCAAT^{Naph}**U**TAACGC)-3'-containing T/T flanking base pair. This sequence context was so chosen as to test the sequence dependency of the probe in the detection of target DNA (**Figure 2.5**).

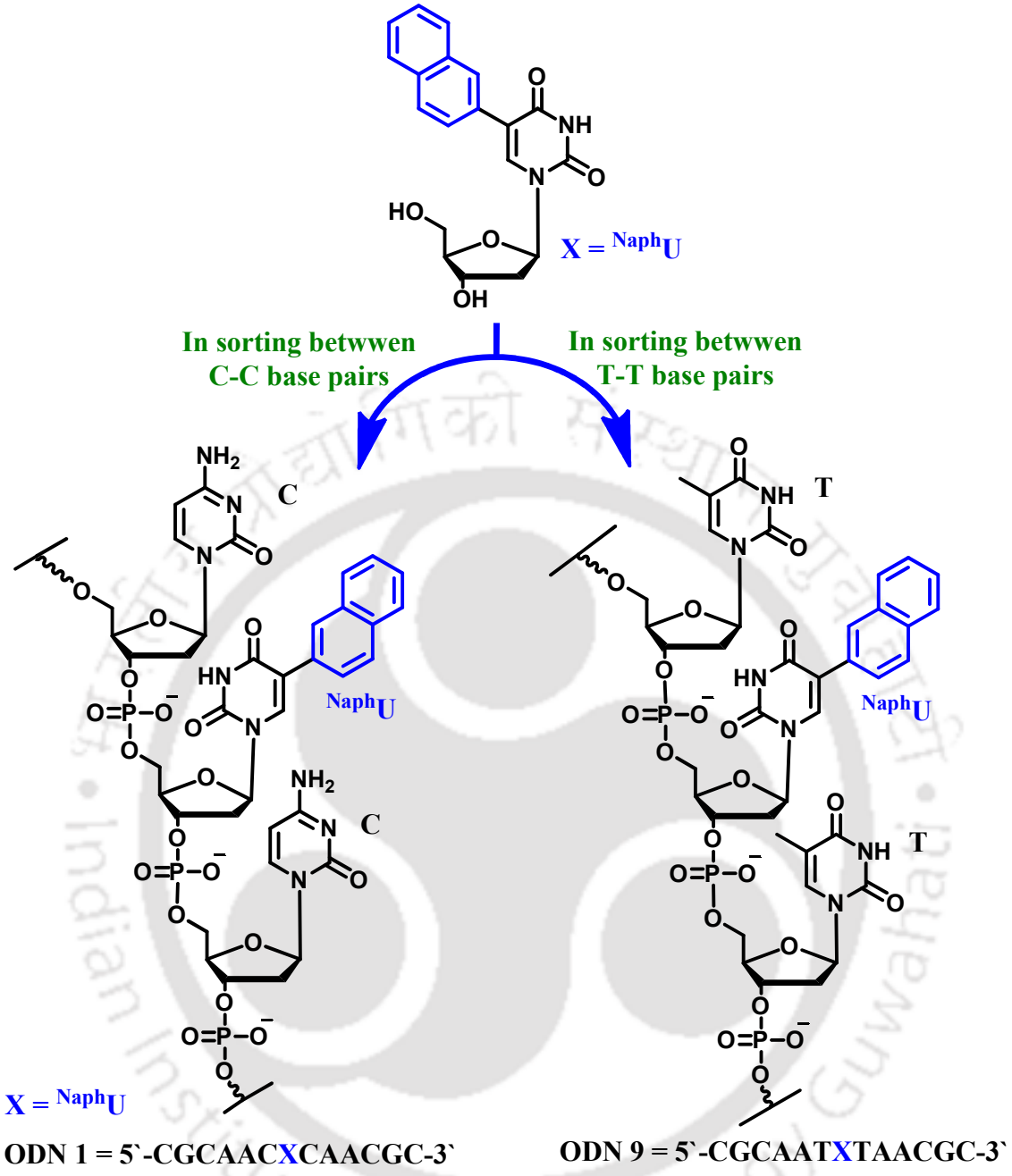

Figure 2.5. Proposed C/C and T/T flanking ^{Naph}U incorporated ODN **1** and ODN **9**.

We envisioned that upon binding with its fully matched complementary sequence, the naphthyl chromophore (^{Naph}U) would emit a strong fluorescence signal. On the contrary, due to lack of Watson–Crick base pairing in the mispaired position in a single base mismatched duplex, the fluorophore would preferably reside inside the duplex and exhibit either very weak or strong fluorescence depending on the nature of the flanking base pair. Thus, with this simple

concept and following the 'Just-Mix & Read strategy' one can just mix the two complementary strands and read the fluorescence signal.

To design of the fluorescently labeled nucleoside we focused on the following design criteria to achieve an environment sensitive fluorescent labelled nucleoside probe which would be able to monitor the local micro-environmental in DNA.

1. The fluorophore should be dielectric sensitive.
2. Emission of the fluorophore should lie in the visible region.
3. Emission must possess high quantum yield in highly polar solvent.
4. Emission and absorption intensities should be so that high fluorescence brightness ($\varepsilon * \Phi_f$) would be observed.

Therefore, with the above design concept we synthesized the naphthyl conjugated nucleoside, ^{Naph}**U** via a Pd(0)-mediated classical Suzuki[18-21] coupling protocol and characterized by NMR and mass spectrometry (**Scheme 2.1**).

2.4. Results and Discussion

Keeping the design criteria of the fluorescent labeled nucleoside in mind we have synthesized a novel naphthalene labeled 2`-deoxyuridine via a Pd (0)-mediated classical Suzuki coupling[18, 20-22] protocol. It was decided that a new naphthalene-based SNP sensor for use in small DNA oligonucleotides should be synthesized. The naphthalene was appended directly to the C-5 position of uridine using classical Suzuki coupling synthetic procedure. The direct link of naphthalene to uridine nucleoside facilitate more electronic cloud on the uridine base. From the early discussed in the introduction section it is clear that, the change in the fluorescence of this type of probes is highly dependent on the geometry that the probe finds itself in under match and mismatch conditions.

2.4.1. Synthesis of Naphthalene Labeled Fluorescent Nucleoside

To synthesis of naphthalene labeled 2`-deoxyuridine fluorescent nucleoside we started with 2-bromonaphthalene which converted to Naphthalene-2-boronic acid pinacol ester (**2.9, Scheme 2.1**). 2-bromonaphthalene under nitrogen atmosphere at 0 °C treated with n-butyl lithium, triisopropyl borate in dry diethylether and the reaction solution was allowed to stir at room temperature for overnight. After treatment with 1:1 Et_2O-5% HCL under reflux condition for about 2h naphthalene-2-boronic acid pinacol ester was afforded. Now taking the purified condition of naphthalene-2-boronic acid pinacol ester treated with 5-iodo-2`-deoxyuridine using tetrakis (triphenylphosphine) palladium (0) in 2:1 MeOH-1M Na_2CO_3 under refluxed

condition for about 6 h in nitrogen atmosphere to afford the desired naphthalene labeled fluorescent nucleoside (**Scheme 2.1**). The final product was isolated pure by column chromatography and characterized by NMR and mass spectrometry which is detail outlined in the experimental section.

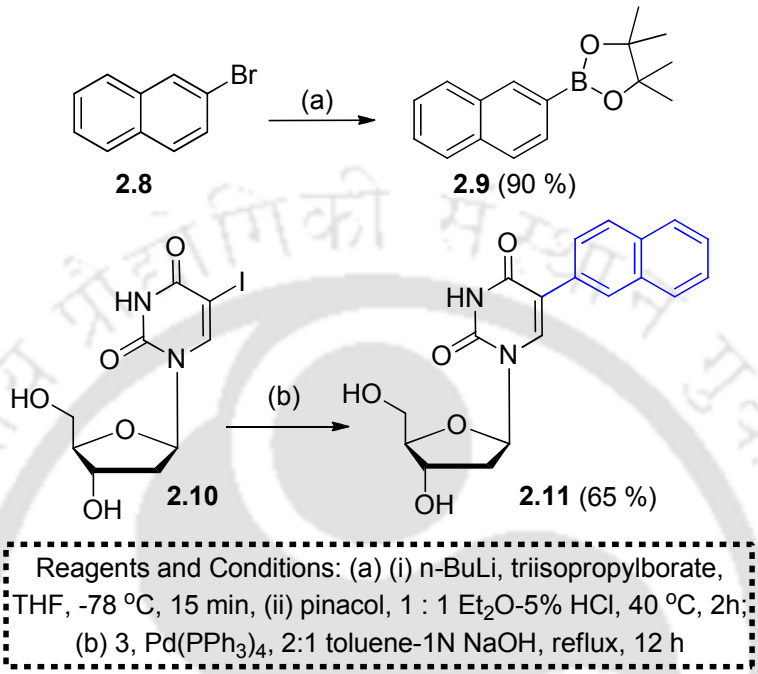

Scheme 2.1. Synthesis of naphthalene labeled fluorescent nucleoside **2.11**.

2.4.2. Study of Photophysical Properties of Naphthalene Labeled Fluorescent Nucleoside

Before going to incorporate into various oligonucleotides and DNA detection study, the spectral properties of ^{Naph}**U**, **2.11** was carried out in different solvent environment varying from non-polar (dioxane) to polar (water). The observed UV-visible spectra showed a little blue shifting pattern with increasing absorption as the polarity of the solvent increases (**Figure 2.6a**). A hypsochromic shift was observed from less polar solvent such as from Toluene (λ_{abs} = 312 nm) to more polar solvent such as methanol (λ_{abs} = 300 nm). Furthermore, ^{Naph}**U** was studied in binary or mixture of solvent like dioxane-water mixture (**Figure 2.7a**). With increasing the percentage of water in dioxane, a decreasing pattern of absorbance with a little blue shift of wavelength. The UV-visible spectrum of **2.11** indicates a strong electronic interaction between the uridine moiety and the covalently attached naphthalene as evident from the bathochromic shift of absorbance between **2.11** and pure naphthalene [e.g. λ_{max} (naphthalene) = 280-290 nm → λ_{max} (**2.11**) = 310-312 nm].

The fluorescence spectra of ^{Naph}U (**2.11**) were measured in various solvents and a mixture of solvent having differing polarity and viscosity. Upon excitation of ^{Naph}U (**2.11**) at 310 nm in a less polar solvent such as 1,4-dioxane (ε = 2.25), a strong emission band was observed at 380 nm as shown in **Figure 2.6b**. Upon excitation of ^{Naph}U (**2.11**) in methanol (ε = 32.7), we observed an emission band was bathochromic shift to 404 nm (**Figure 2.6b-c**). In polar solvents such as water (ε = 80.1), the emission band was red-shifted to 453 nm (**Figure 2.7b-c**). As shown in emission spectra in dioxane-water, **Figure 2.7b**, this broad and bathochromic shift emission band exhibited a typical solvatofluorochromicity, which can be assigned to ICT fluorescence.

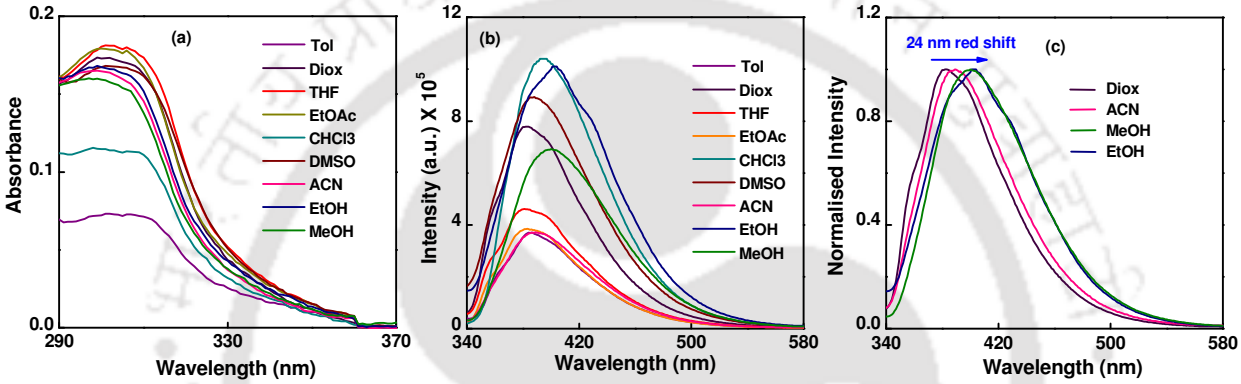

Figure 2.6. (a) UV-visible, (b) fluorescence emission (λ_{ex} = 310 nm) and (c) fluorescence normalised emission of naphthalene linked 2`-deoxyuridine**,** (**^{Naph}U, 2.11**) in different solvent.

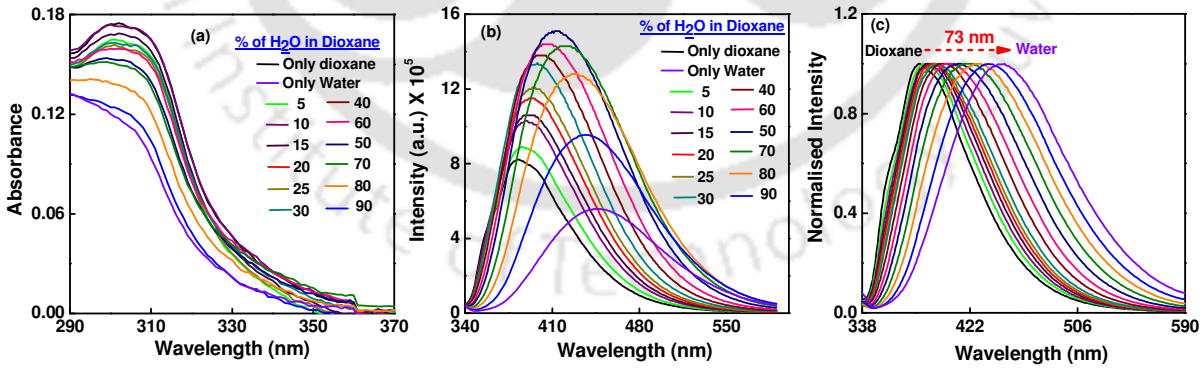

Figure 2.7. (a) UV-visible, (b) fluorescence emission (λ_{ex} = 310 nm) and (c) fluorescence normalised emission of naphthalene linked 2`-deoxyuridine**,** (**^{Naph}U, 2.11**) in dioxane-water mixture of solvent.

In this molecular configuration, a significant large resonance interaction was generated and the emission from the ICT state was observed at longer wavelengths. These results suggest

that ^{Naph}**U** (**2.11**) can be act as a solvatochromic environmentally sensitive fluorescence (ESF) nucleoside and that it exhibits broad ICT emission in low viscosity environments. In contrast, when ^{Naph}**U** (**2.11**) is introduced to restricted spaces such as the narrow DNA groove, and twisted, a blue-shifted LE emission should be observed. The combination of both fluorescence modes expands the emission wavelength range and may enhanced the applicability of ^{Naph}**U** as a sensor molecule. Interestingly, both the fluorescence intensity and wavelength of ^{Naph}**U** were markedly affected by solvent polarity (**Figure 2.6b, 2.7b**). Thus, **Table 2.1** shows the photophysical summary of the nucleoside (^{Naph}**U, 2.1**) in different solvents and **Table 2.2** in dioxane-water mixture of solvent.

Table 2.1. Photophysical summary of the ^{Naph}**U (2.11)** in different solvents

Solvents	λ_{abs}(nm)	ε_{max}(L/mole*cm)	λ_{em}(nm)	Φ_f	ε_{max} X Φ_f
Tol	312	7220	380	0.14	1010.8
Diox	303, 279	17220	380	0.13	2238.6
THF	304, 280	17990	379	0.07	1259.3
EtOAc	303, 278	17850	380	0.06	1071
CHCl3	305, 281	11250	395	0.25	2812.5
DMSO	304, 281	16760	388	0.16	2681.6
ACN	301, 278	16670	390	0.07	1166.9
EtOH	302, 277	16851	404	0.20	3370.2
MeOH	300, 278	15940	402	0.15	2391

Table 2.2. Photophysical summary of the ^{Naph}**U (2.1)** in dioxane-water mixture of solvents

% of H_2O in Dioane	λ_{abs}(nm)	ε_{max} (L/mole*cm)	λ_{em}(nm)	$\Delta\lambda_{em}$(nm)	Φ_f	ε_{max} * Φ_f
Dioxane	303	17220	380	0	0.13	2238.6
10	305	17500	390	10	0.17	2975
15	305	16660	394	14	0.19	3165.4
20	304	17590	396	16	0.2	3518
25	305	15780	399	19	0.23	3629.4
30	305	16080	400	20	0.26	4180.8
40	305	13700	405	25	0.29	3973
50	304	15910	410	30	0.32	5091.2
60	303	14930	416	36	0.37	5524.1
70	304	14900	425	45	0.39	5662
80	303	13715	433	53	0.39	5348.85
90	303	12141	439	59	0.34	4127.94
Water	303	11540	453	73	0.23	2654.2

Such an environmentally sensitive fluorescent nucleoside provides a potentially useful tool for structural studies of nucleic acids, as well as for the detection of target genes, and for

SNP typing. Thus, the newly synthesized ESF nucleoside ^{Naph}**U** (**2.11**) was incorporated into oligodeoxynucleotides via automated DNA/RNA synthesis and their thermal stability and photophysical properties were assessed.

2.4.3. Theoretical Calculation

All these spectroscopic properties clearly supported the strong electronic coupling between the two aromatic parts of naphthalene and uridine in ^{Naph}**U** (**2.11**) that were our expectation from the design and theoretical study.[22f] The possibility of electronic coupling between uridine nucleus and the aromatic π-cloud of naphthalene core in ^{Naph}**U** nucleoside was first investigated by a theoretical calculation using Gaussian 03 program package.[19] Thus, based on time dependent density functional (TD-DFT) calculation at B3LYP/6-31G* level of theory we observed that the nucleoside ^{Naph}**U** has a large LUMO coefficient on the carbon at the 2-position of naphthalene that connects to the C-5 of uridine moiety. Moreover, a significant amount of LUMO coefficient was present on the ⟩C=O and ⟩C=C⟨ functionalities of uridine nucleus (**Figure 2.8**). The significant overlap of the uridine acceptor and naphthalene donor orbitals supported the strong electronic coupling between them. Therefore, the nucleoside ^{Naph}**U** reasonably would show modulated optical properties upon incorporation into short oligonucleotide sequence and can sense DNA microenvironment via a change in absorption/emission intensity and wavelength.

The emissive state of the nucleoside ^{Naph}**U** was characterized with significant electron redistribution, that is, ICT feature as was revealed from the overlapping of HOMO–LUMO as well as the transition oscillator strength. Thus, the calculated excitation energy (in vacuum) for the transition of S0→ S1 of ^{Naph}**U** was found to be 316 nm (with $f = 0.17$ and $CI = 0.522$) which was in close agreement with the experimental result of 312 nm (in toluene). As the naphthalene is electronically coupled with the aromatic system of the uridine nucleus we expected that ^{Naph}**U** would be usable for sensing the dielectric property of the local microenvironment in DNA via the shift in wavelength of emission and enhanced intensity.

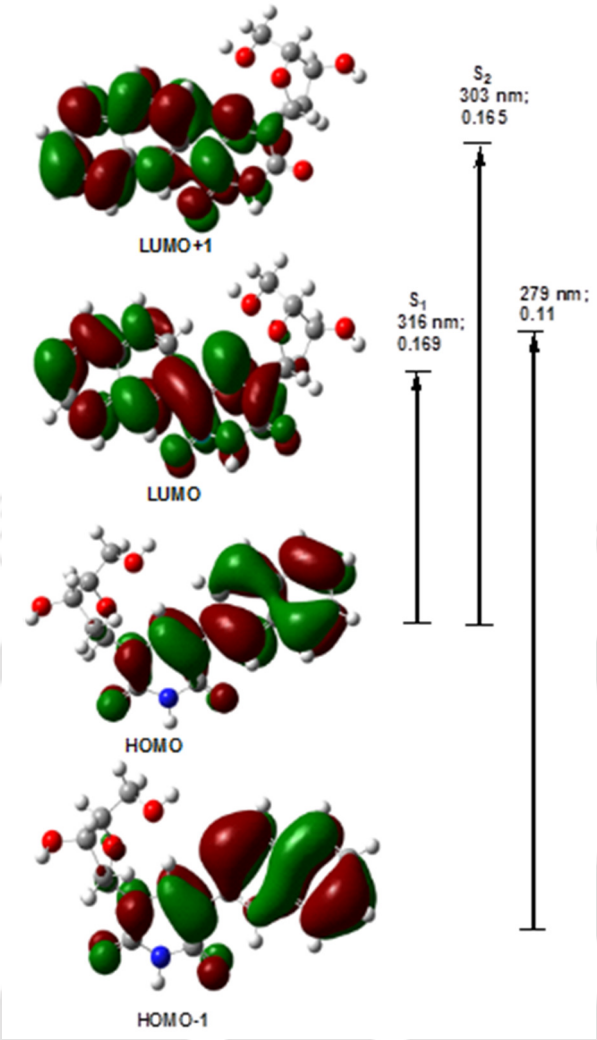

Figure 2.8. MO diagram with electronic transition of compound ^{Naph}**U (2.11).**

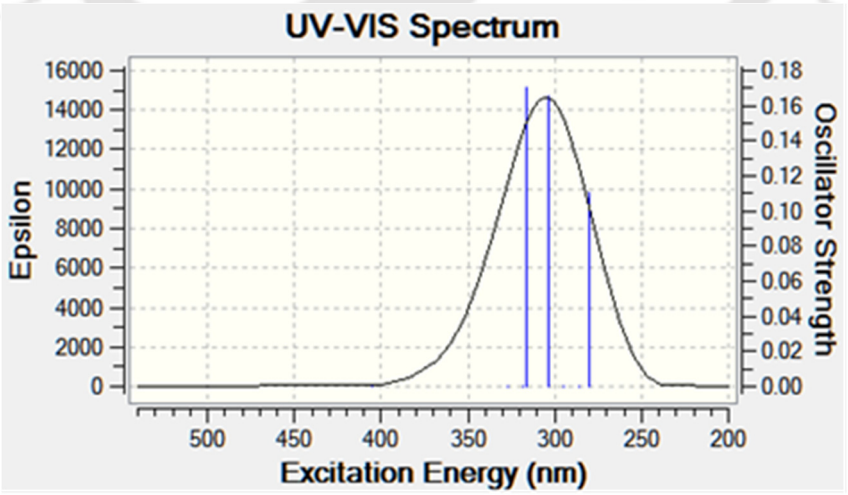

Figure 2.9. Calculated UV-Visible spectrum of nucleoside ^{Naph}**U (2.11)**.

Table 2.3. Summary of TD-DFT calculation

Entry	Electronic transition	Energy (eV) (wavelength)	*f*	Composition	CI
^{Naph}U (2.11)	$S_0 \rightarrow S_1$	3.9188 eV 316.38 nm	0.1699	HOMO → LUMO (93 → 94)	0.52167
	$S_0 \rightarrow S_2$	4.0892 eV 303.20 nm	0.1657	HOMO-1 → LUMO (92 → 94)	0.29483
	$S_0 \rightarrow S_1$			HOMO → LUMO (93 → 94)	0.38393
	$S_0 \rightarrow S_2$			HOMO → LUMO+1 (93 → 95)	0.43602
	$S_0 \rightarrow S_2$	4.4309 eV 279.82 nm	0.1101	HOMO-1 → LUMO (92 → 94)	0.45489

Center Number	Atomic Number	Atomic Type	Coordinates (Angstroms) X	Y	Z
1	1	0	1.01037	-3.345195	0.320648
2	8	0	1.710351	-2.679940	0.399486
3	6	0	2.724823	-2.967772	-0.561885
4	1	0	2.306621	-3.023214	-1.576801
5	1	0	3.218624	-3.926818	-0.340326
6	6	0	3.769662	-1.860974	-0.532071
7	1	0	4.596201	-2.151033	-1.191978
8	8	0	3.198049	-0.640099	-1.027049
9	6	0	3.277361	0.392467	-0.050814
10	1	0	4.074616	1.094966	-0.297927
11	7	0	2.035104	1.172680	-0.096953
12	6	0	0.819212	0.525211	-0.094482
13	1	0	0.902229	-0.552928	-0.021055
14	6	0	-0.389838	1.147924	-0.170433
15	6	0	-0.393382	2.617462	-0.226525
16	8	0	-1.367236	3.356077	-0.256908
17	7	0	0.894857	3.184576	-0.245105
18	1	0	0.923759	4.196928	-0.292952
19	6	0	2.128973	2.564330	-0.185304
20	8	0	3.184514	3.177117	-0.190043
21	6	0	4.344397	-1.543210	0.862694
22	1	0	4.218764	-2.385217	1.556526
23	6	0	3.531870	-0.316959	1.287464
24	1	0	2.585738	-0.635046	1.734441
25	1	0	4.060514	0.324250	1.999946
26	8	0	5.724334	-1.242576	0.665738
27	1	0	6.091888	-0.954176	1.515927
28	6	0	-1.649019	0.369901	-0.210975
29	6	0	-2.838323	0.867865	0.298414
30	6	0	-1.655131	-0.940428	-0.781196
31	6	0	-4.033061	0.102733	0.280210
32	1	0	-2.867222	1.869017	0.710865

33	6	0	-2.795363	-1.705227	-0.807112
34	1	0	-0.744594	-1.327602	-1.229745
35	6	0	-5.253495	0.608980	0.805710
36	6	0	-4.018991	-1.216134	-0.276697
37	1	0	-2.778131	-2.695171	-1.258181
38	6	0	-6.401526	-0.150620	0.781029
39	1	0	-5.263616	1.611655	1.226158
40	6	0	-5.219105	-1.973832	-0.290367
41	6	0	-6.385117	-1.454667	0.227402
42	1	0	-7.327709	0.249272	1.185044
43	1	0	-5.203325	-2.973682	-0.718680
44	1	0	-7.298228	-2.043733	0.212340

2.4.4. Synthesis and Characterization of the Oligonucleotide Probe

Therefore, to establish our expectation the nucleoside ^{Naph}**U** was next incorporated into short 13-mer oligonucleotide sequence containing cytosine as the flanking base for DNA detection via standard DNA synthesis protocol in an automated DNA/ RNA synthesizer (**Scheme 2.2, Table 2.4**). The ODN was purified and characterized by MALDI-TOF mass spectrometry (**Table 2.4**). Therefore, from the photophysical study of the fluorescent nucleoside revealed that the nucleoside is environment sensitive and could potentially be used for SNP sensing in DNA microenvironment. After observing the excellent photophysical property of naphthalene appended uridine nucleoside in different solvent condition we being interested to incorporate into short oligonucleotide sequences. To do the oligonucleotide synthesis, we first protected the 5'-OH of the nucleoside ^{Naph}**U, 2.11** with 4,4′-dimethoxytrityl group by reaction with 4,4′-dimethoxytrityl chloride in presence of catalytic amount of *N, N*-dimethylamino pyridine (DMAP) in dry pyridine solvent. The 5'-DMTr protected nucleoside **2.12** was isolated pure by a silica gel column chromatography using 20:1 methanol-chloroform solvent mixture and characterized by NMR and mass spectrometry. Next, the DMTr protected nucleoside **2.12** was converted to its phosphoramidite derivative **2.13** by reaction with 2-cyanoethyl-*N,N,N',N'*-tetraisopropyl-diphosphoramidite in presence of (1*H*)-tetrazole in anhydrous acetonitrile under nitrogen atmosphere. The phosphoramidite derivative **2.13,** so produced was used for the DNA synthesis without further purification (**Scheme 2.2**).

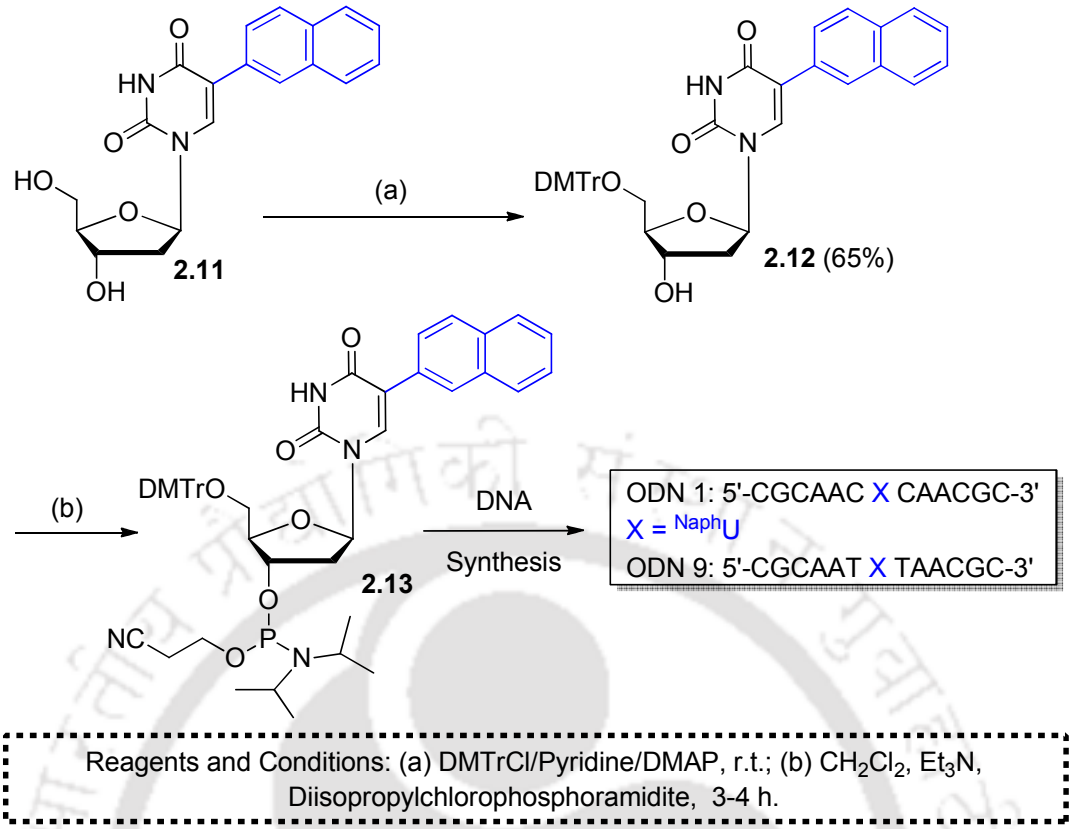

Scheme 2.2. Synthesis of fluorescently labeled ODNs.

Table 2.4. Synthesized fluorescently labeled ODNs and their MALDI-TOF MS

ODNs	Sequence	MALDI-TOF mass calcd. $[M+1]^+$	MALDI-TOF mass calcd. $[M+1]^+$
1	5'-d(CGCAAC ^{Naph}**U**CAACGC)-3'	4001.75	4002.60
9	5'-d(CGCAAT ^{Naph}**U**TAACGC)-3'	4031.76	4031.61

Finally, using naphthalene labeled nucleoside, 13-mer oligomer ODN **1**, and ODN **9** were synthesized via standard DNA synthesis protocol using an automated DNA/RNA synthesizer. ODN **1** synthesized in such a way that, the naphthalene labeled uridine will have flanked in-between G/C bases after hybridized to duplex formation and that of ODN **9** will have flanked in-between A/T bases after hybridized to duplex formation. After the synthesis ODNs were purified by reversed phase HPLC and characterized by MALDI-TOF mass spectrometry (**Figure 2.10, Table 2.4**). Thus, 13-mer ODN **1** and **9** contained singly labeled ^{Naph}**U** and differed only by flanking bases near the labeled nucleoside (ODN **1** contained C, while ODN **9** contained T as the flanking bases). As was mentioned earlier, while ODN **1** and ODN **9** were synthesized to test the sequence dependency in DNA detection.

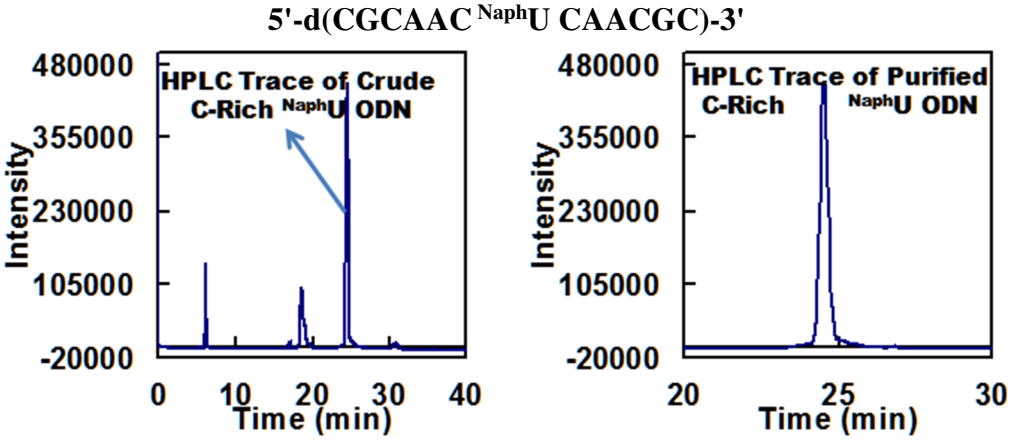

Figure 2.10. HPLC traces of synthesized crude and purified oligonucleotide probe containing fluorescent nucleoside, ^{Naph}**U**.

Synthesized ODNs were purified by reverse phase HPLC on a 5-ODS-H column (10×150 mm, elution with 50 mM ammonium formate buffer (AF), pH 7.0, linear gradient over 45 min from 3% to 40% acetonitrile at a flow rate 2.0 ml/min). The ODNs purified by HPLC were characterized by MALDI-TOF mass spectrometry. The calculated masses of the ODNs are in good agreement with the experimentally found masses. **Table 2.4** shows the calculated MALDI-TOF masses and experimentally found MALDI-TOF mass data of the synthesized ODNs.

2.4.5. DNA Detection by Measuring Photophysical Properties

2.4.5.1. Spectral Study of ODN 1 and ODN 9 with Its Various Duplexes

After synthesizing ODN **1** and ODN **9**, the UV-visible absorption and fluorescence emission properties of the single strand ODN **1** with its various duplexes formed by hybridization with various complementary ODNs were carried out (**Table 2.5**). Thus, from the UV–visible spectra (**Figure 11a-b**), the single base mismatched duplexes of ODN **1** exhibited a bathochromic shift along with a hypochromic effect in comparison to the corresponding single strand ODN **1** (**Figure 2.11b, Table 2.6**). In contrast, the fully matched duplex ODN **1•2**, ^{Naph}**U/A** base pair showed minimal hypsochromic shift (ODN **1**, λ_{max} = 313 nm → OND **1•2**, λ_{max} = 310 nm) in absorption band with a little hyperchromicity (**Figure 2.11b**). This was might be due to in the mismatched duplexes the rotation of ^{Naph}**U** of probe ODN **1** lead to pairing between the mismatched base of the target ODN **3**–**7** and naphthyl unit of probe ODN **1** resulting in an intercalation of naphthyl moiety between the base stack. This intercalation reasonably was more prominent when the opposite base of target ODN was an

abasic site (Φ) wherein the bathochromic shift and hypochromism was maximum. For the fully matched duplex ODN **1•2**, this clearly supported that ^{Naph}**U** of probe ODN **1** involved in Watson–Crick base pairing with the opposite matched base adenosine of target ODN **2**. Thus, rigid naphthyl unit extorted pointing along the groove site of compact hydrophobic environment.[24]

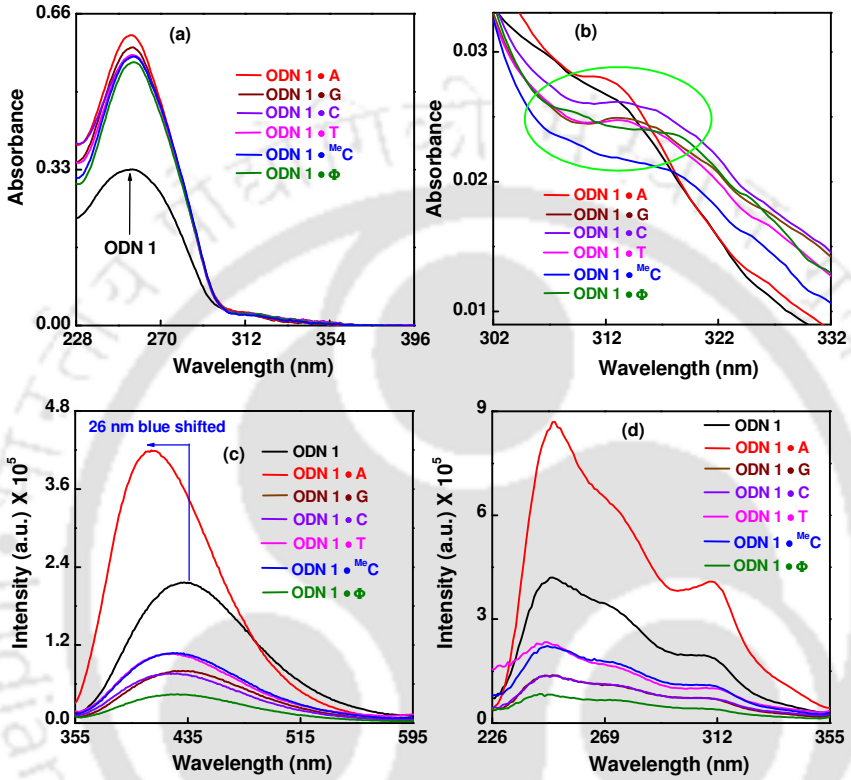

Figure 2.11. (a) UV-visible, (b) expanded UV-visible (302nm to 332 nm), (c) emission and (d) excitation spectra of probe oligonucleotide (ODN **1**) containing nucleoside, ^{Naph}**U**, and its various duplexes with natural bases A, G, C, T and ^{Me}C and Abasic DNA (Φ).

Table 2.5. Oligonucleotide sequences used for DNA detection study

Entry	Sequence (5`→3`)
ODN **1**	CGCAAC^{Naph}**U**CAACGC
ODN **2**	GCGTTG**A**GTTGCG
ODN **3**	GCGTTG**G**GTTGCG
ODN **4**	GCGTTG**C**GTTGCG
ODN **5**	GCGTTG**T**GTTGCG
ODN **6**	GCGTTG^{Me}**C**GTTGCG
ODN **7**	GCGTTG**Φ**GTTGCG
ODN **8**	CGCAAC**T**CAACGC

Table 2.6. Summary of photophysical propertiies of probe oligonucleotide (ODN **1**) containing nucleoside, ^{Naph}**U**, and its various duplexes with A, G, C, T and ^{Me}C and AP site (Φ)

Entry	λ_{abs} (nm)	$\Delta\lambda_{abs}$ (nm)	λ_{em} (nm)	$\Delta\lambda_{em}$ (nm)	Φ_f	Anisotropy
ODN **1**	313	---	434	---	0.054	0.12
ODN **1•A**	**310**	**-3**	**408**	**26**	**0.088**	**0.24**
ODN **1•G**	318	5	432	2	0.023	0.17
ODN **1•C**	318	5	424	10	0.02	0.1
ODN **1•T**	317	4	421	13	0.03	0.18
ODN **1•^{Me}C**	317	4	427	7	0.014	0.15
ODN **1•Φ**	319	6	429	5	0.034	0.11

Being interested by the solvent polarity dependent fluorescence property of the fluorescent nucleoside (**2.11,** ^{Naph}**U**), we thought that ^{Naph}**U** would be usable for monitoring the change in DNA microenvironment. Therefore, we studied the fluorescence properties of single stranded ODN **1**, (5′-CGCAAC ^{Naph}**U** CAACGC-3′) in the presence and absence of their various complementary strands. As revealed from the fluorescence spectra (**Figure 2.11c** and **Table 2.6**) the fluorescence spectrum of the duplex, ODN **1•2** containing a ^{Naph}**U/A** base pair showed a strong enhanced emission at 408 nm on excitation at 310 nm which was Hypsochromic shift to 26 nm (ODN **1**, λ_{max} = 434 nm → OND **1•2**, λ_{max} = 408 nm). In contrast, the fluorescence of duplexes, ODN **1•3-7** containing ^{Naph}**U/N** base pairs (N = C, G, T, ^{Me}C or Φ) showed drastically quenched fluorescence emission. This might be because of the intercalate of naphthyl moiety between the flanking GC/GC base pair which was also supported from the shift in UV–visible spectra. This fluorescence quenching, along with spectral blue shift, might be attributable to a combination of an electron transfer process between the fluorescent nucleoside and adjacent guanosine residues,[25, 26] a desolvation effect[27] and alterations in the conformation of the naphthalene moiety relative to the nucleobase.[28] Moreover, all the duplexes exhibited blue shifted emission compared to their corresponding single stranded ODN **1**. Most notably, the blue shift in emission wavelength was maximum (26 nm) in case of the fully matched duplex ODN **1•2**. Therefore, the probe ODN **1** having GC/GC flanking pair was able to detect matched adenosine base of the target ODN **2** opposite of labeled base ^{Naph}**U** of probe ODN **1** via the generation of a distinct, drastically enhanced and maximally blue shifted fluorescence signal. The drastic change in fluorescence emission intensity along with a maximum blue shift of wavelength for perfectly matched duplex ODN **1•2** perhaps the naphthyl moiety located in the compact hydrophobic microenvironment pointing toward the

groove of the duplex. Similar result of blue shifting (13 nm) was also observed with other fluorescent probe ODN **9** (ODN **9**: 5`-CGCAAT $^{Naph}$**U** TAACGC-3`) containing –T– flanking base which showed reasonably non-discriminating fluorescence enhancement upon pairing with any of the complementary target ODNs (**Figure 2.12**). In case of all mismatched duplexes the naphthyl moiety, similar to the case of GC/GC flanking pair sequence, also involved in intercalation between the flanking non-quenching AT/AT base pair. However, in contrast to the GC/GC flanking base pair (**Figure 2.11c**), the non-quenching nature of AT/AT flanking pair resulted in enhanced fluorescence signals from all the mismatched duplexes comparable to the intensity of the signal generated from fully matched duplex (**Figure 2.12**). This was so obvious and a positive result of our expectation that the flanking GC/GC base pair is responsible for the quenching of ^{Naph}**U** fluorescence. Thus, ^{Naph}**U** could potentially be useful in designing G-quenched molecular beacon as well.

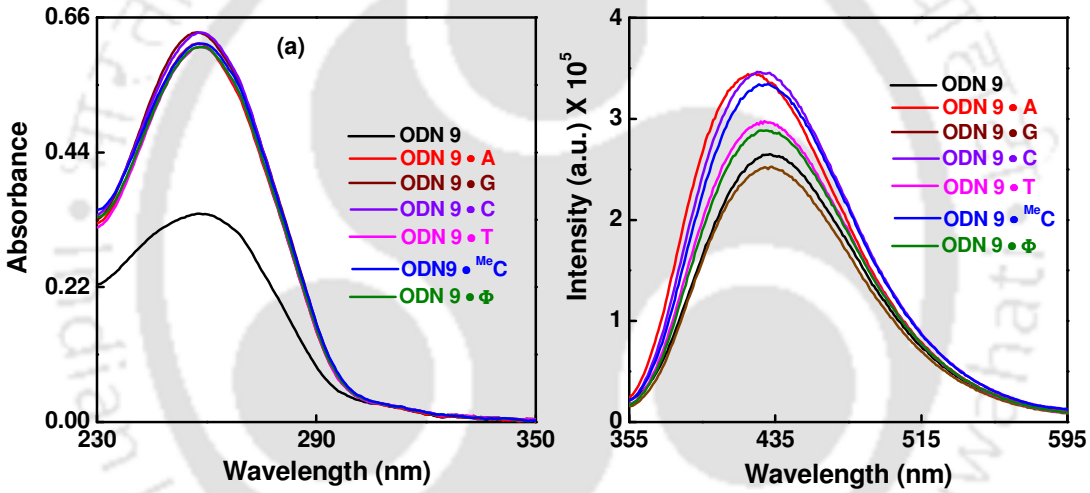

Figure 2.12. (a) UV-visible, (b) emission spectra of probe oligonucleotide (ODN **9**) containing nucleoside, ^{Naph}**U**, and its various duplexes with natural bases A, G, C, T and ^{Me}C and Abasic DNA (Φ).

It is worth noting that the nucleoside labels attached via multiple C–C covalent bonds and flanking between GC/GC base pair were found to be unable to generate discriminating fluorescence signal in sensing of opposite base of target DNAs which might be because of quenching of fluorescence by GC/GC flanking base pair.[29h,i,l, 30b] On the contrary and very interestingly, in spite of flanked between GC/GC base pair, our present probe ODN **1** is capable of sensing opposite matched base –A– of target ODN **2** with a clear discriminating signal to noise ratio (S/N = 2.0). This might be because of more rigid disposition of the labeled nucleoside ^{Naph}**U** compared to the nucleoside labeled with fluorophore via multiple C–C bonds

within the duplex. Though, the present probe relies on the light of excitation in the UV–region, the concept of wavelength shift-guided DNA detection and our inspiring result would shed light for the design of more of such long wave length emissive probe which could be utilized for DNA detection even under the quenching environment of GC/GC flanking base pair.

2.4.5.2. Evaluation of Thermal Stability of the Duplexes Derived from ODN 1

The effect on thermal stability of various duplexes in the presence (modified) and absence (unmodified) of naphthalene were verified. There should be no or minimal effect on the thermal stability for fully matched duplex ODN **1•2** (**^{Naph}U/A**), because the naphthalene moiety was not intercalating between GC/GC flanking bases but it was resides pointing towards the hydrophobic groove site. The comparable thermal melting stability of the fully matched duplex (presence of naphthalene) ODN **1•2, ^{Naph}U/A** (T_m = 59.3 °C) to that of an unmodified duplex (absence of naphthalene) ODN **8•2** (T_m = 58.8 °C) (**Figure 2.13**, **Table 2.7**) completely supported.[23e,f] Thus, we observed that the matched duplexes with modified ODNs ODN **1/A** shows almost same stability with the unmodified one implies naphthlene resides along the hydrophobic compact groove site, as a result there is not marked effect on the duplexes stability (**Figure 2.13**) as well as the helicity of the duplex too (**Figure 2.14**).

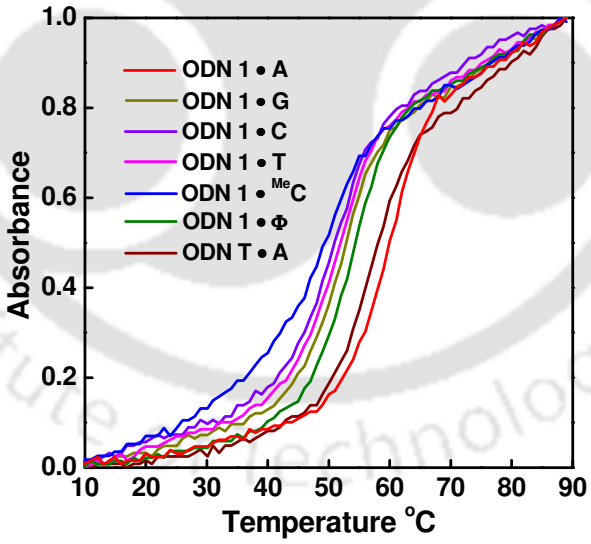

Figure 2.13. *Tm* curve of (ODN **1** = 5'-CGCAAC **X** CAACGC-3') containing nucleoside, **^{Naph}U**(= X), and its various duplexes with natural bases A, G, C, T and ^{Me}C and Abasic DNA (Φ).

Table 2.7. Thermal melting temperatures of duplex ODNs

Duplexes	T_m (°C)
ODN **1•A**	59.3
ODN **1•G**	53.1
ODN **1•C**	53.5
ODN **1•T**	53.4
ODN **1•^{Me}C**	51.3
ODN **1•Φ**	54.2
ODN **2•8**, (**A•T**)	58.8

2.4.5.3. Circular Dichroism Measurement

To know about the spatial disposition of the naphthyl chromophoric moiety inside the duplex, we examined the global property of all possible duplexes using circular dichroism (CD) spectroscopy. Thus, all spectra showed a positive band at around λ = 281–285 nm and a negative band at around λ = 250–252 nm of varying magnitude with intersection at around λ = 263–265 nm (**Figure 2.14**) which is the characteristic CD spectra of B-DNA. Thus, CD spectra reflected that the naphthyl unit of ^{Naph}**U** stabilized B-form conformation of the duplexes. The fully matched duplex ODN **1•2** showed a distinct CD signal with a 4 nm blue shift of positive band of highest intensity indicating a strong stacking interaction between naphthyl unit of ^{Naph}**U** and the base pairs of duplex. The induced CD signal between 300–330 nm corresponding to the chromophores' absorption band supported that the conformational freedom of naphthyl moiety was restricted in the groove in case of fully matched duplex (ODN **1•2**, ^{Naph}**U/A**) and inside the duplex upon intercalation in case of single base mismatched duplexes (ODN **1•3-6**) and abasic duplex (ODN **1•7**) (**Figure 2.14**).[31] This observation was also supported by the increase in fluorescence anisotropy of the duplexes (**Table 2.6**) in comparison to the single strand probe ODN **1**.

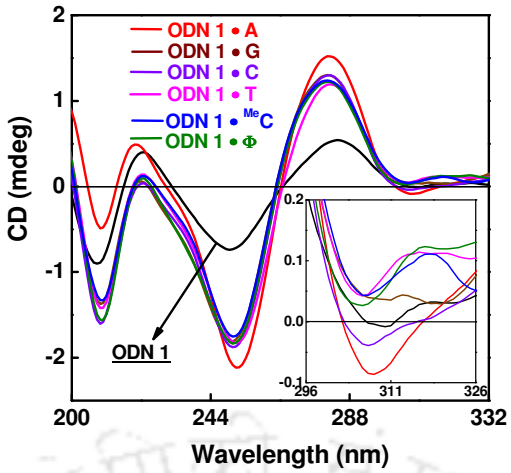

Figure 2.14. (a) Circular Dichroism (CD) and (b) Induced CD spectra of probe oligonucleotide (ODN **1**) containing nucleoside, ^{Naph}**U**, and its various duplexes with natural bases A, G, C, T and ^{Me}C and Abasic DNA.

2.4.5.4. Molecular Modeling Study

To support the experimental result, we carried out the molecular modeling study of the duplexes (fluorescently labeled ODNs and the complementary ODNs) by MacroModel calculation (Maestro vs. 9.0) using AMBER* force field in water. Thus, the optimized structure of duplex ODN **2•8** [N = A] showed that the fluorophore resides along the major groove and thus it would experience more hydrophilic environment (**Figure 2.15**). As a result, a strong fluorescence emission would be expected. On the other hand, as the fluorophore resides along the major groove it brings no affect on stability of the duplex (ODN **2•8** [N = A]). Both molecular modeling and photophysical studies strongly support expected result.

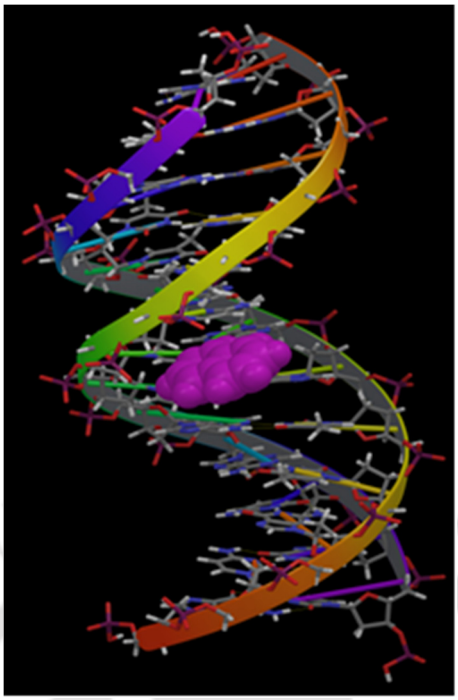

Figure 2.15. AMBER* energy minimized conformations in water of the duplex ODN **1•2**.

2.5. Conclusion

In conclusion, we established that the strong electronic coupling between naphthalene π-cloud and uridine nucleus linked via a single C–C bond led to a modulated photophysical property in ^{Naph}**U** which was explored, for the first time, in DNA detection. The oligonucleotide probe containing ^{Naph}**U** was found to be highly specific for the detection of matched base adenosine of a target DNA opposite to the labeled base (^{Naph}**U**) of probe DNA via maximum shift in emission wavelength. Interestingly, the probe nucleoside flanking between GC/GC base pair could sense efficiently the presence of opposite matched base –A– of target DNA both via the maximum shift in wavelength and enhancement of intensity of fluorescence signal. The concept of wavelength shift-guided DNA detection is very important and would shed light in the design of long wavelength emissive fluorescent nucleoside which could be applied in cellular DNA detection. Designing more of such probes for DNA detection is our current research focus.

2.6. Experimental Section

^{1}H NMR spectra were measured with a 600 MHz machine; ^{13}C NMR spectra were measured with 100 MHz spectrometer. Coupling constant (*J* value) is reported in hertz. The chemical shifts are shown in ppm downfield from tetramethylsilane, using residual chloroform (δ = 7.24 in ^{1}H NMR, δ = 77.0 in ^{13}C NMR) dimethyl sulfoxide (δ = 2.48 in ^{1}H NMR, δ = 39.5 in ^{13}C NMR), and methanol (δ = 3.30 in ^{1}H NMR, δ = 49.0 in ^{13}C NMR), as an internal standard. FAB masses were recorded on a mass spectrometer.

The reagents for DNA synthesis were purchased from Glen Research and used. Mass spectra of oligodeoxynucleotides were determined with a MALDI-TOF MS (acceleration voltage 20 kV, positive mode) with 2′,3′,4′-trihydroxyacetophenone as a matrix. Concentration was measured from molar extinction coefficient at 260 nm at 80 ºC for all ODNs. All aqueous solutions utilized purified water. Reversed-phase HPLC was performed on reverse phase columns (10 × 150 mm, 4.6 × 150 mm) with a chromatograph, using a UV detector, at 254 nm.

2.6.1 Synthesis and Characterization

Synthesis of 4,4,5,5-tetramethyl-2-(naphthalen-2-yl)-1,3,2-dioxaborolane (2.9): A two-neck 50 mL flask fitted with magnetic stirring bar, was charged with 2-Bromonaphthalene (200 mg,0.97 mmol) under nitrogen atmosphere. Dry Et_2O (6 mL) was added, and the solution was cooled to 0 °C. To this solution was added *n*-butyl lithium (0.5 mL, 15% in hexane, 1.152mmol) drop wise over 5 minutes. The solution was stirred at 0°C for 15 minutes where upon triisopropyl borate (216.66mg, 1.152mmol) dissolved in 5 mL of dry Et_2O was added drop wise to the reaction system. The solution was allowed to warm to room temperature for overnight. After that, pinacol (136.13 mg, 1.152 mmol) and 2 ml of 1:1 Et_2O-5% HCl (0.93 mL HCl in 1 ml Et_2O) was added to the reaction mixture and heated it under reflux for 2 h. The resulted biphasic solution was extracted with Et_2O (3 X 10 mL). This was washed with water (mL), dried over sodium sulfate, and filtered, and the solvents removed under reduced pressure to yield Naphthalene-2-boronic acid pinacol ester (109.2mg, 89%).^{1}H NMR (400 MHz, $CDCl_3$, ppm) δ8.21-8.35 (s, 1H), 7.75-7.85(m, 4H), 7.37-7.50 (m, 2H), 1.2-1.32 (s, 12H), ESI-TOF-MS m/z 254 $[M+H]^+$.

***Synthesis of 5-(2-naphthyl)-2'-deoxyuridine (2.11)*:** To a solution of **2.9** (100 mg, 0.40 mmol), 5-iodo-2`-deoxyuridine (141 mg, 0.40 mmol), and tetrakis(triphenylphosphine) palladium (0) (35 mg, 0.03 mmol) in methanol (10 mL) was added 1 M Na_2CO_3 (5 mL) under nitrogen. The mixture was refluxed for 6 h. The completion of the reaction was monitored by

TLC extracted with ethyl acetate. The organic layer was washed with brine, dried over Na_2SO_4, filtered, and evaporated under reduced pressure. The crude product was purified by silica gel chromatography to provide 5-(2-Naphthyl)-2`-deoxyuridine (92 mg, 65 %). ^{1}H NMR (600 MHz, CD_3OD) δ 8.32 (s, 1H), 8.0 (s, 1H), 7.71-7.76 (m, 3H), 7.55-7.57(dd, 1H, *J* = 10.2 Hz), 7.34-7.37 (m, 2H), 6.27 (t, 1H, *J* = 6.6, 6 Hz), 4.35-4.37 (q, 1H, *J* = 4.8, 3.6 Hz), 3.85-3.87 (q, 1H, *J* = 3, Hz), 3.64-3.74 (ddd, 2H, *J* = 3.0 Hz), 2.25-2.27 (q, 2H, J = 4.8, 1.2, 5.4 Hz); 13C NMR (CD_3OD, DMSO-d6, 100 MHz) δ 41.8, 62.6, 72. 1, 86.9, 86.2, 115.8, 127.4, 127.5, 128.3, 128.7, 128.8, 129.4, 132.0, 134.2, 134.8, 140.2, 151.9, 164.7; ESI-TOF-MS m/z 355 $[M+H]^+$.

Synthesis of 5-(2-naphthyl)-5'-O-dimethoxytrityl-2'-deoxyuridine (2.12): A solution of *5-(2-naphthyl)-2'-deoxyuridine* **2.11**, (201.8 mg, 0.57 mmol) with 4-(dimethylamino) pyridine (catalytic amount) and4,4′-dimethoxytrityl chloride (212 mg, 0.627 mmol) in dry pyridine (6.0 mL) was stirred at room temperature for 16 h. After concentration of the solution to dryness, the residue was purified by silica gel column chromatography to yield the tritylated product as a pale solid (243 mg, 65%).^{1}H NMR (400 MHz) δ6.50-6.55 (dd, 1H, *J* = 2.12 Hz), 4.35-4.4 (m, 1H, *J* = 3.36, 1.12, 3.84 Hz), 3.45-3.48 (m, 1H), 3.27-3.37 (m, 9H, *J* = 4.76, 4.88, 5 Hz), 2.43-2.52 (m, 1H, *J* = 6.96, 6.92,6.60 Hz), 2.57-2.65 (m, 1H), 8.0-8.1 (s, 1H), 6.75-7.65 (m, 20 H). ESI-TOF-MS m/z 657 $[M+H]^+$.

5'-O-dimethoxytrityl-5-naphthyl-2'-deoxyuridine-3'-yl-2-Cyanoethyl N,N-diisopropylphosphoramidite (2.13): To a solution of **2.12** (50.0 mg, 0.076 mmol) and triethylamine (13.8 µL, 0.099 mmol) in anhydrous CH_2Cl_2, 22 µL (0.099 mmol) 2-cyanoethyl *N,N*- diisopropylchlorophosphorodiamidite was added under nitrogen atmosphere. The mixture was stirred at room temperature for 3-4 h. Then the mixture was filtered off and used for oligodeoxynucleotide synthesis without further purification.

2.6.2. Synthesis, Characterization and Concentration Determination of the ODNs

All the reagents for DNA synthesis were purchased from Glen Research. ODNs were synthesized by a conventional phosphoramidite method by using an automated DNA/RNA synthesizer. Synthesized ODNs were purified by reverse phase HPLC on a 5-ODS-H column (10×150 mm). Elution was done with 50 mM ammonium formate buffer (AF), pH 7.0, with a linear gradient over 45 min from 3% to 40% acetonitrile at a flow rate of 2.0 ml/min. The ODNs purified by HPLC were characterized by MALDI-TOF MS (**Table 2.4**). The concentration of each purified ODN was determined from molar extinction coefficient at 260 nm at 80 ^{o}C.

2.6.2.1. Studies on Photophysical Properties of the Nucleoside/Oligonucleotides

2.6.2.1.1. UV-Visible and Fluorescence Measurements of Nucleoside Monomer: The *UV*–visible spectra of the nucleoside monomer (10 μM) were recorded in different organic solvents using a UV-Visible spectrophotometer (Shimadzu UV-2550 UV-visible) with a cell of 1 cm path length at 25 °C. Equal volume of each samples' solution in different solvents were used. The measurements were taken in absorbance mode. The absorbance values of the sample solutions were measured in the wavelength regime of 200–550 nm. All the sample solutions were prepared just before doing the experiment.

The Fluorescence spectra were obtained using a fluorescence spectrophotometer (fluoromax 4) at 25 °C using 1 cm path length cell. The excitation wavelength for monomer was set at $\lambda_{abs,\,max}$ of each solvent and emission spectra were recorded in the wavelength regime of 300–600 nm with an integration time of 0.1 sec. The fluorescence quantum yields (Φ_f) were determined using quinine sulphate as a reference with the known Φ_f (0.54) in 0.1 molar solution in sulphuric acid.

2.6.2.1.2. UV-visible and Thermal Melting Temperature (T_m) Measurements of the Oligonucleotides: All UV-visible and T_m of the ODNs (2.5 μM, final duplex concentration) were measured in 50 mM sodium phosphate buffers (pH 7.0) containing 100 mM sodium chloride. The measurements were taken in absorbance mode a UV-Visible spectrophotometer (Shimadzu UV-2550 UV-visible) with a cell of 1 cm path length. The absorbance values of the sample solutions were measured in the wavelength regime of 200–500 nm. All the sample solutions were prepared just before doing the experiment. Total volume of 120 μL from a stock solution of 700 μL of 2.5 μM concentration for each set was used for UV and *Tm* experiments in 8-micro cell. Absorbance *vs*. temperature profiles were measured at 260 nm using a UV-visible spectrophotometer equipped with a Peltier temperature controller using 1 cm path length cell. The absorbance of the samples was monitored at 260 nm from 5 to 90 °C with a heating rate of 1 °C/min. From these profiles, average method was used to determine T_m values.

2.6.2.1.3. Fluorescence Experiments of the Oligonucleotides: ODNs solutions were prepared as described in UV-visible and T_m measurement experiments. Fluorescence spectra were obtained using a fluorescence spectrophotometer (Fluoromax 4) at 25 °C using 1 cm path length cell. The excitation wavelengths for single strand duplex ODN were set at $\lambda_{abs,\,max}$ (310 nm), and emission spectra were measured in the wavelength regime of 300–600 nm with an integration time of 0.2 sec. All the sample solutions were prepared just before doing the

experiment. Total volume of 500 µL from a stock solution of 700 µL of 2.5 µM concentration for each set was used for fluorescence experiment in 1 ml cell of 1 cm path length. The fluorescence quantum yields (Φ_f) were determined using quinine sulphate as a reference with the known Φ_f (0.54) in 0.1 molar solution in sulphuric acid.

2.6.2.1.4. Circular Dichroism Measurement: CD experiments were performed with a CD Spectropolarimeter (Jasco *J-810* circular dichroism spectropolarimeter) equipped with a Peltier thermoelectric type temperature control system. The data were collected using a 1 cm path length quartz cuvette with scanning from 400 to 190 nm, a time constant of 3 s and a wavelength step size of 0.5 nm at 25°C. The final duplex concentration was 2.5 µM in 50 mM sodium phosphate, 0.1 M sodium chloride, pH 7.0, room temperature.

2.6.3. Macro Model Study

Molecular modeling study of the duplexes (fluorescently labeled ODNs and the complementary ODNs) were carried out by Macro Model (Maestro vs. 9.0) using AMBER* force field in water.

2.6.4. Theoretical Calculations

The ground state structures of the fluorophores were optimized using density functional theory (DFT) with B3LYP functional and 6-31G (d) basis set. The excited state related calculations were carried out with the Time dependent density functional theory (TD-DFT) with the optimized structure of the ground state (B3LYP/6-31G (d)). There are no imaginary frequencies in frequency analysis of all the calculated structures; therefore, each calculated structure is a local energy minimum.

B3LYP/6-31G* Optimized Structure and Energy and Cartesian Co-ordinate of ^{Naph}**U** (**2.11**)

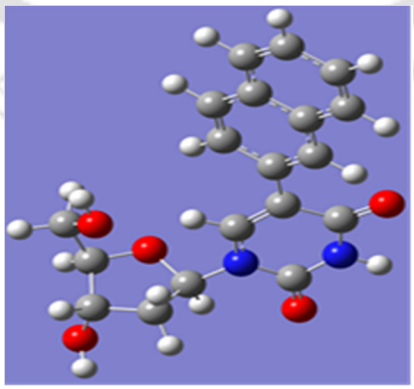

E(UB+HF-LYP) = -1220.50692045 a.u.

2.7. NMR Spectra of ^{Naph}U Nucleoside

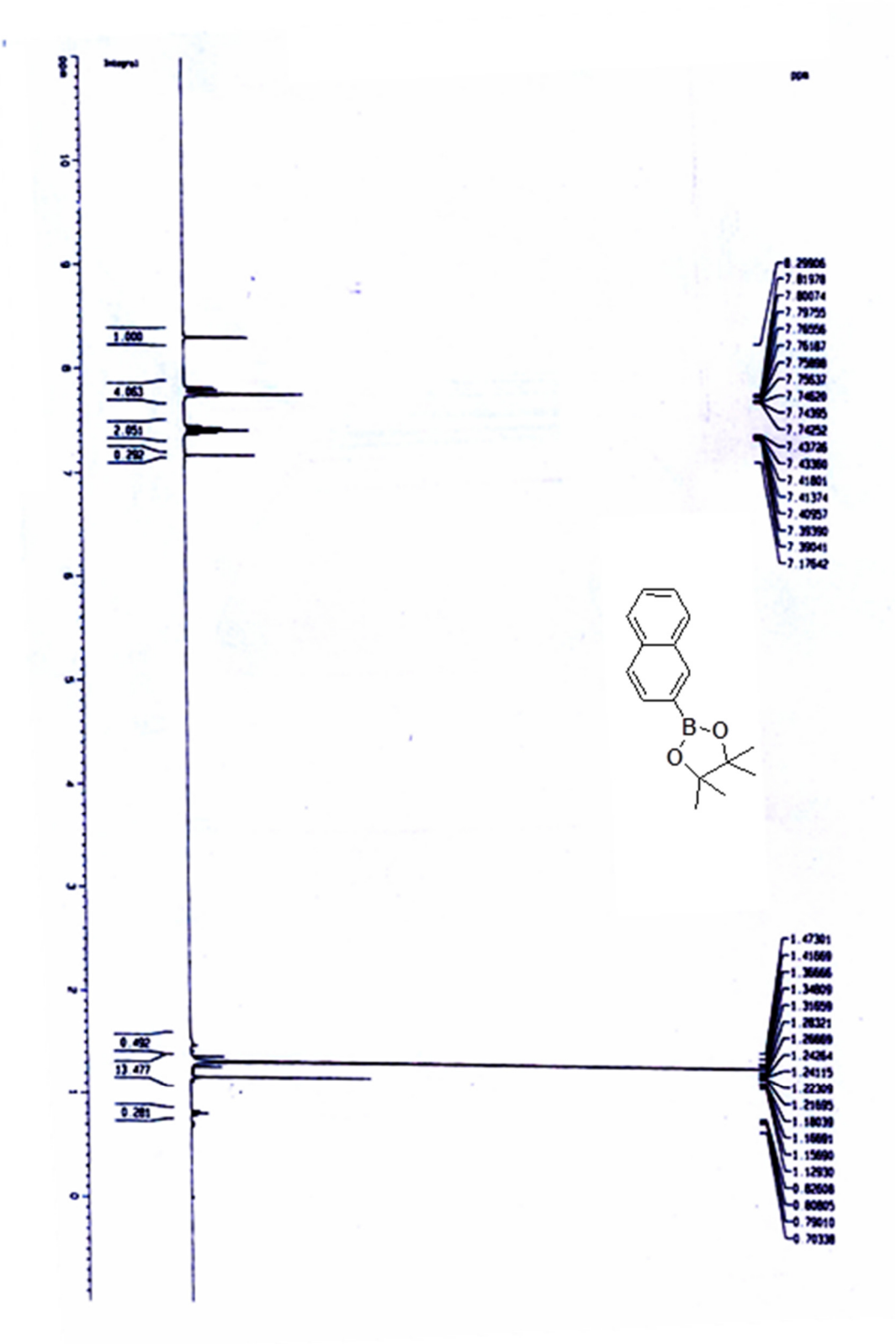

Figure 2.16. ^{1}H NMR spectra of Naphthyl boronic ester (**2.9**).

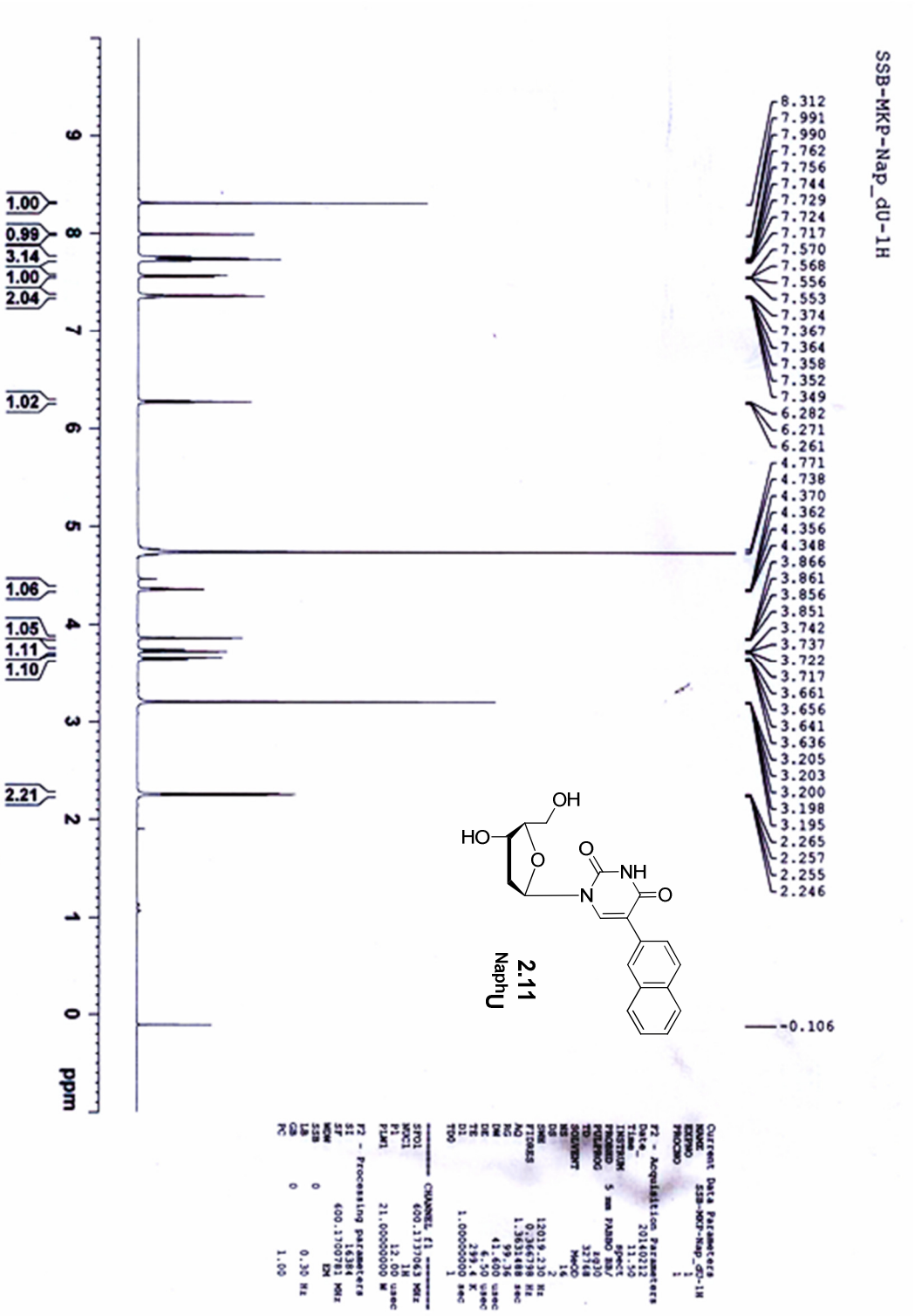

Figure 2.17. ^{1}H NMR 5-(2-naphthyl)-2'-deoxyuridine (**2.11**).

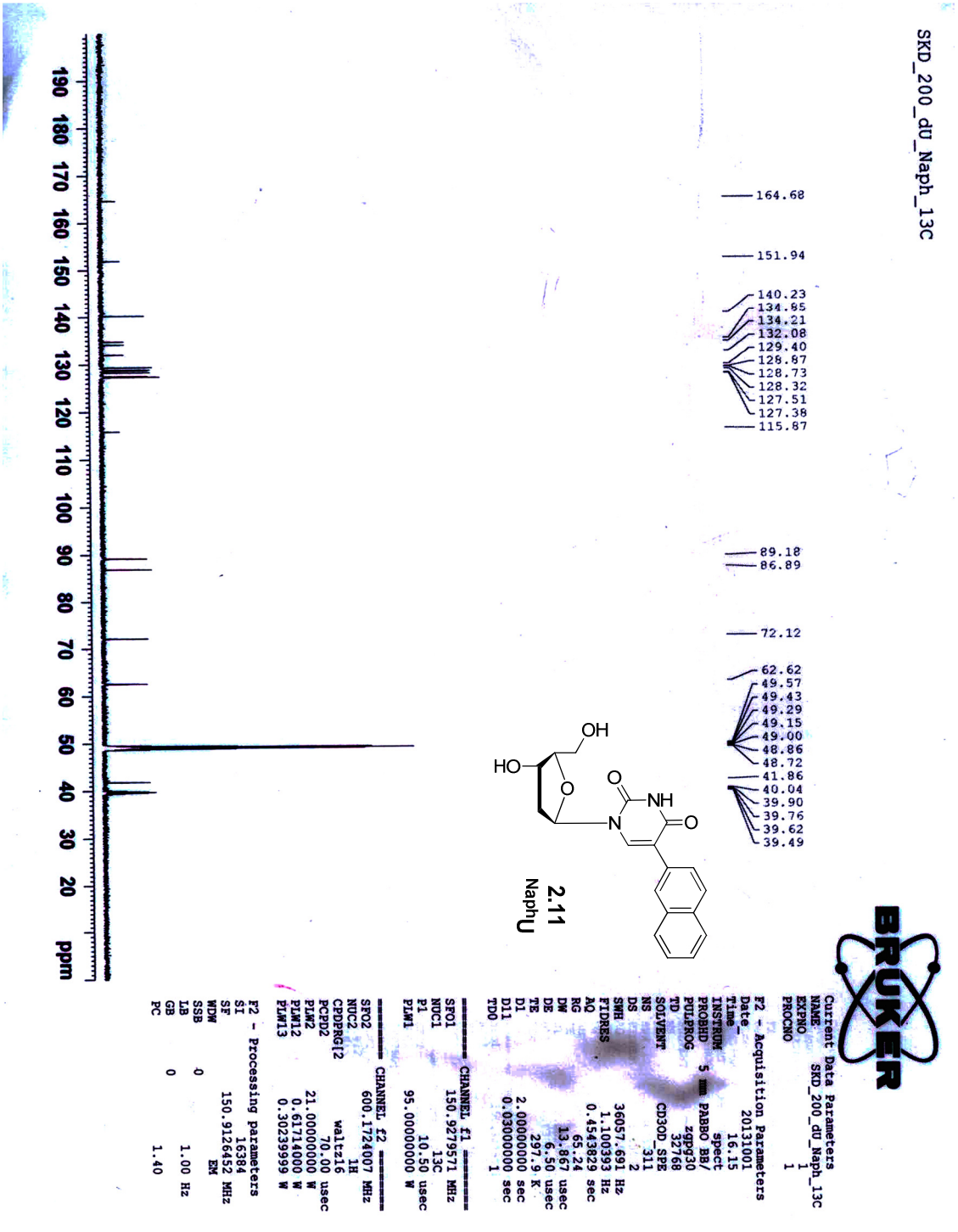

Figure 2.18. ^{13}C NMR 5-(2-naphthyl)-2'-deoxyuridine (**2.11**).

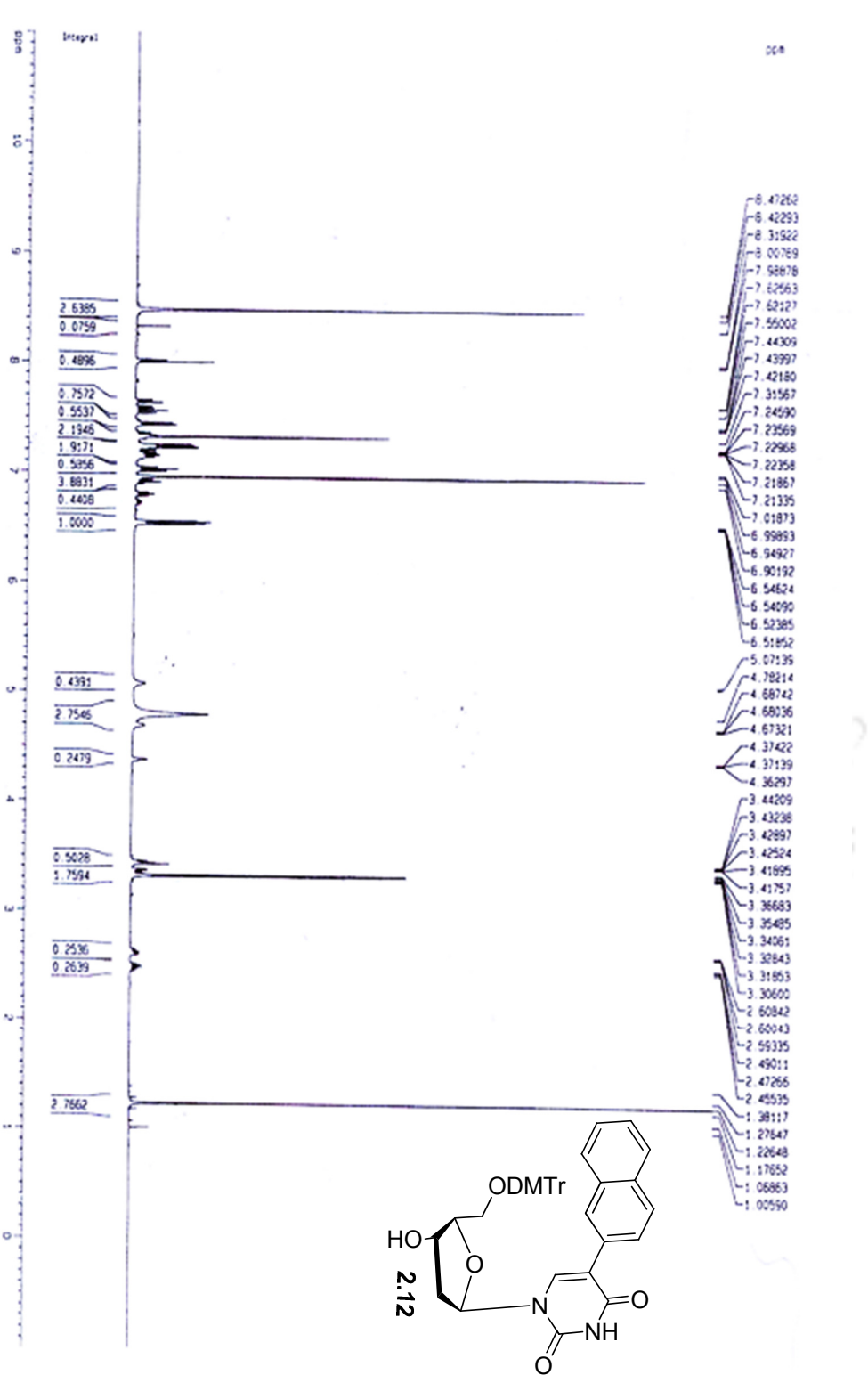

Figure 2.19. ^{1}H NMR spectra of DMTr protected ^{Naph}**U** nucleoside (**2.12**).

2.8. References

1. (a) Okamoto, A.; Tainaka, K.; Saito, I. *J. Am. Chem. Soc*. **2003**, *125*, 4972. (b) Okamoto, A.; Kanatani, K.; Saito, I. *J. Am. Chem. Soc*. **2004**, *126*, 4820. (c) Saito, Y.; Bag, S. S.; Kusakabe, Y.; Nagai, C.; Matsumoto, K.; Kodate, S.; Suzuka, I.; Saito, I. *Chem. Commun*. **2007**, 2133. (d) Rajendar, B.; Rajendran, A.; Sato, Y.; Nishizawa, S.; Teramae, N. *Bioorg. Med. Chem*. **2009**, *17*, 351. (e) Thiagarajan, V.; Rajendran, A.; Satake, H.; Nishizawa, S.; Teramae, N. *ChemBioChem.* **2010**, *11*, 94. (f) Saito, Y.; Suzuki, A.; Okada, Y.; Yamasaka, Y.; Nemoto, N.; Saito, I. *Chem. Commun*. **2013**, *49*, 5684.
2. (a) Rist M. J.; Marino, J. P. *Curr. Org. Chem*. **2002**, *6*, 775. (b) Xia, T. *Curr. Opin. Chem. Biol*. **2008**, *12*, 604. (c) Pawar M. G.; Srivatsan, S. G. *Org. Lett*. **2011**, *13*, 1114. (d) Sinkeldam, R. W.; Marcus, P.; Uchenik, D. Tor, Y. *ChemPhysChem* **2011**, *12*, 2260. (e) Riedl, J.; Pohl, R.; Rulíšek, L.; Hocek, M. *J. Org. Chem*. **2012**, *77*, 1026.
3. (a) For reviews, see; Hawkins, M. E. *Cell Biochem. Biophys.* **2001**, *34*, 257. (b) Okamoto, A.; Saito Y.; Saito, I. *J. Photochem. Photobiol. C*. **2005**, *6*, 108. (c) Ranasinghe, R. T.; Brown, T. *Chem. Commun*. **2005**, 5487. (d) Wilson J. N.; Kool, E. T. *Org. Biomol. Chem*. **2006**, *4*, 4265. (e) Tor, Y. *Tetrahedron symposium in print, ed*. **2007**, *63*. (f) Venkatesan, N.; Seo, Y. J.; Kim, B. H. *Chem. Soc. Rev*. **2008**, *37*, 648.
4. (a) Smith, L. M.; Sanders, J. Z.; Kaiser, R. J.; Hughes, P.; Dodd, C.; Connell, C. R.; Heiner, C.; Kent, S. B. H.; Hood, L. E. *Nature* **1986**, *321*, 674. (b) Guo, J.; Xu, N.; Li, Z.; Zhang, S.; Wu, J.; Kim, D. H.; Marma, M. S.; Meng, Q.; Cao, H.; Li, X.; Shi, S.; Yu, L.; Kalachikov, S.; Russo, J. J.; Turro, N. J.; Ju, *J. Proc. Natl. Acad. Sci. U.S.A*. **2008**, *105*, 9145.
5. Tyagi, S.; Kramer, F. R. *Nat. Biotechnol*. **1996**, *14*, 303.
6. (a) Greco, N. J.; Tor, Y. *Tetrahedron* **2007**, *63*, 3515. (b) Greco, N. J.; Tor, Y. *J. Am. Chem. Soc*. **2005**, *127*, 10784. (c) Srivatsan, S. G.; Tor, Y. *J. Am. Chem. Soc*. **2007**, *129*, 2044. (d) Greco, N. J.; Sinkeldam, R. W.; Tor, Y. *Org. Lett*. **2009**, *11*, 1115. (e) Wanninger-Weiss, C.; Valis, L.; Wagenknecht, H.-A. *Bioorg. Med. Chem*. **2008**, *16*, 100.
7. (a) Hudson, R. H. E.; Ghorbani-Choghamarani, A. *Org. Biomol. Chem*. **2007**, *5*, 1845. (b) Capobianco, M. L.; Cazzato, A.; Alesi, S.; Barbarella, G. *Bioconjugate Chem*. **2008**, *19*, 171. (c) Ryu, J. H.; Seo, Y. J.; Hwang, G. T.; Lee, J. Y.; Kim, B. H. *Tetrahedron* **2007**, *63*, 3538. (d) Xiao, Q.; Ranasinghe, R. T.; Tang, A. M. P.; Brown, T. *Tetrahedron*

2007, *63*, 3483. (e) Sessler, J. L; Sathiosatham, M.; Brown, C. T.; Rhodes, T. A.; Wiederrecht, G. *J. Am. Chem. Soc*. **2001**, *123*, 3655. (f) Skorobogatyi, M. V.; Malakov, A. D.; Pchelintseva, A. A.; Turban, A. A.; Bondarev, S. L.; Korshun, V. A. *ChemBioChem* **2006**, *7*, 810.

8. (a) Okamoto, A.; Tainaka, K.; Saito, I. *J. Am. Chem. Soc*. **2003**, *125*, 4972. (b) Okamoto, A.; Tanaka, K.; Fukuta, T.; Saito, I. *J. Am. Chem. Soc*. **2003**, *125*, 9296. (c) Gardarson, H.; Kale, A.; Sigurdsson, S. T. *ChemBioChem* **2011**, *12*, 567. (d) Cekan, P; Sigurdsson, S. T. *Chem. Commun*. **2008**, *29*, 3393. (e) Xie, Y.; Maxson, T.; Tor, Y. *Org. Biomol. Chem*. **2010**, *8*, 5053. (f) Srivatsan, S. G.; Weizman, H.; Tor, Y. *Org. Biomol. Chem*. **2008**, *6*, 1334. (g) Datta, K.; Johnson, N. P.; Villani, G.; Marcus, A. H.; von Hippel, P. H. *Nucleic Acids Res*. **2011**, E-pub ahead of print, DOI: 10.1093/nar/gkr858.
9. (a) Karunakaran, V.; Perez Lustres, J. L.; Zhao, L.; Ernsting, N. P.; Seitz, O. *J. Am. Chem. Soc*. **2006**, *128*, 2954. (b) Kummer, S.; Knoll, A.; Socher, E.; Bethge, L.; Herrmann, A.; Seitz, O. *Angew. Chem., Int. Ed*. **2011**, *50*, 1931. (c) Holzhauser, C.; Berndl, S.; Menacher, F.; Breunig, M.; Göpferich, A.; Wagenknecht, H.-A. *Eur. J. Org. Chem*. **2010**, *7*, 1239. (d) Berndl, S.; Wagenknecht, H.-A. *Angew. Chem., Int. Ed*. **2009**, *48*, 2418. (e) Asanuma, H.; Kashida, H.; Liang, X.; Komiyama, M. *Chem. Commun*. **2003**, *7*, 1536. (f) Coleman, R. S.; Berg, M. A.; Murphy, C. J. *Tetrahedron* **2007**, *63*, 3450.
10. (a) Okamoto, A.; Kanatani, K.; Saito, I. *J. Am. Chem. Soc*. **2004**, *126*, 4820. (b) Tainaka, K.; Tanaka, K.; Ikeda, S.; Nishiza, K.-I.; Unzai, T.; Fujiwara, Y.; Saito, I.; Okamoto, A. *J. Am. Chem. Soc*. **2007**, *129*, 4776. (c) Saito, Y.; Motegi, K.; Bag, S. S.; Saito, I. *Bioorg. Med. Chem*. **2008**, *16*, 107.
11. Saito, Y.; Kugenuma, K.; Tanaka, M.; Suzuki, A.; Saito, I. *Bioorg. Med. Chem. Lett*. **2012**, *22*, 3723.
12. (a) The International HapMap Consortium, *Nature*, **2005**, *437*, 1299. (b) Haga, H.; Yamada, Y.; Ohnishi, Y.; Nakamura, Y.; Tanaka, T. *J. Hum. Genet*. **2002**, *47*, 605. (c) Brookes, A. J.; *Gene*, **1999**, *234*, 177. (d) Chakravarti, A.; *Nat. Genet. Suppl*. **1999**, *21*, 56.
13. (a) Pastinen T.; Hudson, T. J.; *Science* **2004**, *306*, 647. (b) McCarthy J. J.; Hilfiker, R. *Nat. Biotechnol.* **2000**, *18*, 505.
14. (a) Reviews: Suh Y.; Cantor, C. *Mutat. Res*. **2005**, *573*, 1. (b) Sobrino, B.; Brion M.; Carracedo, A. *Forensic Sci. Int*. **2005**, *154*, 181. (c) Twyman, R. M.; *Curr. Top. Med.*

Chem. **2004**, *4*, 1423. (d) Nakatani, K. *ChemBioChem* **2004**, *5*, 1623. (e) Carlson, C. S.; Newman T. L.; Nickerson, D. A. *Curr. Opin. Chem. Biol*. **2001**, *5*, 78. (f) Kwok, P. Y.; *Annu. Rev. Genomics Hum. Genet.* **2001**, *2*, 235.

15. (a) Friedrich, A.; Hoheisel, J. D.; Marm´e, N.; Knemeyer, J.-P. *FEBS Lett.* **2007**, *581*, 1644. (b) Kumar, T. S.; Wengel J.; Hrdlicka, P. J. *ChemBioChem.* **2007**, *8*, 1122. (c) Ergen, E.; Weber, M.; Jacob, J.; Herrmann A.; M¨ ullen, K. *Chem.–Eur. J*. **2006**, *12*, 3707. (d) Asseline, U.; Chassignol, M.; Aubert Y.; Roig, V. *Org. Biomol. Chem*. **2006**, *4*, 1949. (e) Valis, L.; Amann, N.; Wagenknecht, H.-A. *Org. Biomol. Chem*. **2005**, *3*, 36. (f) Yamana, K.; Fukunaga, Y.; Ohtani, Y.; Sato, S.; Nakamura, M.; Kim, W. J.; Akaike, T.; Maruyama, A. *Chem. Commun.* **2005**, 2509. (g) Crockett A. O.; Wittwer, C. T. *Anal. Biochem*. **2001**, *290*, 89. (h) Paris, P. L.; Langenhan J. M.; Kool, E. T. *Nucleic Acids Res*. **1998**, *26*, 3789.
16. Okamoto, A.; Saito Y.; Saito, I. *Photochem. Photobiol. C: Photochem. Rev*. **2005**, *6*, 108.
17. (a) Tainaka, K.; Tanaka, K.; Ikeda, S.; Nishiza, K.-I.; Unzai, T.; Fujiwara, Y.; Saito I.; Okamoto, A. *J. Am. Chem. Soc*. **2007**, *129*, 4776. (b) Saito, Y.; Mizuno, E.; Bag, S. S.; Suzuka I.; Saito, I. *Chem. Commun*. **2007**, 4492. (c) Takei, F.; Suda, H.; Hagihara, M.; Zhang, J.; Kobori, A.; Nakatani, K. *Chem.–Eur. J*. **2007**, *13*, 4452. (d) Hudson R. H. E.; Ghorbani-Choghamarani, A. *Org. Biomol. Chem*. **2007**, *5*, 1845. (e) Ryu, J. H.; Seo, Y. J.; Hwang, T.; Lee J. Y.; Kim, B. H. *Tetrahedron* **2007**, *63*, 3538. (f) Xiao, Q.; Ranasinghe, R. T.; Tang A. M. P.; Brown, T. *Tetrahedron* **2007**, *63*, 3483. (g) Moran, N.; Bassani, D. M.; Desvergne, J.-P.; Keiper, S.; Lowden, P. A. S.; Vyle J. S.; Tucker, J. H. R. *Chem.Commun*. **2006**, 5003. (h) Mayer-Enthart E.; Wegenknecht, H.-A. *Angew. Chem., Int. Ed*. **2006**, *45*, 3372. (i) Hurley, D. J.; Seaman, S. E.; Mazura J. C.; Tor, Y. *Org. Lett*. **2002**, *4*, 2305.
18. (a) Sartori, G.; Enderlin, G.; Herve, G.; Len, C. *Synthesis* **2012**, *44,* 767. (b) Kazzouli, S.; Berteina-Raboin, S.; Agrofoglio, L. A. *Nucleotides & Nucleic Acids* **2007**, *26*, 1395. (c) Okamoto, A.; Tainaka, K.; Unzai, T.; Saito, I. *Tetrahedron* **2007**, *63*, 3465. (d) Al-Razzak, L. A.; Schwepler, D.; Decedue, C. J.; Balzarini, J.; De Clercq, E.; Mertes, M. P. *J. Med. Chem.* **1987**, *30*, 409. (e) Jacobsen, M. F.; Ferapontova, E. E.; Gothelf, K. V. *Org. Biomol. Chem.* **2009**, *7*, 905. (f) Wanninger-Weiss, C.; Wagenknecht, H.-A.; *Eur. J. Org. Chem.* **2008**, *1*, 64. (g) Bag, S. S.; Talukdar, S.; Matsumoto, K.; Kundu, R.

J. Org. Chem. **2013**, *78*, 278. (h) Bag, S. S.; Kundu, R.; Matsumoto, K.; Saito, Y.; Saito, I. *Bioorg. Med. Chem. Lett*. **2010**, *20*, 3227.

19. Frisch, M. J. et al., Gaussian 03, revision C.02; *Gaussian, Inc.: Wallingford, CT*, **2004**.
20. (a) Tanpure A.; Srivatsan, S. G. *ChemBioChem* **2012**, *13*, 2392. (b) Greco, N. J.; Tor, Y. *J. Am. Chem. Soc*. **2005**, *127*, 10784. (c) Riedl, J.; Pohl, R.; Rulíšek, L.; Hocek, M. *J. Org. Chem*. **2012**, *77*, 1026. (d) Ehrenschwender, T.; Wagenknecht, H. –A. *J. Org. Chem*. **2011**, *76*, 2301. (e) Jacobsen, M. F.; Ferapontova, E. E.; Gothelf, K. V. *Org. Biomol. Chem*. **2009**, *7*, 905.
21. (a) Miyaura, N.; Yamada, K.; Suzuki, A. *Tetrahedron Lett.* **1979**, *20*, 3437. (b) Miyaura, N.; Suzuki, A. *Chem. Rev.* **1995**, *95*, 2457.
22. (a) Dougherty, G.; Pilbrow, J. R. *Int. J. Biochem.* **1984**, *16*, 1179. (b) Nakamura, M.; Fukunaga, Y.; Sasa, K.; Ohtoshi, Y.; Kanaori, K.; Hayashi, H.; Nakano, H.; Yamana, K. *Nucleic Acids Res.* **2005**, *33*, 5887.
23. (a) Sartori, G.; Enderlin, G.; Herve, G.; Len, C. *Synthesis* **2012**, *44*, 767. (b) Kazzouli, S.; Berteina-Raboin, S.; Agrofoglio, L. A. *Nucleotides Nucleic Acids* **2007**, *26*, 1395. (c) Okamoto, A.; Tainaka, K.; Unzai, T.; Saito, I. *Tetrahedron* **2007**, *63*, 3465. (d) Al-Razzak, L. A.; Schwepler, D.; Decedue, C. J.; Balzarini, J.; De Clercq, E.; Mertes, M. P. *J. Med. Chem*. **1987**, *30*, 409. (e) Jacobsen, M. F.; Ferapontova, E. E.; Gothelf, K. V. *Org. Biomol. Chem*. **2009**, *7*, 905. (f) Wanninger-Weiss, C.; Wagenknecht, H.-A. *Eur. J. Org. Chem*. **2008**, *1*, 64.
24. (a) Dougherty, G.; Pilbrow, J. R. *Int. J. Biochem*. **1984**, *16*, 1179. (b) Nakamura, M.; Fukunaga, Y.; Sasa, K.; Ohtoshi, Y.; Kanaori, K.; Hayashi, H.; Nakano, H.; Yamana, K. *Nucleic Acids Res*. **2005**, *33*, 5887.
25. a) Kawai, M.; Lee, M. J.; Evans, K. O.; Nordlund, T. M.; *J. Fluoresc*. **2001**, *11*, 23. b) Jean, J. M.; Hall, K. B. *Proc. Natl. Acad. Sci. USA* **2001**, *98*, 37.
26. a) Seidel, C. A. M.; Schulz, A.; Sauer, M. H. M. *J. Phys. Chem.* **1996**, *100*, 5541. b) Kelley, S. O.; Barton, J. K. *Science* **1999**, *283*, 375. c) Torimura, M.; Kurata, S.; Yamada, K.; Yokomaku, T.; Kamagata, Y.; Kanagawa, T.; Kurane, R. *Anal. Sci*. **2001**, *17*, 155.
27. a) Ward, D. C.; Reich, E.; Stryer, L. *J. Biol. Chem*. **1969**, *244*, 1228. b) Rachofsky, E. L.; Osman, R.; Ross, J. B. A. *Biochemistry* **2001**, *40*, 946.
28. Sinkeldam, R. W.; Wheat, A. J.; Boyaci, H.; Tor, Y. *ChemPhysChem* **2011**, *12*, 567.
29. (a) Kwok, P. Y. *Annu. Rev. Genomics Hum. Genet*. **2001**, *2*, 235. (b) Chicurel, M. *Nature* **2001**, *412*, 580. (c) Tyagi, S.; Bratu, D. P.; Kramer, F. R. *Nat. Biotechnol*. **1998**,

16, 49. (d) Kim, S.; Misra, A. *Annu. Rev. Biomed. Eng*. **2007**, *9*, 289. (e) Kwok, P. Y.; Chen, X. *Curr. Issues Mol. Biol*. **2003**, *5*, 43. (f) Ryu, J. H.; Heo, J. Y.; Bang, E.- K.; Hwang, G. T.; Kim, B. H. *Tetrahedron* **2012**, *68*, 72. (g) Lee, J.; Cho, H. Y.; Hwang, G. T. *ChemBioChem* **2013**, *14*, 1353. (h) Okamoto, A.; Kamei, T.; Saito, I. *J. Am. Chem. Soc*. **2006**, *128*, 658. (i) Okamoto, A.; Kamei, T.; Tanaka, K.; Saito, I. *J. Am. Chem. Soc*. **2004**, *126*, 14732. (j) Seo, Y. J.; Rhee, H.; Joo, T.; Kim, B. H. *J. Am Chem. Soc*. **2007**, *129*, 5244. (k) Malinovskii, V. L.; Samain, F.; Häner, R. *Angew. Chem., Int. Ed*. **2007**, *46*, 4464. (l) Yoshida, Y.; Niwa, K.; Yamada, K.; Tokeshi, M.; Baba, Y.; Saito, Y.; Okamoto, A.; Saito, I. *Chem. Lett*. **2010**, *39*, 116.

30. (a) Bag, S. S.; Talukdar, S.; Matsumoto, K.; Kundu, R. *J. Org. Chem*. **2013**, *78*, 278. (b) Bag, S. S.; Kundu, R.; Matsumoto, K.; Saito, Y.; Saito, I. *Bioorg. Med. Chem. Lett*. **2010**, *20*, 3227.

31. (a) Kypr, J.; Kejnovska, I.; Renciuk, D.; Vorlıckova, M. *Nucleic Acids Res*. **2009**, *37*, 1713. (b) Saha, I.; Kumar, G. S. *J. Fluoresc*. **2011**, *21*, 247.

Chapter 3

Studies on the Label Free Detection of Mismatched, Abasic and Bulge DNA Utilizing Fluorescent Tetrazolyl Pyrene Unnatural Nucleoside

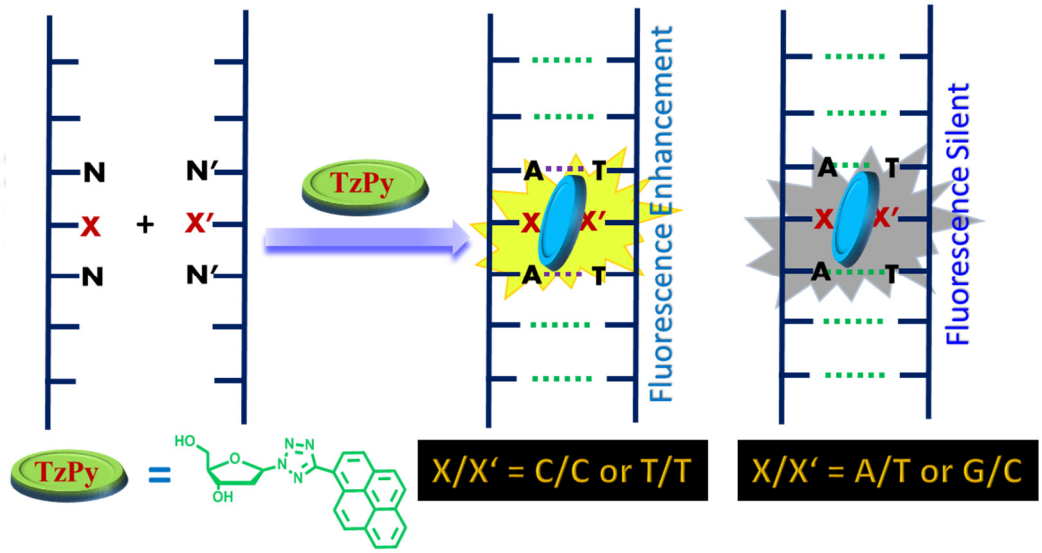

3.1. Introduction

In recent time due to simplicity, label-free DNA recognition by fluorescent small molecules has received much attention in mutation identification and drug screening. The use of covalently-modified or labeled nucleic acids have certain drawbacks in this regard. The covalent attachment of fluorophores or labeling agents to the functional oligonucleotide may have affect on the structural conformity, biological stability and recognition events.[1] Furthermore, the labeling of an analyte to nucleic acid are costly, tedious and time consuming. On the other hand, ‘‘label-free’’ detection concept aims to overcome these drawbacks.[2]

In label-free approach, fluorescent ligands are not covalently attached to the nucleic acid backbone but it interacts noncovalently with DNA through a number of binding modes such as intercalation, groove-binding, end-stacking or electrostatic interactions. The fluorescent molecules used in label-free DNA detection are in general non-emissive or weakly emissive in aqueous solution, due to quenching by solvent-solute interactions. However, they show fluorescence enhancement upon binding to defined DNA structures due to the protection of their excited states within the hydrophobic interior of the oligonucleotide.[3] Label-free DNA detection based approach offers unique advantage, which can be carried out in homogenous solution without any pre-labeling or immobilization step. So, label free detection are less time consuming and moderate cost. Furthermore, single nucleotide polymorphism (SNP) typing or single base mismatch detection could be easily achieved by label free strategy.

Mismatched (non-Watson–Crick) base pairs represent the most common type of DNA damage. Mismatch are occurred in living cells due to erroneous insertion, deletion and misincorporation of bases.[1] Scientists have developed a lot of chemically modified small organic molecule/drug and metal complexes that could specifically bind to mismatch base pairs over fully match paired double-stranded DNA. A label-free fluorescence based DNA detection technique to discriminate between mismatched duplex DNA over matched duplex DNA with high accuracy is an attractive research area. In the previous, chapter 2 we represent the DNA base discrimination of match and mismatch pair by using a covalently labeled naphthalene oligonucleotide.[4] As compared with the previous work which was focused to covalent labeled DNA detection methods, the label-free technique is apparently simple, less time consuming and inexpensive.

3.2. DNA Mismatch Detection

A large number of research works in this regard have been reported in literature. Few of them are discussed below.

Sato[6] *et. al*., exploited 2-amino-5,6,7-trimethyl- 1,8-naphthyridine (**3.1**, ATMND; **Figure 3.1**) as selective C-C mismatch binding probe in the hairpin structures of $(CCG)_n$ trinucleotide repeats, which are associated with neurological diseases. The binding characteristics of ATMND to $(CCG)_n$ were examined by UV-visible absorption, fluorescence, and isothermal titration calorimetry (ITC) measurements. ATMND is able to bind selectively to $(CCG)_n$ trinucleotide repeats with fluorescence quenching.

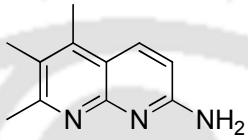

3.1, ATMND

Figure 3.1. Structure of 2-amino-5,6,7-trimethyl- 1,8-naphthyridine (ATMND).

Granzhan[7] *et.al*., explored bisanthracene macrocycle **3.2** (**Figure 3.2**) as fluorescent probe to discriminate between matched and mismatched base pair containing DNA. Its binding affinity to the fully matched and mismatched base pair containing DNA was investigated by the thermal denaturation experiments. In addition, the binding stoichiometry of macrocycle **3.2** to the matched and mismatched base pair containing duplexes was obtained from UV-vis, fluorescence and circular-dichroism (CD) spectrophotometric titrations. Addition of DNA resulted hypochromism and red-shift of the absorption spectrum of the anthracene derivative **3.2**. Moreover, when the mismatched base is thymine, binding of the probe **3.2** results in a quasi-complete quenching of its fluorescence, which allows an easy differentiation from the sequences in which the middle thymine is matched with adenine. Thus, the probe **3.2** is able to signal the presence of a single mismatched thymine residue in the duplexes that contain 16 other AT and GC base pairs. The selective recognition of thymine-containing mismatches is relevant in the context of SNP detection, since thymine is involved in 49% of point mutations in human genome, with the C–T transition representing about 33% of all substitutions.

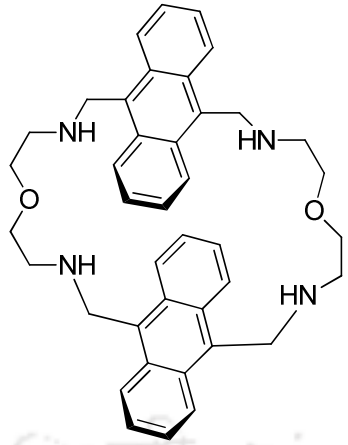

3.2

Figure 3.2. Structure of bisanthracene macrocycle **3.2**.

3.3. Abasic Site Detection

Zhao *et al*., in 2006 demonstrated that amiloride (N-amidino-3,5-diamino-6-chloro-pyrazinecarboxamide hydrochloride) (**Figure 3.3**) can recognize thymine base opposite an abasic site in DNA duplexes with high selectivity and affinity.[8] Amiloride (N-amidino-3,5-diamino-6-chloro-pyrazinecarboxamide hydrochloride),[9] has two sets of hydrogen-bond forming sites on either end of the system, i.e., a hydrogen-bonding profile fully complementary to thymine, and a guanidinium moiety suitable for recognition of the phosphodiester DNA backbone (**Figure 3.3**). The binding of amiloride to 11-mer AP site-containing duplexes (5'-TCC AGX GCA AC-3'/3'-AGG TCY CGT TG-5', X = AP site, Y = target), with an emphasis on the effect of the guanidinium moiety, and a highly selective interaction to T with a nanomolar range of binding affinity have been investigated. Amiloride exhibits significant quenching of its fluorescence upon addition of DNA duplexes containing T opposite the AP site, while almost no responses are observed in the presence of normal duplexes containing no AP sites. Amiloride is capable of selectively binding to T over C, A and G.

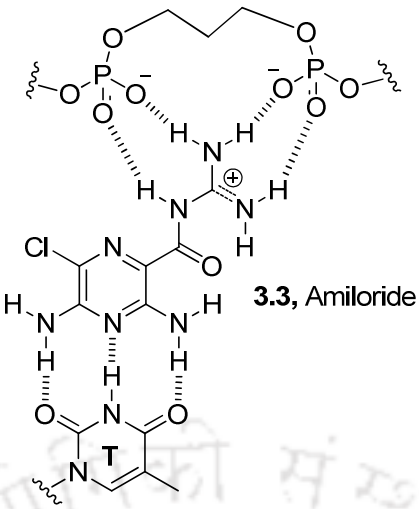

Figure 3.3. Possible binding mode of amiloride with T in the AP site-containing DNA duplexes.

Zhao *et al*., again demonstrated pyrazine derivative, 3,5-diamino-6-chloro-2-pyrazine carbonitrile (DCPC, **Figure 3.4**) which can bind to thymine selectively over other nucleobases opposite an abasic site in DNA duplexes (5'-GTGTG CGTTG ANA TGGAC GCAGA-3'/3'-CACAC GCAAC TXT ACCTG CGTCT-5', X = abasic site, N = target nucleotide).[10] The binding of DCPC is accompanied by a significant enhancement of its fluorescence (λ_{max}, 412 nm), and the response is highly selective to thymine base. In the absence of DNAs, the ligand shows a very weak emission with a maximum at 412 nm, and almost no response is observed for guanine, even in the presence of 5 equivalent of DNA (50 μM). Similarly, the response of DCPC is only moderate for adenine and cytosine. By contrast, DCPC exhibits a significant enhancement of its fluorescence for thymine. In the presence of 1 equivalent of DNA (10 μM), the emission intensity at 412 nm is indeed, enhanced by a factor of 25, and this is accompanied by a 3 nm red-shift of the emission maximum. The response for thymine is concentration-dependent which is explained by 1:1 binding with a dissociation constant, K_d, of 2.6 μM.

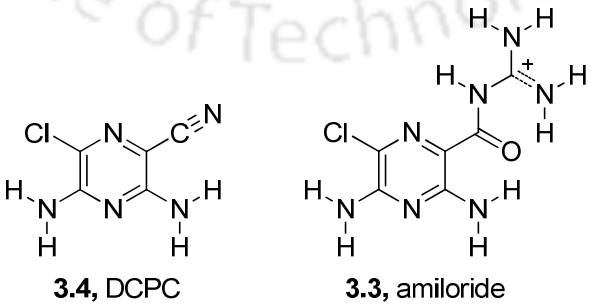

Figure 3.4. Chemical structures of DCPC and amiloride.

Rajendran *et al*., explored the interaction of amiloride (**Figure 3.4**) with thymine which was found to depend on the bases flanking the AP site.[11] The flanking base dependent recognition of AP site phosphates was investigated by ^{31}P NMR experiments. The interaction of amiloride in the absence and presence of 23-mer AP site-containing DNA duplex with two different flanking bases (GXG and TXT, where X is the AP site) was investigated. The fluorescence response of amiloride strongly depends on the bases flanking the AP site. When guanine bases were flanked with the AP site (GXG), fluorescence of amiloride at 415 nm was quenched and the emission peak became broader upon addition of the DNA duplex, while its fluorescence was enhanced and the peak was narrowed when the flanking bases were T (TXT). Further, the emission maximum of amiloride was red shifted about 5 nm upon addition of one equivalent of the DNA duplex having T flanking bases at the AP site, whereas no noticeable shift was observed for the DNA duplex containing an AP site with G flanking bases. Amiloride absorption, centered at 362 nm, decreased upon addition of DNA and a red shift in the absorption spectrum of amiloride by 12.5 nm was observed by the addition of one-equivalent of DNA with G flanking bases, while it was 9.5 nm with T flanking bases.

Wu *et al*., investigated the binding property of berberine (**Figure 3.5**) to DNA contain AP site.[12] Berberine weakly binds to the fully matched DNAs without the AP site but it strongly binds to the DNA containing AP site. Berberine's fluorescence light-up behaviours are highly dependent on the target nucleobases opposite the AP site in which the targets thymine and cytosine produced dual emission bands, while the targets guanine and adenine only gave a single emission band. The emission of berberine alone was rather weak; while the presence of the fully matched DNA (FM) slightly increases the fluorescence response with emissions at 538 nm by exciting at either 360 or 465 nm. However, upon addition of DNA1-Y (**Figure 3.5**) with guanine (DNA1-G) or adenine (DNA1-A) opposite the AP site to the berberine solution, berberine's emission was blue shifted to 534 nm, which was accompanied by an increase in intensity of 5 (DNA1-A) or 6 (DNA1-G) times higher than that for FM under excitation at either 360 or 465 nm, respectively. Interestingly, the enhancement became more pronounced for cytosine (DNA1-C) or thymine (DNA1-T) opposite the AP site with the intensities increased up to about 26 times when excited at 465 nm. Importantly, when the excitation wavelength was set to 360 nm, dual emission bands appear at 492 and 584 nm for DNA1-C or DNA1-T with their intensities being 9 and 14 times higher than the FM's emission at 538 nm, respectively. From the absorbance spectra, the presence of DNA1- C and DNA1-T also resulted in more pronounced bathochromic and hypochromic changes than those for DNA1-G and

DNA1-A. It was explained that the target pyrimidines cause berberine to be stacked well within DNA base pairs near the AP site, which resulted in a strong resonance coupling of the electronic transitions to the particular vibration mode to produce the dual emissions.

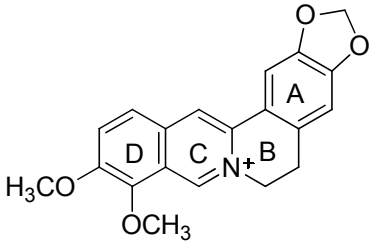

3.5, berberine

DNA1-Y: 5'-ATGGTGT**X**TGCAGCG-3' Probe strand
3'-TACCACA**Y**ACGTCGC-5' Target strand
X = AP site, Target base **Y** = A, C, G or T

DNA2-Y: 5'-CACACTP**X**GTCGAAA-3'
3'-GTGTGAT**Y**CAGCTTT-5'
P = 2-aminopurine, **Y** = C or G

DNA3-Y: 5'-ATGGTGA**X**AGCAGCG-3' Probe strand
3'-TACCACT**Y**TCGTCGC-5' Target strand
X = AP site, Target base **Y** = A, C, G or T

Figure 3.5. Structure of berberine, **3.5** and the sequences used by Wu[7] *et al*. X = AP site (dSpacer, tetrahydrofuran residual) for AP site-containing DNAs. Fully matched DNAs (FM-DNA) with X/Y = G/C and A/T are used as controls.

3.4. Bulge DNA Detection

Verma *et al*., explored a new fluorescence probe PyDANP (**Figure 3.6**) which detects Cytosine Bulge DNA via a turn-on fluorescence response.[13] Upon binding of DANP moiety in PyDANP to cytosine bulge DNA, the fluorescence from DANP bound to C-bulge increased by ~12-fold with A-T flanking base pairs, showing that PyDANP is a turn-ON probe for the detection of C-bulge DNA. PyDANP binding to C-bulge DNA was associated with 1:1 complex formation. The absorption spectrum of PyDANP with DNA containing C-bulge flanked by TA/AT base pairs (TCA/T_A) showed a bathochromic shift in the peak at 342 to 350 nm and the unstructured peak at 380 to 390 nm with increased absorbance. Similar spectral changes were also observed for the DNA containing C-bulge flanked by GC/GC base pairs (GCG/ C_C). With the fully matched double-stranded DNA (GC/ GC), peak at 342 nm was shifted but the shift of peak at 380 nm was not significant.

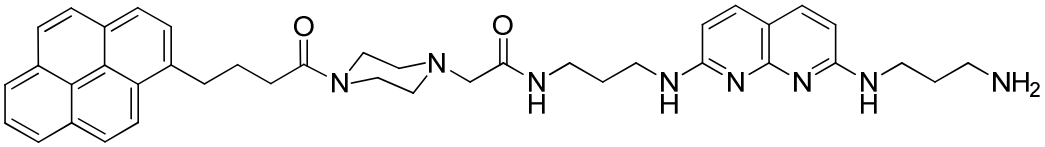

3.6, PyDANP

Figure 3.6. Structures of PyDANP.

Suda *et al*., observed ligand 2,7-diamino-1,8-naphthyridine (DANP, **3.7 Figure 3.7**) that strongly and specifically binds to the single cytosine and thymine bulges over the purine bulge and fully matched duplexes with exclusively 1:1 stoichiometry.[14] The observed absorbance maximum for free DANP in phosphate buffer (pH 7.0) showed at 364 nm with a shoulder at 376 nm. The presence of fully matched duplex as well as adenine bulge duplex resulted in a small hypochromic shift but not a bathochromic shift of the absorption maximum. In contrast, the cytosine bulge duplex (T_A/ACT) induced a bathochromic shift by 30 nm to 394 nm with a concomitant hypochromic shift by 65%. Bathochromic shift of DANP absorption was also induced by the thymine bulge (T_A/ATT) producing the absorption maximum at 390 nm. Whereas guanine bulge duplex was intermediate between the pyrimidine and adenine bulge duplex in terms of the bathochromic shift. The emission maximum of DANP was not virtually affected by the presence of fully matched duplex and adenine bulge duplex. However, a broad emission with the emission maximum at 424 nm was observed in the presence of the cytosine and thymine bulge.

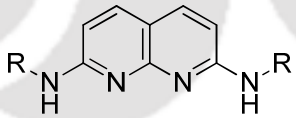

3.7, DANP

R = $CH_2CH_2CH_2NH_2$

Figure 3.7. Chemical structure of DANP, **3.7**.

Takei et al., also investigated and exploited *N,N'*-bis(3-aminopropyl)- 2,7-diamino-1,8-naphthyridine (DANP, **3.7**, **Figure 3.7**) as allele specific C-bulge probe DNA and a fluorescent molecule selectively binding to the C-bulge.[15] The fluorescence of the DANPH+ bound to the C-bulge was, in fact, selectively modulated by the neighboring matched or mismatched base pair formation. The profile in the fluorescence change of DANPH+ regarding the allele specific C-bulge probes may be used for the determination of the allele type at the predetermined SNP site.

Ong et al., developed a water-soluble derivative 7-Deazaguanine (7-DeG, **3.8**, **Figure 3.8**) as a hydrogen-bonding module capable of displaying high affinity and selectivity toward DNA and RNA duplexes containing single T- and U-bulges.[16] In the presence of ligand **3.8**, DNA duplex containing a single T-bulge flanked by guanines was stabilized by +7.0 °C. From fluorescence titration experiment a 1:1 binding stoichiometry was evaluated.

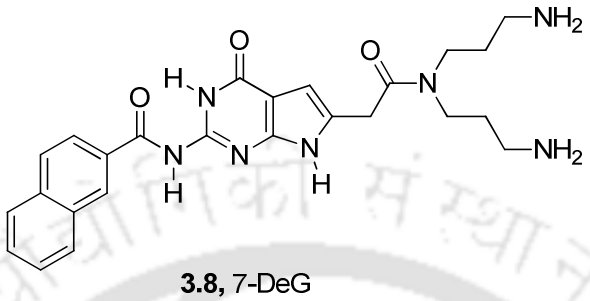

3.8, 7-DeG

Figure 3.8. 7-Deazaguanine, **3.8** (7-DeG), deazaguanine-based hydrogen-bonding ligand.

3.5. Background

Development of small fluorescent molecules/biomolecular building blocks that can recognize biomacromolecules with highly specific fluorescence signal generation is recently an emerging research trend in chemical biology. In the field of DNA, the detection of sequence alteration is highly important for reliable and early disease diagnosis. In particular, DNA base pair mismatch and abasic site are the two most frequently encountered DNA sequence alteration. The mismatched base pairs in DNA mainly arises due to replication errors, damages or lesions or sometimes due to the spontaneous deamination. On the other hand, abasic site is one of the most frequently encountered DNA lesion mainly arises due to a rise in temperature, a drop in pH, or the presence of alkylations on the base. If left unrepaired by cellular machinery, both the form of deformed DNA may result in deleterious mutation in DNA that are dangerous to cellular survival and replication. Therefore, the detection and targeting of both the mismatched and abasic DNA is highly important which would ultimately help in designing new diagnostics and chemotherapeutics. As a result of tremendous research efforts several fluorescent oligonucleotide probes containing fluorescent nucleoside/non-nucleoside analogues have been reported as fluorescent signal transducer for reporting variety of events including probing DNA hybridization, typing single-nucleotide polymorphism (SNP), and monitoring the dynamics of DNA/protein complexes or the detection DNA base mismatches or for targeting the abasic site in DNA.

Therefore, a brief introduction of the label free DNA detection with various small fluorescent molecules is described in this chapter.

3.6. Objective

As a part of our ongoing research activity, we previously have reported the design of fluorescent nucleosides/labelled nucleosides for the detection of SNPs and abasic site in a short DNA with a probe containing triazolylphenanthrene nucleoside opposite to the abasic site.[17] However, labeling of DNA with fluorescent nucleoside to get oligonucleotide probe is extensive time consuming, laborious and high cost demanding. Thus simple, cost effective labell free strategies would be much more beneficial for the detection of mismatched DNA or abasic DNA. Utilization of small fluorescent molecules as probe would be ideal candidate in terms of less time consuming, less laborious, cost-effective and operational simplicity. In this respect, fluorescent nucleoside as a small ligand would be advantageous which can easily recognize DNA hybridization status because of the natural self-recognition property between bare nucleosides and DNA. Inspired by our earlier results and ongoing research on the design of tetrazolyl nucleosides we thought that the tetrazolylpyrene nucleoside could serve as an efficient probe for sensing DNA.[18] We envisaged that the natural self-recognition/organization property between the bare nucleoside and DNA and H-bonding/hydrophobic force mediated interaction would be an efficient strategy for sensing deformed DNA. The bare fluorescent nucleoside would thus be advantageous over simple intercalative dyes as the sugar unit could impart extra binding interaction possibly in the minor groove and the aromatic base could engage in intercalation into the cavity at the locally destabilised site similar to the action of drug, daunomycine.

With this concept and idea, we framed our objective as below:

a) Utilisation of our previously reported tetrazolylpyrene nucleoside (**TzPy**, **Figure 3.9**) for sensing of mismatched DNA
b) Label free detection of abasic DNA
c) Studies on the interaction of the same nucleoside with single base bulge-out DNA

We thought that the tetrazolylpyrene (**TzPy**) moiety of the nucleoside with large surface area, high polarizability, high stacking propensity could reinstate the DNA base stack (AT or GC) via intercalation into the cavity leading to stabilization of the abasic duplex as well as it can have held in binding interaction at the mismatched base pair site. We expected that the

voids created by pyrimidine base mismatched pairs (T•T or C•C) and the pyrimidine abasic pairs (T•Φ or C•Φ) would be covered by the triazolylpyrene unit of the fluorescence nucleoside much better way compared to purine base. We expected that insertion of the probe at the mispair sites would displace a T or C into an extra helical position. This would led to the generation of a discriminating fluorescence signal and allow us for the detection of the same. **Figure 3.9**, represented the proposed binding of **TzPy** to matched/mismatched DNAs.

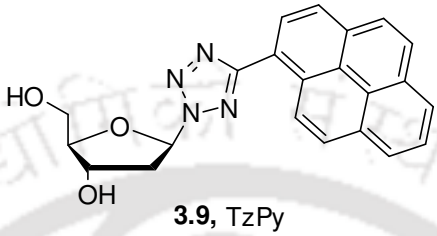

3.9, TzPy

Chemical structure of **TzPy, 3.9**.

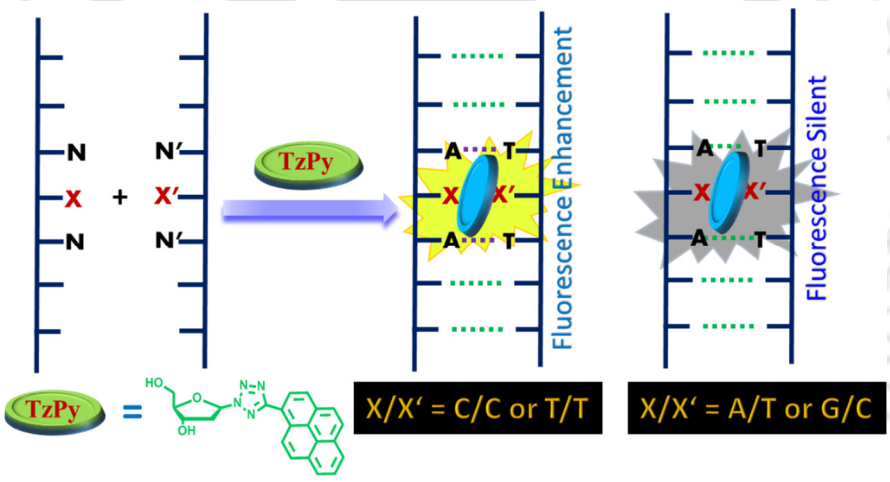

Figure 3.9. Chemical structure of **TzPy**, **3.9** and Proposed bind of **TzPy** to A/T flanked homo pyrimidine mismatched duplexes and matched duplex (X, X' = C/C or T/T, X = C/T, X' = Abasic or bulge site).

3.7. Result and Discussion

3.7.1. Study of Photophysical Properties of TzPy in dioxane-water mixture

Before going to detail study on interaction of different form of DNA (match and mismatch pair) with **TzPy**, we have performed the spectral study of **TzPy** in mixed dioxane-water environment. The study may give a basic idea of spectral characteristics of **TzPy** in non-polar and polar mixed environment. The absorption and fluorescence spectra of **TzPy** were recorded in dioxane-water mixed solvents and in buffer. From the absorption spectra (**Figure**

3.10a), it is seen that the absorption wavelength of **TzPy** was blue-shifted by addition of water/buffer to dioxane solution (**Figure 3.10c**). This might be a possibility of solvent-solute interaction/H-bonding interaction in H_2O. It was also found that absorption band is blue shifted as the solvent polarity increases.[19] A close look to **figure 3.10a, b** and **Table 3.1** suggested that the absorption spectrum of **TzPy** in dioxane (monomer) blue-shifted to 9 nm in higher water fraction. In addition, the band at 360-365 nm in dioxane became disappeared in water/buffer. With increase in water content the polarity of the environment changes and that decreases the solubility of **TzPy** in higher water fraction in dioxane and favours blue shifting of absorption wavelength.

To gain a further insight, we have performed the fluorescence measurements in dioxane and water. **Figure 3.10d** depicts the change in fluorescence behaviour in dioxane-water mixture. With increasing the percentage of water up to 30 % an increase in emission intensity observed but further increase of water percentage resulted a quenching of fluorescence intensity and almost quenched in water (**Figure 3.10d**). The initial minimum increases in fluorescence intensity may be due to combination of solubility and hydrophobic interaction of **TzPy** with water. But, the dramatic decrease of fluorescence is not due to effect of solubility alone. It perhaps due to intermolecular hydrogen bonding/hydrophobic interaction. This reflects quenching is due to less solubility as % water increases.

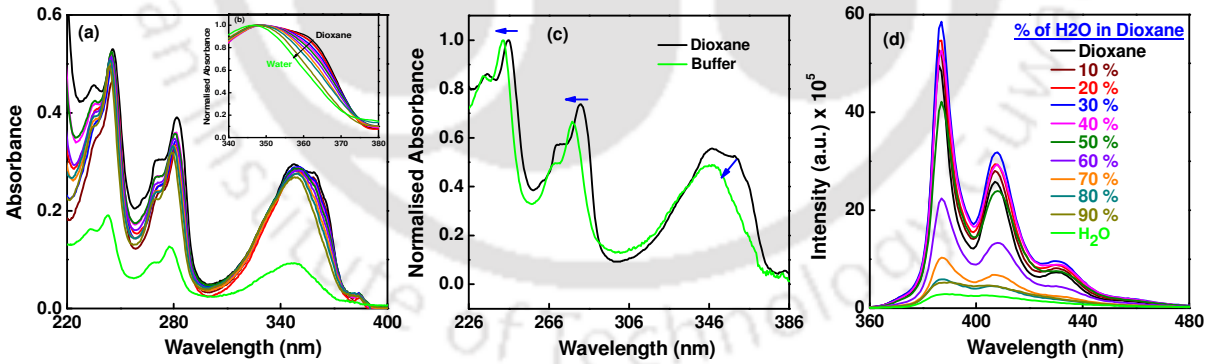

Figure 3.10. (a) UV-visible (b) inset normalised UV-visible of **TzPy** (c) normalised UV-visible absorbance in dioxane and buffer and (d) fluorescence emission spectra (λ_{ex} = 350 nm) in dioxane with increasing percent of water.

Table 3.1. Photophysical summary of Dioxane-water mixture of solvent

Entry	λ_{abs}	$\Delta\lambda_{abs}$	λ_{em}
Dioxane	347, 360, 366	---	386, 407, 431
10 % H2O	347, 358, 364	1	386, 407, 431
20 % H2O	347, 358, 363	2	387, 407, 430
30 % H2O	349, 363	2	387, 407, 430
40 % H2O	350, 362	3	387, 407, 430
50 % H2O	350, 361	4	387, 407, 430
60 % H2O	351, 360	5	387, 408, 430
70 % H2O	351, 360	5	387, 408, 430
80 % H2O	349, 359	6	387, 405
90 % H2O	348, 358	7	388, 404
H2O	344	3 nm	389, 403

3.7.2. DNA Mismatch Detection

3.7.2.1. Spectral Study of TzPy with Various Form of Match and Mismatch Duplexes Having Both AT/AT and GC/GC Flanking

Since **TzPy** exhibited low fluorescence in water/buffer, it will be interesting to study the interaction with DNA in aqueous buffer. The study will focus to investigate whether **TzPy** interact with DNA or not. In this regard, we examined the interaction of **TzPy** in buffer with various form of match pair and mismatch pair DNAs. The interaction of the nucleoside probe with short 13-mer duplex DNAs containing both match and mismatch pair having both A:T and G:C flanking base pair. This sequence context was so chosen as to study the effects of flanking bases (T−A and C−G base pairs) on the sensing of base mismatches. The DNAs used in this study is tabulated (**Table 3.2**).

Table 3.2. DNA sequences used in this study

ODNs	**T:A flanking base sequences**
1.	5'-CGCAAT **X** TAACGC-3' [**X** = A, G, C, T]
2.	5'-GCGTTA **Y** ATTGCG-3' [**Y** = A, G, C, T, Φ]
	C:G flanking base sequences
3.	5'-CGCAAC **X** CAACGC-3' [**X** = A, G, C, T]
4.	5'-GCGTTG **Y** GTTGCG-3' [**Y** = A, G, C, T, Φ]
5.	5'-CGCAAT_TAACGC-3'

To investigate mismatched DNA recognition over matched DNA, UV-visible experiment of **TzPy** were carried out with 13 mer matched and mismatched DNA (**Table 3.2**) in sodiaum phosphate buffer solutions (50 mM sodium phosphate and 100 mM NaCl in water, pH = 7). **Figure 3.11a and 3.11d** depict the absorption plot of **TzPy** with various match and mismatch pair DNA. **TzPy** exhibited a predominant band around 344 nm in buffer. Upon mixing with various matched and mismatched pair DNA, a dramatic changes of the absorption peaks were observed. The intensity of the peak around 344 nm gradually increased and 8-9 nm red shifted with addition of AT/AT flanking homopyrimidine mismatched DNA, [ODN **1•2** (X•Y = C•C/T•T)]. In addition, two new shoulder peaks at 374 nm and 388 nm appeared in the absorption spectra. Interestingly, for the case of AT/AT flanked matched (X•Y = A•T/G•C), homopurine mismatched (X•Y = A•A/G•G) duplexes only 1-2 nm of red shift was observed. Furthermore, when **TzPy** interacted with GC/GC flanking matched and various mismatched DNAs, [ODN **3•4**, (X•Y = A•T, G•C, A•A, G•G, C•C, T•T)] there was also no shift and no new absorption band observed but only enhanced absorbance band was observed. So, this result suggested that there was minimal effect on the absorbance of **TzPy** with other matched and mismatched DNAs having AT/AT and GC/GC base flanking duplexes, except AT/AT flanking homopyrimidine mismatched (C•C/T•T) duplexes. Upon addition AT/AT flanking homopyrimidine mismatched duplex (C•C/T•T) to the solution of TzPy gave a clear and visible color change upon irradiated with UV-transilluminator (**Figure 3.11e**). Meanwhile, we might be applied **TzPy** for the detection of AT/AT flanking homopyrimidine (C•C/T•T) mismatch pair. Due to the specific interaction of **TzPy** with AT/AT flanked homopyrimidine (X•Y = C•C) (**Figure 3.11c**), the absorbance at 374 nm gradually increases and the peak at 344 nm was red shifted to 353 nm with increasing addition of DNAs.

On the basis of above results, we proposed that **TzPy** interacts with homopyrimidine mismatch (C•C/T•T) specifically at the mismatch site. The **TzPy** occupies the cavity formed by mismatched cytosines, stacking with the flanking base pairs without affecting the helicity of DNAs, which was also supported from circular dichroism spectroscopic study.

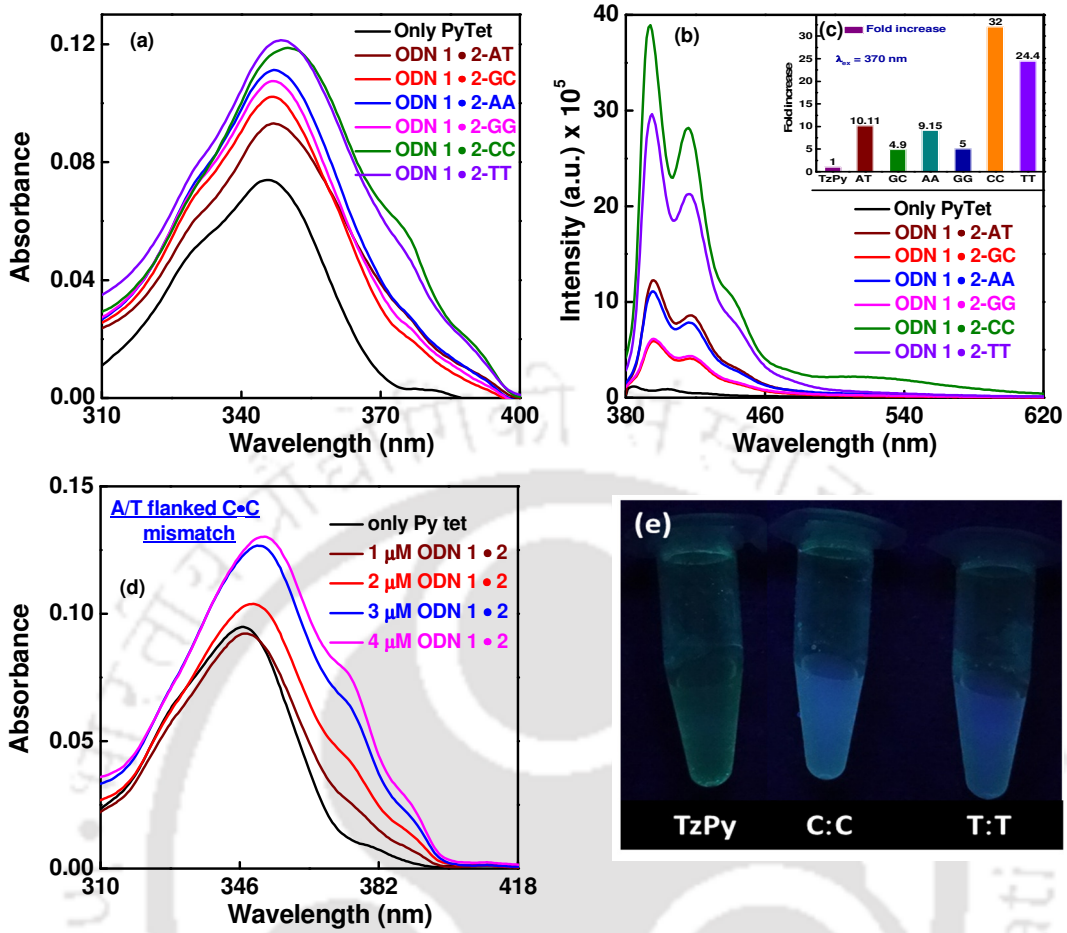

Figure 3.11. (a) UV-visible, (b) emission (c) in set fold increase in fluorescence of the probe (10 μM) in absence and presence of various mismatched/matched DNA duplexes (4 μM, pH 7), (d) UV-visible of **TzPy** with increase concentration of AT/AT flanking C•C mismatch duplex and (e) color change under UV- transilluminator.

Table 3.3. Photophysical Summary and Thermal melting (T_m) of **TzPy** non-natural nucleoside with AT/AT flanking various mismatch/match DNA duplexes

Entry	$\lambda_{abs.}$ (nm)	$\lambda_{em.}$ (nm)	Anisotropy	T_m (°C)	ΔT_m (°C)
Only TzPy	344	384, 404, 424	0.01	---	---
ODN 1•2–AT	---	---	---	52.03	---
ODN 1•2–AT + 3.9	348	396, 417, 440	0.05	52.03	---
ODN 1•2–GC	---	---	---	55.9	---
ODN 1•2–GC + 3.9	346	396, 417, 440	0.03	55.2	-0.7
ODN 1•2–AA	---	---	---	41.6	---
ODN 1•2–AA + 3.9	346	394, 417, 439	0.05	41.2	-0.4
ODN 1•2–GG	---	---	---	45.4	---
ODN 1•2–GG + 1	346	395, 417, 439	0.04	44.5	-0.9
ODN 1•2–CC	---	---	---	37.5	---
ODN 1•2–CC + 3.9	353, 374, 388	393, 415, 436	0.08	40.2	**2.7**
ODN 1•2–TT	---	---	---	42.4	---
ODN 1•2–TT + 3.9	352, 374, 388	394, 416, 439	0.076	43.6	**1.2**

$\Delta T_m = T_m$ with probe $-T_m$ without probe; Error in Tm is estimated at ±0.3 °C.

To investigate mismatched DNA recognition over matched DNA, fluorescence titrations of **TzPy** was also carried out with 13 mer matched and mismatched DNA (**Table 3.2**). Interestingly, the fluorescence of **TzPy** exhibited drastic change upon excitation at 370 nm in presence of AT/AT flanked homopyrimidine mismatch duplex ODN **1•2** (X•Y = C•C/T•T) (**Figure 3.11b**). On the other hand, the fluorescence intensity of AT/AT flanking fully matched duplexes ODN **1•2** (X•Y = A•T/G•C)] or homopurine mismatch duplexes ODN **1•2** (X•Y = A•A/G•G) are little affected on emission intensity compared to fluorescence intensity of **TzPy** (**Figure 3.11b**). Fluorescence enhancement upon binding may result from the hydrophobic microenvironment. Interestingly, **TzPy** exhibited a higher emission response in the presence of DNA homopyrimidine mismatch relative to the full matched DNA (**Figure 3.11b**). Given a 32-fold (at 393 nm) higher fluorescence intensity toward the C•C mismatch pair and 24-fold (at 393 nm) higher for T•T mismatch pair. This inferred that **TzPy** was quite selective for binding to the single base mismatch particularly homopyrimidine (**Figure 3.11b**). This selectivity might stem from the structural impact of C•C/T•T mismatch, which clearly alters the groove dimensions and the capability to binding through the simultaneously very low DNA breathing dynamics and a narrow minor groove.

The strong binding near the hydrophobic mismatched site leads to the enhanced fluorescence in case of homopyrimidine mismatched DNA with AT/AT flanked bases. This

specific detection of homopyrimidine might be due to the insertion of **TzPy** into the hydrophobic cavity generated at pyrimidine-pyrimidine mismatch site specifically. So, the **TzPy** got tightly captured at the hydrophobic site which got restricted in its rotational movement, resulting in an enhanced emission intensity. This was also supported by steady state anisotropy (**Table 3.3**) and the increased thermal stability (**Figure 3.14d, e**).

Furthermore, the effect of flanking bases on the interaction of **TzPy** was examined by fluorescence measurements. **Figure 3.12b** showed the fluorescence emission spectra of **TzPy** in the presence of 13-mer GC/GC flanking homopyrimidine mismatched duplexes. Interestingly, fluorescence changes were minimum upon addition of 13-mer GC/GC flanking homopyrimidine mismatched duplexes (**Figure 3.12b**). Furthermore, the emission maximum of **TzPy** was red shifted by about 12 nm in presence of DNA containing AT/AT flanking homopyrimidine mismatch duplexes, whereas no noticeable shift was observed for the DNA duplex containing homopyrimidine mismatch with GC/GC flanking duplexes. This is due to the more polar nature of guanine and cytosine. Therefore, the G•C base pair is also very polar. On the other hand, thymine has smaller dipole moment and adenine is even less polar. As a result, the whole A•T base pair is much less polar than the G•C one [20]. This might be the reason that high polar cavity created by GC/GC flanking bases has no effect on the fluorescence of **TzPy**. Also GC/GC flanking duplexes exhibited quenching character. Hence, **TzPy** may experience different polarity with different flanking bases, which in turn may affect its fluorescence.

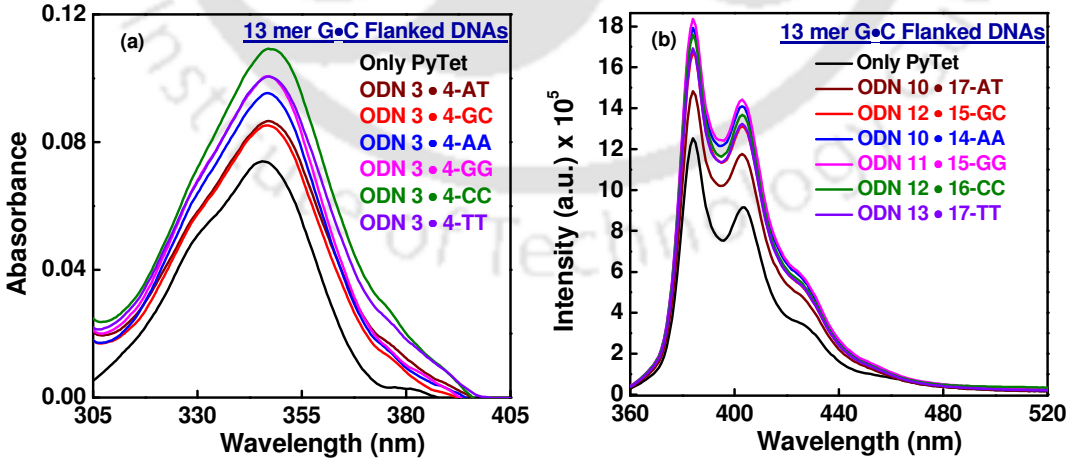

Figure 3.12. (a) UV-visible and (b) fluorescence emission spectra of the probe (10 μM) in absence and presence of GC/GC flanking various mismatch/match DNA duplexes (4 μM, pH 7).

Table 3.4. Photophysical Summary and Thermal melting (T_m) of **TzPy** non-natural nucleoside with GC/GC flanking various mismatch/match DNA duplexes

Entry	$\lambda_{abs.}$ (nm)	$\lambda_{em.}$ (nm)	Anisotropy	T_m (°C)	ΔT_m (°C)
Only TzPy, 3.9	344	384, 404, 424	0.01	---	---
ODN 3•4–AT	---	---		60.6	---
ODN 3•4–AT + 3.9	346	384, 403, 422	0.012	59.6	-1
ODN 3•4–GC	---	---		62.0	---
ODN 3•4–GC + 3.9	346	384, 403, 422	0.013	61.5	-0.5
ODN 3•4–AA	---	---		50.6	---
ODN 3•4–AA + 3.9	346	384, 403, 422	0.01	49.6	-1
ODN 3•4–GG	---	---		52.0	---
ODN 3•4–GG + 3.9	346	384, 403, 422	0.01	51.5	-0.5
ODN 3•4–CC	---	---		44.2	---
ODN 3•4–CC + 3.9	346	384, 403, 422	0.014	43.4	-0.8
ODN 3•4–TT	---	---		51.3	---
ODN 3•4–TT + 3.9	346	384, 403, 422	0.013	50.5	-0.8

$\Delta T_m = T_m$ with probe $-T_m$ without probe; Error in Tm is estimated at ±0.3 °C.

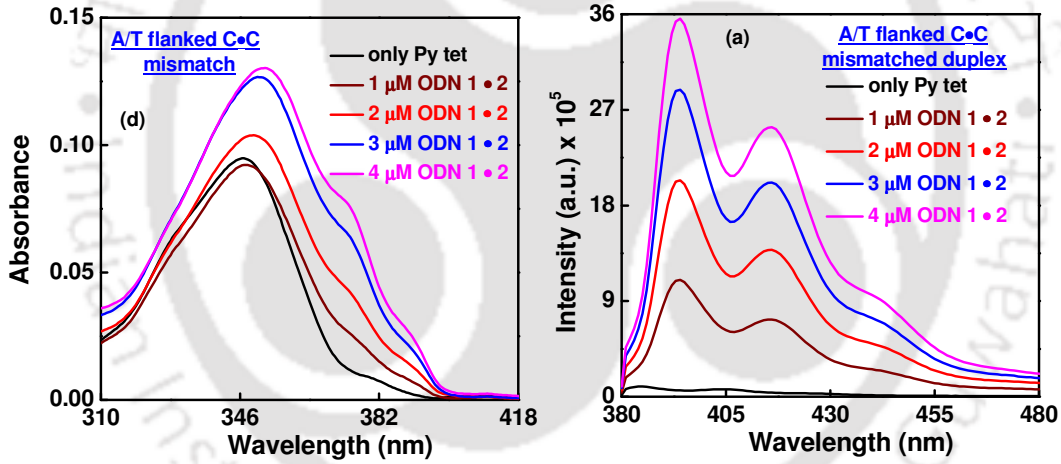

Figure 3.13. (a) UV-visible, (b) fluorescence emission spectra of the probe (10 μM) in absence and presence of increasing concentration of AT/AT flanking C•C mismatch duplex, ODN **1•2**, X•Y = C•C, (4 μM, pH 7).

3.7.2.2. Effect of TzPy On the Thermal Stability of Various Match and Mismatch Duplexes Having Both AT/AT and GC/GC Flanking Base Pairs

The effect of **TzPy** on the thermal stability of various matched and mismatched duplexes with both AT/AT and GC/GC flanking base pairs was assayed by recording the melting profiles of DNAs in presence and absence of **TzPy**. Groove binding by a combination of electrostatic, van der Waals, and hydrogen-bonding interactions exerted stabilizing effects on DNA structure, which leads to a rise in its melting temperature. The more and stronger the

interactions are, the higher the melting temperature of duplex DNA is. The thermal stability of AT/AT flanking C•C mismatch pair increased by 2.8 °C and that of T•T mismatch pair was by 1.2 °C (**Figure 3.14 d, e**); whereas no such marked effect was found for other homopurine mismatched and matched DNA (**Figure 3.14, Table 3.3**). This might be due to the probe **TzPy** inserted to the compact hydrophobic cavity of the mismatch site and got stacked between the flanking bases which might increase the stability of the AT/AT flanking homopyrimidine mismatch duplexes. No such types of stabilization occurred for other form of DNAs including GC/GC flanking matched and mismatched duplexes (**Figure 3.15, Table 3.4**).

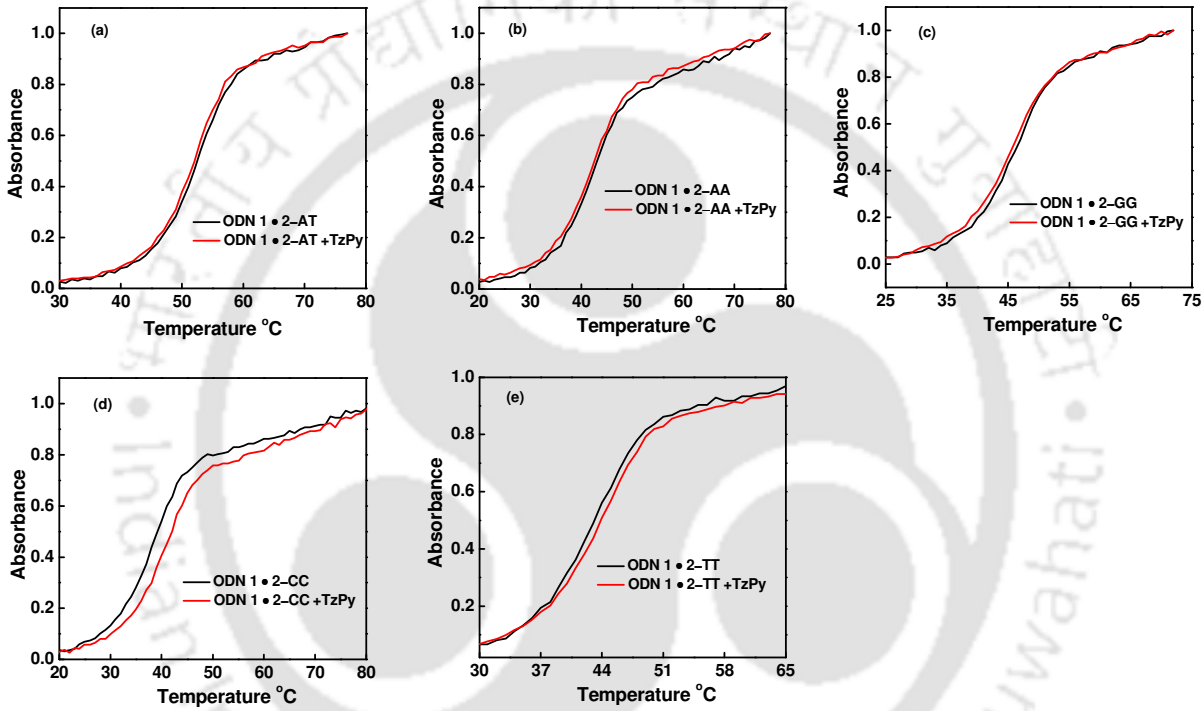

Figure 3.14. Melting temperature curve (T_m) of A:T flanking various match and mismatch duplexes, ODN **1•2**, X•Y = (a) A•T, (b) A•A, (c) G•G, (d) C•C and (e) T•T in absence and presence of **TzPy**.

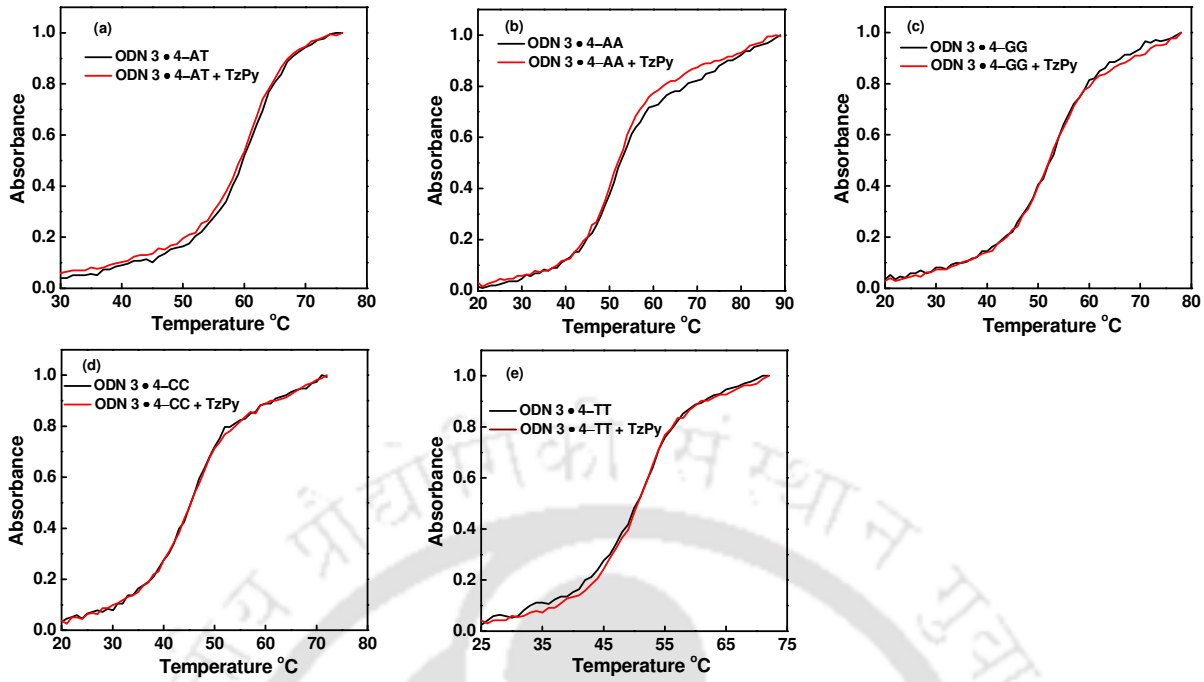

Figure 3.15. Melting temperature curve (T_m) for G:C flanking various match and mismatch duplexes, ODN **1•2**, X•Y = (a) A•T, (b) A•A, (c) G•G, (d) C•C, (e) T•T in absence and presence of **TzPy**.

3.7.2.3. Effect of TzPy On the Circular Dichroism Spectra of Various Match and Mismatch Duplexes Having Both AT/AT and GC/GC Flanking Base Pairs

The effect of **TzPy** on the conformation of various matched and mismatched duplexes with both AT/AT and GC/GC flanking base pairs was studied using CD spectropolarimeter. **Figure 3.16-3.17** depicts CD characteristic spectra for AT/AT and GC/GC flanking matched and mismatched DNAs respectively. In the absence of **TzPy**, the CD spectra of all DNAs exhibited a characteristic positive peak at 222 and 282 nm and a negative peak at 252 nm, which was assigned as the characteristic of B-DNA. Interestingly, **TzPy** had a negligible impact on the B-DNA conformation of mismatched/matched DNA duplexes. Thus, we did not observe any significant change in CD spectra in presence of **TzPy** (**Figure 3.16, 3.17**). This insignificant change of the CD spectrum following the addition of **TzPy** suggested the presence of **TzPy** did not disturbed the topological conformation of DNAs. Furthermore, there was also no such noticeable effect observed for AT/AT flanking homopyrimidine mismatched duplexes in presence of **TzPy**. **TzPy** interacted with homopyrimidine mismatched (C•C/T•T) duplexes specifically at the mismatch site, inserting deeply in DNA without disturbing the helical conformation and got π-π stacking with the flanking bases protruding into the opposite major

groove.[21] **TzPy** occupied the place (cavity) made by two mismatched cytosines and held via stacking with the flanking base pairs. So, this specific type of binding mode of **TzPy** to homopyrimidine mismatched DNA termed as insertion not intercalation, because intercalation which leads to unwinding and elongation of the helix in contrast to insertion does not unwind DNA helix.[22]

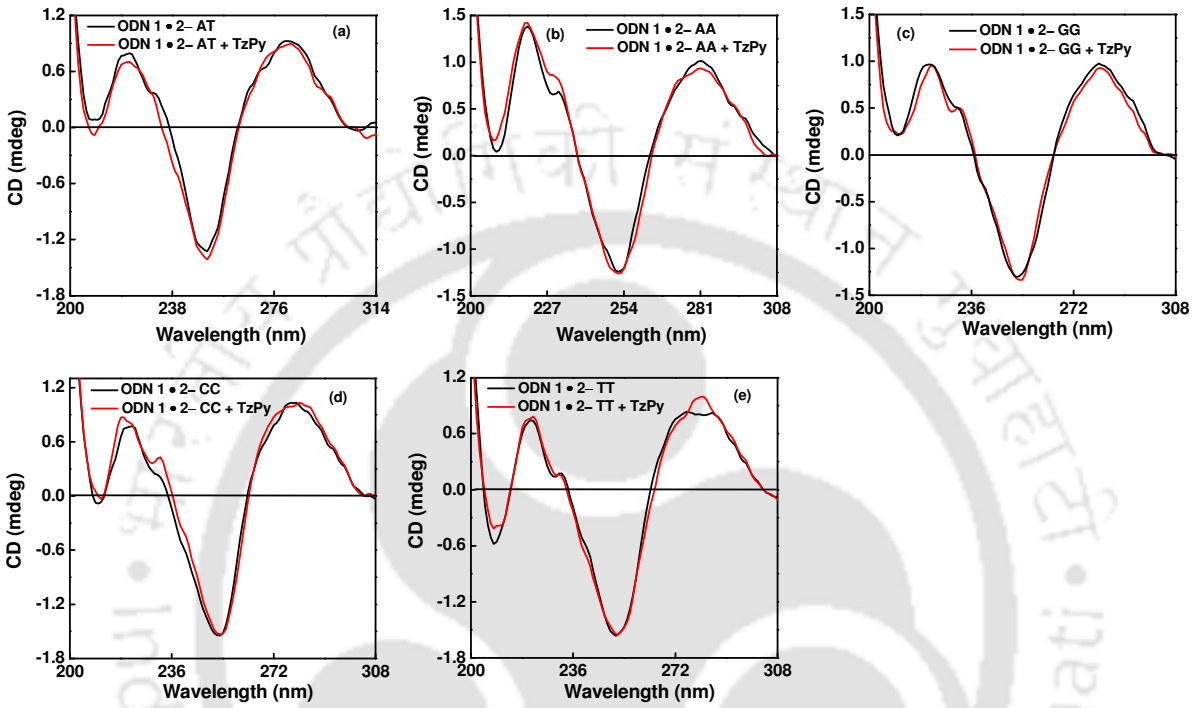

Figure 3.16. Circular Dichroism (CD) spectra of of AT/AT flanking various match and mismatch duplexes, ODN **1•2**, X•Y = (a) A•T, (b) A•A, (c) G•G, (d) C•C, (e) T•T in absence and presence of TzPy.

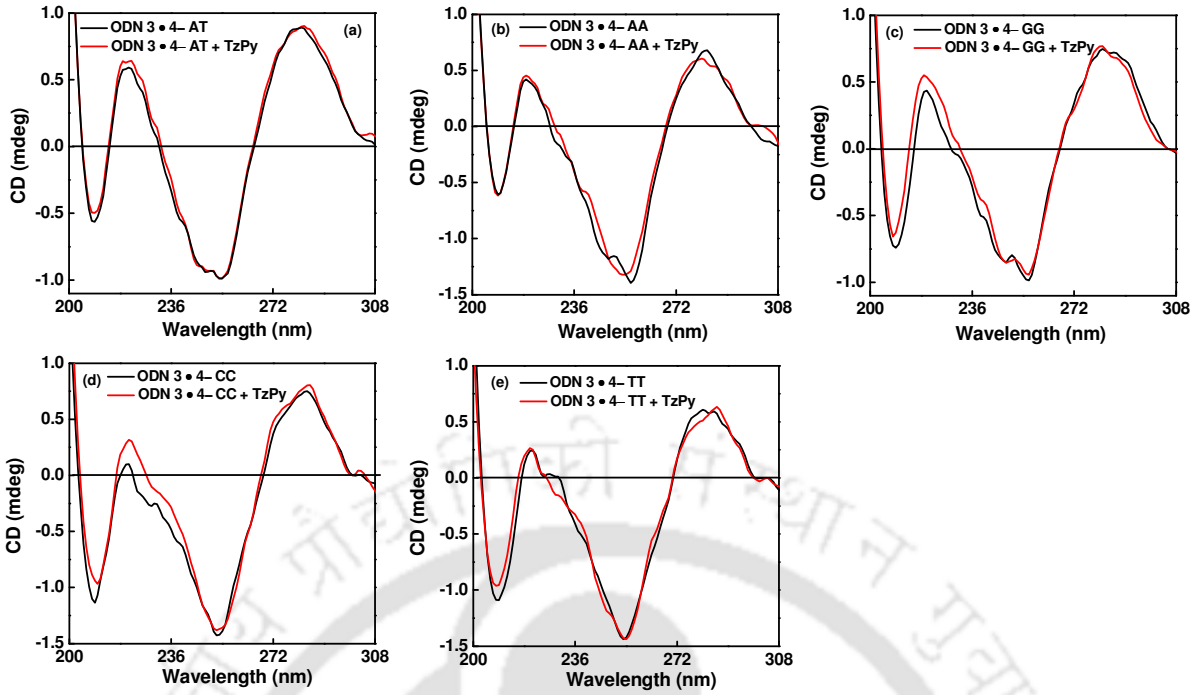

Figure 3.17. Circular Dichroism (CD) spectra of of GC/GC flanking various match and mismatch duplexes, ODN **1•2** (X•Y = (a) A•T, (b) A•A, (c) G•G, (d) C•C, and (e) T•T) in absence and presence of **TzPy**.

3.7.3. Detection of Abasic Site (AP site) Positioned Opposite to Pyrimidines in Duplex DNA

Previous experiment showed that **TzPy** interact strongly in the hydrophobic site generated by homopyrimidine mismatched DNAs. The change in absorption and emission intensity might be due to hydrophobic base stacking interaction by flanking bases in the mismatch site. This result was highly selective and made us to think whether the same probe can be utilized for detecting an abasic site. In this context ODN **2** and ODN **1** (**Table 3.1**) were chosen for pyrimidine detection positioned opposite to abasic site. ODN **2** in which Y = absic site, (Φ) flanked between adenine bases and ODN **1** is a complementary to ODN **2** wherein, X = C/T were placed opposite to abasic site. Herein, an abasic site (AP site) in a DNA duplex was employed as a binding site for **TzPy**. The proposed binding interaction of **TzPy** to abasic site opposite to pyrimidine in AT/AT flanking bases represented in **Figure 3.18**.

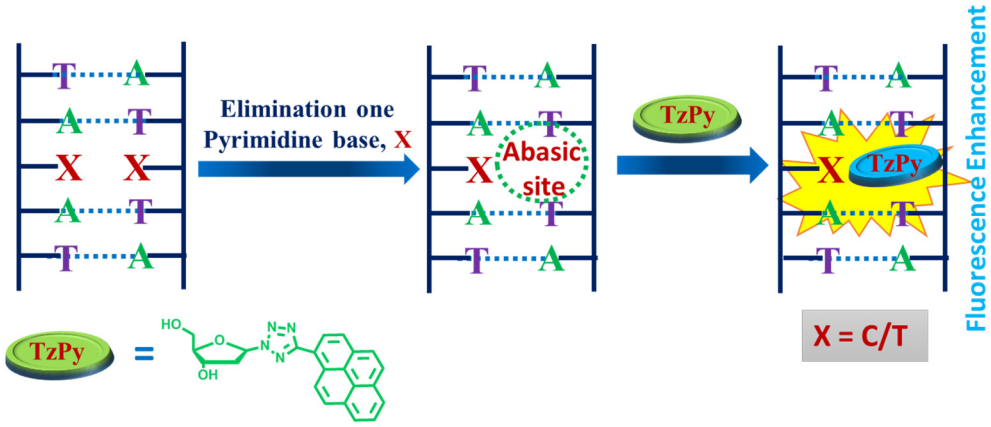

Figure 3.18. Pictorial presentation of the proposed binding of **TzPy** to abasic site opposite to pyrimidines (X = C/T).

3.7.3.1. Spectral Study of TzPy with Abasic Site Positioned Opposite to Pyrimidine in AT/AT Flanking Duplex DNA

As is shown in **Figure 3.19a**, **TzPy** showed significant red shift of about 9 nm, (λ_{abs} = 344 nm to λ_{abs} = 353 nm) and a new shoulder peak at 373 nm appeared, which was assigned as characteristic of **TzPy** upon binding with AP site containing duplex (the base opposite from the AP site is C/T). It is interesting to note that **TzPy** showed the selectivity for C or T opposite to AP site over full match pair (ΔT_m = -0.4) which also supported from an increasing thermal stability (**Figure 3.20, Table 3.5**) (C, ΔT_m = +4.8 or T, ΔT_m = +1.9).

Unlike weak binding of **TzPy** to the fully matched DNAs without the AP site, strong binding of **TzPy** to the AP site occurred and the **TzPy**'s fluorescence light-up behaviours are highly dependent on the target nucleobases opposite the AP site in which the targets thymine and cytosine produced enhanced emission band, while the targets full match pair only gave a minimal effect on emission band (**Figure 3.19b, Table 3.5**). While abasic site was positioned opposite to cytosine, the fluorescence increment was about 19 fold (at 394 nm), the abasic site positioned opposite of thymine experienced a 14 fold (at 394 nm) enhanced intensity. Interestingly there was very minimal effect on fluorescence for full matched pair, which also investigated earlier. It was expected that the target pyrimidines cause **TzPy** would be stacked well within DNA base pairs near the AP site, which results in a strong hydrophobic environments and π-π stacking electrostatic interaction with the flanking base pairs reduced the rotational movement which leads to enhanced fluorescence emissions. The increased in steady state anisotropy (**Table 3.5**) also supported the restricted rotation of **TzPy** due to strong

binding in the mutated site (abasic site positioned opposite to pyrimidine base). The result further supported by the increase in thermal stability of these mutated DNAs in presence of **TzPy** (**Figure 3.20**). We expect that this approach would shed light to develop a practical device for differentiating pyrimidines positioning opposite to an AP site from full match pair.

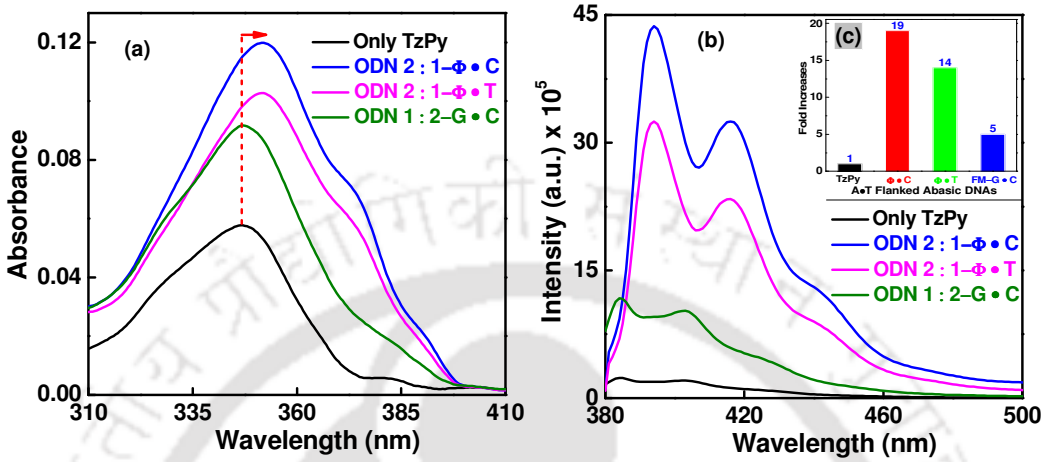

Figure 3.19. (a) UV-visible, (b) emission and (c) in set fold increase in fluorescence of the probe **TzPy** (10 μM) in presence and absence of AP site in opposite to pyrimidine base ODN **2•1** (X = C and T) and full match DNA duplexes (4 μM, pH 7).

Table 3.5. Photophysical summary of TzPy with AT/AT flanking Abasic site DNAs

Entry	$\lambda_{abs.}$ (nm)	$\lambda_{em.}$ (nm)	Anisotropy	T_m (°C)	ΔT_m (°C)
Only TzPy	344	384, 404, 424	0.01	---	---
ODN 2•1–ΦC	---	---	---	33.9	---
ODN 2•1–ΦC + TzPy	353, 373, 390	394, 416, 439	0.1	38. 7	4.8
ODN 2•1–ΦT	---	---	---	36.4	---
ODN 2•1–ΦT + TzPy	353, 373, 390	394, 416, 439	0.09	38.3	1.9
ODN 1•2-GC	---	---	---	55.2	---
ODN 1•2-GC + TzPy	346	384, 403, 426	0.013	54.8	-0.4

3.7.3.2. Effect of TzPy On the Thermal Stability of Abasic Site Positioned Opposite to Pyrimidine in AT/AT Flanking Duplex DNA

Thermal stability of AP site (abasic site) opposite to pyrimidine also evaluated in the absence and presence of **TzPy**. As shown in **Figure 3.20** abasic site opposite to cytosine was stabilized more (ΔT_m = 4.8, **Figure 3.20a, Table 3.5**) compared to that positioned opposite to thymine (ΔT_m = 1.9, **Figure 3.20b**). Earlier we showed that there was no or minimal effect on

full match pair. The increase thermal stability might be due to π-π stacking of **TzPy** with the flanking bases in the AP site positioned opposite to pyrimidine.

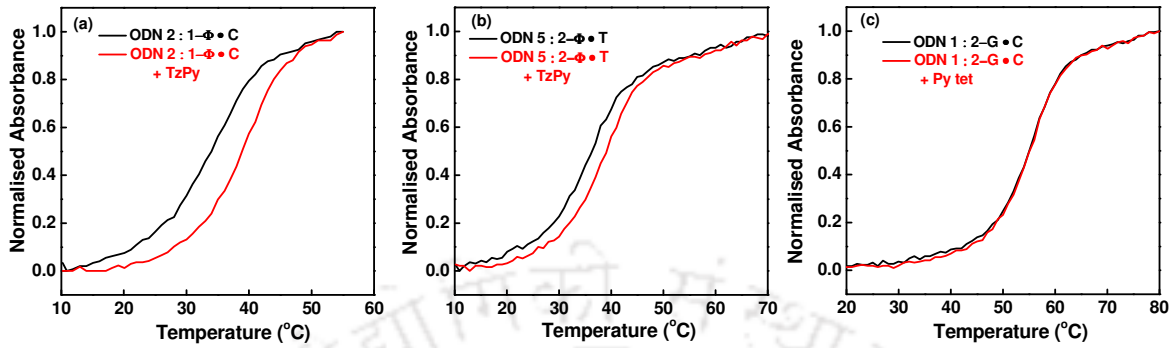

Figure 3.20. Melting temperature curve (T_m) for AT/AT flanking abasic site opposite to pyrimidine duplexes, ODN **2•1**, Y•X = (a) Φ•C, (b) Φ•T and (c) full match duplex in absence and presence of **TzPy**.

3.7.3.3. Effect of TzPy On the Circular Dichroism of Abasic Site Positioned Opposite to Pyrimidine in AT/AT Flanking Duplex DNA

In absence of **TzPy**, the CD spectra of abasic site positioned opposite to Pyrimidine and fully matched duplex exhibited a characteristic positive peak at 222 and 282 nm and a negative peak at 252 nm, which is the characteristic of B-DNA (**Figure 3.21**). Interestingly, **TzPy** had a negligible impact on the conformation of absic DNAs.

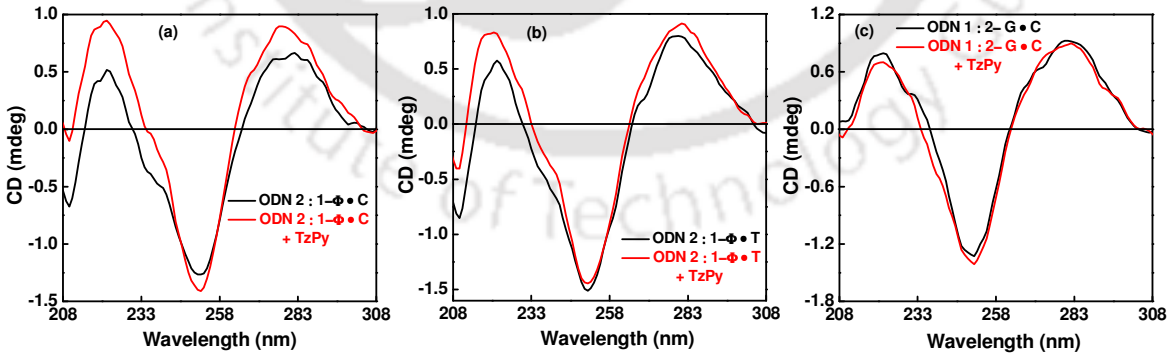

Figure 3.21. Circular Dichroism (CD) spectra for AT/AT flanking abasic site opposite to pyrimidine duplexes, ODN **2•1**, Y•X = (a) Φ•C, (b) Φ•T and (c) full match duplex in absence and presence of **TzPy**.

3.7.4. Detection of Pyrimidine Bulge DNAs

Single-base bulge in DNA is also a common type of DNA damage which arise due to either insertion or deletion of one or more bases during the replication process[23,24] or from recombination between imperfectly homologous sequences.[25] However, the mutated DNAs including homopurine, homopyrimidine, abasic site and bulge structures have widespread biological consequences inducing frame-shift mutagenesis,[23,26] which leads to highly harmful diseases[27] including cancers,[30] hypercholesterolemia[28] and Alzheimer's[29] etc. Therefore, there is much demand to develop more reliable methods for the recognition of such types of mutated DNAs in order to find disease-related mutations and identify the mutated site which can be potentially targeted by drug design.

Previously, we found that the homopyrimidine mismatch site and abasic site selectively when positioned opposite to pyrimidine base provided a well-defined space to interact with **TzPy**. Thus, **TzPy** got tightly captured at the hydrophobic pocket which reduced its rotational movement, resulted an increased steady state anisotropy and strong enhanced emission intensity. Interestingly the driving forces of the interaction of **TzPy** with mutated DNAs mainly resulted from the strong hydrophobicity of the DNA-**TzPy** complexes, which compromises the binding selectivity for the **TzPy** with mutated site in DNA. Herein, we focus to test whether the space provide by extra single base or bulge site in DNA will be able to interact with **TzPy** in the same manner or not. So, we carried out all experiments with AT/AT flanking pyrimidine bulges which was performed previously for homopyrimidine mismatch and abasic site with the same condition and solution environment. The pictorial presentation of the formation of pyrimidine bulge DNA and interaction with **TzPy** proposed in **Figure 3.22**.

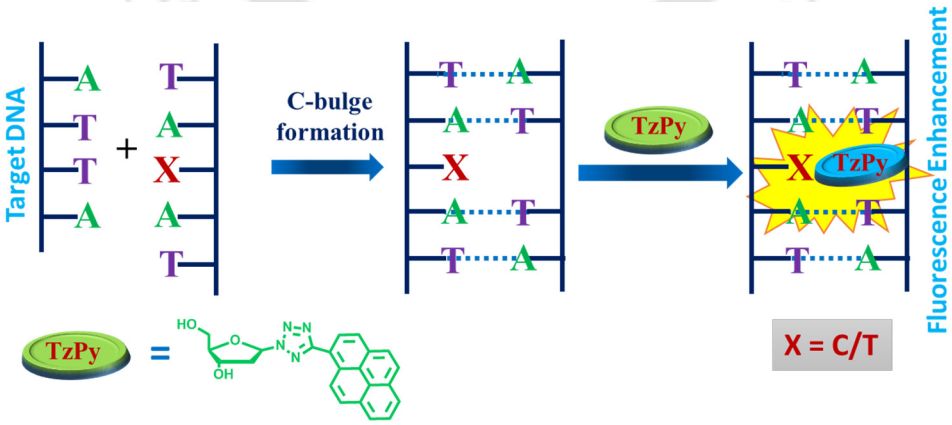

Figure 3.22. Pictorial presentation of the proposed binding of **TzPy** to pyrimidines (X = C/T) bulge.

In order to elucidate the role of the bulge site in interaction with **TzPy**, the bulge site-containing DNA was compared with the fully matched DNA. As we previously observed that, fully matched DNA provided no or minimal effect on the photophysical outcome of **TzPy**, whereas the mismatched/abasic DNAs made changes in photophysical property. A close look at the structural features of fully match DNA and mutated DNA, both DNAs provides the common grove binding sites, but the big difference was the mutated site which was provided by mutated DNAs. This mutated site might be play a vital rule for the specific recognition of mutated DNAs. This inferred, the strong binding between **TzPy** and mutated DNAs occurred by inserting into the mutated cavity and π-π stacking with the flanking bases. Fully matched DNA had no effect on **TzPy**, meanwhile groove site had no rule to binds with **TzPy**. So, it the only mutated site which responsible for binging and changes in photophysical property of **TzPy**.

3.7.4.1. Spectral Study of TzPy with AT/AT Flanking Pyrimidine-Bulge

All spectral studies of **TzPy** carried out in buffer containing 100 mM NaCl, 50 mM sodium phosphate buffer having pH 7 in absence and presence of pyrimidine bulge and fully matched DNA. As shown in **figure 3.23a**, upon addition of pyrimidine bulge DNA (ODN **2•5** = AXA/T_T, X = C/T) to the solution of **TzPy** the band at 344 nm faced bathochromic shift to 13 nm (344 nm → 357 nm) with a new shoulder peak at 374 nm. These facts support the strong binding of **TzPy** acquired to bulge site. On the other hand, no significant absorption spectrum observed in the presence of FM duplex (**Figure 3.23a**). Thus, as we discussed earlier, the DNA groove did not support to bind **TzPy**. So, only the bulge site provided the well-defined space for **TzPy** to insert into the cavity via stacking between the flanking bases. The increase in thermal stability in presence of **TzPy** further supported our assumption (**Figure 3.24**).

Next the interaction between **TzPy** with pyrimidine bulge DNA was studied using fluorescence spectroscopy. From the fluorescence spectrum (**Figure 3.23b**) a drastic enhancement of fluorescence emission intensity was observed in presence of pyrimidine bulge DNA. **TzPy** emitted strongly at 394 nm under excitation at 370 nm for both C-bulge and T-bulge respectively ODN **2•5** (ACA/T_T, ATA/T_T). Interestingly, C-bulge DNA showed more selectivity over T-bulge DNA. C-bulge DNA (ODN **2•5** = ACA/T_T) gave 42-fold increase in fluorescence intensity whereas T-bulge (ODN **2•5** = ATA/T_T) 37.4 fold at 394 nm. The increased thermal stability (**Figure 3.24, Table 3.6**) and increased steady state anisotropy (**Table 3.6**) also support our assumption. On the other hand, no observable emission

was detected with the corresponding fully matched DNA in the same solution conditions as we observed earlier. Thus, in this case the DNA groove did not support the interaction with **TzPy**. On the basis of our assumption of **TzPy** to a defined size at the bulge site, a similar emission wavelength could be envisaged under excitation with varied wavelengths at 280 nm and 350 nm.

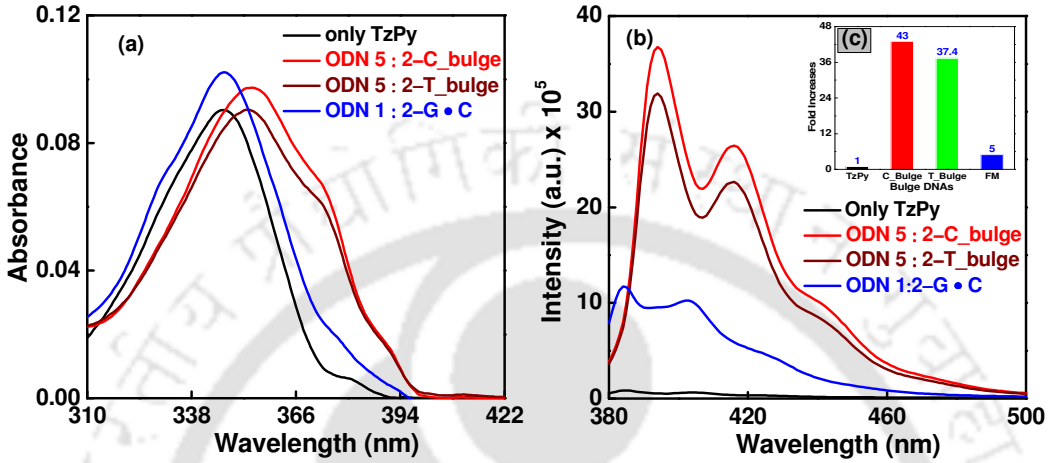

Figure 3.23. (a) UV-visible, (b) emission and (c) in set fold increase in fluorescence of the probe **TzPy** (10 μM) in presence and absence of pyrimidine bulge ODN **2•5** (T_T/ACA and T_T/ATA) and full match DNA duplexes (4 μM, pH 7).

Table 3.6. Photophysical summary of **TzPy** with AT/AT flanking Bulge DNAs

Entry	$\lambda_{abs.}$ (nm)	$\lambda_{em.}$ (nm)	Anisotropy	T_m (°C)	ΔT_m (°C)
Only TzPy	344	384, 404, 424	0.01	---	---
ODN 2•5–C	---	---	---	42.7	---
ODN 2•5–C + TzPy	357, 374, 390	393, 415, 438	0.01	44.6	1.9
ODN 2•5–T	---	---	---	41.1	---
ODN 2•5–T + TzPy	356, 374, 390	393, 415, 438	0.09	42.4	1.3
ODN 3•4–GC	---	---	---	55.2	---
ODN 1•2–GC + TzPy	346	384, 403, 426	0.013	54.8	-0.4

3.7.4.2. Effect of TzPy On the Thermal Stability of Pyrimidine-Bulge

A qualitative structure–function relationship was established by thermal denaturation studies of DNA oligonucleotides containing a single pyrimidine-bulge (**Figure 3.24**). In the presence of TzPy, DNA duplex containing a single pyrimidine-bulge flanked by AT/AT was stabilized by +1.9 °C and +1.3 °C for C-bulge and T-bulge respectively (**Figure 3.24a, b**).

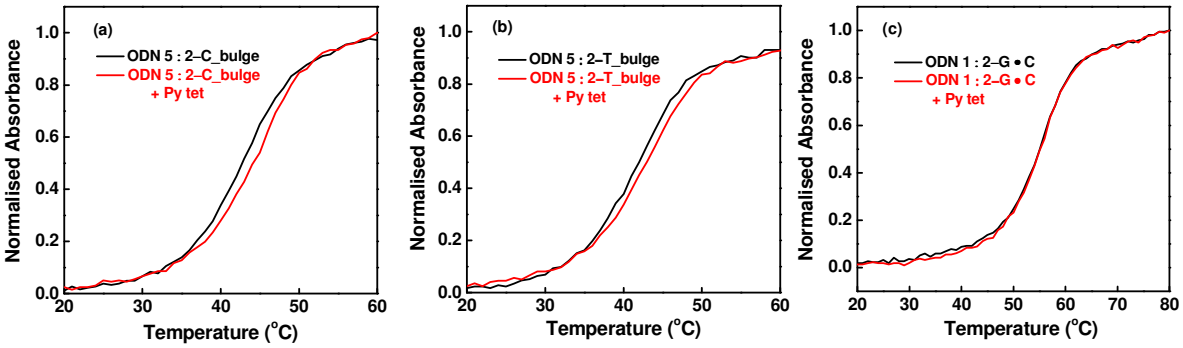

Figure 3.24. Thermal melting curve of AT/AT flanking pyrimidine bulge and fully matched duplex, ODN **2•5**, (a) C-bulge, (b) T-bulge and (c) fully match pair in absence and presence of **TzPy**.

3.7.4.3. Effect of TzPy On the Circular Dichroism of Pyrimidine-Bulge

In the absence of **TzPy**, the CD spectra of abasic site opposite to Pyrimidine and fully matched duplex exhibited a characteristic positive peak at 222 and 282 nm and a negative peak at 252 nm, which assign the characteristic of B-DNA. Interestingly, **TzPy** had a negligible impact on the characteristic peaks of pyrimidine-bulge DNA, there was no such spectral changed observed in presence of **TzPy** (**Figure 3.25**). This minimal change of the CD spectrum following the addition of **TzPy** suggested that the **TzPy** did not disturbed the topological conformation of pyrimidine-bulge DNAs.

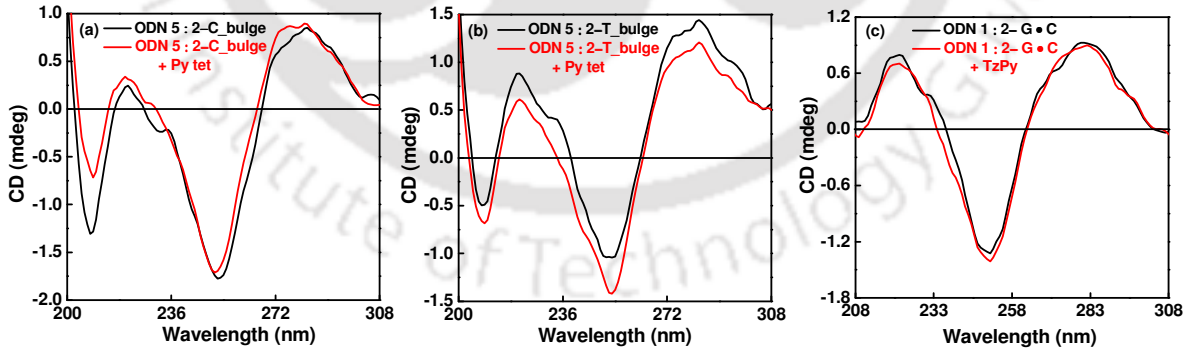

Figure 3.25. Circular Dichroism (CD) spectra of AT/AT flanking pyrimidine-bulge and fully matched duplex, ODN **2•5**, (a) C-bulge, (b) T-bulge and (c) fully match pair in absence and presence of **TzPy**.

3.8. Conclusion

In conclusion, **TzPy** serves as a versatile fluorescent light-up probe for label free detection of pyrimidine base mispair. The probe further was found to bind strongly to abasic site positioned opposite to pyrimidine bases. In addition, the probe, **TzPy** represents an attractive probe for recognizing pyridine base bulge-out in DNA bulge hairpin. The binding of the probe to all the three mutated DNA duplexes is accompanied by an increase in the thermal stability. So, **TzPy** exhibits highly sensitive, selective and fluorescent detection of mutated DNAs over fully matched duplexes without affecting the helical conformation. The high degree of specificity towards mutated DNAs comes mainly from the **TzPy** inserting into the hydrophobic mutated site of DNAs. All the spectral evidences open up a multitude of possibilities for the probe **TzPy** to be an efficient fluorescent light-up bioprobe for label free DNA detection. The label free fluorescent light-up sensing of DNA base mismatches, abasic DNAs and DNA bulge over matched duplexes makes **TzPy** exploitable as a potential diagnostic tool for the diseases that are associated with these types of mutated DNAs. The **TzPy** might also find future applications for the detection and targeting of DNA lesion with a less laborious, simple and cost effective way. Recognition of such DNA lesions may give clues about the initial DNA recognition event(s) by repair enzymes in the complex repair machinery.

3.9. Experimental Section

3.9.1. Spectroscopic Measurements:

3.9.1.1. UV-visible measurements:

UV-visible spectra of probe (10 uM fixed concentration) and all the ODNs (4 μM concentration of each single strand) were measured in 50 mM sodium phosphate buffers (pH 7.0) containing 100 mM sodium chloride using Shimadzu UV-2550 UV-Visible spectrophotometer, with quartz optical cell of 1.0 cm path length and scanning rate of 0.5 nm with wavelength range of 200-500 nm and slit width of 1 nm.

3.9.1.2. Thermal melting temperature (T_m) experiments of the oligonucleotides:

The thermal denaturation studies (T_m), absorbance *vs.* temperature profiles of the duplexes (4 μM concentration of each single strand) were measured at 260 nm using Shimadzu UV-2550

UV-Visible spectrophotometer equipped with a Peltier temperature controller using 1 cm path length cell in 50 mM sodium phosphate buffers (pH 7.0) containing 100 mM sodium chloride. The absorbance of the samples was monitored at 260 nm from 10 to 90 °C with a heating rate of 0.5 °C/min. From these profiles, average method was used to determine T_m values using in built software.

3.9.1.3. Steady state fluorescence experiments:

ODNs solutions were prepared as described in UV-visible and T_m measurement experiments. Fluorescence spectra were recorded using Fluoromax–4 fluorescence spectrophotometer at 25 °C using quartz cell of 1.0 cm path length with a slit width of 4 nm, wavelength range 350-650 nm. Excitation spectra were monitored at 410 nm emission wavelength. Fluorescence emissions were collected exciting the ODNs at the wave length corresponding to their absorption maxima. Steady-state fluorescence emission spectra were recorded at room temperature as an average of ten scans using an excitation slit of 5.0 nm, emission slit 5.0 nm. The steady state anisotropy experiment was performed with the same fluorescence spectrophotometer at 25 °C using 1 cm path length cell. The fluorescence anisotropy (r) was calculated using the following equation-

$$r = \frac{(I_{VV} - I_{VH}G)}{(I_{VV} + 2I_{VH}G)};\ G = \frac{I_{HV}}{I_{HH}}$$

where, I_{VV} and I_{VH} are the emission intensities when the excitation polarizer is vertically oriented and the emission polarizer is oriented vertically and horizontally respectively. G is the correction factor. The terms I_{HV} and I_{HH} are the emission intensity when the excitation polarization is horizontally oriented and the emission polarization is oriented vertically and horizontally, respectively.

3.9.1.4. Circular dichroism (CD) measurement:

CD spectra were recorded with JASCO CD J-810 Spectorpolarimeter equipped with a Peltier thermoelectric type temperature control system (4 μM concentration of each strand in 50 mM sodium phosphate, 100 mM sodium chloride, pH 7.0, at room temperature). The data were collected using quartz optical cells with a 1.0 cm path length. Measurements were conducted using 4 μM of strands in buffer. Corrections were made for buffer background CD spectra (200-400 nm) were recorded at 25 °C as an average of three scans and with a scan speed of 200 nm/min. The spectral data were analyzed with the spectra manager software.

3.10. References

1. Navani, N. K.; Li, Y. *Curr. Opin. Chem. Biol*., **2006**, *10*, 272.
2. Ma, D. -L.; He, H. -Z.; Leung, K. -H.; Zhong, H. -J.; Chana, D. S.-H.; Leung, C. -H. *Chem. Soc. Rev*., **2013**, *42*, 3427.
3. Joseph, M. J.; Taylor, J. C.; McGown, L. B.; Pitner, J. B.; Linn, C. P. *Biospectrum*, **1996**, *2*, 173.
4. Bag, S. S.; Pradhan, M. K.; Das, S. K.; Jana, S.; Bag, R. *Bioorg. Med. Chem. Lett*. **2014**, *24*, 4678.
5. (a) Mukherjee, A.; Lavery, R.; Bagchi, B.; Hynes, J. T. *J. Am. Chem. Soc*., **2008**, *130*, 9747. (b) Neidle, S.; Thurston, D. E. *Nat. Rev. Cancer***, 2005**, *5*, 285.
6. Sato, Y.; Honjo, A.; Ishikawa, D.; Nishizawa, S.; Teramae, N. *Chem. Commun*., **2011**, *47*, 5885.
7. Granzhan, A.; Teulade-Fichou, M. -P. *Chem. Eur. J*. **2009**, *15*, 1314.
8. Zhao, C.; Dai, Q.; Seino, T.; Cui, Y. -Y.; Nishizawa, S.; Teramae, N. *Chem. Commun*. **2006**, 1185.
9. (a) Glitzer, M. S.; Steelman, S. L. *Nature*, **1966**, *212*, 191; (b) Benos, D. J. *Am. J. Physiol*., **1982**, *242*, 131; (c) Tewey, K. M.; Rowe, T. C.; Yang, L.; Halligan, B. D.; Liu, L. F. *Science*, **1984**, *226*, 466; (d) Besterman, J. M.; Elwell, L. P.; Blanchard, S. G.; Cory, M. *J. Biol. Chem*., **1987**, *262*, 13352.
10. Zhao, C.; Rajendran, A.; Dai, Q.; Nishizawa, S.; Teramae, N. *Anal. Sci.***2008**, *24*, 693.
11. Rajendran, A.; Zhao, C.; Rajendar, B.; Thiagarajan, V.; Sato, Y.; Nishizawa, S.; Teramae, N. *Biochim. Biophys. Acta.* **2010**, *1800*, 599.
12. Wu, F.; Shao, Y.; Ma, K.; Cui, Q.; Liu, G.; Xu, S. *Org. Biomol. Chem*., **2012**, *10*, 3300.
13. Verma, R. K.; Takei, F.; Nakatani, K. *Org. Lett.* **2016**, *18*, 3170.
14. Suda, H.; Kobori, A.; Zhang, J.; Hayashi, G.; Nakatani, K. *Bioorg. Med. Chem*. **2005**, *13*, 4507.
15. Takei, F.; Suda, H.; Hagihara, M.; Zhang, J.; Kobori, A.; Nakatani, K. *Chem. Eur. J*. **2007**, *13*, 4452.
16. Ong, H. C.; Arambula, J. F.; Ramisetty, S. R.; Baranger, A. M.; Zimmerman, S. C. *Chem. Commun*., **2009**, 668.
17. (a) Bag, S. S.; Kundu, R.; Sangita, T. *RSC Advances* **2013**, *3*, 21352. (b) Bag, S. S.; Talukdar, S.; Matsumoto, K.; Kundu, R. *J. Org. Chem*. **2013**, *78*, 278.
18. Bag, S. S.; Talukdar, S.; Anjali S.J. *Bioorg. Med. Chem. Lett*. **2016**, *26*(8), 2044.

19. Fu, B.; Huang, J.; Bai, D.; Xie, Y.; Wang, Y.; Wang, S.; Zhou, X. *Chem. Commun*., **2015**, *51*, 16960.
20. Hobza, P.; Sponer, J. *Chem. Rev*. **1999**, *99*, 3247.
21. Cordier, C.; Pierre, V. C.; Barton, J. K. *J. Am. Chem. Soc*., **2007**, *129*, 12287.
22. Granzhan, A.; N. Kotera, Teulade-Fichou, M. –P. *Chem. Soc. Rev*., **2014**, *43*, 3630.
23. Baase, W. A.; Jose, D.; Ponedel, B. C.; von Hippel, P. H.; Johnson, N. P. *Nucleic Acids Res*., **2009**, *37*, 1682.
24. Loeb, L. A.; Loeb, K. R.; Anderson, J. P. *Proc. Natl. Acad. Sci. U. S. A*., **2003**, *100*, 776.
25. (a) Friedberg, E. C.; Walker, G. C.; Siede, W. *DNA Repair and Mutagenesis, ASM Press, Washington*, **1995**; (b) Ionov, Y.; Peinado, M. A.; Malkhosyan, S.; Shibata, D.; Perucho, M. *Nature*, **1993**, *363*, 558; (c) Streisinger, G.; Okada, Y.; Emrich, J.; Newton, J.; Tsugita, A.; Terzaghi, E.; Inouye, M. *Cold Spring Harbor Symp. Quantum Biol*., **1966**, *31*, 77.
26. Cannistraro, V. J.; Taylor, J. S. *J. Biol. Chem*., **2007**, *282*, 11188.
27. Abdel-Rahman, W. M. *Curr. Genomics*, **2008**, *9*, 535.
28. Austin, M. A.; Hutter, C. M.; Zimmern, R. L.; Humphries, S. E. *Am. J. Epidemiol*., **2004**, *160*, 407.
29. McNally, E. M.; Duggan, D.; Gorospe, J. R. *Hum. Mol. Genet*., **1996**, *5*, 1841.
30. Boiteux, S.; Guillet, M. *DNA Repair*, **2004**, *3*, 1.

Chapter 4

Studies on the Label Free Detection of G-Quadruplex DNA Utilizing Fluorescent Tetrazolyl Pyrene Unnatural Nucleoside

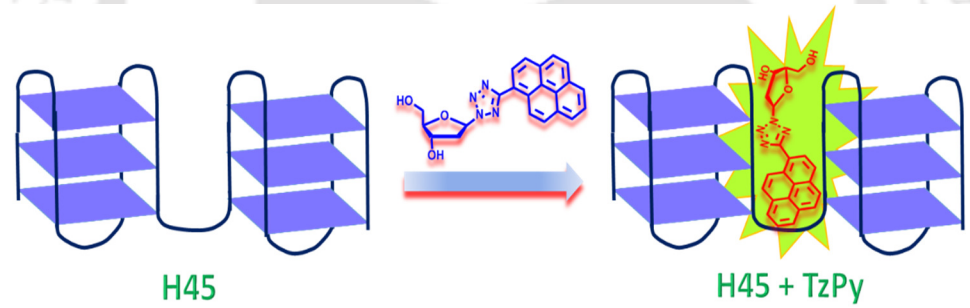

4.1. Introduction

DNA has been recognised as a classical and effective drug target in anticancer chemotherapy. Out of several topological isomers of DNA, the discovery of guanine-rich G-quadruplex DNA has got tremendous attention as a specific and effective drug target at gene level. The unique structural features exhibited by the diverse array of G-quadruplex topologies offer the potential for highly specific interactions with array of organic/inorganic molecule. DNA containing guanine-rich sequences can fold into a four-stranded DNA helical secondary structure through guanine-guanine Hoogsteen H-bonding termed a G-quadruplex.[1] The G-quadruplexes could be monomeric or multimeric depending upon DNA sequence. Compared with G-quadruplex monomeric, multimeric G-quadruplexes are more biologically relevant and a predominant factor in recognizing long telomeric DNA *in vivo*. Monomeric G-quadruplex formed by short human telomeric DNA sequences (typically 21−26 nt) is usually used as the model to screen G-quadruplex-drug interaction. Subsequently the telomeric terminal overhang with ~200 nt has the ability to form higher-order G-quadruplex structures (dimer or multimer).[2] In higher order G-quadruplex structure each single consecutive monomeric G-quadruplex units are connected by TTA linkers. To date, most studies focused on ligand binding to monomeric G-quadruplexes.[3] There are very few reports of ligand binding to higher-order G-quadruplexes.[4-8] There also some diseases which are highly associated with expansion repeats of G-rich sequences capable of forming multimeric G-quadruplexes, such as ALS, cancer and Fragile X syndromes.[9–12] Research on multimeric G4 is at a very early stage, and the structures and functions of these G-rich sequences are poorly understood. Searching for a highly specific multimeric G4 ligands and fluorescent probes are important to understand the structures and functions of G-quadruplexes. Distinction among the higher-order G-quadruplexes might be a promising strategy for developing selective anticancer agents.[13,14]

4.2. Detection of Higher-Order G-Quadruplexes

Long human telomeric DNA can form stable, higher-order G-quadruplex structures, which are potential drug targets. However, there are very few examples of ligand binding to higher-order G-quadruplexes. Searching for highly specific multimeric G4 ligands is important for structure probing and for study of the function of G-rich gene sequences, as well as for the design of novel anticancer drugs. Studies on interactions between ligands and multimeric G-quadruplexes could provide a new route for screening specific telomeric G-quadruplex-

targeting ligands. There are very few number of research works in this regard have been reported in literature and discussed below.

Zhao[4] *et.al*., exploited nanosized zinc-finger-like chiral supramolecular complexes which prefer to bind with multimeric G-quadruplexes over monomeric G-quadruplex units with ~200-fold different selectivity (**Figure 4.1**). A limited number of ligands are reported which can distinguish higher-order G-quadruplexes over monomeric G-quadruplexes with high selectivity. The nanosized chiral metallosupramolecular complex bind to the well-matched two G-quadruplex units instead of binding to the cleft between the two G-quadruplexs like other reported ligands (**Figure 4.1**). The supramolecular complex, Ni-M specifically bound to higher-order G2T1 with 1:1 binding ratio as was verified by various methods such as, DNA UV melting studies, Job's plot, isothermal titration calorimetry (ITC).

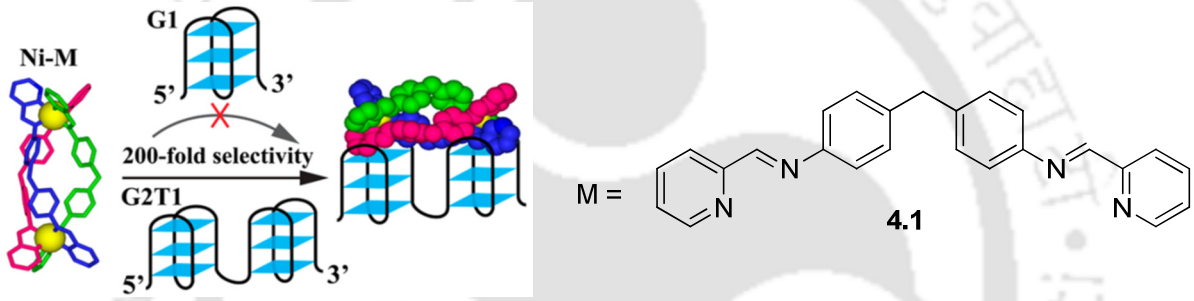

G1: AGGGTTAGGGTTAGGGTTAGGG

G2T1: AGGGTTAGGGTTAGGGTTAGGGTTAGGGTTAGGGTTAGGGTTAGGG

Figure 4.1. Pictorial presentation of the preferred binding of a chiral metallosupramolecular complex to dimeric G-quadruplex over a monomeric G- quadruplex.

Zhou[8a] *et.al*., explored the highly selective, sensitive and topology-specific fluorescent sensing of dimeric G-quadruplexes, G2T1 (G2T1: 5`-AGGGTTAGGGTTAGGGTTAGGGTTAGGGTTAGGGTTAGGGTTAGGG-3`), by a polyether-tethered dimeric berberine **4.2** (**Figure 4.2**). Dimeric berberine displayed high selectivity for binding with dimeric G-quadruplexes over monomeric one. Berberine subunits intercalate into G-quadruplexes through π–π stacking interactions with base pairs.[15–20] Photofluorimetric titrations revealed that compound **4.2** interacted with G2T1 in a 1:1 stoichiometry. The two berberine subunits of compound **4.2** simultaneously interacted with the two G-quartets of G2T1. The binding constants (K_a's) of compound **4.2** decreased with the length of the linkers which suggests that a short TTA linker favoured its binding over long TTA linkers, because of the increasing special distance between the two G-quadruplex units.

Specifically, compound **4.2** bound into the adjacent planes of dimeric G-quadruplexes probably through π–π stacking interactions, which might be restricted the rotation of the berberine plane and generated the enhanced fluorescence emission.[21] Compound **4.2** exhibited a fluorescent "turn-on" response toward dimeric G-quadruplexes and showed no effect towards ss-DNA, ds-DNA, ct-DNA or other monomeric G-quadruplexes such as, c-kit2 and G1 (G1: AGGGTTAGGGTTAGGGTTAGGG).

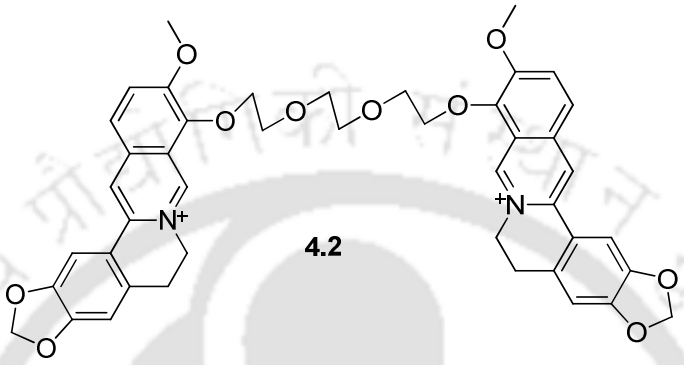

Figure 4.2. Structure of dimeric berberine **4.2**.

Zhang[7] et.al., reported a number of tetraphenylethene (TPE) derivatives positively charged side-arm substituents (**Figure 4.3**) and studied their interactions with different multimeric G-quadruplexes. 1,2-Bis{4-[(trimethylammonium)- butoxy]phenyl}-1,2-tetraphenylethene dibromide (DATPE) (**Figure 4.3**), which contains two side arms and gave a fluorescence response to only multimeric G4. The DATPE has a low level of cytotoxicity and little or no effect on multimeric G4 conformation or stability. 1,1,2,2-Tetrakis{4-[(trimethylammonium) butoxy]phenyl}tetraphenylethene tetrabromide (QATPE) (**Figure 4.3**) contains four side arms has a lower level of recognition specificity for multimeric G4 compared to DATPE but its binding affinity to multimeric G4 was found to be higher compared to other structural DNAs. The high multimeric G4-binding affinity, excellent multimeric G4-stabilizing ability, and the promotion of parallel G4 formation make QATPE a novel anticancer agent. The DATPE has a fluorescence response to only multimeric G4. Its high degree of specificity towards multimeric G4 came mainly from the DATPE molecules intercalating into the pocket site of multimeric G4. The specific fluorescence response to multimeric G4, the lack of effect on G4 conformation or stability, and low cytotoxicity make DATPE a promising fluorescent probe for multimeric G4 detection in biological samples or *in vivo*. QATPE had a fluorescence response higher to multimeric G4 compared to monomeric G4. In addition, QATPE could promote the formation of parallel G4 and had strong multimeric G4-stabilizing

ability. QATPE exhibited a higher K_a value to the same multimeric G4 compared to DATPE. This suggested the π–π stacking and electrostatic interaction between positively charged side arms and negatively charged phosphate backbones of G4 contributed to binding interactions between the TPE derivatives and G4s. The CD spectra of the monomeric and multimeric G4s had a negative and a positive peak at around 240 and 290 nm, respectively, and a positive shoulder peak at about 265 nm, which indicated all of these telomeric DNAs fold into a parallel/antiparallel mixed hybrid G4 structure.[22]

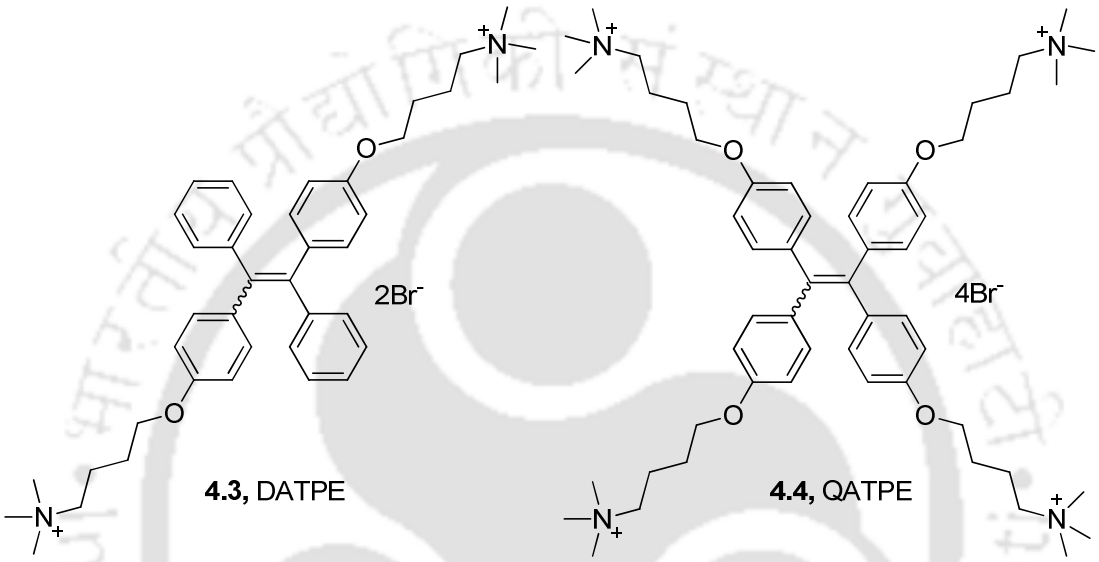

Figure 4.3. Chemical structures of the two tetraphenylethene (TPE) derivatives used by Zhang[23] *et.al*.

Zhu[5] *et.al*., explored TMPipEOPP (**Figure 4.4**), a cationic porphyrin derivative as a promising multimeric telomeric G-quadruplex ligand under molecular crowding conditions using a combined spectroscopic technique (UV, fluorescence and CD). TMPipEOPP interacted with monomeric G-quadruplexes in sandwich-like end-stacking mode of quadruplex/TMPipEOPP/quadruplex and interacted with multimeric human telomeric G-quadruplexes via intercalation into the pocket between two adjacent G-quadruplex units. The pocket size greatly affected TMPipEOPP binding. A larger pocket was advantageous for the intercalation of TMPipEOPP. TMPipEOPP discriminated G-quadruplexes magnificently over duplex, single-stranded and triplex DNAs under molecular crowding conditions.

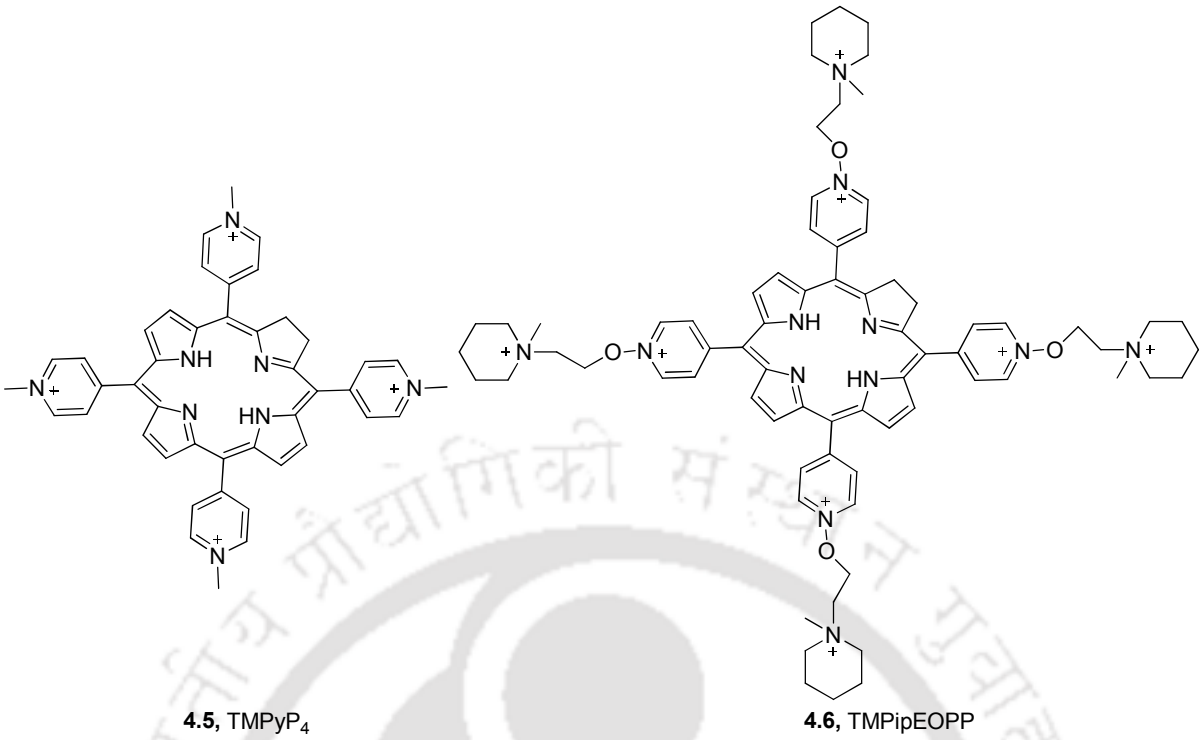

Figure 4.4. The chemical structures of TMPyP4 and TMPipEOPP.

Huang[8b] *et al*., explored the synthesis of a new triaryl-substituted imidazole derivative called IZNP-1 (**4.7, Figure 4.5**), and its multimeric G-quadruplex recognition specificity. IZNP-1 had an excellent ability to discriminate between telomeric multimeric and monomeric G-quadruplexes. They found that IZNP-1 selectively bound to telomeric multimeric G-quadruplexes with a much stronger affinity than it did with monomeric G-quadruplexes. The strong affinity toward a multimeric G-quadruplex was explained on the basis of intercalation into the pocket between the two quadruplex units and forming a tight complex.

The interactions of IZNP-1 with different nucleic acids using UV-visible and fluorescence spectroscopy, including four telomeric multimeric G-quadruplexes, six monomeric G-quadruplexes and one duplex DNA were studied. Free IZNP-1 had weak fluorescence with maximum emission wavelength at 540 nm. However, the addition of the telomeric multimeric G-quadruplexes (htg45, htg51, htg57 and htg69) significantly enhanced the fluorescence of IZNP-1, while monomeric G-quadruplexes (htg21, c-kit2, RET, EAD, HRAS and TBA) and duplex DNA (hairpin) had very little effect on the level of fluorescence. With the addition of the multimeric G-quadruplex htg45, the absorption bands of IZNP-1 at both 323 and 400 nm continuously increased but monomeric G-quadruplex htg21 had a little effect on the absorption spectrum of IZNP-1.

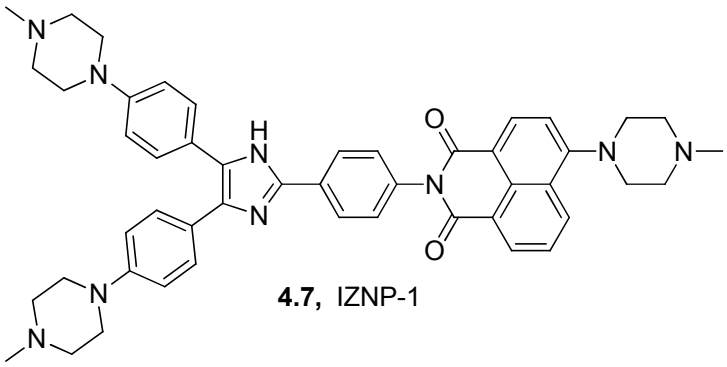

4.7, IZNP-1

Figure 4.5. The chemical structures of IZNP-1.

4.3. Background

The acquired knowledge on the role in many biological processes and in disease generation that G-quadruplex plays and to get insight into those processes, the design of highly sensitive fluorescent probes has attracted much research attention in recent time for the detection of G-quadruplex structure. Toward this end, many fluorescent probes based on organic architectures as well as metal complexes have been developed. However, many of the quadruplex-binding fluorescent dyes have been found to be non-specific and very few have shown specificity for a targeted quadruplex over other quadruplex topologies. The challenges for the design of highly selective fluorescent probe for one type of quadruplex and discriminating for any other form of DNA lies on the common structural features of all types of G-quadruplexes. Toward this end most of these studies have focused only on monomeric G-quadruplexes. However, targeting telomeric multimeric G-quadruplexes is most promising for anticancer drugs development research. Only very few reports exist which targeted multimeric G-quadruplexes. Therefore, there is a high demand to develop fluorescent probe for the recognition of G-quadruplex with high specifity for recognition of DNA and selectivity in sensing a particular quadruplex topology. In a rational approach of G-quadruplex selective fluorescent probe one has to consider the factors such as G-quadruplex topology and the binding mode along with end stacking interaction.

In this quest, unnatural nucleoside containing a fluorophoric moiety as a ligand would be beneficial over the reported classes of organic/inorganic fluorescent dyes or ligand because of the natural self-recognition property via electrostatic/H-bonding interaction through the involvement of sugar unit of the designed probe. Though many nucleosides are recently found applications in cancer treatment via groove binding and/or stacking interaction with the cancer cell DNA there is no report of study that a nucleoside can be a good binder of a selective G-

quadruplex. Only in 2009, Tang et al. have shown the G-quadruplex-groove binding event by two propeimine derivatives via H-bonded, electrostatic and van-der Walls interaction [Y. Tang, X. Xu, Q. Li, et al., CN101352445; 2009.]. Therefore, design of fluorescent nucleoside as a specific probe of G-quadruplex DNA is of considerable interest.

4.4. Objective

As a part of our ongoing research for the design of fluorescent DNA sensor, DNA stabilising/binding fluorescent unnaral nucleosides[13c-d] and design of tetrazolyl class of fluorescent nucleosides[13e-f] we recently observed the tetrazolylpyrene nucleoside as an effective switch-on sensor for DNA lession. Inspired by our recent results, we thought that the tetrazolylpyrene nucleoside could serve as an efficient probe for sensing G-quadruplex. The fluorescent nucleoside with tetrazolylpyrene as nucleobase is expected to have the following advantageous property to interact with G-quadruplex over the reported other classes of ligands: (a) the natural self-recognition/organization property, (b) The sugar unit of the nucleoside would interact with the loops and grooves possibly through H-bonding interaction enhancing the binding affinities with the phosphate backbone, (c) specific molecular shape of tetrazole unit might also offer recognition to the groove regions of G-quadruplex through H-bonding built on backbone and the nucleoside core, (d) the planar pyrenyl aromatic system along with the tetrazole could involve in π–π stacking interaction with G-quartet. Therefore, we envisaged that the H-bonding/electrostatic/stacking interaction force mediated binding would be an efficient strategy for sensing G-quadruplex with fluorescent nucleoside. The bare fluorescent nucleoside would thus be advantageous over simple intercalative dyes as the sugar unit could impart extra binding interaction possibly in the groove and the aromatic base could engage in π–π stacking interaction with G-quartet similar to the action of drug, daunomycine. Thus, the sugar unit extending from the triazolylpyrene aromatic core would simultaneously interact with loops or bind the grooves of the G-quadruplex extending the aromatic core to the G-quartet planes for π–π stacking interaction. Therefore, we expected that the present nucleoside with a tetrazolylpyrene core size comparable to the G-quartet and with sugar unit might provide good selectivity over duplex DNA.

Based on the consideration above, utilised our previously reported tetrazolylpyrene nucleoside (**TzPy, Figure 4.6**) for selective sensing of G-quadruplex DNA. We thought that the tetrazolylpyrene (**TzPy**) moiety of the nucleoside with large surface area, high polarizability, high stacking propensity could involve in p-p stacking interaction with G-tetrad

while the sugar unit involved in interaction with the groove or loop via H-bonding/electrostatic interaction leading to stabilization of the G-quadruplex. Thus, the binding event would lead to the generation of a discriminating fluorescence signal and allow us for the selective detection of the G-quadruplex. Furthermore, we envisaged that the planar aromatic **TzPy** unit of the probe could insert/intercalate between two G-tetrad planes of a multimeric G-quadruplex leaving the sugar unit for electrostatic/H-bonding interaction in both the planes.

Based on the consideration above we framed our objective as below to utilise our previously reported tetrazolylpyrene nucleoside (**TzPy**) for specific sensing of multimeric G-quadruplex DNA over other DNAs.

(a) Study of photophysical properties of **TzPy** in the presence of various kind of G-quadruplex DNAs, duplexes and single stranded DNAs.

(b) Comparison of binding property of the probe between monomeric human telomeric (Hum21) with dimeric human telomeric G-quadruplex (Hum45).

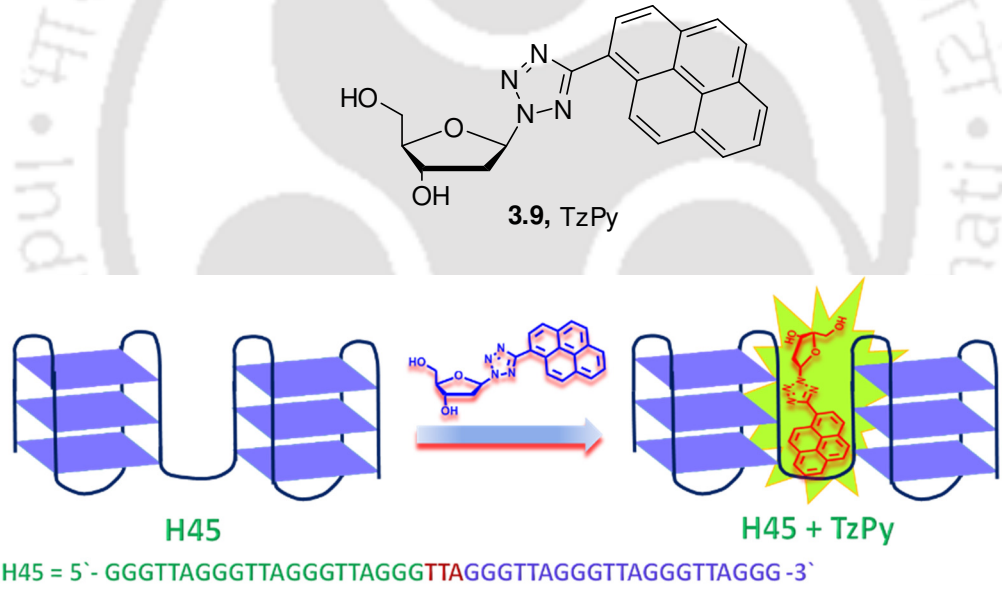

Figure 4.6. Proposed bind of **TzPy** to the cleft between the G-qudruplex of Hum45.

4.5. Result and Discussion

4.5.1. Spectral Study of TzPy with Various Kind of G-quadruplex and Other DNAs

As we have seen earlier in chapter 3 that **TzPy** shows negligible fluorescence properties in aqueous buffer. **TzPy** have been exploited before as fluorescent light up probe for the label-

free detection of DNA lesions. To our knowledge, however, no study of their G-quadruplex recognition abilities has been reported. In this work, **TzPy** exploited as G4 (including monomeric and multimeric G4) recognition probe. First, the comparative fluorescence responses of **TzPy** with different types of structural DNAs were carried out. To achieve this, 11 oligonucleotides, including six monomeric G4s, one dimeric G4, two duplex DNAs including ct-DNA and two single-stranded DNA were used (**Table 4.1**). The interaction of **TzPy** with different types of DNAs are discussed with regard to their fluorescence response and also effect on multimeric G4 conformation and stabilizing ability.

Table 4.1. DNA sequences used in this study

Oligo Code	Oligo Sequence (5`→3`)	ε (L/mole*cm)	Structure
TBA	GGTTGGTGTGGTTGG	143300	monomeric
HIV	TGGCCTGGGCGGGACTGGG	175400	monomeric
Hum21	$GGG(TTAGGG)_3$	215000	monomeric
Hum45	$GGG(TTAGGG)_7$	459400	multimeric
O_{XY} 3.5	$GGGG(TTTTGGGG)_4$	262000	monomeric
Bom 17	$GG(TTAGG)_3$	174600	monomeric
Cmyc	GGGGAGGGTGGGGAGGGTGGGGAAGG TGGGG	321500	monomeric
SS 1	CGCAATCTAACGC	121800	single-stranded
SS 2	GCGTTAGATTGCG	125300	single-stranded
dS	SS1 + SS2	---	duplex
ct-DNA	---	6600	long duplex

To investigate dimeric G4 (Hum45) recognition over monomeric G4s, various spectral studies were carried out in sodiaum phosphate buffer solutions (50 mM sodium phosphate and 100 mM NaCl in water, pH = 7). The genuine structure of long human telomeric sequence in K^+ solution is still inconceivable.[23] In contrast, the conformation of long human telomeric sequence in Na^+ solution is clear.[24-26] Thus, we chose Na^+ buffer throughout our experiments.

As shown in **Figure 4.7a**, **TzPy** exhibited a predominant absorption band at around 344 nm in buffer. A dramatic changes of the absorption peaks were observed upon mixing with various G-quadruplexes, specifically with dimeric human telomere G-quadruplex (Hum45) in which one single G-quadruplex linked to another via a TTA unit. The peak around 344 nm gradually increased and bathochromically shifted by 13 nm (344 nm → 357 nm) with addition of dimeric G-quadruplex. In addition, a new shoulder peaks at 373 nm and 390 nm were appeared. Furthermore, a clear change in absorption peak of **TzPy** also appeared in addition of

Cmyc and Oxy 3.5. The new shoulder peak at 375 nm appeared and the peak at 344 nm faced bathochromic shift of 7 nm for Cmyc (344nm → 351 nm) and 6 nm for Oxy 3.5 (344 nm → 350 nm). Interestingly, there was no such shift observed for other monomeric G-quadruplex DNAs. This result suggested that there was a minimal effect on the absorption spectra of **TzPy**, when it interacted with monomeric G-quadruplexes, duplexes and single stranded DNAs. The discriminative interaction behaviour of **TzPy** was also clear and from a color change of the solution upon irradiation with UV-transilluminator (**Figure 4.8**). Therefore, we can apply **TzPy** for the detection of dimeric G-quadruplex over monomeric G-qudruplex.

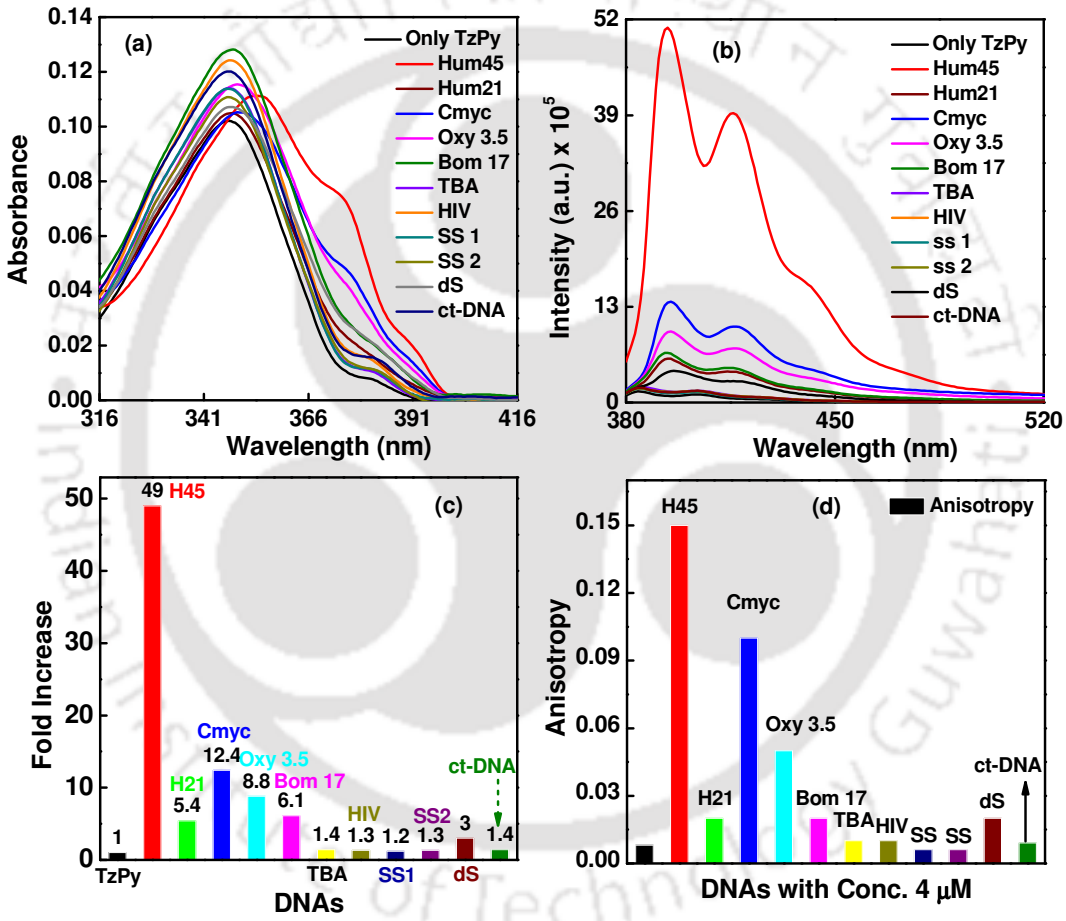

Figure 4.7. (a) UV-visible, (b) emission (c) fluorescence fold increase (d) steady state anisotropy of the probe (10 μM) in absence and presence of ss-DNA, ds-DNA, ct-DNA, Cmyc, Oxy3.5, TBA, HIV, Hum21 and Hum45.

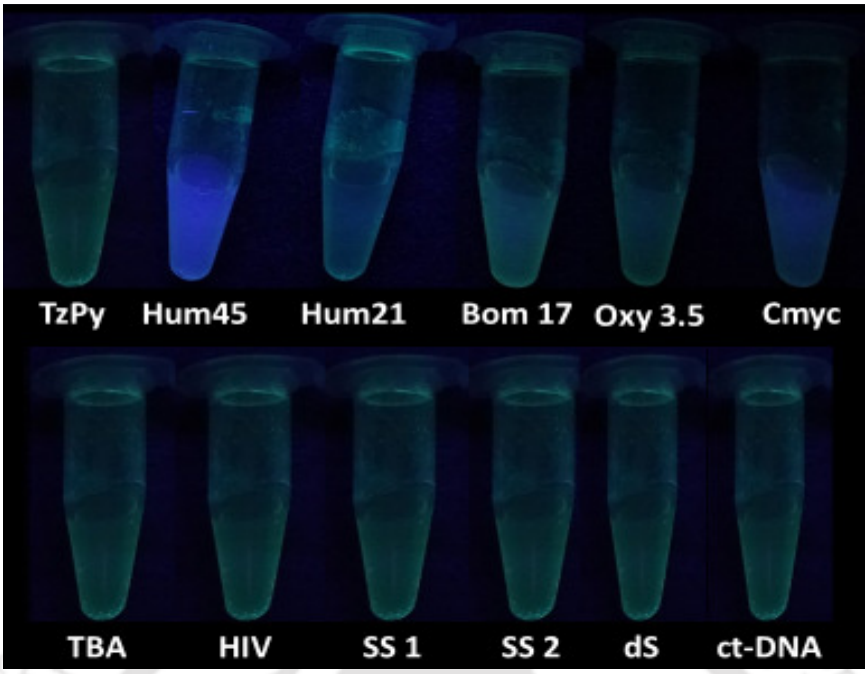

Figure 4.8. Color change under UV-transilluminator in presence of **TzPy**.

Table 4.2. Photophysical Summary of **TzPy** non-natural nucleoside with various G-quadruplexes, single and duplexes DNAs.

Entry	λ_{abs} (nm)	$\Delta\lambda_{abs}$ (nm)	λ_{em} (nm)	$\Delta\lambda_{em}$ (nm)	Anisotropy
TzPy	344, 379	---	384, 404, 421	---	0.01
Hum45	357, 373, 390	13	394, 416	12	0.15
Hum21	348, 381	4	395, 416	12	0.02
Cmyc	351, 375, 389	7	395, 417	13	0.1
Oxy 3.5	350, 375	6	395, 416	12	0.05
Bom 17	348, 379	4	394, 415	11	0.02
TBA	346, 379	2	385, 404,424	---	0.01
HIV	346, 379	2	385, 404,424	---	0.01
SS1	346, 380	2	384, 404, 423	--	0.01
SS2	346, 380	2	384, 404, 423	---	0.01
dS	349, 377	4	395, 417	13	0.02
ct-DNA	347, 381	2	384, 404, 423	---	0.01

Further to get more insight into the binding properties of **TzPy** with G4s fluorescence spectra were recorded in presence of all DNAs used in this work (**Table 4.2**). As shown in **Figure 4.7b**, free **TzPy** emitted almost negligible fluorescence at 384 nm when excited at 370 nm, but dramatically **TzPy** exhibited a higher emission response in addition of dimeric G-quadruplex. On the other hand, the fluorescence intensity for other G-quadruplexes were insignificant. Fluorescence enhancement upon binding might be a result of π-π stacking interaction of the probe in hydrophobic microenvironment. Interestingly, **TzPy** exhibited a

higher emission response in the presence of Hum45 which gives 49-fold higher fluorescence intensity compared to free **TzPy** and 5.4-fold increase with Hum21. This indicated that **TzPy** is quite selective for binding to Hum45. This selectivity might stem from the structural impact of dimeric G-quadruplex, Hum45. The lack of fluorescence response of **TzPy** to other monomeric G4s, ss, ct-DNA and dS DNAs implied that such a stacking interaction did not occured with **TzPy**. The increased steady state anisotropy also further supported the strong binding of **TzPy** to Hum45 (**Figure 4.7d, Table 4.2**). **TzPy** exhibited a fluorescent "turn-on" response toward dimeric G-quadruplexes and showed negligible effect towards ss-DNA, ds-DNA, ct-DNA, Cmyc, Oxy3.5, TBA, HIV and Hum21.

4.5.2. Effects of TzPy On Circular Dichroism Spectra of G-quadruplexes

Circular dichroism (CD) spectroscopy is widely used to investigate the conformation of G-quadruplexes and to investigate the interactions between ligands and G-quadruplexes.[27-33] To define the structural features of the G-quadruplexes and effect of **TzPy** on the conformation of G4s was investigated by measuring the CD spectra of G4s. In the absence of **TzPy**, the CD spectra of all G4s exhibited a characteristic positive peak at 245 nm and 293 nm and a negative peak at 263 nm, which was assigned as antiparallel-stranded G-quadruplex conformation, except for Cmyc and HIV (**Figure 4.9**). In contrast, the Cmyc and HIV sequence, which formed a well-defined hybrid-type G-quadruplex, exhibited a distinct CD spectrum containing a strong positive peak at 298 nm and a characteristic shoulder peak at 260 nm and a negative peak at 240 nm (**Figure 4.9**). Interestingly, **TzPy** had a negligible impact on the characteristic peaks of both anti-parallel and mixed types G-quadruplexes. This minimal change of the CD spectrum following the addition of **TzPy** suggested that the presence of **TzPy** did not disturbed the topological conformation of G4s. This feature made **TzPy** more suitable for the study of multimeric G4 as a fluorescent probe.

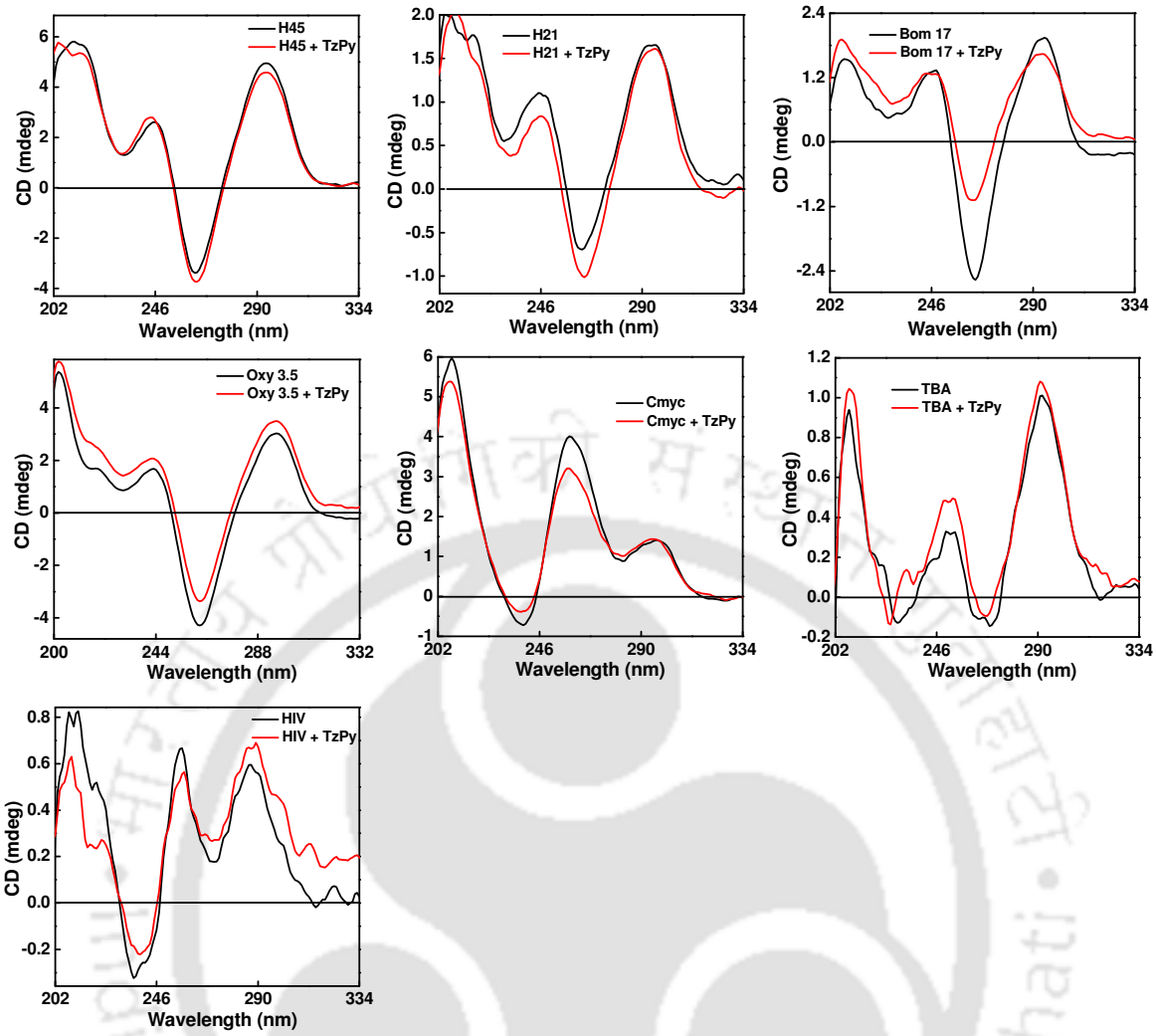

Figure 4.9. Circular dichroism spectra of Hum45, Hum21, Bom 17, Oxy 3.5, Cmyc, TBA and HIV in presence and absence of **TzPy**.

4.5.3. Comparative Binding Study of TzPy with Human Monomeric G4 (Hum21) and Human Dimeric G4 (Hum45)

To gain more insight into the understanding of the binding properties of **TzPy** with monomeric human telomeric G-quadruplex (Hum21) and higher order (dimeric) human telomerc G-quadruplex (Hum45) comparative studies were carried out utilising UV-visible, DNA melting profile and fluorescence spectroscopic methods.

As shown in **figure 4.10a**, **TzPy** exhibited a predominant absorption band around 344 nm in buffer. Upon increased addition of Hum21 to **TzPy** the absorption of the band at 344 nm enhanced without shifting and appearance of a new shoulder peak. This might be due to **TzPy** remain unaffected with Hum21. The color of **TzPy** solution also not even changed upon the addition of Hum21 when irradiated with UV-transilluminator (**Figure 4.8**). On the other hand,

as shown in f**igure 4.11a**, a dramatic changes of the absorption peaks were observed upon addition of dimeric human telomere G-quadruplex (Hum45) in which one single G-quadruplex linked to another via TTA unit. The peak around 344 nm gradually enhanced and shifted bathochromically by 13 nm (344 nm → 357 nm) upon addition of increased concentration of dimeric G-quadruplex. In addition, a new shoulder peak at 373 nm and 390 nm appeared, which was due to the strong binding of **TzPy** with Hum45. Upon addition of dimeric G-quadruplex to TzPy solution a clear and visible color change of **TzPy** solution appeared upon irradiated with UV-transilluminator (**Figure 4.8**).

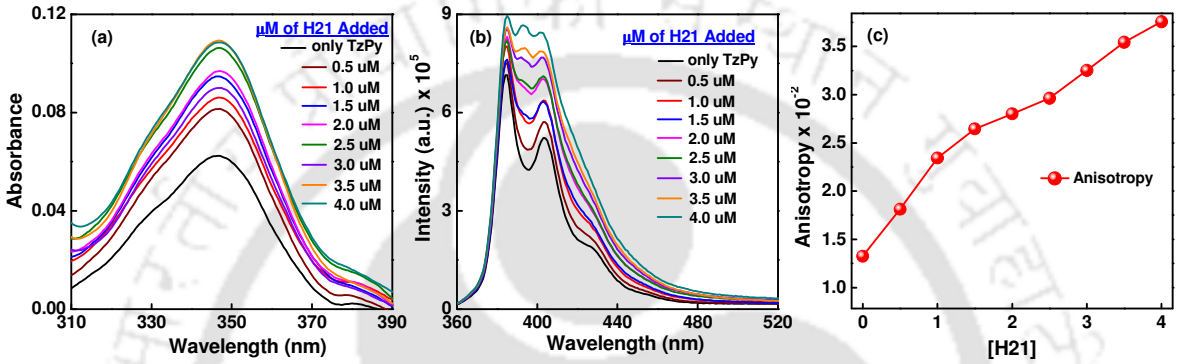

Figure 4.10. (a) UV-visible and (b) fluorescence emission spectra and (c) steady state anisotropy of **TzPy** (10 μM) in absence and presence of Hum21 (4 μM, pH 7).

Table 4.3. Photophysical summary of **TzPy** with Hum21

μM of H21	λ_{abs}	$\Delta\lambda_{abs}$	λ_{em}, 350 nm	$\Delta\lambda_{em}$	Anisotropy
TzPy	344, 379	---	384, 403	---	0.01
0.5	347, 380	3	384, 403	---	0.01
1.0	348, 380	4	384, 403	---	0.018
1.5	348, 380	4	384, 403	---	0.02
2.0	348, 380	4	385, 402	1	0.026
2.5	348, 380	4	385, 402	1	0.028
3.0	348, 380	4	385, 401	1	0.028
3.5	348, 380	4	385, 401	1	0.03
4.0	348, 380	4	385, 401	1	0.035

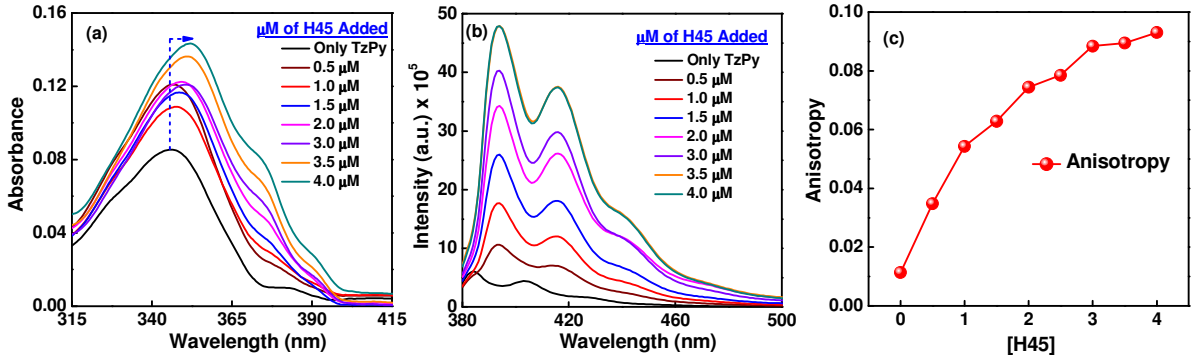

Figure 4.11. (a) UV-visible and (b) fluorescence emission spectra and (c) steady state anisotropy of **TzPy** (10 μM) in absence and presence of Hum45 (4 μM, pH 7).

Table 4.4. Photophysical Summary of **TzPy** with Hum45

μM of H45	λ_{abs}	$\Delta\lambda_{abs}$	λ_{em} 370 nm	$\Delta\lambda_{em}$	Anisotropy
TzPy	344, 379	---	384, 404	---	0.01
0.5	349, 377	5	395, 416	12	0.03
1.0	350, 377	6	395, 416	12	0.05
1.5	351, 376	7	395, 416	12	0.06
2.0	351, 375	7	395, 416	12	0.07
2.5	351, 375	7	395, 416	12	0.08
3.0	353, 375	9	395, 416	12	0.9
3.5	355, 373	11	395, 416	12	0.9
4.0	357, 372	13	395, 416	12	0.1

Next the fluorescence response of **TzPy** in addition of increasing concentration of Hum21 and Hum 45 was investigated. **TzPy** responded well in addition of dimeric human telomeric G-quadruplex (**Figure 4.11b**) compared to monomeric human telomere, Hum21 (**Figure 4.10b**). **TzPy** preferred to bind with both Hum21 and Hum45. Interestingly, **TzPy** bound to monomeric human telomere, Hum21 was not so strong that its fluorescence response was weak. On the contrary, a strong binding was the result with dimeric G-quadruplex, Hum45. With addition of increasing concentration of Hum45 a predominant bathochromic shift of emission bands by 12 nm (384 nm → 394nm and 404 nm → 416 nm) with enhanced intensity and around 49-fold increased intensity was observed compared to free **TzPy**. The increased steady state anisotropy (**Figure 4.11c, Table 4.4**) also revealed that **TzPy** bound strongly at the most hydrophobic pocket.

A close look at the fluorescence response and the structural features of both multimeric G4 and monomeric G4, revealed that both the quadruplexes exhibited the common stacking,

grove binding and loop binding sites, with a prominent difference in the presence of a hydrophobic cleft present in multimeric G4 (Hum45). The cleft provided by Hum45 might play the vital role for the specific recognition of multimeric G4 by the probe. This inferred the strong binding between **TzPy** and multimeric G4 (Hum45) occurred by inserting and π-π base stacking on the cleft between two consecutive G-quadruplex linked by TTA unit.[4] As a result, **TzPy** molecules intercalated into the cleft, such a G4/TzPy/G4 binding mode (**Figure 4.6**) that not only restricted the skeletal vibration and rotation of the **TzPy** molecule, but also promoted the strong fluorescence response.[8] So, **TzPy** got tightly captured at the hydrophobic cleft which restricted its rotational movement, result an enhanced emission intensity which was also supported by increased steady state anisotropy (**Figure 4.11c, Table 4.4**). Thus, **TzPy** inserted into the cleft site were mainly responsible for the fluorescence enhancement. The **TzPy** exhibited a fluorescent "turn-on" response toward dimeric G-quadruplexes over monomeric G-quadruplex.

4.5.4. Binding Affinity of TzPy to Dimeric G4 (Hum45) DNA

Dimeric G4 DNA-binding behavior of **TzPy** were investigated from fluorescence titration experiments (**Figure 12, Table 4.5**). The apparent binding constants (*K*) between **TzPy** and Hum45 were analyzed.[34] The excellent multimeric G4 recognition specificity of **TzPy** might come mainly from the **TzPy** intercalating into the cleft between two G4 units. Binding constant was calculated according to the Benesi-Hildebrand equation 1.

$$\frac{1}{(I-I_o)} = \frac{1}{(I_\alpha - I_o)} + \frac{1}{(I_\alpha - I_o)K[H45]} \quad \ldots\ldots\ldots\ldots\ldots\ldots (1)$$

Where I_o is the fluorescence intensity of **TzPy** in the absence of Hum45, I is the fluorescence intensity recorded in the presence of added Hum45, I_∞ is fluorescence intensity in presence of added $[Hum45]_{max}$ and *K* is the association constant. The association constant (*K*) was determined from the slope of the straight line of the plot of $1/(I-I_o)$ against 1/[Hum45] and is found to be 4.7×10^5 M^{-1}.

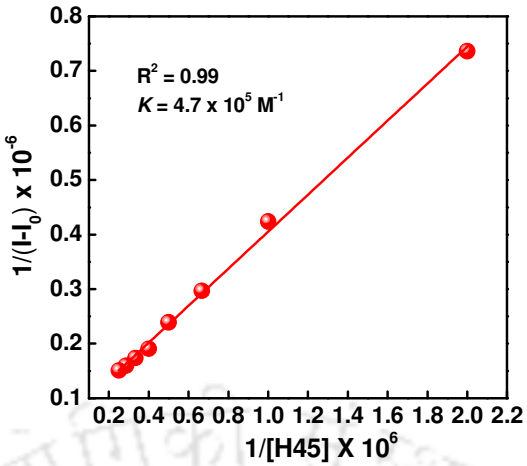

Figure 4.12. Benesi-Hildebrand plot for **TzPy** with increasing concentration of Hum45.

4.5.5. Effect of TzPy On the Thermal Stability of Hum21 and Hum45

The effects of **TzPy** on the thermal melting stability of Hum45 and Hum21 was measured by determining the changes of the melting temperature (ΔT_m) in absence and presence of **TzPy**.[35] DNA UV melting studies clearly indicated that **TzPy** had negligible influence on the melting temperature (T_m) of Hum21 (**Figure 13**) whereas it significantly enhanced (2 °C) the T_m of Hum45 (**Figures 13, Table 4.5**).[36] Combining the experimental results presented above, we concluded that **TzPy** had no or negligible effect on the conformation/stability of monomeric G4 and holds great potential as a fluorescence probe for multimeric G4. The probe **TzPy** exhibited strong multimeric G4-stabilizing ability which could act as novel anticancer agent targeting multimeric G4s.

Table 4.5. T_m values and Binding constant (K_a) values of H21 and H45 with **TzPy**

Entry	T_m (°C)	ΔT_m (°C)	K_a, M^{-1}
Hum45	59	----	---
Hum45 + TzPy	61	+2	4.7×10^5
Hum21	68	----	---
Hum21 + TzPy	68	0	---

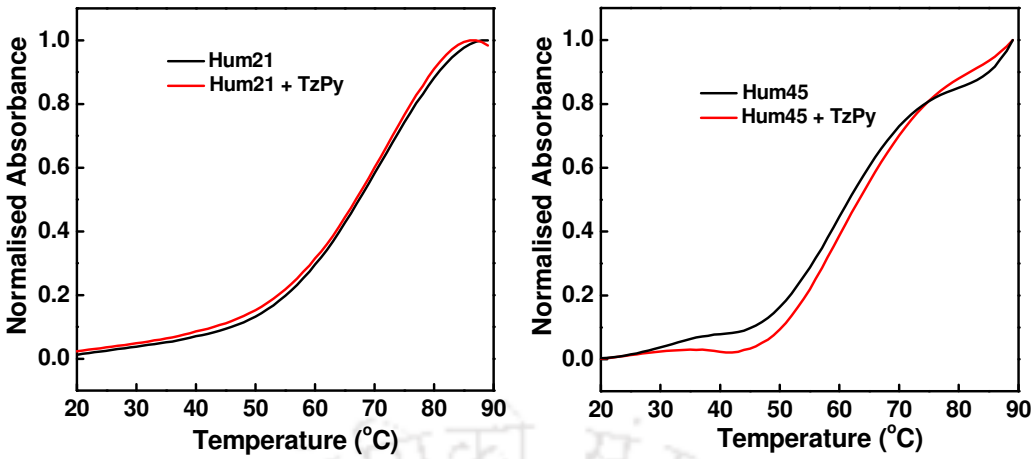

Figure 4.13. T_m profile for Hum21 and Hum45 in absence and presence of **TzPy**.

4.6. Conclusion

In conclusion, we successfully demonstrated that the bare fluorescent tetrazolylpyrene nucleoside served as a versatile fluorescent light-up probe for label free detection of multimeric G-quadruplex DNA with high specificity. The strong binding of the probe via intercalative stacking inside the TTA pocket connecting two G-quadruplex units of H45 multimeric G-quadruplex DNA and discrimination to other monomeric and long DNA duplex were accompanied by a drastic enhancement of emission intensity without compromising the conformation and thermal melting stability. Thus, the probe **TzPy** had an excellent ability to discriminate between telomeric multimeric and monomeric G-quadruplexes. To the best of our knowledge, this is the first example of a fluorescent nucleoside as ligand that can specifically distinguish multimeric G-quadruplexes from monomeric ones. The label free fluorescent light-up sensing by our fluorescent nucleoside probe with a less laborious, simple and cost effective way would be very useful and might find future applications for the specific detection and targeting of multimeric G-quadruplex DNA and help in designing such unnatural nucleoside as multimeric G-quadruplex specific binder/drug like candidates for cancer therapy. The design of multimeric G-quadruplex specific fluorescent probe with enhanced G-quadruplex stabilizing ability is our current research focus.

4.7. Experimental Section

4.7.1. Spectroscopic Measurements

4.7.1.1. UV-visible Measurements

UV-visible spectra of all the ODNs (4 μM concentration of each single strand) were measured in 50 mM sodium phosphate buffers (pH 7.0) containing 100 mM sodium chloride using Shimadzu UV-2550 UV-Visible spectrophotometer, with quartz optical cell of 1.0 cm path length and scanning rate of 0.5 nm with wavelength range of 200-500 nm and slit width of 1 nm.

4.7.1.2. Thermal Melting Temperature (T_m) Experiments of The Oligonucleotides

The thermal denaturation studies (T_m), absorbance *vs.* temperature profiles of the duplexes (4 μM concentration of each single strand) were measured at 260 nm using Shimadzu UV-2550 UV-Visible spectrophotometer equipped with a Peltier temperature controller using 1 cm path length cell in 50 mM sodium phosphate buffers (pH 7.0) containing 100 mM sodium chloride. The absorbance of the samples was monitored at 260 nm from 20 to 90 °C with a heating rate of 0.5 °C/min. From these profiles, average method was used to determine T_m values using in built software.

4.7.1.3. Steady State Fluorescence Experiments

ODNs solutions were prepared as described in UV-visible and T_m measurement experiments. Fluorescence spectra were recorded using Fluoromax–4 fluorescence spectrophotometer at 25 °C using quartz cell of 1.0 cm path length with a slit width of 4 nm, wavelength range 350-650 nm. Excitation spectra were monitored at 410 nm emission wavelength. Fluorescence emissions were collected exciting the ODNs at the wave length corresponding to their absorption maxima. Steady-state fluorescence emission spectra were recorded at room temperature as an average of ten scans using an excitation slit of 5.0 nm, emission slit 5.0 nm. The steady state anisotropy experiment was performed with the same fluorescence spectrophotometer at 25 °C using 1 cm path length cell. The fluorescence anisotropy (r) was calculated using the following equation-

$$r = \frac{(I_{VV} - I_{VH}G)}{(I_{VV} + 2I_{VH}G)};\ G = \frac{I_{HV}}{I_{HH}}$$

where, I_{VV} and I_{VH} are the emission intensities when the excitation polarizer is vertically oriented and the emission polarizer is oriented vertically and horizontally respectively. G is the correction factor. The terms I_{HV} and I_{HH} are the emission intensity when the excitation polarization is horizontally oriented and the emission polarization is oriented vertically and horizontally, respectively.

4.7.1.4. Circular Dichroism (CD) Measurement

CD spectra were recorded with JASCO CD J-810 spectropolarimeter equipped with a Peltier thermoelectric type temperature control system (4 μM concentration of each strand in 50 mM sodium phosphate, 100 mM sodium chloride, pH 7.0, at room temperature). The data were collected using quartz optical cells with a 1.0 cm path length. Measurements were conducted using 4 μM of strands in sodium phosphate buffer. Corrections were made for buffer background CD spectra (200-400 nm) were recorded at 25 °C as an average of three scans and with a scan speed of 200 nm/min. The spectral data were analyzed with the spectra manager software.

4.8. References

1. Neidle, S. *J. Med. Chem*. **2016**, *59*, 5987. (b) Burge, S.; Parkinson, G. N.; Hazel, P.; Todd, A. K.; Neidle, S. *Nucleic Acids Research* **2006**, *34* (19), 5402.
2. (a) Bugaut, A.; Alberti, P. *Biochimie* **2015**, *113*, 125. (b) Tóthová, P.; Krafčíková, P.; Víglaský, V. *Biochemistry* **2014**, *53*, 7013.
3. Ma1, D. –L.; Chan, D. S. –H.; Yang, H.; He1, H. –Z.; Leung, C. –H. *Current Pharmaceutical Design* **2012**, *18*, 2058. (b) Lavrado, J.; Ohnmacht, S. A.; Correia, I.; Leitão, C.; Pisco, S.; Gunaratnam, M.; Moreira, R.; Neidle, S.; dos Santos, D. J. V. A.; Paulo, A. *Chem. Med. Chem.* **2015**, *10*, 836. (c) Guyen, B.; Schultes, C. M.; Hazel, P.; Mann, J.; Neidle, S. *Org. Biomol. Chem*. **2004**, *2*, 981. (d) Amato, J.; Morigi, R.; Pagano, B.; Pagano, A.; Ohnmacht, S.; Magis, A. D.; Tiang, Y. –P.; Capranico, G.; Locatelli, A.; Graziadio, A.; Leoni, A.; Rambaldi, M.; Novellino, E.; Neidle, S.; Randazzo, A. *J. Med. Chem*. **2016**, *59*, 5706. (e) Paul, A.; Maji, B.; Misra, S. K.; Jain, A. K.; Muniyappa, K.; Bhattacharya, S. *J. Med. Chem*. **2012**, *55*, 7460. (f) Neidle, S. *Chem. Rec*. **2015**, *15*, 691.
4. Zhao, C.; Wu, L.; Ren, J.; Xu, Y.; Qu, X. *J. Am. Chem. Soc*. **2013**, *135*, 18786.
5. Zhu, L. –N.; Wu, B.; Kong, D. –M. *Nucleic Acids Research* **2013**, *41* (7), 4324.

6. Zhang, L.; Liu, H.; Shao, Y.; Lin, C.; Jia, H.; Chen, G.; Yang, D.; Wang, Y. *Anal. Chem*. **2015**, *87*, 730.
7. Zhang, Q.; Liu, Y. –C.; Kong, D. –M.; Guo, D. –S. *Chem. Eur. J*. **2015**, *21*, 13253.
8. (a) Zhou, C. –Q.; Yang, J. –W.; Dong, C.; Wang, Y. –M.; Sun, B.; Chen, J. –X.; Xu, Y. –S.; Chen, W. –H. *Org. Biomol. Chem*. **2016**, *14*, 191. (b) Hu, M.-H.; Chen, S.-B.; Wang, B.; Ou, T.-M.; Gu, L.-Q.; Tan, J.-H.; Huang, Z.-S. *Nucleic Acids Research* 2016, 1. *doi: 10.1093/nar/gkw1195.*
9. Reddy, K.; Zamiri, B.; Stanley, S. Y. R.; Macgregor Jr., R. B.; Pearson, C. E. *J. Biol. Chem.* **2013**, *288*, 9860.
10. Zamiri, B.; Reddy, K.; Marcgegor Jr., R. B.; Pearson, C. E. *J. Biol. Chem*. **2014**, *289*, 4653.
11. Brčić, J.; Plavec, J. *Nucleic Acids Res*. **2015**, *43*, 8590.
12. Zamiri, B.; Mirceta, M.; Bomsztyk, K.; Macgregor Jr., R. B.; Pearson, C. E. *Nucleic Acids Res.* **2015**, DOI: 10.1093/nar/ gkv1008.
13. (a) Dai, J.; Carver, M.; Hurley, L. H.; Yang, D. *J. Am. Chem. Soc*. **2011**, *133*, 17673. (b) He, H. Z.; Chan, D. S.; Leung, C. H.; Ma, D. L. *Nucleic Acids Res*. **2013**, *41*, 4345.
14. (a) Huang, X. X.; Zhu, L. N.; Wu, B.; Huo, Y. F.; Duan, N. N.; Kong, D. M. *Nucleic Acids Res*. **2014,** *42*, 8719. (b) Nikan, M.; Antonio, M. D.; Abecassis, K.; McLuckie, K.; Balasubramanian, S. *Angew. Chem., Int. Ed*. **2013**, *52*, 1428.
15. Ma, Y.; Ou, T.-M.; Tan, J.-H.; Hou, J.-Q.; Huang, S.-L.; Gu, L.-Q.; Huang, Z.-H. *Eur. J. Med. Chem.* **2011**, *46*, 1906.
16. Liao, S.-R.; Zhou, C.-X.; Wu, W.-B.; Ou, T.-M.; Tan, J.-H.; Li, D.; Gu, L.-Q.; Huang, Z.-S. *Eur. J. Med. Chem*. **2012**, *53*, 52.
17. Ma, Y.; Ou, T.-M.; Hou, J.-Q.; Lu, Y.-J.; Tan, J.-H.; Gu L.-Q.; Huang, Z.-H. *Bioorg. Med. Chem*. **2008**, *16*, 7582.
18. Ma, Y.; Ou, T.-M.; Tan, J.-H.; Hou, J.-Q.; Huang, S.-L.; Gu, L.-Q.; Huang, Z.-H. *Bioorg. Med. Chem. Lett.* **2009**, *19*, 3414.
19. Zhang, W.-J.; Ou, T.-M.; Lu, Y.-J.; Huang, Y.-Y.; Wu, W.-B.; Huang, Z.-S.; Zhou, J.-L.; Wong, K.-Y.; Gu, L.-Q. *Bioorg. Med. Chem*. **2007**, *15*, 5493.
20. Zhang, L.; Liu, H.; Shao, Y.; Lin, C.; Jia, H.; Chen, G.; Yang, D. Z.; Wang, Y. *Anal. Chem.* **2015**, *87*, 730.
21. Lu, Y.-J.; Yan, S.-C.; Chan, F.-Y.; Zou, L.; Chung, W.-H.; Wong, W.-L.; Qiu, B.; Sun, N.; Chan, P.-H.; Huang, Z.-S.; Gu, L.-Q.; Wong, K.-Y. *Chem. Commun*. **2011**, *47*, 4971.

22. Ambrus, A.; Chen, D.; Dai, J.; Bialis, T.; Jones, R. A.; Yang, D. *Nucleic Acids Res*. **2006**, *34*, 2723.
23. Petraccone, L. *Top. Curr. Chem*. **2013**, *330*, 23.
24. Amrane, S.; Adrian, M.; Heddi, B.; Serero, A.; Nicolas, A.; Mergny, J.-L.; Phan, A. T. *J. Am. Chem. Soc*. **2012**, *134*, 5807.
25. Wang, Y.; Patel, D. *J. Structure* **1993**, *1*, 263.
26. (a) Xu, Y.; Kaminaga, K.; Komiyama, M. *J. Am. Chem. Soc*. **2008**, *130*, 11179. (b) Gray, R. D.; Chaires, J. B. *Nucleic Acids Res*. **2008**, *36*, 4191. (c) Nicoludis, J. M.; Barrett, S. P.; Mergny, J.-L.; Yatsunyk, L. A. *Nucleic Acids Res*. **2012**, *40*, 5432.
27. Chen, S.-B.; Wu, W.-B.; Hu, M.-H.; Ou, T.-M.; Gu, L.-Q.; Tan, J.-H.; Huang, Z.-S. *Chem. Commun*. **2014**, *50*, 12173.
28. Jin, B.; Zhang, X.; Zheng, W.; Liu, X.; Qi, C.; Wang, F.; Shangguan, D. *Anal. Chem*. **2014**, *86*, 943.
29. Nikan, M.; Antonio, M. D.; Abecassis, K.; McLuckie, K.; Balasubramanian, S. *Angew. Chem., Int. Ed*. **2013**, *52*, 1428.
30. Liao, G.-L.; Chen, X.; Ji, L.-N.; Chao, H. *Chem. Commun*. **2012**, *48*, 10781.
31. Ambrus, A.; Chen, D.; Dai, J.; Bialis, T.; Jones, R. A.; Yang, D. *Nucleic Acids Res*. **2006**, *34*, 2723.
32. Laguerre, A.; Stefan, L.; Larrouy, M.; Genest, D.; Novotna, J.; Pirrotta, M.; Monchaud, D. *J. Am. Chem. Soc*. **2014**, *136*, 12406.
33. Jin, B.; Zhang, X.; Zheng, W.; Liu, X.; Zhou, J.; Zhang, N.; Wang, F.; Shangguan, D. *Anal. Chem*. **2014**, *86*, 7063.
34. a) Xie, X.; Choi, B.; Largy, E.; Guillot, R.; Granzhan, A.; Teulade-Fichou, M. P. *Chem. Eur. J*. **2013**, *19*, 1214. b) Stootman, F. H.; Fisher, D. M.; Rodger, A.; Aldrich-Wright, J. R. *Analyst* **2006**, *131*, 1145. c) Jin, B.; Zhang, X.; Zheng, W.; Liu, X.; Zhou, J.; Zhang, N.; Wang, F.; Shangguan, D. *Anal. Chem*. **2014**, *86*, 7063.
35. a) Mergny, J. L.; Phan, A. T.; Lacroix, L. *FEBS Lett*. **1998**, *435*, 74. b) Murat, P.; Singh, Y.; Defrancq, E. *Chem. Soc. Rev*. **2011**, *40*, 5293.
36. Zhao, C.; Ren, J.; Gregoliński, J.; Lisowski, J.; Qu, X. *Nucleic Acids Res*. **2012**, *40*, 8186.

Chapter 5

Studies on the Synthesis, Photophysical Properties of Naphthalimide and Fluorescence Switch-on Sensing of ct-DNA

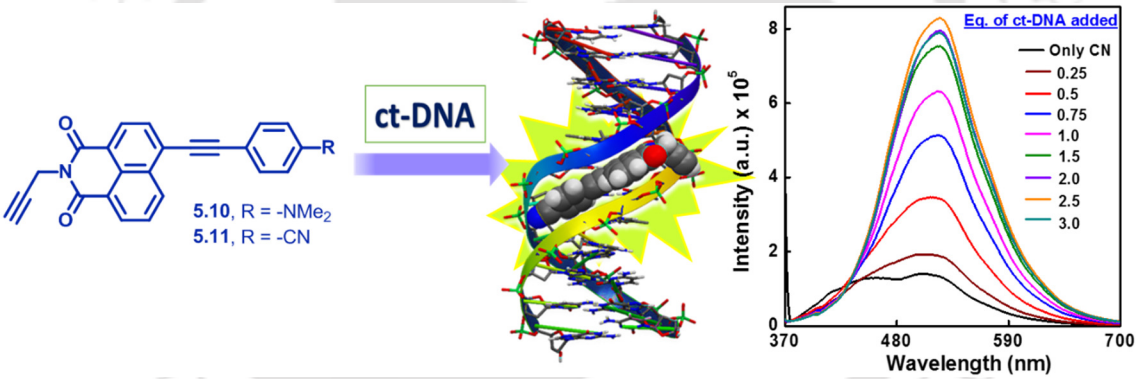

5.1. Introduction

The interactions between small molecules and DNA have been the focus of research in the fields of chemistry, biochemistry, drug design and clinical medicine.[1–4] Interaction of DNA-drug molecules, in general, is of two types. (1) Covalent or label DNA-drug interaction and (2) non-covalent DNA-drug interaction. Covalent DNA-drug interaction is irreversible. Non-covalent DNA-drug interactions occur via three types of binding modes: (i) electrostatic external binding between the negatively charged sugar phosphate backbone along the DNA double helix and the cationic or positive end of the polar drug, (ii) groove binding involving hydrogen bonding or van der Waals interaction with the nucleic acid bases in the deep major groove or the shallow minor groove of the DNA helix and (iii) intercalative binding where the drug intercalates itself within the nucleic acid base pairs.[5,6] Among the three modes, intercalative binding is the most effective for drugs targeted to DNA.[7] Intercalation is one of the most important binding mode in which small molecules intercalate between the base pairs of the double helix DNA forming π–π overlapping interactions, simultaneously lengthening and unwinding the DNA helix.[8] In such an event an unwanted small molecule if intercalates into DNA, it may damage the DNA even altering the genetic information. So, because of easy availability among various types of DNA ct-DNA is used as model DNA-drug interaction study. For investigating such binding characteristics of organic dyes to DNA, sensitive spectral techniques have been successfully exploited along with various other techniques.[7]

The 4-amino and/ or alkyl amino-1,8-naphthalimide chromophore or their anologues have been reported for their several interesting photophysical properties and utilized for chemosensory applications.[9i] Because of the 'push–pull' nature of its internal charge transfer (ICT) excited state, these have been utilized in several biological applications.[9] Naphthalenimides show a diversified interaction behaviour towards biological substrates including DNA and proteins. Brana *et al* [10] first synthesized a series of 3-nitro-naphthalimide derivatives which were proven to effectively bind DNA. Among the single naphthalimide derivatives, mitonafide [11] and amonafide [12] have been used in clinical trials and both bind DNA and influence the functions of DNA and RNA. Furthermore, because of their potential anti-tumor activity upon electronic excitation with UV light 1,8-naphthalimides have attracted much attention in the fields of biology and medicine. 4-Amino-1,8-naphthalimide also have been utilized in supramolecular fields as well as DNA targeting molecule. Troger's base compounds as well as metal complexes of napthalimides have been developed and found to interact strongly with DNA.[9i–l]

Calf-thymus DNA (ct-DNA) is one of the most important biological macromolecule used as a model for DNA-drug interaction. The model study with ct-DNA-small molecule can gives an important information about drug design, biological functions and stability factors of DNA. A large number of research works in this regard have been reported in literature, few of them are discussed below.

The binding property of highly photocarcinogenic and phototoxic fluoroquinolones (FQs), lomefloxacin (LOM) (**Figure 5.1**) and enoxacin (ENX) (**Figure 5.1**) to calf thymus DNA (ct-DNA) were investigated by Sortino[14] *et. al*. Both the nature and efficiency of the binding are markedly dependent on the buffer concentration. In 10^{-3} M phosphate buffer the interaction with ct-DNA seems to involve mainly the cationic form of both FQs, which bind to the helix with different efficiency. An increase of one order of magnitude of the buffer concentration induced a displacement of the molecules from the DNA interior, leading to significant decrease of the association constants. In this overall scenario, the positively charged piperazinyl ring of both molecules was thought to act as a pivot, going from one binding mode to another. The absorption spectra of LOM and ENX showed significant hypochromic effects accompanied by change in the shape of the absorption bands and fairly clear isosbestic points. These findings provide a first indication of the formation of ground-state complexes of LOM and ENX with double-helical ct-DNA. The fluorescence intensity was markedly quenched by the addition of the polynucleotide. In contrast, no shifts of the emission maxima were observed. The positively charged piperazinyl ring of LOM and ENX is thought to behave as a pivot, going from one binding mode to another. In fact, in both cases it can interact with the negatively charged phosphates of the DNA stem via a highly favored electrostatic interaction.

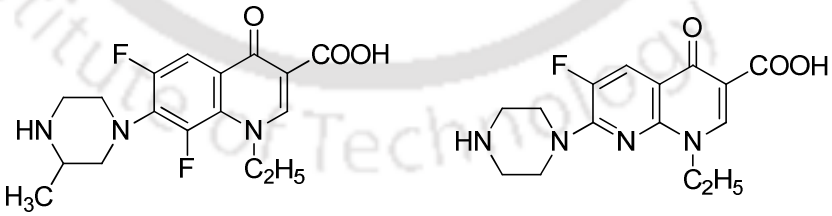

5.1, LOM **5. 2,** ENX

Figure 5.1. Structure of Highly photocarcinogenic and phototoxic fluoroquinolones (FQs), lomefloxacin (LOM) and enoxacin (ENX).

Zhang[15] *et.al*., investigated the binding characteristics of sodium saccharin (SSA) (**Figure 5.2**), an artificial sweetener, with calf thymus DNA (ct-DNA) by a combined fluorescence and UV−vis spectroscopic. The binding mode of SSA to ct-DNA was principally

through groove binding as revealed by ct-DNA melting temperature studies, viscosity measurements, iodide and salt quenching effects. SSA **5.3** preferentially bound to the guanine base of ct-DNA and led to a transformation from B-like DNA structure to A-like conformation.

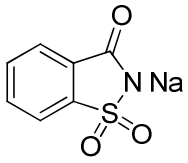

5.3

Figure 5.2. Structure of sodium saccharin SSA.

Huo[16] *et.al*., explored the interaction between neodymium–naproxen complex (Nd–NAP) (**Figure 5.3**) with calf thymus DNA (ct-DNA). Nd- NAP intercalated with the ct-DNA base pairs. Analysis of fluorescence quenching data of Nd–NAP by ct-DNA at different temperatures using a Stern–Volmer equation revealed dynamic and static quenching occurred simultaneously. The thermodynamic parameters ΔG, ΔH, and ΔS calculated at different temperatures indicated that hydrogen bonding and van der Waals force were the main binding forces. The absorbance values of Nd–NAP at 218 nm decreased with increasing concentration of ct-DNA; a red shift was also detected, indicating that there was a strong interaction between Nd–NAP and ctDNA that might be intercalation.

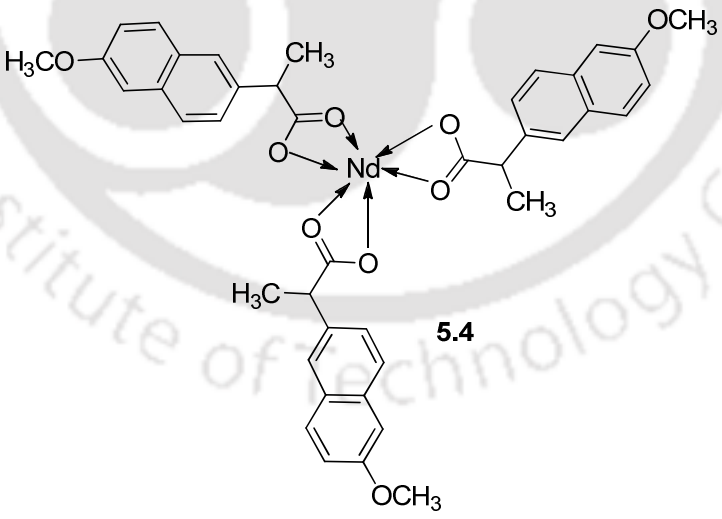

5.4

Figure 5.3. Structure of neodymium–naproxen complex (Nd–NAP).

Zhou[17] *et.el*., investigated the binding characteristics of daphnetin (**Figure 5.4**) with calf thymus DNA (ct-DNA) by using multi spectroscopic and chemometric approaches coupled with DNA viscosity measurements, melting studies and molecular docking technique. The groove mode of daphnetin binding to ct-DNA was concluded by little change in melting

temperature, viscosity of ct-DNA and iodide quenching effect as well as increase in single-stranded DNA quenching effect. Circular dichroism spectra showed the groove binding of daphnetin to ct-DNA led to the conformational change in ct-DNA from B-form to A-form. The interaction mechanism of daphnetin with ct-DNA expected to help understanding the pharmacological effects of daphnetin, and the combined methods used the study of interaction between other small molecules and DNA.

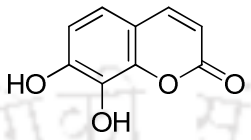

Daphnetin, **5.5**

Figure 5.4. Structure of daphnetin.

The ability of small molecules to bind and interfere with DNA replication and transcription provides further insight into how the drugs control the expression of genes so, Rehman[18] *et.al*., explored the interaction of an antimetabolite anticancer drug 6 mercaptopurine (6 MP) (**Figure 5.5**) with calf thymus DNA. From UV-visible spectroscopy, hyperchromism with increasing concentration of ct-DNA confirming the interaction of 6MP and DNA. Steady state fluorescence revealed an increase in the fluorescent intensity with increasing DNA concentration with a moderate binding constant of 7.48 x 10^3 M^{-1} which was consistent with an external binding mode. Competitive displacement assays confirmed a non-intercalative binding mode of 6MP which was further confirmed by CD and viscosity experiments.

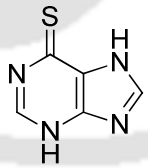

6 Mercaptopurine, **5.6**

Figure 5.5. Structure of 6 mercaptopurine (6 MP).

Zhang[19] *et.al*., studied the interaction between farrerol (**Figure 5.6**) and calf thymus DNA in a physiological pH (*i.e.,* at 7.4) Tris-HCl buffer. Farrerol molecules intercalated into the base pairs of DNA as evidenced by decreases in iodide quenching effect and single-stranded DNA (ssDNA) quenching effect, induced CD spectral changes, and significant increases in relative viscosity and denaturation temperature of DNA. Moreover, the thermodynamic parameters enthalpy change (ΔH) and entropy change (ΔS) were calculated to be, 16.49 ± 0.51

kJ mol^{-1} and 32.47 ± 1.02 J mol^{-1} K^{-1} via the van't Hoff equation, suggested that the binding of farrerol to DNA was driven mainly by hydrophobic interactions and hydrogen bonds.

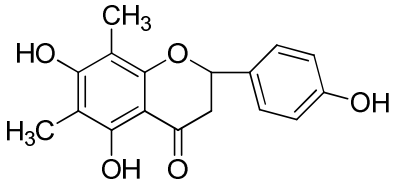

Farrerol, **5.7**

Figure 5.6. Structure of farrerol.

Shi[20] *et. al*., proposed the binding interaction of gefitinib (**Figure 5.7**) with calf thymus DNA (ct-DNA) under the simulated physiological pH condition. Gefitinib preferred to bind to the minor groove of ct-DNA with the binding constant (K_b) of 1.29 x 10^4 L mol^{-1} at 298 K. Base on the signs and magnitudes of the enthalpy change (ΔH^0 = - 60.4 kJ mol^{-1}) and entropy change (ΔS^0 = - 124.7 J mol^{-1} K^{-1}) in the binding process and the results of molecular docking, concluded that the main interaction forces between gefitinib and ct-DNA in the binding process were van der Waals force and hydrogen bonding interaction. CD spectra revealed that gefitinib did not disturb native B-conformation of ct-DNA.

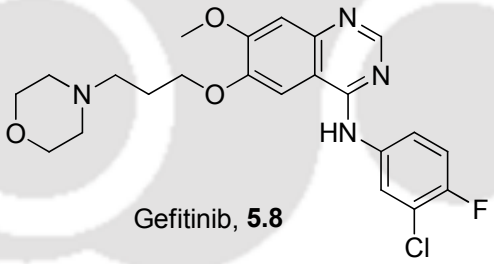

Gefitinib, **5.8**

Figure 5.7. Structure of gefitinib.

The interaction of one anthraquinone derivative (AOMan, **Figure 5.8**) with calf thymus deoxyribonucleic acid (ct-DNA) was systematically investigated by Cui[21] *et. al*., at physiological pH 7.4. Thermodynamic parameters, enthalpy and entropy changes were calculated according to Van't Hoff equation, indicated that the reaction was spontaneous and predominantly enthalpically driven. ct-DNA can quench the fluorescence of AOMan by a static quenching procedure. The molecular modeling showed anthraquinone ring tended to slide into the G–C rich region of ct-DNA through the hydrogen bond, which are consistent with the results from experimental methods. Studying the binding interaction of target anthraquinones with DNA is one of the key steps in their DNA-changing action and the design of new drugs.

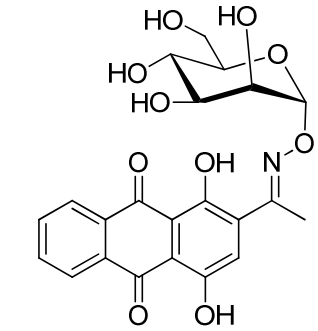

Anthraquinone derivative (AOMan), **5.9**

Figure 5.8. Structure of anthraquinone derivative (AOMan).

5.2. Background

Solvatochromic fluorescent molecules are widely known to serve as extremely sensitive probes in biological systems for the detection and probing of structures, dynamics, micropolarity around a biomolecule and interbiomolecular interactions. Therefore, the development of such fluorescent molecules is a very important research target for understanding biological events associated with interbiomolecular interactions. As for example, highly solvatochromic fluorescent probes and fluorescently labeled bio-molecular building blocks such as solvofluorochromic nucleosides/amino acids have been successfully utilized for the sensing and detection of bio-molecular microenvironment/ biomolecules. However, many of such explored fluorophores emitted at a short wavelength region, possessed low emission intensity and/or suffered from a quenching incidence rendering them unsuitable for practical use. Therefore, bright and long-wavelength emissive fluorescent molecules with emission in the visible region have attracted great interest in recent time as new fluorescent probes for the detection and sensing of biomolecules without any interference by the background signal generated from the auto absorption and auto fluorescence of biomolecules.

Therefore, a brief introduction of the interaction of small fluorescent molecules as probes of calf thymus DNA is given in this chapter.

5.3. Objective

With the growing interest in DNA binding agents, like, intercallators, groove binders and reported limited number of switch on long wavelength emissive biomolecular probe, it is thus pertinent to develop new designer molecules and study the binding interaction with DNA

to reveal how the compound may be further modified to enhance its binding activity or to provide guidelines for the development of more potent compounds with novel photophysical properties. Naphthalimide derivatives aroused the interest of chemists, physicists and biologists for various reasons such as chemosensory applications, several biological applications, as interacting molecule for DNA and proteins and in the field of medicine. However, there is no report of 1,8-naphthalimide in which 4-position is conjugated to donor/acceptor substituted phenylacetylenes to achieve much longer absorption wavelength.

Therefore, as a part of our ongoing program for the design and synthesis of highly solvatochromic fluorophores with a linker unit for possible future use in lebelling of biomolecular building blocks and taking into consideration of the importance of naphthalimide derivatives in biological applications, we were very much interested in the possibility of synthesizing 1,8-naphthalimide derivatives with donor/acceptor substituents as new potential solvatochromic fluorophores (**Figure 5.9**).

Thus, we framed our objective as below:

a) Synthesis of donor/acceptor containing 1,8-naphthalimide
b) Study of photophysical property
c) Study of interaction with ct-DNA

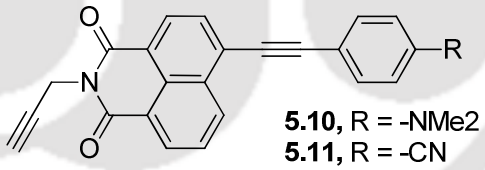

Figure 5.9. Structure of **5.10** and **5.11**.

5.4. Results and Discussions

5.4.1. Synthesis of Donor/Acceptor Labeled Naphthalimide Solvatocromic Fluoroprobe

A Pd(0)-mediated 'click-reagent version' of Sonogashira coupling[9b,22] of anhydride **5.12** with 4-ethynyl-*N,N*-dimethylaniline and 4-ethynylbenzonitrile, respectively, was carried out in dry DMF at 80 ^{o}C for 4 h, to afford 4-substituted- 1,8-naphthalic anhydrides, **5.15** and **5.16**. After recrystallization from hot toluene pure naphthalic anhydride derivatives **5.15** and **5.16** in 65% and 70% yields, respectively, were afforded. Next, conjugated anhydrides **5.15** and **5.16** were allowed to react with propargylamine in dry ethanol under reflux for 50 h to

afford 4-(4-*N, N*-dimethylaminophenylethynyl)- *N*-(2-propynyl)-1,8-naphthalimide (**5.10,** $^{4\text{-DMAPE}}$**NI**) and 4-(4-cyanophenylethynyl)-*N*-(2-propynyl)-1,8-naphthalimide (**5.11,** $^{4\text{-CPE}}$**NI**), respectively, with good yields (**Scheme 5.1**). Washing the products in water and ethanol and recrystallization gave pure compound **5.10** as red crystalline solid and **5.12** as yellow powder in very good yields. The structures of the final products were characterized by NMR, mass spectrometry, and by X-ray single crystal analysis of compound **5.10**.

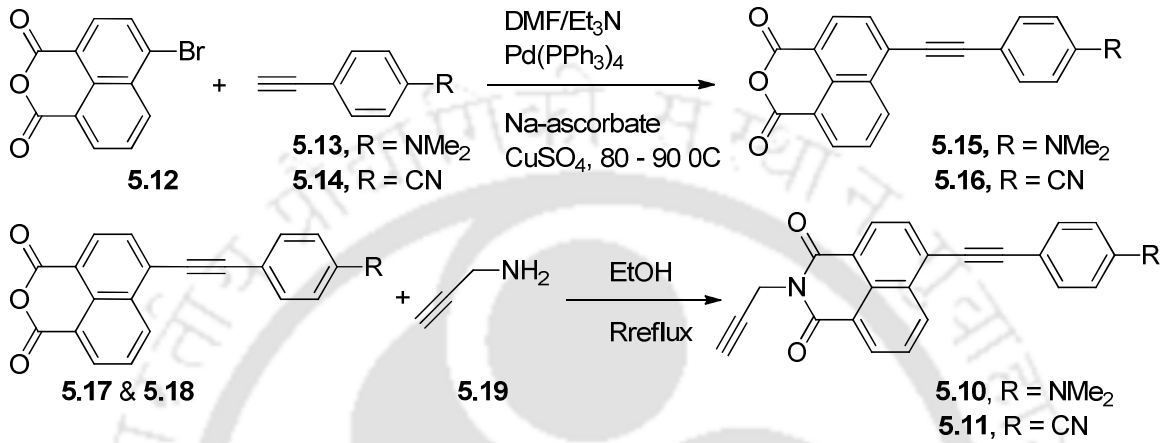

Scheme 5.1. Synthesis of donor/ accepter labeled naphthalimide fluorophore **5.10** and **5.11**.

The structures of the final products were characterized by NMR, mass spectrometry, and by X-ray single crystal analysis of compound **5.10**. To examine the biomolecule sensing ability of probe **5.10** and **5.11**, first the photophysical property in different solvent environment varying from non-polar to polar investigated.

5.4.2. Crystallographic Description of 5.10

The crystal structure of fluorophore **5.10** showed very interesting arrangement (**Figure 5.11**). Thus, the donor substituted planar naphthalimide with the pendent propargyl arm crystallized in a layered sheet-like arrangement. The planar sheets are layered on top of each other, with slip-stacked ArCH–π-bonding (3.29 Å) between internal alkyne and aromatic C–H of naphthalimide core. The layers are held by C–C–π (3.37 Å) bonding between donor/acceptor aromatics and π-stacking between the donor unit in one layer and the acceptor naphthalimide core of the other layer (**Figure 5.11a**). Head-to-tail arrangements of donor *N,N*-dimethylanilino unit of one molecule in one layer and acceptor naphthalimide core of a separate molecule in second layer makes the system stable by forming a strongly π-stacked and charge transfer stabilized stacked layer like structure. The layers are so arranged that the donor-*N,N*-dimethylphenyl moiety interacts via π-stacking and charge transfer interactions with the

acceptor naphthalimide ring in the molecule in the layer above and below with an average interlayer distance being 3.31 Å. The pendant terminal acetylenic-H involved in H-bonding with –C=O of naphthalimide group (2.37 Å) of a molecule in a different layer giving rise to a bent-stair-like arranged third stacked layer (**Figure 5.11 a and b**).

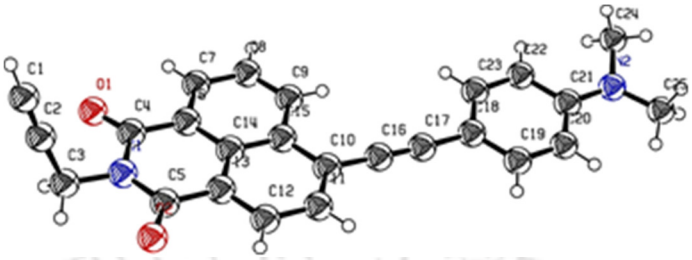

Figure 5.10. ORTEP molecular diagram with ellipsoid at 50% probability of **5.10**.

Crystallographic description of 5.10: Crystal dimension (mm): 0.35 x 0.25 x 0.20. $C_{25}H_{18}N_2O_2$, Mr = 378.41; Monoclinic, space group P2(1)/c; a = 28.621(3) Å, b = 9.4187(8) Å, c = 15.0718(14) Å; α = 90.00°, β = 104.256(5)°, γ = 90.00°, V = 3937.9(6) $Å^3$; Z = 8; ρcal = 1.317 Mg/m^3; μ (mm^{-1}) = 0.083; *F (000)* = 1680.0; Refinement method = Full-matrix least-squares on F^2; Final R indices [$I>2\sigma_I$] R1 = 0.2650, wR2 = 0.5213, R indices (all data) R1 = 0.1826(3683), wR2 = 0.5213(8879); goodness of fit = 1.593. [CCDC no.-CCDC 882241].

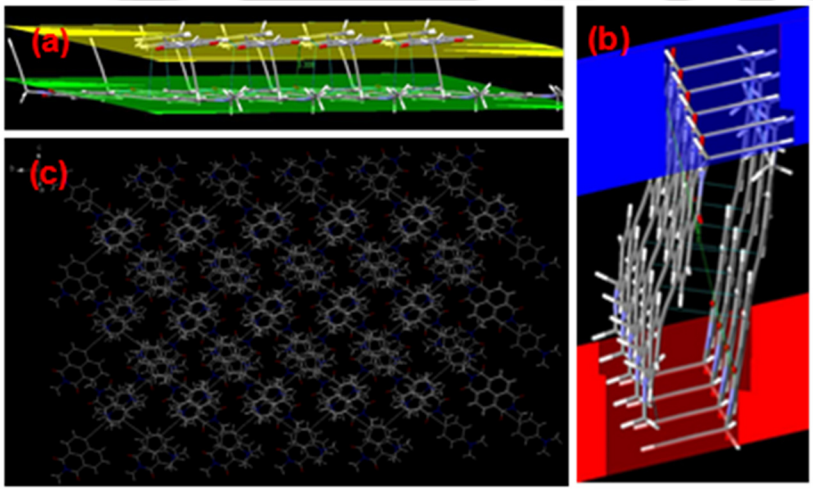

Figure 5.11. Crystal structure (a-b) showing inter planar distance and the two planes formed by two pendent acetylenic arms. (c) Crystal network of the molecule **5.10**.

5.4.3. Spectral Study of 5.10 and 5.11 in Different Solvent

After getting all the compounds in hand in very pure form, we turned our attention to study their photophysical properties. Thus, the UV-visible absorption spectra of the naphthalimide fluorophores **5.10** and **5.11** were studied in various solvents of different polarity.

The longest wavelength absorption of compound **5.10** was characterized by a broad band with the maxima appearing between 450 and 467 nm depending on the polarity of the solvents (**Figure 5.12a**). This band was unambiguously assigned as intramolecular charge transfer (ICT) band that was generated out of charge transfer from the donor 4-*N,N*-dimethylaminophenyl group to the acceptor naphthalimide ring system via the internal alkyne. The origin of ICT was also evident from the fairly broad, intense and the large solvatochromicity of the band.[13b,23] Thus, an increase in polarity of the media led to a red shift of the absorption maxima of about 14–24 nm when changing the solvent from hexane to chloroform to DMSO suggesting that the ground state of the molecule was significantly polar. However, for the fluorophore **5.11**, a blue shift of about 17 nm of the absorption band on changing the solvent from dioxane to trifluoroethanol (between 389 and 372 nm) was observed which might be because of the presence of electron acceptor cynophenyl unit in conjugation with the naphthalimide ring system (**Figure 5.12b**). This observation indicated that the ground state was not so polar and the fluorophore **5.11** was lipophilic in nature. Therefore, the donor *N,N*-dimethylaminophenyl unit was responsible for the enhancement of the charge separation in the molecule **5.10** which ultimately led to a large red shift of the absorption maxima.

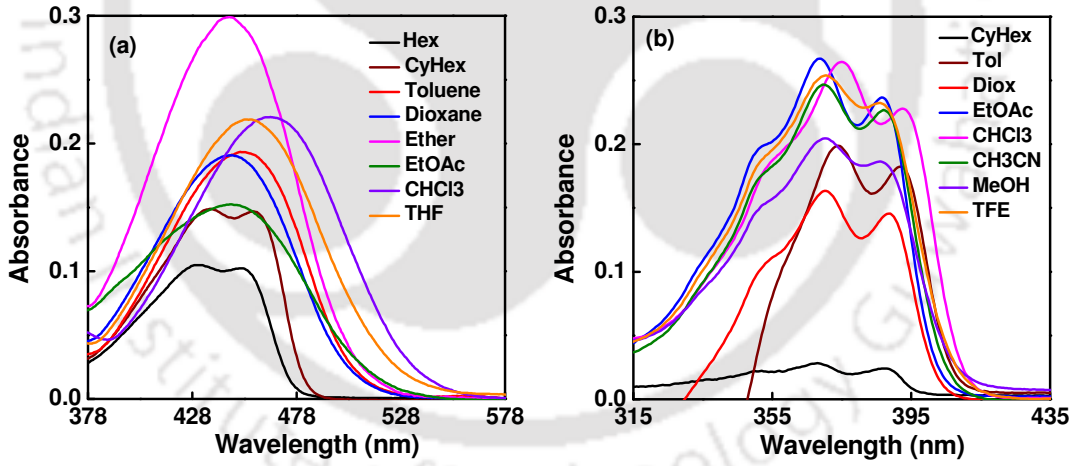

Figure 5.12. (a) UV-visible spectra for **5.10** and (b) UV-visible spectra for **5.11** in different solvents.

Next, we evaluated the fluorescence photophysical properties of the fluorophores. The fluorescence spectra of all the compounds consisted of structureless broad band except in hexane, cyclohexane where some structured bands appeared. However, an increase in the polarity of the solvent led to large Stokes shift of emission maxima for compound **5.10** (**Figure 5.13a**). Thus, from the fluorescence spectra of imide fluorophore **5.10**, it was clear that as the solvent polarity increases a strong red shift of about 140 nm (λ_{max}, hexane 474 nm, and λ_{max},

chloroform 611 nm) was observed with decrease in both the fluorescence intensity and the quantam yield (**Table 5.1**). The red shift and signal broadening of the spectra indicated that the conjugation is extended well between the acceptor imide carbonyl group and the donor *N, N*-dimethylanilino unit through internal alkyne. Same observation was reflected in the fluorescence images of the compound in different solvents at a wavelength of 254 nm under a trans illuminator (**Figure 5.13c**). Thus, in hexane/cyclohexane it showed a strong greenish blue color while the color changed from greenish blue to yellow in toluene, pink in dioxane and ultimately to red in chloroform. Surprisingly, no emission was observed when polarity of the solvent increased to methanol through ethylacetate.

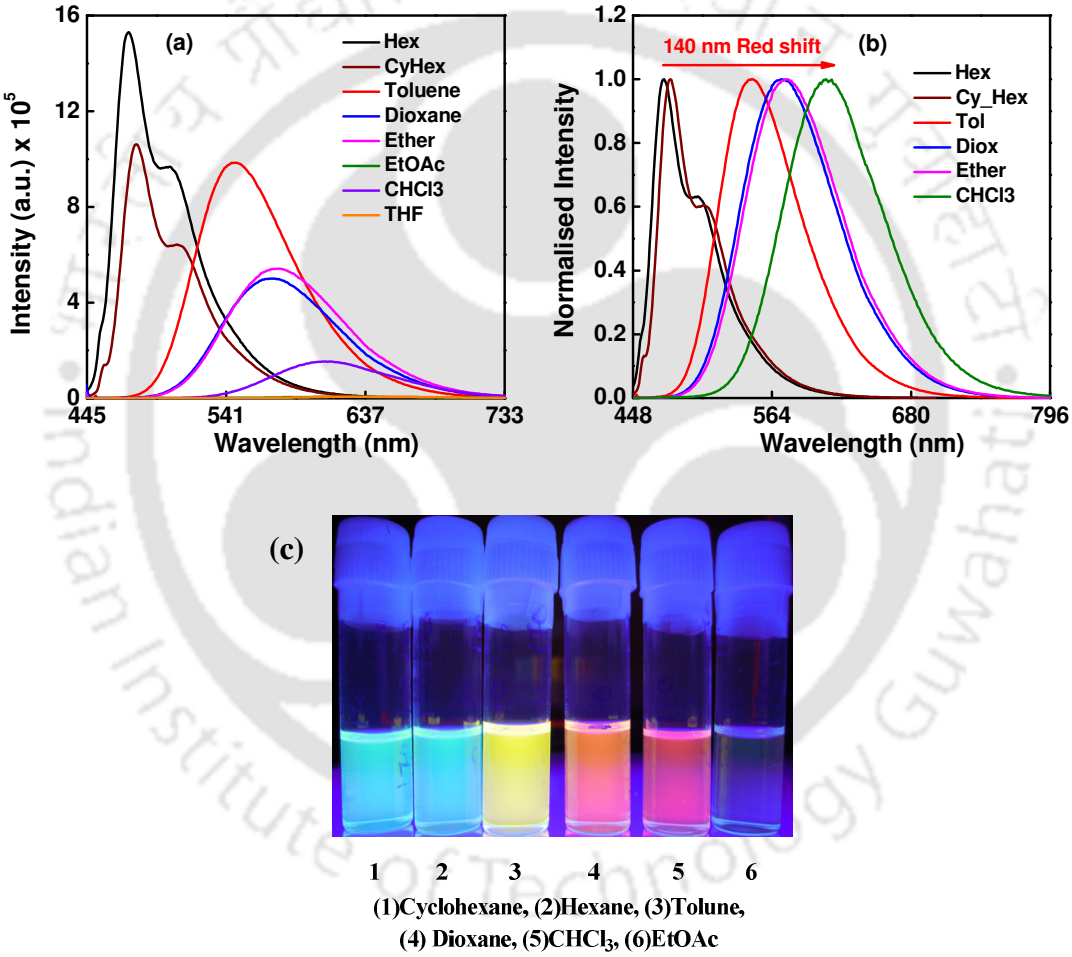

Figure 5.13. (a) emission and (b) normalized emission spectra of **5.10** ($^{4\text{-DMAPE}}$**NI**) in different solvents (λ_{ex} = 445 – 465 nm). (c) Colours in different solvents after irradiation of **5.10** in UV light (λ = 254 nm).

Table 5.1. Absorption ($\lambda_{abs.}$, nm), Emission (λ_{em}, nm), Lifetime (τ_1, ns), Quantum Yield (Φ_f), Radiative Rate Constant (k_f, $10^7 s^{-1}$) and Non-radiative Rate Constant (k_{nr}, $10^7 s^{-1}$) of 5.10 ($^{4\text{-DMAPE}}$NI) in different solvents.

Solvents	$\lambda_{abs.}$	λ_{em}	Φ_f[1]	τ_1 (ns)	χ^2	k_f (10^9 s^{-1})	k_{nr} (10^9 s^{-1})
Hexane	453	474	0.79	2.80	1.05	0.28	0.07
CyHex	459	480	0.66	2.84	1.02	0.23	0.12
Toluene	454	548	0.53	3.74	1.03	0.14	0.13
Dioxane	448	572	0.24	3.75	1.17	0.06	0.20
Ether	446	577	0.23	---	---	---	---
$CHCl_3$	467	611	0.14	2.58	1.04	0.05	0.33

Red colored crystalline nature, highly ICT character and non-emissive nature of the fluorophore **5.10** in protic polar solvent drew our attention to evaluate its' solid-state photophysical property for possible future material applications. Thus, the solid-state UV–visible spectra showed two absorption bands at 444 and 560 nm (**Figure 5.14a**). The solid-state emission spectra revealed a strong emission at 721 nm with a Stokes shift of 161 nm when excited at its long wavelength absorption band (**Figure 5.14a**). The time resolved fluorescence in solid state showed a longer lifetime (τ_1 = 5.59 ns) compared to its solution state (**Figure 5.14b**). More interestingly, the gas phase/solution phase energy gap between HOMO and LUMO (2.6–2.7 eV) remained very closer to that of a band gap of an organic semiconductor.[24] Thus, our observations on solid state photophysical property clearly showed that the fluorophore **5.10** might find applications in material sciences such as in organic semiconductors/ electronic devices.

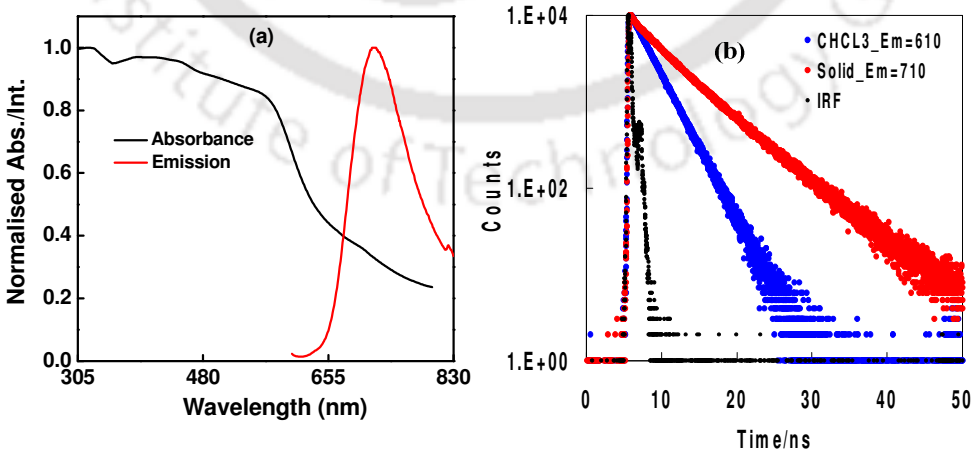

Figure 5.14. (a) Normalized absorbance and emission spectra of **5.10** ($^{4\text{-DMAPE}}$**NI**) in solide state (λ_{ex} = 560 nm). (b) Time resolved fluorescence spectra of **5.10** in both solvent and solid state.

After investigating the photophysical properties of fluorophore **5.10** both in solution and in solid state, we next evaluated the fluorescence photophysical property of fluorophore **5.11**. Thus, for the case of acceptor containing naphthalimide fluorophore **5.11**, upon changing the solvent polarity, both the intensity and the quantam yield of emission were found to be increased with a moderate Stokes shift of about 39 nm when compared between the solvents dioxane and TFE (**Figure 5.15a, b, Table 5.2**).

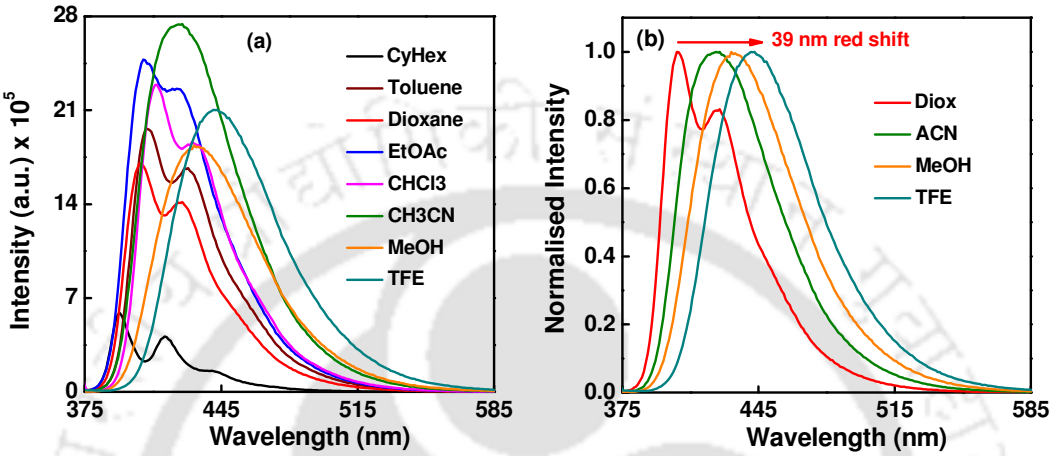

Figure 5.15. (a) emission and (b) normalized emission spectra of **5.11** (**$^{4\text{-CPE}}$NI**) in different solvents (λ_{ex} = 370 nm).

Table 5.2. Absorption (λ_{abs}, nm), Emission (λ_{em}, nm), Lifetime (τ_1, ns), Quantum Yield (Φ_f), Radiative Rate Constant (k_f, 107s−1) and Non-radiative Rate Constant (k_{nr}, 107s−1) of Fluorophore 5.11 ($^{4\text{-CPE}}$NI) in different solvents.

Solvents	$\lambda_{abs.}$	λ_{em}	Φ_f [2]	τ_1 (ns)	χ^2	k_f (10^9 s^{-1})	k_{nr} (10^9 s^{-1})
Dioxane	389	403	0.57	1.45	1.11	0.39	0.30
Toluene	392	408	0.48	1.62	1.03	0.29	0.32
EtOAc	387	406	0.56	1.52	1.17	0.36	0.29
$CHCl_3$	393	411	0.49	1.38	1.16	0.35	0.37
CH_3CN	387	423	0.54	1.66	1.13	0.32	0.28
MeOH	387	434	0.54	1.79	1.04	0.30	0.25
TFE	372	442	0.55	2.05	1.10	0.27	0.22

To understand the fluorescence behavior more precisely, we measured fluorescence lifetime in different solvents and found that the decay followed a single exponential fitting for all the fluorophores. The effect of polarity was very similar to what was observed for the fluorescence quantum yield (**Table 5.1**). While in case of compound **5.10** increase in the polarity of the solvent led to a shortening of the lifetime, in case of compound **5.11**, lifetime increased as the polarity of the solvent was increased (**Figure 5.16a** and **b, Table 5.1-2**). The dependence of the quantum yield of fluorescence of **5.10** on the nature of the solvent was

mainly dictated by changes in the rate of radiationless deactivation as was revealed from the change in the rate constants of radiationless deactivation on going from hexane to chlorofom (**Table 5.1**). However, the opposite was obviously the result in case of fluorophore **5.11** correlating its dependency of quantum yield with the change in solvent polarity (**Table 5.2**).

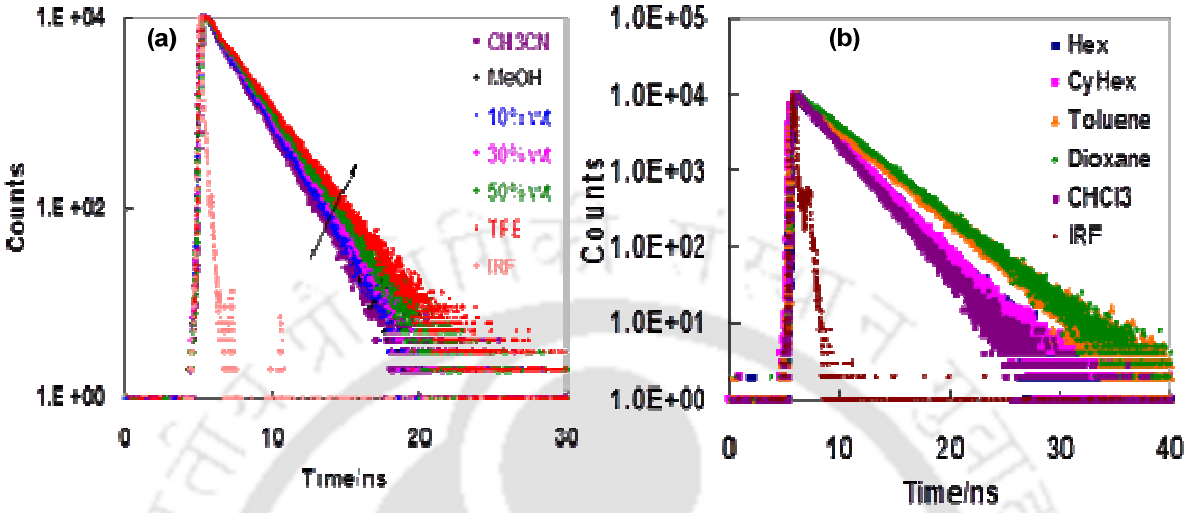

Figure 5.16. Time resolved fluorescence spectra of (a) **5.10** and (b) **5.11** in different solvent of varying polarity.

Overall, it was observed that the fluorescence quantum yields markedly decreased with increase in solvent polarity for the case of fluorophore **5.10**. Protic solvents, like methanol, are known to induce fluorescence quenching through non-radiative pathways via hydrogen bonding. Thus, the fluorescence in methanol was died away due to protic solvent–solute interactions. These properties indicated that compound **5.10** has strong charge transfer (CT) character. The conjugation between the *N,N*-dimethyl aminophenyl moiety as an electron donor and the naphthalimide core as an electron acceptor played an important role in the large dipole change during excitation and made fluorophore **5.10** highly solvatochromic.

Time dependent DFT calculation[28] also revealed that the emissive state of **5.10** was characterized with more significant electron redistribution, that is, ICT feature and rationalized the explanation of ICT origin and the solvent polarity dependency of the fluorophores' emission (**Figure 5.17** and **5.18**).

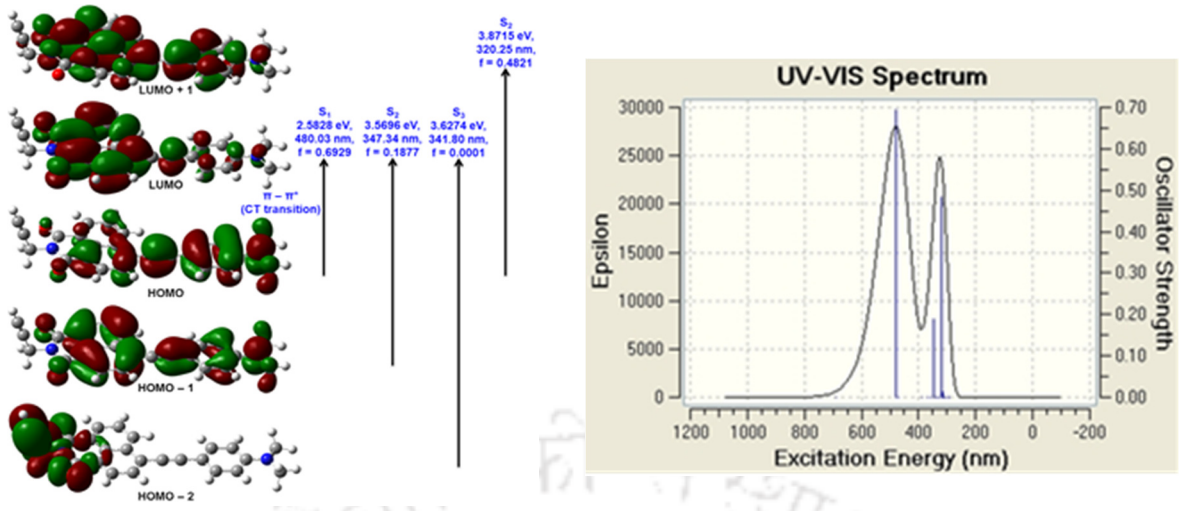

Figure 5.17. Excited-state energy levels of probe **5.10** based on TD-DFT calculations. The surface plots represent densities of the MOs with the largest contribution to the *CI*-eigenvectors.

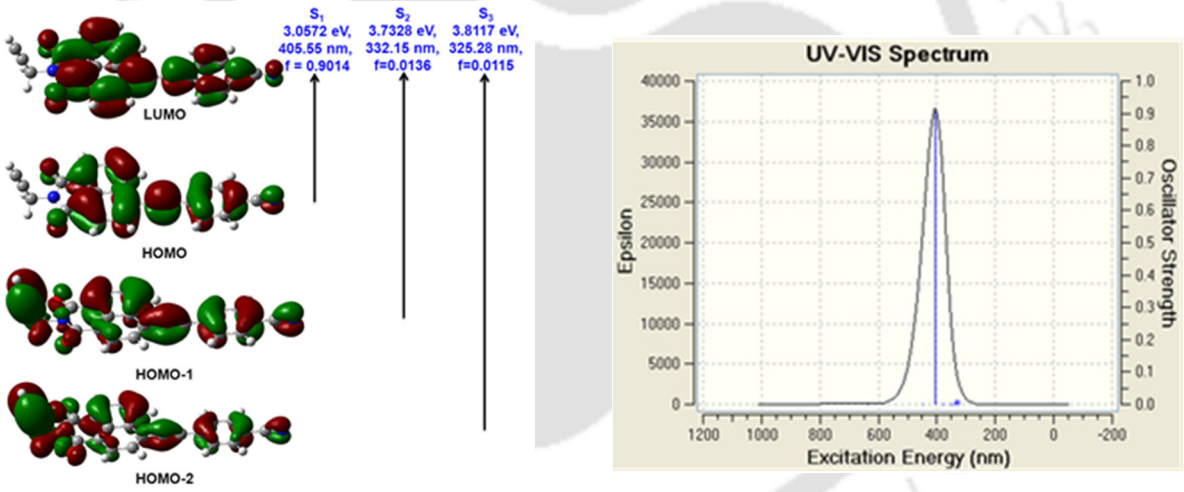

Figure 5.18. Excited-state energy levels of probe **5.11** based on TD-DFT calculations. The surface plots represent densities of the MOs with the largest contribution to the *CI*-eigenvectors.

5.4.4. Lippert and Mataga Plots

To get an insight into the strong solvent polarity sensitive emission behaviors of compounds **5.10** and **5.11**, the fluorescence spectral dependency on solvent polarity parametres (Δf) was studied on the basis of Lipert-Mataga model.[25]

Thus, a good linear correlation of the absorption and fluorescence maxima (~λ_{abs}, and ~λ_{fl} max respectively, in cm^{-1}) of fluorophores **5.10** and **5.11** with the solvent polarity functions

Δf indicated that for the fluorophore **5.10**, the ~λ_{abs} values apparently correlated linearly with Δf. This result suggested that the ground state of **5.10** was moderately polar in nature. However, a less correlation was observed in case of the fluorophore **5.11**, suggesting a nonpolar ground state (**Figure 5.19**). The reasonably high slopes of ~ $\tilde{\nu}_{fl}$ versus Δf plots for all the fluorophores **5.10 and 5.11** further suggested that the fluorescent states of these fluorophores were highly polar in nature, most possibly of intramolecular charge transfer (ICT) character.[26,27] Thus, the change of emission wavelength of the fluorophores with solvent polarity indicated their potential ICT features. A good linear correlation with large slopes of the $\Delta\tilde{\nu}$ versus Δf plots suggested that the fluorescence states were highly polar in nature for all the fluorophores (**Figure 5.19**). Substantially high values of ($\mu_e - \mu_g$) obtained from the plot (22.6 D for **5.10** and 13.9 D for **5.11**) indicated that the fluorescence state of **5.10** is of higher ICT character than **5.12** (**Table 5.3**). The excited state dipole moment determined from Stokes shift was found to be more than the ground state for fluorophore **5.10**. This might be associated with partial transfer of electron from the donor *N,N*-dimethylamino group to the acceptor naphthalimide core.

The Lippert-Mataga polarity parameter (Δf) has been considered as the measure of the polarity of different solvents and solvent mixtures used and was calculated using following equation.

$$\Delta f = \frac{\varepsilon - 1}{2\varepsilon + 1} - \frac{n^2 - 1}{2n^2 + 1} \quad \ldots\ldots\ldots\ldots\ldots\ldots\ldots\ldots\ldots\ldots (5.1)$$

In different solvents, the absorption and fluorescence spectra involve the electronic transitions between the same two ground and excited electronic states, the Stokes' shift ($\Delta\tilde{\nu}$) is expected to follow a linear relation with Δf, as suggested by the Lippert and Mataga equation as

$$\Delta\tilde{\nu} = \Delta\tilde{\nu}_0 + \frac{2(\mu_e - \mu_g)^2}{hca^3}\Delta f \quad \ldots\ldots\ldots\ldots\ldots\ldots (5.2)$$

where μ_e and μ_g are the excited (fluorescent) state and the ground state dipole moments of the fluorophore, h is Planck's constant, c is the velocity of light, and a is the Onsager radius of the dipole-solvent interaction sphere. The $\Delta\tilde{\nu}$ values for **5.10** and **5.11** compounds in different solvents were estimated (in cm^{-1}) considering the λ_{max}^{abs} and λ_{max}^{fl} values from non-polar to polar

or low polar to high polar solvents. The $\Delta\tilde{\nu}$ values thus estimated for the **5.10** and **5.11** compounds are listed in **Table 5.4.**

Table 5.3. Summary table of $\tilde{\nu}_{max}^{abs}$ and $\tilde{\nu}_{max}^{fl}$ of the fluorophores and fluorescent nucleoside and solvent polarity parameter (Δf)

5.10				**5.11**			
Solvents	Δf	$\tilde{\nu}_{max}^{abs}$ (cm^{-1})	$\tilde{\nu}_{max}^{fl}$ (cm^{-1})	Solvents	Δf	$\tilde{\nu}_{max}^{abs}$ (cm^{-1})	$\tilde{\nu}_{max}^{fl}$ (cm^{-1})
Hex	0.001	22075	19841	CyHex	0	27173	25445
CyHex	0	21786	19801	Tolune	0.013	26666	24509
Toluene	0.013	22026	18083	Dioxane	0.021	27027	24813
Dioxane	0.021	22321	17301	EtOAc	0.201	27100	24630
Ether	0.163	22422	17065	$CHCl_3$	0.148	26666	24330
EtOAc	0.201	22272	16234	CH_3CN	0.305	27027	23640
$CHCl_3$	0.148	21413	16529	MeOH	0.309	27027	23041

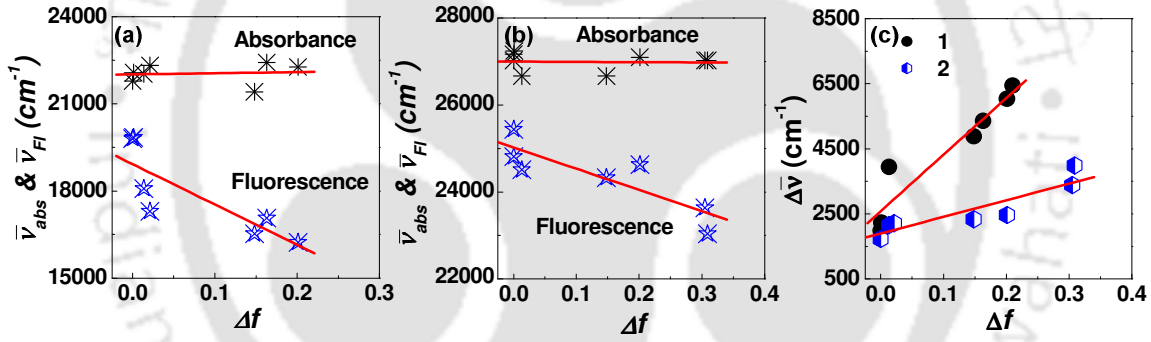

Figure 5.19. Plots of $\tilde{\nu}_{abs}$ & $\tilde{\nu}_{fl}$ values against solvent polarity parameter Δf for fluorophore (a) **5.10** and (b) **5.11** (c) Plots of $\Delta\tilde{\nu}$ values against Δf in different solvents for **5.10** and **5.11** and the corresponding dipole moment and excitation energy values.

Table 5.4. Summary table of $\Delta\tilde{\nu}$ of the fluorophores and solvent polarity parameter (Δf)

5.10			**5.11**		
Solvents	Δf	$\Delta\tilde{\nu}$(cm^{-1})	Solvents	Δf	$\Delta\tilde{\nu}$(cm^{-1})
Hex	0.001	2234.0	CyHex	0	1728
CyHex	0	1985.4	Tolune	0.013	2157
Tolune	0.013	3943.2	Dioxane	0.021	2214
Dioxane	0.021	5020.3	$CHCl_3$	0.148	2336
Ether	0.163	5356.6	EtOAc	0.201	2470
$CHCl_3$	0.148	4884.3	CH_3CN	0.305	3387
EtOAc	0.201	6037.9	MeOH	0.309	3986
THF	0.21	6450	---	---	---

Table 5.5. Summary of Physical parameters of **5.10** and **5.11**

Parameter	**5.10 (NMe_2)**	**5.11 (CN)**
Onsager radius[a] (Å)	6.67	7.26
$\Delta\mu^{[b]} = (\mu_e - \mu_g)$ in Debye	22.64	13.93
$\mu_g^{[c]}$ in Debye	10.60	0.43
Excitation energy (calcd) in eV	2.58	3.05
Excitation energy (exptl) in eV	2.72	3.18

[a] Onsager radii for **5.10** and **5.11** were obtained from B3LYP/6-31G* optimized geometry; [b] Calculated from **Eq. 2** and slope from the Plots of $\Delta\tilde{\nu}$values against Δf; [c] Gas phase dipole moment obtained from B3LYP/6-31G* optimized geometry.

Being inspired by the interesting solvatochromic emission property, we next turned our attention to explore the possible sensing of microenvironment of ct-DNA using fluorophore **5.10** and **5.11**. Naphthalimides are well known as probes of nucleic acids and many naphthalimide chromophores have been utilized in fluorescence based elucidation of structure, dynamics and conformation of proteins.[9c–h] Therefore, we envisaged that the naphthalimide moiety of our probes might significantly interact with the aromatic bases in DNA via intercalative stacking/H-bonding and/ or electrostatic interaction. This idea along with the intense emission of the probes in low polar media compared to high polar media and/or buffer drew our attention to exploit fluorophores **5.10** and **5.11** in the possible sensing of microenvironment of calf-thymus DNA (ct- DNA) which is easily available biomolecules with widespread applications.[29]

5.4.5. Studies On the Interaction of Fluorophores 5.10 and 5.11 with ct-DNA

5.4.5.1. UV-visible Study of 5.10 and 5.11 with ct-DNA

After observing very exciting photophysical properties in different solvent environment, we next motivated to explore the possible sensing of microenvironment of ct-DNA using fluorophore **5.10** and **5.11**. Naphthalimides are well known as probes of nucleic acids and many naphthalimide chromophores have been utilized in fluorescence based elucidation of structure, dynamics and conformation of DNA.[9c–h] Therefore, we envisaged that the naphthalimide moiety of our probes might significantly interact with the aromatic bases in DNA *via* intercalative π-π stacking/H-bonding and/ or electrostatic interactions. Thus, the absorption maxima of fluorophore **5.10** and **5.11** located at 445 and 395 nm, respectively,

showed a negligible effect on the change in wavelength position and enhanced absorbance intensity as ct-DNA was added gradually (**Figure 5.20**).

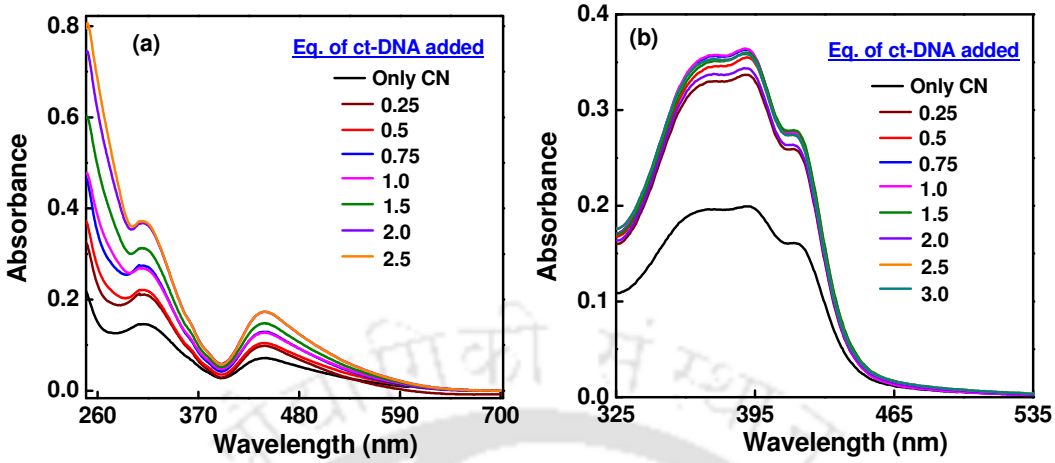

Figure 5.20. (a) UV-Visible of fluorophore **5.10** and (b) UV-visible spectra of fluorophore **5.11** in presence of increasing concentration of ct-DNA. [**Probe**] = 30 μM and [ct-DNA] = 7.5, 15, 22.5, 30, 37.5, 45, 60 and 75 μM.

5.4.5.2. Fluorescence Study of 5.10 and 5.11 With ct-DNA

Next, fluorescence titration experiment was carried out. Thus, upon gradual addition of ct-DNA, the emission intensity (λ_{em} = 525 nm) of the fluorophore **5.11** was found to be significantly enhanced with slightly red shifted pattern. The emission became saturated at 75 μM concentration of ct-DNA compared to 30 μM probe concentration (**Figure. 5.21a**). This observation clearly indicated a well-defined binding of the probe **5.11** with ct-DNA. On the contrary, fluorophore **5.10**, which is of greater ICT character compared to fluorophore **5.11**, showed a sudden enhancement of fluorescence intensity with very little blue shifted pattern at probe: ct-DNA concentration ratio of 1:1. Beyond this ratio, no regular trend in decreased emission upon addition of increasing amount of ct-DNA was observed when excited at 460 nm (**Figure. 5.21b, Table 5.6**). The emission response of fluorophore **5.11** upon binding with ct-DNA represented the possible binding of the probes along the groove side thereby facing more polar microenvironment leading to an enhancement of fluorescence intensity of probe **5.11** and an anomalous behavior in emission for the case of fluorophore **5.10**. The quenching incidence of probe **5.10** could easily be explained if we consider the non-radiative deactivation via solvent solute H-bonding interaction when exposed to the more polar microenvironment along the groove side. These observations are in accord with the intrinsic emission behaviors of the probes as was reveled from the solvent polarity dependent emissions of each fluorophore. [15]

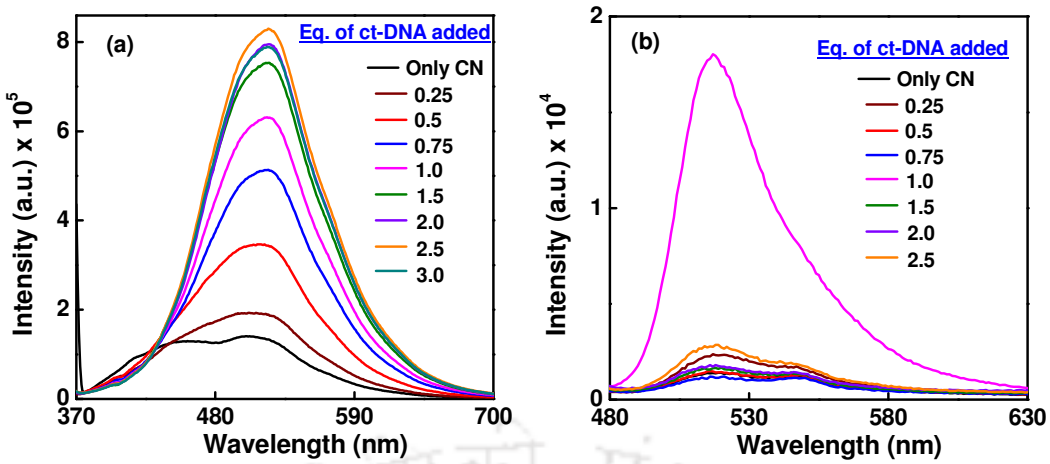

Figure 5.21. (a) Emission spectra of fluorophore **5.11** (λ_{ex} = 370 nm) and (b) Emission spectra of fluorophore **5.10** (λ_{ex} = 460 nm) in presence of increasing concentration of ct-DNA. [Probe] = 30 µM and [ct-DNA] = 0, 7.5, 15, 22.5, 30, 45, 60 and 75µM.

Table 5.6. UV-visible, Fluorescence and T_m values of ct-DNA in presence of Fluorophore **5.11** ($^{4\text{-CPE}}$NI)

Fluorophore **2 :** CT-DNA	UV-Vis & Fluorescence			T_m (°C)
	λ_{max}^{abs} (nm)	λ_{max}^{fl} (nm)	Φ_f	
1 : 0	305, 370, 395, 421	521	----	----
0 : 1	260	----	----	65.83
0 : 0.25	304, 371, 391, 418	513	0.038	----
1 : 0.5	305, 369, 394, 418	517	0.037	65.56
1: 0.75	307, 370, 393, 418	522	0.049	----
1: 1	307, 371, 393, 418	523	0.057	64.88
1 : 1.5	308, 372, 394, 418	524	0.068	64.26
1 : 2	307, 370, 393, 418	524	0.072	----
1 :2.5	307, 371, 392, 417	524	0.079	-----
2 : 1	---	----	----	63.21

5.4.5.3. Evaluation of Binding Constant "Benesi-Hildebrand plot"

The association constant (K) of the fluorophore **5.11** with ct-DNA was determined by a Benesi-Hildebrand plot using the following equation 1,

$$\frac{1}{(I - I_o)} = \frac{1}{(I_\alpha - I_o)} + \frac{1}{(I_\alpha - I_o)K[ct-DNA]} \quad \text{..... (1)}$$

Where I_0, I and I_α are the emission intensities of fluorophore **5.11** in the absence of ct-DNA, in the presence of an intermediate and at infinite concentration of ct-DNA, respectively. From the slop of the 1/ (I – I_0) *vs.* 1/[ct-DNA] plot of equation 1, binding constant K was determined

which was found to be 3.98×10^4 M^{-1} (**Figure. 5.22**). The free energy of binding (ΔG) also calculated using the equation 2, which was found to be −6.3 kcal/mol.

$$\Delta G = -RT \ln K \quad \text{..... (2)}$$

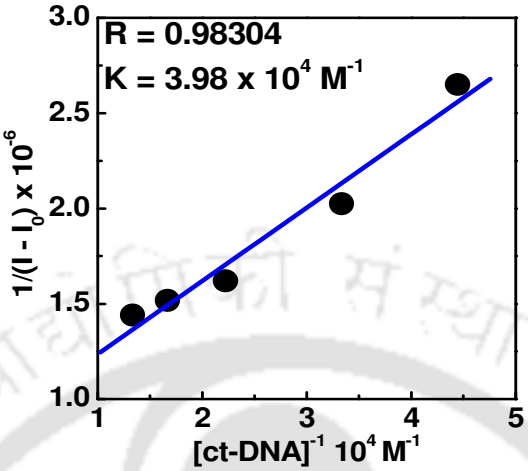

Figure 5.22. Benesi- Hildebrand plot of fluorophore **5.11** in presence of increasing ct-DNA concentration. [fluorophore 5.2] = 30 μM and [ct-DNA] = 15, 22.5, 30, 45, 60 and 75 μM.

5.4.5.4. DNA Melting Experiments

Thermal denaturation experiment indicated no destabilization of ct-DNA upon binding with the probe **5.11** suggesting that the probe possibly binds to a groove of ct-DNA (**Figure 5.23, Table 5.6**).[30]

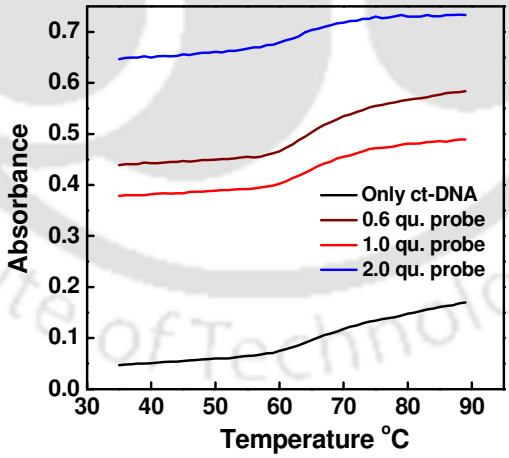

Figure 5.23. T_m study of ct-DNA in presence of fluorophore **5.11.**

5.4.5.5. Evaluation of Binding Mode of the Fluorophore 5.10 and 5.11 with ct-DNA by a Dye (Ethidium Bromide) Displacement Study

To investigate the binding mode of the probes with ct-DNA an intercalation or a groove binding, a competitive binding experiment was performed. Thus, upon addition of increasing amount of probe **5.10** and/or **5.11**, no significant change in fluorescence of ethidium bromide of EB–ct-DNA complex was observed indicating that both the probes were not interacting with ct-DNA as intercalators but may be groove binders (**Figure 5.24**).[31] Though, naphthalimides are known as intercalators,[9] because of appended propergyl units the probes were unable to intercalate sterically between the DNA bases rather they preferred to bind alongside the groove position of ct-DNA via possible π-stacking/H-bonding interactions which was also supported from the fluorescence experiment.

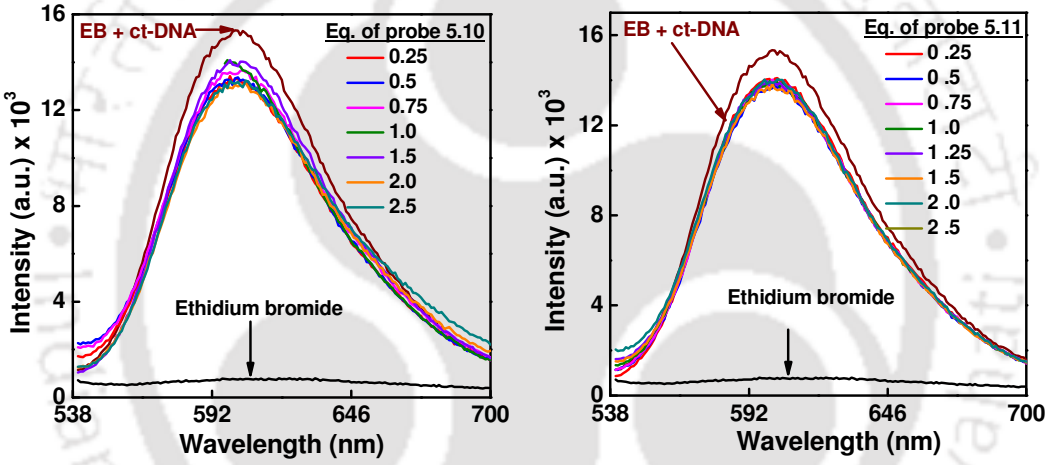

Figure 5.24. (a) Emission spectra (λ_{ex} = 520 nm) of EB, EB-ct-DNA complex and EB-ct-DNA complex mixed with **5.10**. (b) Emission spectra (λ_{ex} = 520 nm) of EB, EB-ct-DNA complex and EB-ct-DNA complex mixed with fluorophore **5.11**. [EB] = 6 μM, [ct-DNA] = 25 μM and [**Probe 5.10 or 5.11**] = 7.5, 15, 22.5, 30, 37.5, 45, 60 and 75 μM.

5.4.5.6. Molecular Modeling Study

To support minor groove binding event, we have carried out MacroModel calculation by Maestro, version 9.0 with AMBER/ force field in water.[32] For the optimization we chose the DNA sequence [5`-d(*CP *GP*CP*GP*AP*AP*TP*TP*CP*GP*CP*G)-3` , (PDB Id: 1DNH)] where Hoechst 33258 dye enter into the minor groove. Thus, Amber* optimized geometry of our probe **5.11** with the model DNA sequence (**Figure 5.25**) showed and support our experimental observation of groove binding event especially in the minor groove.

Therefore, it was clear from the above findings that the probe **5.11** was more efficient compared to probe **5.10** in sensing microenvironment of ct-DNA via the generation of enhanced fluorescence signal. The low fluorescence intensity of the probes in phosphate buffer in absence of biomolecules is not due to the insolubility of the probe but may be attributed to the radiationless channel assisted by intermolecular hydrogen bonding present in aqueous solution.[13a,b] However, as the probes bound to the groove side they experienced restricted radiationless channel inside the groove of ct-DNA ultimately leading to a fluorescence switch-on signal with high intensity and quantum yield.

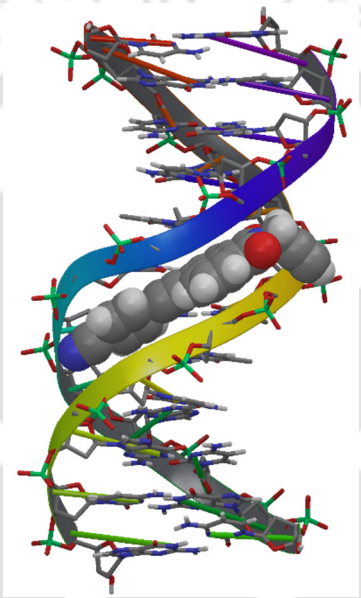

Figure 5.25. Amber* energy minimized geometry of **5.11** with DNA, showing the minor groove binding of the probe **5.11**. The DNA sequence was 5'-d(*CP*GP*CP*GP*AP*AP*TP*TP*CP*GP*CP*G)-3', (**PDB Id: 1DNH**).

5.5. Conclusion

In conclusion, we developed new donor/acceptor conjugated fluorescent naphthalimide based fluorophores. The fluorescence of naphthalimide containing terminal alkynes were of highly ICT character and very sensitive to solvent polarity. We also investigated that both the probes are capable of sensing of microenvironment of ct-DNA via a generation of enhanced fluorescence signal. The solid state fluorescence property of the probe **5.10** might find application in materials sciences. The exploitation of the terminal acetylenes to the synthesis

of fluorescently labeled biomolecular building blocks such as labeled nucleosides and amino acids and their applications thereof is our current research target.

5.6. Experimental Section

5.6.1. General Methods

All reactions were carried out under a nitrogen atmosphere in flame-dried glassware using nitrogen filled balloon. Organic extracts were dried over anhydrous sodium sulphate. Solvents were removed in a rotary evaporator under reduced pressure. Silica gel (60-120 mesh size) was used for the column chromatography. Reactions were monitored by TLC on silica gel 60 F254 (0.25mm). ^{1}H NMR spectra were recorded at 400 MHz spectrometer and ^{13}C NMR spectra were recorded at 100 MHz spectrometer. Coupling constant (*J* value) was reported in hertz. The chemical shifts were shown in ppm downfield from tetramethylsilane, using residual chloroform (δ = 7.24 in ^{1}H NMR, δ = 77.23 in ^{13}C NMR), dimethyl sulfoxide (δ = 2.5 in ^{1}H NMR, δ = 39.5 in ^{13}C NMR), as an internal standard. Mass spectra were recorded using HR mass spectrometer and data analyzed using the inbuilt software. IR spectra were recorded in KBr or neat on a FT-IR spectrometer.

5.6.2. Crystallographic Description

Crystal data were collected with a CCD diffractometer using graphite monochromatedMoKα radiation (λ = 0.71073 Å) at 298 K. Cell parameters were retrieved using and refined with softwares on all observed reflections. Data reduction was performed with the software and corrected for Lorentz and polarization effects. Absorption corrections were applied with the program. The structure was solved by direct methods implemented in a program and refined by full-matrix least-squares methods on F2. All non-hydrogen atomic positions were located in difference Fourier maps and refined anisotropically. The hydrogen atoms were placed in their geometrically generated positions. colourless crystals were isolated in rectangular shape from acetonitrile at room temperature.

5.6.3. Synthetic Procedure and Characterization Data

Synthesis of 4-(2-(4-(N,N-dimethylamino)phenyl)ethynyl)-1,8-naphthalic anhydride (5.15): To a solution of 4-bromo naphthaline anhydride in 1: 1 DMF-Et_3N under N_2, $Pd(PPh_3)_4$

followed by terminal alkyne was added. After 5 minutes of stirring under N_2 atmosphere, 6 mole% of a solution of sodium ascorbate in DMF was added followed by addition of 1 mole% of a solution of $CuSO_4$ in DMF. The reaction mixture was stirred for 4 hrs at 80 ^oC. After completion of the reaction monitored by TLC, the reaction mixture corresponding to the compound (**5.15**) was extracted with ethyl acetate, washed with ammonium chloride, brine and dried over anhydrous Na_2SO_4. The pure product was isolated by column chromatographyfollowed by recrystallization from hot toluene, (65% yield)**.** ^{1}H NMR (400 MHz, $CDCl_3$) δ 3.04 (s, 6H), 6.69 (d, 2H, *J* = 8.4), 7.52 (d, 2H, *J* = 8.4), 7.83 – 7.91 (m, 2H), 8.53 (d, 1H, *J* = 7.6), 8.63 (d, 1H, *J* = 7.2), 8.82 (d, 1H, *J* = 8.4);^{13}C NMR (100 MHz, $CDCl_3$) δ40.3, 85.3, 87.9, 104.0, 111.9, 125.8, 127.7, 130.2, 132.2, 132.9, 133.7, 133.9, 134.5, 151.3, 162.8, 167.5; ESI-TOF-MS *m/z* 342 $[M+H]^+$; HRMS calcd. for $C_{22}H_{16}NO_3$ $([M+H]^+)$ 342.1130, found 342.1125.

Synthesis of 4-(2-(4-(cyano)phenyl)ethynyl)-1,8-naphthalic anhydride (5.16): This was synthesised following same procedure as that was followed for the synthesis of compound **5.15**. Because of poor solubility, the product was isolated by filtration followed by washing with ethanol-water to a yellow powder, (65% yield)**.** ^{1}H NMR (400 MHz, d_6-DMSO) δ8.00 – 8.09 (m, 5H), 8.21 (d, 1H, *J* = 7.6), 8.55 (d, 1H, *J* = 7.6),8.63 (d, 1H, *J* = 6.4), 8.92 (d, 1H, *J* = 8.4); ESI-TOF-MS *m/z* 324 $[M+H]^+$; HRMS calcd. for $C_{21}H_{10}NO_3$ $([M+H]^+)$ 324.0660, found 324.0653.

Synthesis of 4-(4-N,N-dimethylaminophenylethynyl)-N-(2-propynyl)-1,8-naphthalimide (5.10, $^{4\text{-DMAPE}}$NI): To a solution of 0.2 g (0.5865 mmol) of 4-(2-(4-(*N,N*-dimethylamino)phenyl)ethynyl)-1,8-naphthalic anhydride (**5.15**) in dry ethanol, 120 µL (1.8736 mmol) of propergylamine was added and the reaction mixture was stirred at 70 - 75 ^oC for 50 – 60h. One equiv. excess of propergylamine was added after 30h of reaction. The reaction was monitored by TLC and the product was separated by column chromatography. Further the product was recrystallized from hot toluene and 0.14 g (0.3703 mmol) red crystalline pure compound **1** was isolated, (63% yield)**.** ^{1}H NMR (400 MHz, $CDCl_3$) δ 2.18 (t, 1H, *J* = 2.4), 3.05 (s, 6H), 4.94 (d, 2H, *J* = 2.0), 6.79 (bs, 2H), 7.55 (d, 2H, *J* = 8.4), 7.81 (t, 1H, *J* = 8.0), 7.88 (d, 1H, *J* = 7.6), (8.55, 1H, *J* = 7.6), 8.65 (d, 1H, *J* = 8.4), 8.73 (1H, d, *J* = 9.6); ^{13}C NMR (100 MHz, $CDCl_3$) δ 29.6, 40.4, 70.7, 78.9, 85.5, 102.3, 112.1, 120.7, 122.7, 127.3, 128.4, 129.6, 129.9, 130.7, 131.1, 131.6, 132.0, 133.3, 133.5, 150.9, 163.2, 163.5; HRMS calcd. for $C_{25}H_{18}N_2O_2$ $([M+H]^+)$ 379.1441, found 379.1445.

Crystallographic description of 5.10: Crystal dimension (mm): 0.35 x 0.25 x 0.20. $C_{25}H_{18}N_2O_2$, Mr = 378.41; Monoclinic, space group P2(1)/c; a = 28.621(3) Å, b = 9.4187(8) Å, c = 15.0718(14) Å; α = 90.00°, β = 104.256(5)°, γ = 90.00°, V = 3937.9(6) $Å^3$; Z = 8; ρcal = 1.317 Mg/m^3; μ (mm^{-1}) = 0.083; *F (000)* = 1680.0; Refinement method = Full-matrix least-squares on F^2; Final R indices [$I>2\sigma_I$] R1 = 0.2650, wR2 = 0.5213, R indices (all data) R1 = 0.1826(3683), wR2 = 0.5213(8879); goodness of fit = 1.593. [CCDC no.-CCDC 882241].

Synthesis of 4-(4-cyanophenylethynyl)-N-(2-propynyl)-1,8-naphthalimide (5.11, $^{4\text{-CPE}}$NI): To a solution of 0.2 g (0.6191 mmol) of 4-(2-(4-(cyano)phenyl)ethynyl)-1,8-naphthalic anhydride (**5.16**) in dry ethanol, 120 μL (1.8736 mmol) of propergylamine was added and the reaction mixture was stirred at 70 - 75 ºC for 50 – 60h. 1 Equiv. excess of propergylamine was added after 30h of reaction. The reaction was monitored by TLC and the product was separated by filtration and washed with ethanol-water mixture and recrystallized from hot toluene and 0.15 g (0.4166 mmol) yellow crystalline pure compound **5.11** was isolated (67% yield)**.** ^{1}H NMR (400 MHz, $CDCl_3$) δ 2.19 (t, 1H, *J* = 2.4), 4.95 (d, 2H, *J* = 2.8), 7.70 – 7.76 (m, 4H), 7.86 (t, 1H, *J* = 8.0), 7.98 (d, 1H, *J* = 7.6), 8.60 (d, 1H, *J* = 7.6), 8.68 (2H, d, *J* = 8.0); ^{13}C NMR (100 MHz, $CDCl_3$) δ 29.4, 70.7, 78.4, 84.5, 89.8, 96.8, 112.6, 118.1, 122.4, 122.6, 126.7, 126.8, 127.8, 130.6, 131.3, 131.6, 132.1, 132.2, 132.4, 162.7, 162.9; HRMS calcd. for $C_{24}H_{12}N_2O_2$ ($[M+H]^+$) 361.0972, found 361.0971.

5.6.4. Study of Photophysical Properties

5.6.4.1. UV-visible and Fluorescence Measurements

All UV-visible spectra of the compounds (10 μM) were measured in different solvents of varying dielectric constant by UV-visible spectrophotometer using 1 cm path length cell at5 298 K. Fluorescence spectra of the compounds (10 μM) were measured in different solvents of varying dielectric constant by fluorescence spectrophotometer at 298 K using 1 cm path length cell. Time resolved fluorescence decays were measured using time resolved fluorescence spectrophotometer. The fluorescence quantum yields (Φ_f) were determined using perylene[1] as a reference with the known Φ_f = 0.94 in cyclohexane for **5.10** and quinine sulphate[2] as a reference with the known Φ_f = 0.54 in 0.1 molar solution in sulphuric acid for **5.11.** The UV-visible absorbance values for both the reference and the sample solution werekept at around 0.2 at the wavelength corresponding to the wavelength of excitation for boththe sample and the reference. The following equation was used to calculate the quantum yield:

$$\Phi_S = \Phi_R \frac{Fl_S^{Area}}{Fl_R^{Area}} \frac{Abs_R}{Abs_S} \frac{n_S^2}{n_R^2} \quad \text{..... (1)}$$

Where, Φ_R is the quantum yield of standard reference, Fl_S^{Area} (sample) and Fl_R^{Area} (reference) are the integrated emission peak areas, Abs_S (sample) and Abs_R (reference) are the absorbances at the excitation wavelength, and n_S (sample) and n_R (reference) are the refractive indices of the solvents.

5.6.5. General Experiment: Studies on the Interaction of Fluorophores 5.10 and 5.11 with ct-DNA

5.6.5.1 Materials

Calf thymus DNA was purchased from Sigma (USA) and used without further purification. Na_2HPO_4 and $NaH_2PO_4.H_2O$ (for preparation of phosphate buffer) were purchased from Merck, India. Water was obtained from a Milli-Q purification system. All experiments were performed with freshly prepared solutions. The probe molecule was purified according to the procedure described. We recrystallised the column purified material twice, dried under vacuum, again characterized and used the very pure material for study.

5.6.5.2. Preparation of ct-DNA Solution

The supplied ct-DNA was dissolved in 1 ml Milli-Q water and reconstituted overnight at 2 – 8 oC to dissolve all the material and then and filtered through a 0.45 µm filter. The DNA concentration was determined by measuring the absorbance at 260 nm (A260) and using the formula, µg/mL of ct-DNA = A260 x 50 µg/ml x Dilution factor, where A260 = absorbance of the DNA solution at 260 mn and 50 µg/mL is the concentration of 1 A260 unit of double strand DNA.[3a] Thus, from the above formula we determined the concentration of our stock ct-DNA solution as 1.4 mg/mL. The molar concentration of ct-DNA was determined from UV-visible spectra using molar absorption coefficient (ε) of 6600 lit mol^{-1} cm^{-1} at 260 nm[3b] which was found to be 4536.7 µM. The purity of ct-DNA was checked by UV-visible spectroscopy by measuring the ratio of absorbances at 260 nm to 280 nm which was found to be 1.8 – 1.9 indicating that the ct-DNA is sufficiently free of protein.[3c] From that stock solution sub stock of 2000 µM ct-DNA was prepared.

5.6.5.3. UV-Visible Study

The UV–visible absorbance measurements were performed using Shimadzu UV -2550 UV–visible spectrophotometer with a cell of 1 cm path length at 298 K. All the UV-visible

studies were carried out in 5 mM phosphate buffer of pH 7.0 containing 5 mM NaCl solution at 298 K. 2-3 % DMF was used to solubilize the probe. The measurements were taken in absorbance mode and the absorbance values of the sample solutions were measured in the wavelength regime of 200–600 nm. All the experiments were carried out by freshly prepared sample solutions.

5.6.5.4. Melting Temperature (T_m) Measurements

The melting temperature (T_m) of the sample solutions (ct-DNA with probe) were measured in 5 mM sodium phosphate buffer (pH 7.0) containing 5 mM sodium chloride and 1 mM Na_2EDTA. Absorbance *vs*. temperature profiles were measured at 260 nm using a Shimadzu UV-2550 spectrophotometer equipped with a peltier temperature controller using 1 cm path length cell. The absorbance of the samples was monitored at 260 nm from 20 to 90 °C with a heating rate of 1 °C/min. From these profiles, first derivatives were calculated to determine T_m values.

5.6.5.5. Fluorescence Study

All fluorescence and steady state anisotropy experiments were performed using a Fluoromax 4 spectrophotometer with a cell of 1 cm path length at 298 K. All the fluorescence studies were carried out in 5 mM phosphate buffer of pH 7.0 containing 5 mM NaCl solution at 298 K. 2-3 % DMF was used to solubilize the probe. The excitation wavelength for probe **5.11** was set at 370 nm and emission spectra were measured in the wavelength regime of 370–700 nm. The fluorescence quantum yield (Φ_f) for fluorophore **5.11** was determined using quinine sulphate as a reference with the known $\Phi_f = 0.54$ in 0.1 molar solution in sulphuric acid.

5.6.5.6. Theoretical Calculations

The ground state structures of the fluorophores were optimized using density functional theory (DFT) with B3LYP functional and 6-31G (d) basis set. The excited state related calculations were carried out with the Time dependent density functional theory (TD-DFT) with the optimized structure of the ground state (B3LYP/6-31G(d)). There are no imaginary frequencies in frequency analysis of all the calculated structures; therefore, each calculated structure is a local energy minimum.

Table 5.7. Summary of TD-DFT Calculations

Entry	Electronic transition	Energy (eV) (Wavelength)	*f*	Composition	*CI*
Probe 5.10	**99 →100**	**2.5828 eV, 480.03 nm**	**0.6572**	**HOMO → LUMO**	**0.6929**
	98 →100	3.5696 eV, 347.34 nm	0.6459	HOMO-1 → LUMO	0.1877
	97 →100	3.6274 eV, 341.80 nm	0.5604	HOMO-2 → LUMO	0.0001
	99 →101	3.8715 eV, 320.25 nm	0.6453	HOMO → LUMO+1	0.4821
probe 5.11	**93 → 94**	**3.0572 eV, 405.55 nm**	**0.6438**	**HOMO → LUMO**	**0.9014**
	88 → 94 89 → 94 92 → 94	3.7328 eV, 332.15 nm	0.0136	HOMO-5 → LUMO HOMO-4 → LUMO HOMO-1 → LUMO	0.5856 0.1470 0.1054
	89 → 94 91 → 94 92 → 94	3.8117 eV, 325.28 nm	0.0115	HOMO-4 → LUMO HOMO-2 → LUMO HOMO-1 → LUMO	0.3075 0.4729 0.3197

Cartesian Coordinates

B3LYP/6-31G* Energy Optimized geometry and energy of 5.10

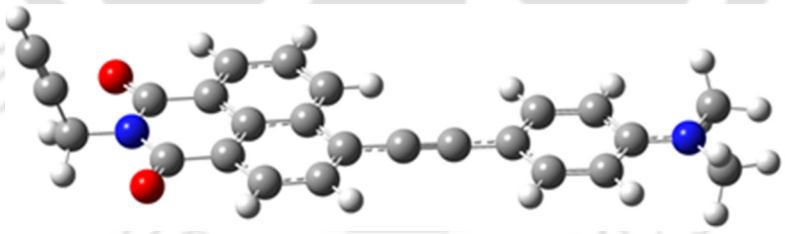

E(RB+HF-LYP) = -1223.37859328 a.u. (Imaginary Freq = 0)

0 1							
O	-4.96554300	-2.42864300	-0.38916000	H	6.63618200	-2.21767000	0.00846500
O	-5.63269100	2.09193000	-0.29050100	C	4.66099100	-1.42746000	-0.02359400
C	-4.47067200	-1.31069200	-0.33363200	H	4.20970800	-2.41282500	-0.09136900
C	-4.83726600	1.16250900	-0.27938900	C	2.41460900	-0.41809000	-0.05430200
C	-2.49248500	0.24262300	-0.21418500	C	1.20059400	-0.52803500	-0.09975900
C	-3.01276000	-1.07533900	-0.27192600	C	4.44810000	0.97110700	0.09117000
C	-3.36865900	1.35931300	-0.21707500	H	3.83145000	1.86482500	0.11314200
C	-1.08220400	0.45634400	-0.15402700	N	-5.28970600	-0.16606600	-0.33490400
C	-0.20573400	-0.68791700	-0.15483000	N	8.03879100	0.07339300	0.18271500
C	3.82537200	-0.29132000	0.00417100	C	-6.74858200	-0.38015600	-0.37218200
C	-2.86320200	2.64667900	-0.16136400	H	-6.91911700	-1.30439200	-0.92809500
H	-3.56051500	3.47792300	-0.16458700	H	-7.18102800	0.46248400	-0.91582100
C	-0.76163900	-1.96956400	-0.21263000	C	-7.34663400	-0.47769800	0.96175600
H	-0.09863400	-2.82843600	-0.21246600	C	-7.86206200	-0.56189900	2.04932100
C	-2.14781200	-2.15922700	-0.27025100	H	-8.30437400	-0.63403700	3.01677900
H	-2.56937600	-3.15807600	-0.31405500	C	8.87625700	-1.11334200	0.13065600
C	-1.47288200	2.85904900	-0.10124900	H	8.67069600	-1.79341600	0.96877600
H	-1.08588800	3.87284500	-0.05738400	H	9.92408100	-0.81557600	0.18975700
C	-0.60135700	1.78704900	-0.09784000	H	8.73498500	-1.67365400	-0.80435600
H	0.47106300	1.94865900	-0.05206100	C	8.65499500	1.38738100	0.25840500
C	5.82609300	1.09622200	0.14861800	H	9.73890300	1.27288100	0.30536600
H	6.25408600	2.08920100	0.21384200	H	8.33443200	1.93556000	1.15503000
C	6.66689900	-0.04516200	0.12271700	H	8.41682500	2.00400700	-0.61999400
C	6.03984000	-1.31368900	0.03336400				

B3LYP/6-31G* Energy Optimized geometry and energy of 5.11

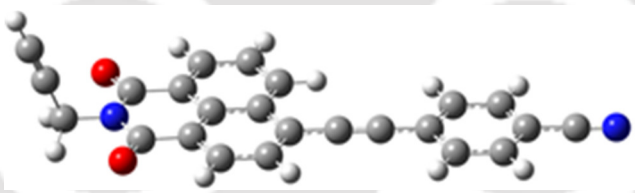

E(RB+HF-LYP) = -1181.64962143 a.u. (Imaginary Freq = 0)

0 1

C	0.34730700	-0.65610200	-0.14423400	H	-6.63124500	0.45341300	-0.92164200
C	-0.53117500	0.48370400	-0.13478900	C	-6.79103900	-0.53340300	0.93333100
C	-0.06081200	1.81800500	-0.05921600	C	-7.30393600	-0.64752900	2.01923300
C	-0.19379000	-1.94033200	-0.22096100	H	-7.74705600	-0.74654400	2.98410000
C	-1.93919400	0.25978100	-0.20653100	H	1.00934900	1.99058700	-0.00447300
C	-2.44780700	-1.06155400	-0.28357600	C	1.75662300	-0.49131400	-0.07828200
C	-1.57996700	-2.14067700	-0.28987700	C	2.96725300	-0.37320800	-0.02451800
C	-3.90849600	-1.30741200	-0.35729500	C	4.38291600	-0.25730200	0.03722200
C	-4.29336000	1.15935600	-0.27513600	C	5.00003800	1.00890900	0.11364000
C	-2.82557900	1.36796600	-0.20123400	C	5.19352200	-1.41213000	0.02260500
C	-2.33139800	2.65787200	-0.12663700	C	6.38190500	1.11816000	0.17366900
C	-0.94223000	2.88083500	-0.05516500	H	4.38321700	1.90148800	0.12528200
H	-0.56493100	3.89737800	0.00351800	C	6.57547500	-1.30523800	0.08257600
H	-3.03460300	3.48404000	-0.12396600	H	4.72462700	-2.38875200	-0.03617100
H	0.47586700	-2.79395300	-0.22696500	C	7.18130300	-0.03851500	0.15857700
H	-1.99479900	-3.14134500	-0.34847400	H	6.85256800	2.09405100	0.23241100
N	-4.73551400	-0.17238000	-0.35133700	H	7.19506600	-2.19591900	0.07112600
O	-5.09377100	2.08279300	-0.27841200	C	8.60836000	0.07342700	0.22027100
O	-4.38701800	-2.43017100	-0.42778700	N	9.76722400	0.16471900	0.27028400
C	-6.19390600	-0.39864200	-0.39715700				
H	-6.35579400	-1.30971700	-0.97688800				

5.7. ^{1}H and ^{13}C NMR Spectra

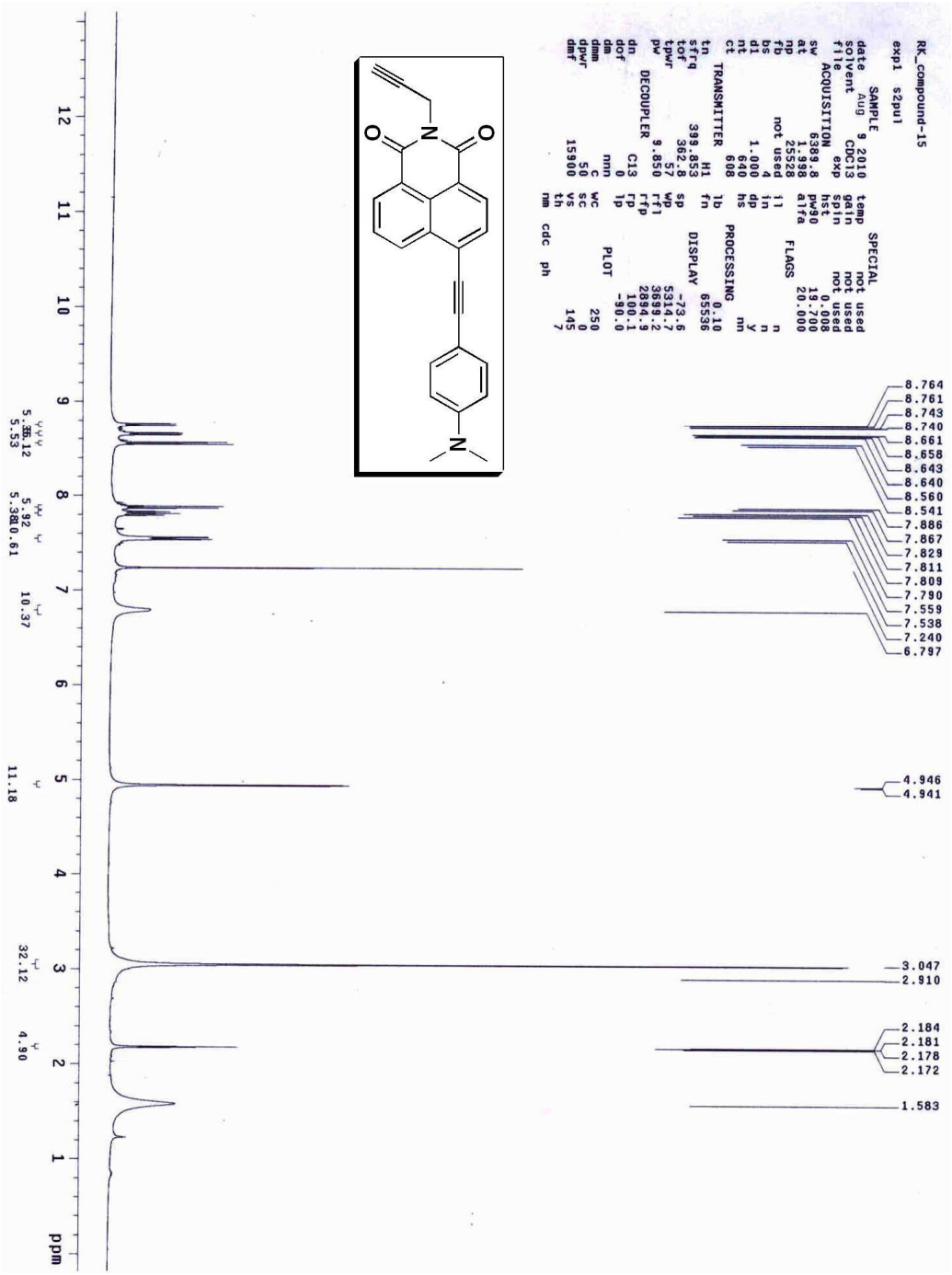

Figure 5.26. ^{1}H NMR of synthesized compound **5.10**.

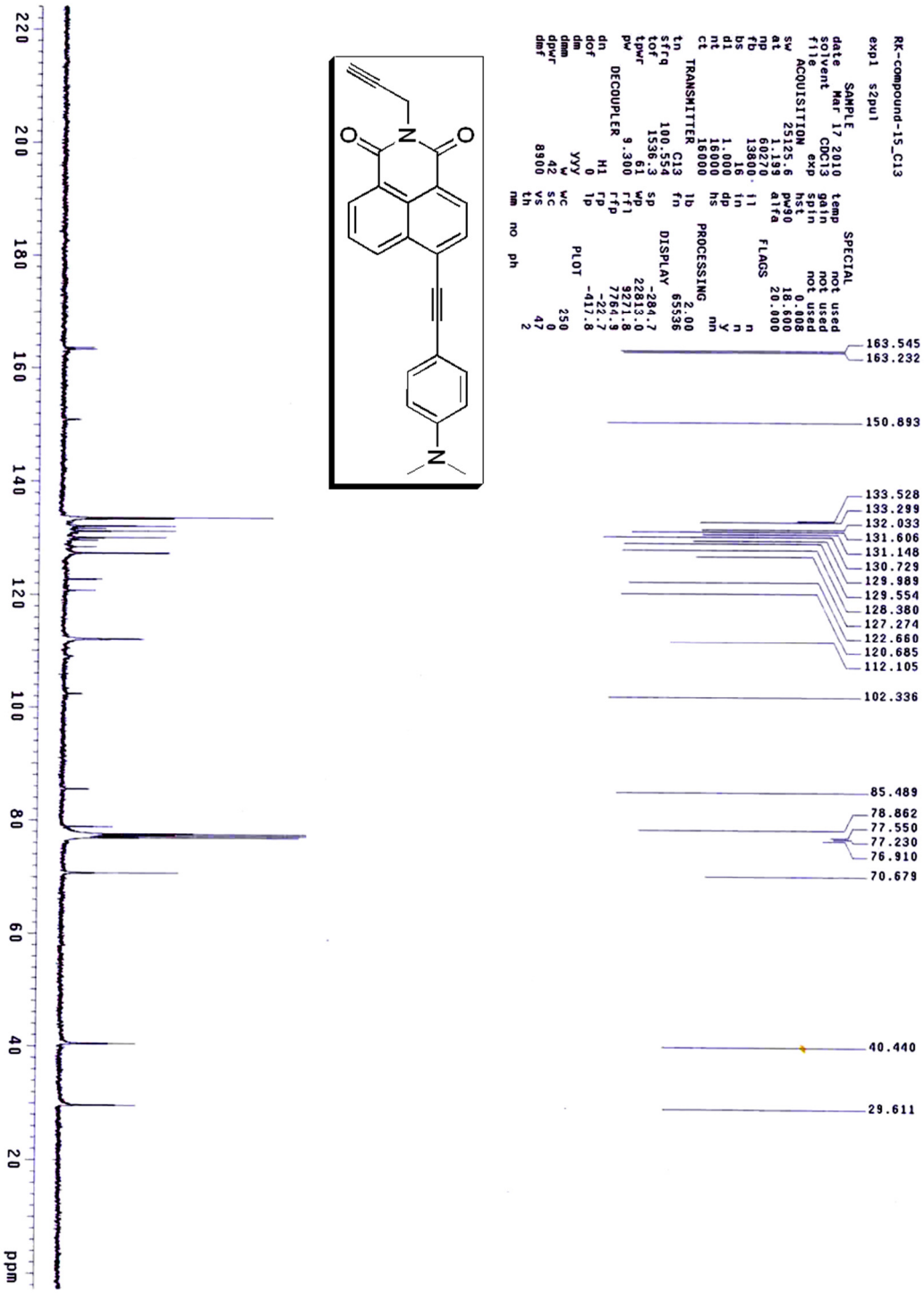

Figure 5.27. ^{13}C NMR of synthesized compound **5.10**.

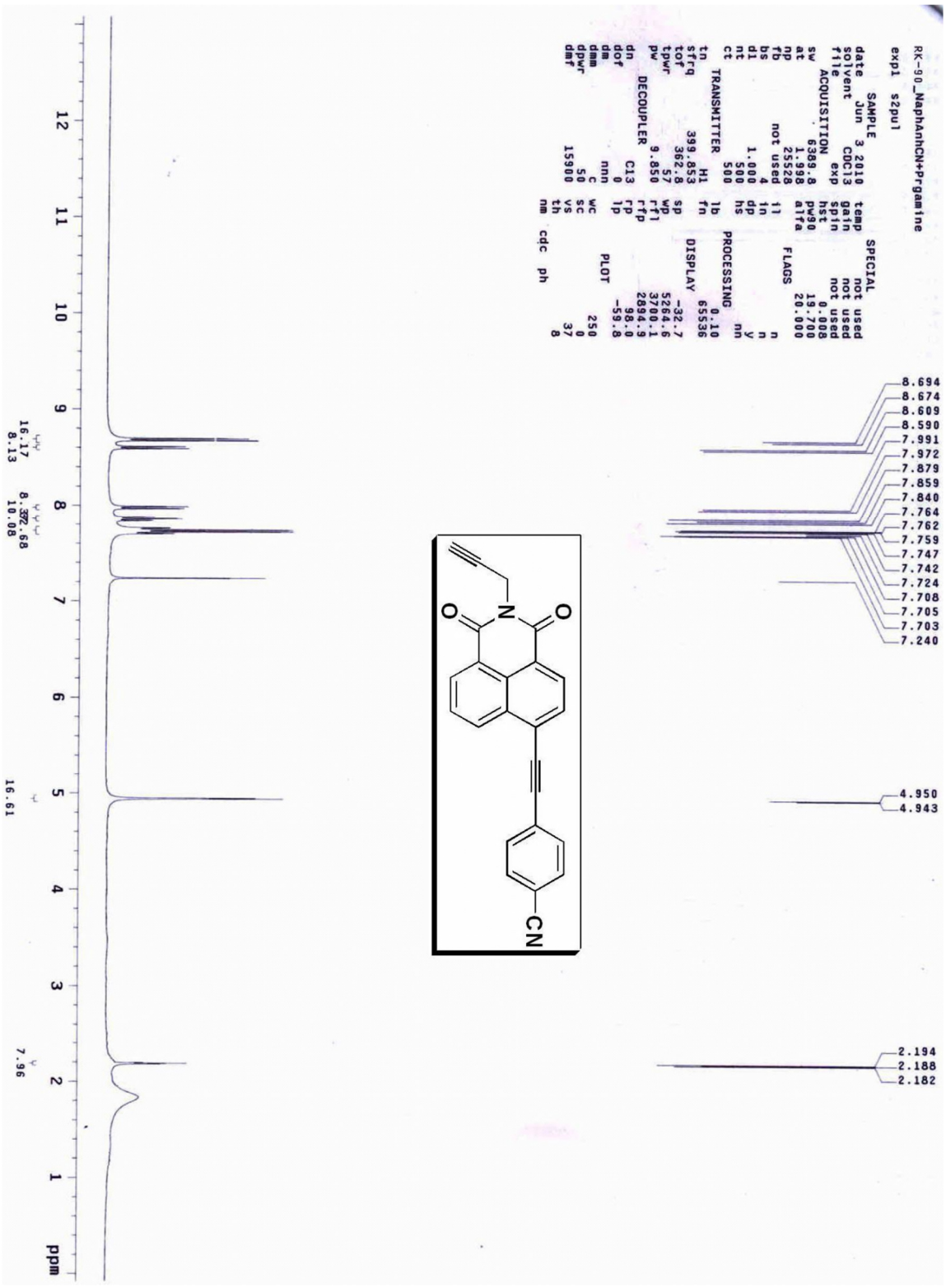

Figure 5.28. [1]H NMR of synthesized compound **5.11**.

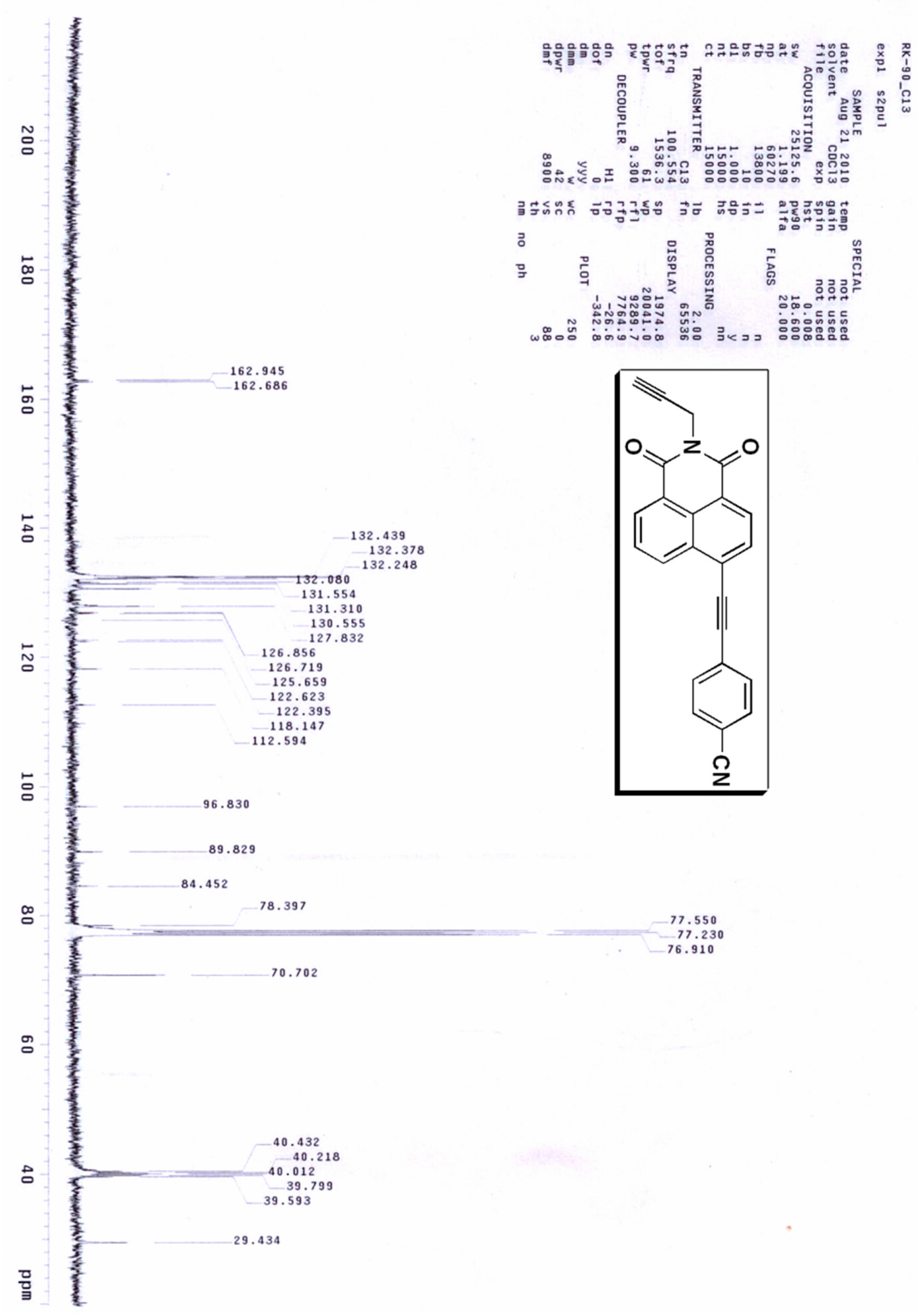

Figure 5.29. ^{13}C NMR of synthesized compound **5.11**.

5.8. References

1. Zhang, G.W.; Wang, L.H.; Zhou, X.Y.; Li, Y.; Gong, D.M. *J. Agric. Food. Chem*. **2014**, *62*, 991.
2. Sarwar, T.; Husain, M.A.; Rehman, S.U.; Ishqi, H.M.; Tabish, M. *Mol. Bio Syst*. **2015**, *11*, 522.
3. Tao, M.; Zhang, G.W.; Pan, J.H.; Xiong, C.H. *Spectrochim. Acta A* **2016**, *155*, 28.
4. Ataci, N.; Arsu, N. *Spectrochimica Acta Part A*, **2016**, *169*, 128.
5. Armitage, B. *Chem. Rev*. **1998**, *98*, 1171.
6. Erkkila, K. E.; Odom, R. T.; Barton, J. K. *Chem. Rev*. **1999**, *99*, 2777.
7. Cao, Y.; He, X. W. *Spectrochim. Acta, Part A* **1998**, *54*, 883.
8. Lu, Y.; Lv, J.; Zhang, G.; Wang, G.; Liu, Q. *Spectrochim. Acta Part A* **2010**, *75*, 1511.
9. (a) Bag, S. S.; Kundu, R. *J. Org. Chem*. **2011**, *76*, 3348. (b) Bag, S. S.; Kundu, R.; Das, M. *J. Org. Chem*. **2011**, *76*, 2332. (c) Sanii, B.; Kudirka, R.; Cho, A.; Venkateswaran, N.; Olivier, G. K.; Olson, A. M.; Tran, H.; Harada, R. M.; Tan, L.; Zuckermann, R. N. *J. Am. Chem. Soc*. **2011**, *133*, 20808. (d) Loving, G.; Imperiali, B. *J. Am. Chem. Soc*. **2008**, *130*, 13630. (e) Vázquez, M. E.; Blanco, J. B.; Imperiali, B. *J. Am. Chem. Soc*. **2005**, *127*, 1300. (f) Loving, G.; Imperiali, B. *Bioconjugate Chem*. **2009**, *20*, 2133. (g) Thielbeer, F.; Chankeshwara, S. V.; Bradley, M. *Biomacromolecules* **2011**, *12*, 4386. (h) Manna, A.; Chakravorti, S. *J. Phys. Chem. B* **2012**, *116*, 5226. (i) Veale, E. B.; Frimannsson, D. O.; Lawler, M.; Gunnlaugsson, T. *Org. Lett*. **2009**, *11*, 4040. (j) Veale, E. B.; Gunnlaugsson, T. *J. Org. Chem*. **2010**, *75*, 5513. (k) Roy, S.; Saha, S.; Majumdar, R.; Dighe, R. R.; Chakravarty, A. R. *Inorg. Chem*. **2009**, *48*, 9501. (l) Ryan, G. J.; Quinn, S.; Gunnlaugsson, T. *Inorg. Chem*. **2008**, *47*, 401.
10. Brana, M.; Cacho, M.; Gradillas, A.; Pascual-Teresa, B. d.; Ramos, A. *Curr. Pharm. Design* **2001**, *7*, 1745.
11. Rosell, R.; Carles, J.; Abad, A.; Ribelles, N.; Barnadas, A.; Benavides, A.; Martín, M. *Invest. New Drug* **1992**, *10*, 171.
12. Malviya, V.K.; Liu, P.; Alberts, D.S.; Surwit, E.A.; Craig, J.B.; Hannigan, E.V. *Am. J. Clin. Oncol.* **1992**, *15*, 41.
13. (a) Ramachandram, B.; Saroja, G.; Sankaran, N. B.; Samanta, A. *J. Phys. Chem. B* **2000**, *104*, 11824. (b) Saha, S.; Samanta, A. *J. Phys. Chem. A* **2002**, *106*, 4763. (c) Duke, R. M.; Veale, E. B.; Pfeffer, F. M.; Kruger, P. E.; Gunnlaugsson, T. *Chem. Soc. Rev*. **2010**, *39*, 3936.

14. Sortino, S.; Condorelli, G. *New J. Chem*. **2002**, *26*, 250.
15. Zhang, G.; Wang, L.; Zhou, X,; Li, Y.; Gong, D. *J. Agric. Food Chem*. **2014**, *62*, 991.
16. Huo, R.; Xu, G.; Jiang, X.; Ge, Y.; Xue, Z.; Cui, F. *J Biochem Molecular Toxicology.* **2012**, *00*, 0.
17. Zhou, X.; Zhang, G.; Pan, J. *Int. J. Biol. Macromolec* **2015,** *74,* 185.
18. Rehman1, S. U.; Yaseen, Z.; Husain, M. A.; Sarwar, T.; Ishqi, H. M.; Tabish, M. *PLOS ONE.* **2014**, *9* (4), 1.
19. Zhang, G.; Fu, P.; Wang, L.; Hu, M. *J. Agric. Food Chem*. **2011**, *59*, 8944.
20. Shi, J. H. Liu, T. T.; Jiang, M.; Chen, J.; Wang, Q. *Journal of Photochemistry and Photobiology B: Biology.* **2015**, *147*, 47.
21. Cui, Y.; Fu, Z.; Geng, S.; Zhang, G.; Cui, F. *J Fluoresc.* **2014,** *24*, 1389.
22. (a) Sonogashira, K.; Tohda, Y.; Hagihara, N. *Tetrahedron Lett*. **1975**, *16*, 4467. (b) Chinchilla, R.; Najera, C. *Chem. Rev*. **2007**, *107*, 874.
23. Wintgens, V.; Valat, P.; Kossanyi, J.; Demeter, A.; Biczok, L.; Berces, T. *New J. Chem*. **1996**, *20*, 1149.
24. (a) Yan, F.; Liu, H. H.; Li, W. L.; Chu, B.; Su, Z. S.; Zhang, G.; Zhu, Y. R. C. J. Z.; Yang, D. F.; Wang, J. B.; Zhang, G. *Appl. Phys. Lett*. **2009**, *95*, 253308. (b) Takahashi, S.; Nozaki, K.; Kozaki, M., et al *J. Phys. Chem. A* **2008**, *112*, 15463. (c) Cao, Z.; Nandhikonda, P.; Penuela, A.; Nance, S.; Heagy, M. D. *Int. J. Photoenergy* **2010**, Article ID 264643. (d) Segura, J. L.; Herrera, H.; Bäuerle, P. *J. Mater. Chem*. **2012**, *22*, 8717.
25. (a) Mataga, N.; Kaifu, Y.; Koizumi, M. *Bull. Chem. Soc. Jpn*. **1956**, *29*, 465. (b) Dahiya, P.; Maity, D. K.; Nayak, S. K.; Mukherjee, T.; Pal, H. *J. Photochem. Photobiol. A*: *Chem*. **2007**, *186*, 218. (c) Masuhara, H.; Mataga, N. *Acc. Chem. Res*. **1981**, *14*, 312. (d) Lippert, V. Z. Z. *Naturforsch*. **1957**, *10a*, 541. (e) Dahiya, P.; Kumbhakar, M.; Maity, D. K.; Mukherjee, T.; Tripathi, A. B. R.; Chattopadhyay, N.; Pal, H. *J. Photochem. Photobiol. A: Chem*. **2006**, *181*, 338.
26. (a) Lakowicz, J. R. *Principles of Fluorescence Spectroscopy, 3rd ed.; Springer: New York*, **2006**. (b) Senthilkumar, S.; Nath, S.; Pal, H. *Photochem. Photobiol.* **2004**, *80*, 104. (c) Nad, S.; Pal, H. *J. Phys. Chem. A* **2003**, *107*, 501. (d) Barik, A.; Nath, S.; Pal, H. *J. Chem. Phys*. **2003**, *119*, 10202. (e) Nath, S.; Pal, H.; Sapre, A. V. *Chem. Phys. Lett*. 2002, 360, 422. (f) Nad, S.; Pal, H. *J. Phys. Chem. A* **2001**, *105*, 1097.
27. (a) Grabowksi, Z. R.; Rotkiewicz, K.; Rettig, W. *Chem. Rev*. **2003**, *103*, 3899. (b) Turro, N. *J. Modern Molecular Photochemistry; University Science Books: Sausalito*,

1991. (c) Fromherz, P. *J. Phys. Chem*. **1995**, *99*, 7188. (d) Albinsson, B. *J. Am. Chem. Soc*. **1997**, *119*, 6369. (e) Chen, X.; Zhao, Y.; Cao, Z. *J. Chem. Phys*. **2009**, *130*, 144307. (f) Thiagarajan, V.; Selvaraju, C.; Malar, E. J. P.; Ramamurthy, P. *ChemPhysChem* **2004**, *5*, 1200. (g) Pham, T. H. N.; Clarke, R. J. *J. Phys. Chem. B* 2008, *112*, 6513. (h) Shim, T.; Lee, M. H.; Kim, D.; Ouchi, Y. *J. Phys. Chem. B*. **1906**, *2008*, 112. (i) Panigrahi, M.; Dash, S.; Patel, S.; Behera, P. K.; Mishra, B. K. *Spectrochim. Acta, Part A* **2007**, *68*, 757. (j) Benniston, A. C.; Harriman, A.; Llarena, I.; Sams, C. A. *Chem. Mater*. **1931**, *2007*, 19. (k) Perez- Inestrosa, E.; Montenegro, J.-M.; Collado, D.; Suau, R. *Chem. Commun*. **2008**, 1085. (l) Shaikh, M.; Mohanty, J.; Singh, P. K.; Bhasikuttan, A. C.; Rajule, R. N.; Satam, V. S.; Bendre, S. R.; Kanetkar, V. R.; Pal, H. *J. Phys. Chem. A* **2010**, *114*, 4507. (m) Birks, J. B. *Photo Physics of Aromatic Molecules; Wiley-Interscience: New York* **1970**.

28. Frisch, M. J. et al. *Gaussian 03, revision C.02*; *Gaussian, Inc.: Wallingford, CT*, **2004**.
29. (a) Granzhan, A.; Ihmels, H. *Org. Lett.* **2005**, *7*, 5119. (b) Wu, F. Y.; Xie, F. Y.; Wu, Y. M.; Hong, J. I. *J. Fluoresc*. **2008**, *18*, 175. (c) Sahoo, D.; Bhattacharya, P.; Chakravorti, S. *J. Phys. Chem. B*. **2010**, *114*, 2044.
30. (a) Ye, B. F.; Zhang, Z. J.; Ju, H. X. *Chin. J. Chem*. **2005**, *23*, 58. (b) Sahoo, B. K.; Ghosh, K. S.; Bera, R.; Dasgupta, S. *Chem. Phys*. **2008**, *351*, 163. (c) Ghosh, R.; Bhowmik, S.; Bagchi, A.; Das, D.; Ghosh, S. *Eur. Biophys. J*. **2010**, *39*, 1243.
31. (a) Bresloff, J. L.; Crothers, D. M. *Biochemistry* **1981**, *20*, 3547. (b) Wu, H. L.; Li, W. Y.; He, X. W.; Miao, K.; Liang, H. *Anal. Bioanal. Chem*. **2002**, *373*, 163. (c) Ghaderi, M.; Bathaie, S. Z.; Saboury, A. A.; Sharghi, H.; Tangestaninejad, S. *Int. J. Biol. Macromol*. **2007**, *41*, 173. (d) Nafisi, S.; Bonsaii, M.; Maali, P.; Khalilzadeh, M. A.; Manouchehri, F. *J. Photochem. Photobiol. B: Biol*. **2010**, *100*, 84.
32. Maestro, version 9.0, Schrödinger, LLC, New York, NY, **2009**.

Summary and Outlook

In this dissertation, we have discussed various types of small organic molecules, which target DNA. A better understanding of DNA–small molecule interactions will be necessary for the rational design of more efficient analogs as potential DNA binding drugs. We also discussed the interaction of G-quadruplexes with small molecule. The continual development of more selective G-quadruplex probes as well as those capable of monitoring G-quadruplex motifs in living cells is essential for further advancing our understanding of G-quadruplex structures in biology. Therefore, there is always a challenge to achieve maximum specific DNA-binding affinity and cellular and nuclear transport activity without affecting the functions of the normal cells.

In *chapter 2*, we synthesised a solvatochromic naphthalene appended uridine nucleoside (^{Naph}**U**) and exploited in SNP detection. Oligonucleotide probe containing ^{Naph}**U** was found to be highly specific for the detection of matched base adenosine of a target DNA opposite to the labeled base (^{Naph}**U**) of a probe DNA via maximum shift in emission wavelength. Interestingly, the probe nucleoside flanking between GC/GC base pair could sense efficiently the presence of opposite matched base –A– of a target DNA both via the maximum shift in wavelength and enhancement of intensity of fluorescence signal. Designing more of such probes for DNA detection is our current research focus.

In *chapter 3*, ^{TzPy}**B**^{Do} was exploited as a probe for label free detection of T-T/C-C base mismatches, abasic site and bulge DNA with increased fluorescence intensity. We proposed that Tetrazolylpyrene (**TzPy**) unit of the probe might involve in stacking interaction along the groove close to the deformed (mismatched/abasic/bulge-out) site that led to the generation of enhanced fluorescence signal. Therefore, **TzPy** exhibits highly sensitive, selective and fluorescent detection of mutated DNAs over fully matched duplexes without affecting the helical conformation. The label free fluorescent light-up sensing of DNA base mismatches, abasic DNAs and DNA bulge over matched duplex makes **TzPy** exploitable as a potential diagnostic tool for the diseases that are associated with these types of mutated DNAs. **TzPy** might also find future applications for the detection and targeting of DNA lesions with a less laborious, simple and cost effective way. Recognition of such DNA lesions may give clues about the initial DNA recognition event(s) by repair enzymes in the complex repair machinery.

In *chapter 4*, the bare fluorescent tetrazolylpyrene nucleoside (^{TzPy}**B**^{Do}) served as a versatile fluorescent light-up probe for label free detection of multimeric G-quadruplex DNA

with high specificity. The strong binding of the probe via intercalative stacking interaction inside the TTA pocket connecting two G-quadruplex units of Hum45 multimeric G-quadruplex DNA and discrimination to other monomeric and long DNA duplex were accompanied by a drastic enhancement of emission intensity without compromising the conformation and thermal melting stability. Thus, the probe **TzPy** had an excellent ability to discriminate between telomeric multimeric and monomeric G-quadruplexes. The probe **TzPy** might find future applications for the specific detection and targeting of multimeric G-quadruplex DNA and help in designing such unnatural nucleoside as multimeric G-quadruplex specific binder/drug like candidates for cancer therapy. The design of multimeric G-quadruplex specific fluorescent probe with enhanced G-quadruplex stabilizing ability is our current research focus.

In *chapter 5*, we developed new donor/acceptor conjugated fluorescent naphthalimide based fluorophores. The fluorescence of naphthalimide containing terminal alkynes were of highly ICT character and very sensitive to solvent polarity. We also investigated that both the probes are capable of sensing of microenvironment of ct-DNA via a generation of enhanced fluorescence signal.